Rothwell, Edward Joseph

RADAR TARGET DISCRIMINATION USING THE EXTINCTION-PULSE TECHNIQUE

Michigan State University PH.D. 1985

RADAR TARGET DISCRIMINATION

USING THE

EXTINCTION-PULSE TECHNIQUE

By

Edward Joseph Rothwell

A DISSERTATION

Submitted to
Michigan State University
in partial fulfillment of the requirements
for the degree of

DOCTOR OF PHILOSOPHY

Department of Electrical Engineering
and Systems Science

1985

ABSTRACT

RADAR TARGET DISCRIMINATION
USING THE
EXTINCTION-PULSE TECHNIQUE

By

Edward Joseph Rothwell

The extinction-pulse (E-pulse) technique is a radar target discrimination scheme which utilizes the natural resonance behavior of conducting scatterers. An E-pulse is a finite duration waveform synthesized in such a way that, upon interaction with a particular target, it excites only a pre-specified portion of the target's natural resonance spectrum. Since the E-pulse waveform is based only on the natural frequencies of the target, it is aspect independent.

This thesis investigates E-pulse synthesis, and a variety of other topics relevant to the technique. Waveforms are synthesized using both a time and a frequency domain approach, and discrimination between differing thin cylinder targets is carried out numerically, demonstrating the success of the technique in the presence of random noise.

The extraction of target natural frequencies from a measured response is also considered, and a variety of techniques is introduced. Particularly successful is the continuation method approach, which proves a viable replacement for the highly noise-sensitive Prony's method.

Edward Joseph Rothwell

As an investigation into the resonance properties of a particular target, a theoretical analysis of a thin wire elliptical loop scatterer is undertaken. A number of the natural frequencies and corresponding surface current distributions of the target are calculated, by solving a homogeneous electric field integral equation in the frequency domain. The natural frequencies are shown to make smooth transitions to those of the limiting cases of a circular loop and a transmission line.

Lastly, an experimental validation of the natural resonance behavior of simple thin wire targets is presented, as well as an experimental verification of the E-pulse concept. Successful discrimination between two realistic aircraft target models is accomplished by utilizing measurements of their scattered field responses.

In loving memory of my father

ACKNOWLEDGMENTS

Foremost thanks are due Dr. Kun-Mu Chen, my academic advisor, for his generous support and guidance throughout this work. Gratitude must also be expressed to Dr. Dennis Nyquist for his unending assistance and to Dr. Byron Drachman for his sincere interest and encouraging advice.

I would also like to thank the members of my guidance committee, Dr. Jes Asmussen and Dr. Bong Ho, for their generous donation of time and assistance.

Finally, I must thank my wife, Kitty, my mother, Mrs. Catherine Rothwell, and my close friend, Rick Nolan, for their support and understanding during my many years of graduate study.

TABLE OF CONTENTS

TABLE OF CONTENTS continued

TABLE OF CONTENTS continued

LIST OF TABLES

LIST OF FIGURES

LIST OF FIGURES continued

LIST OF FIGURES continued

LIST OF FIGURES continued

CHAPTER 1

INTRODUCTION

The topics of radar target identification and discrimination have gained increasing interest in recent years. Reconstructing the geometry and composition of a conducting target based upon a measurement of the electromagnetic field scattered from its surface is known as the "inverse scattering" problem. Since the true inverse problem is extremely difficult to solve, the most promising discrimination techniques have concentrated on extracting simple unique target features from the scattered field. This thesis presents a discrimination scheme called the "Extinction-pulse" or "E-pulse" technique, which utilizes unique features in the time domain scattered field response of a radar target.

It has been hypothesized that the late-time portion of the time domain scattered field response of a conducting radar target is composed entirely of damped sinusoids, oscillating at frequencies which are functions only of target geometry, and not target aspect. These natural frequencies comprise a set of features which uniquely determine the target. An E-pulse is a special aspect independent, finite duration waveform constructed in such a way that, upon interaction with a certain target, results in a scattered field which contains only a pre-specified component of the target's natural mode spectrum. In

particular, the E-pulse can be constructed to result in a null scattered field waveform by eliminating the entired excited portion of the target's natural mode spectrum.

The usefulness of the E-pulse technique is founded on the property that the waveform need not actually be transmitted. It is easily shown that the convolution of the E-pulse waveform and the measured scattered field response of the target gives results completely analogous to transmitting the E-pulse directly. This is important, since it allows the use of any convenient interrogation waveform, as long as it has sufficient frequency content to excite the desired natural modes.

This thesis covers a wide variety of topics pertinent to the E-pulse technique. Chapter 2 gives a review of the singularity expansion method (SEM), which provides an analytical method of exploiting the natural resonance description of the response of a conducting target. Chapter 3 presents a brief overview of some of the more relevant target discrimination schemes developed by other workers, and shows the additional need for the E-pulse technique.

The E-pulse concept is introduced in chapter 4, and expanded upon in great detail. Material in this chapter includes methods of E-pulse synthesis and interpretation. Chapter 5 presents a numerical verification of the E-pulse concept, and provides examples of discrimination between differing thin cylinder targets.

Chapter 6 presents methods for extracting the natural frequencies of conducting targets from measurements of their time domain responses. This is an important topic, since the natural

frequencies of practical targets will not be available from theoretical analyses.

Chapter 7 gives an electromagnetic analysis of a particular scatterer -- a thin wire shaped into an elliptical loop. The natural frequencies of this target are obtained using the singularity expansion method introduced in chapter 2, and E-pulses are constructed for their elimination.

Lastly, chapter 8 introduces experimental validation of both the natural resonance expansion of the field scattered by a conducting target, and of the E-pulse concept itself. Verification of the E-pulse concept is provided using the scattered field measurements of scale aircraft models.

CHAPTER 2

THE SINGULARITY EXPANSION METHOD

2.1 Introduction

The singularity expansion method (SEM) is an analytical technique first formalized by C. E. Baum in the early 1970's for analyzing the transient response of antennas and scatterers to complicated time varying excitations [1]. Its basis is founded on the results of many experiments and theoretical analyses (see [2], [3], or [4] for example) which revealed that the time domain response of such objects is dominated in the late-time period (i. e. after the excitation has been removed) by a sum of exponentially damped sinusoidal functions. The frequencies of these oscillations were seen to be dependent only upon the physical properties of the objects -- geometry, for perfectly conducting bodies -- and not upon the particular form of excitation.

Later developments in the field of SEM have in general taken one of two paths. Many researchers have attempted to investigate the theoretical implications of the method [5]-[13], including the proper expansion of the early and late-time responses, while others have employed the method for the analysis of particular electromagnetic problems [14]-[17]. This chapter will present a short theoretical

overview of the SEM technique the results of which form the basis for a radar target discrimination method which is investigated extensively in later chapters. An electromagnetic analysis of a particular scatterer (a thin wire elliptically shaped loop) will be conducted in chapter seven using the theory developed in this chapter.

2.2 SEM Representation of Scattered Field

The electromagnetic field scattered by a perfectly conducting target results from the surface current and charge induced by the excitation field, as shown in Figure 2.2.1. Experimental evidence suggests that the surface current can be represented in the late-time period by a sum of natural mode damped sinusoidal functions

$$\vec{K}(\vec{r},t) = \sum_{n=1}^{N} A_n \vec{K}_n(\vec{r}) e^{\sigma_n t} \cos(\omega_n t + \phi_n) \qquad (2.2.1)$$

Here $\vec{K}_n(\vec{r})$ is the spatial current distribution of the n'th natural oscillation mode, A_n and ϕ_n are the amplitude and phase of the n'th mode, and $s_n = \sigma_n + j\omega_n$ is the complex natural frequency of the n'th mode. Whereas the phase and amplitude are directly dependent upon the form of excitation (e. g. target aspect), the natural frequencies of any particular conducting target are determined by the object's geometry only.

Calculation of the transient scattered field maintained by the induced surface current and charge is simplified greatly by using a transform domain analysis. The Laplace transform of a function f(t) is defined as [18]

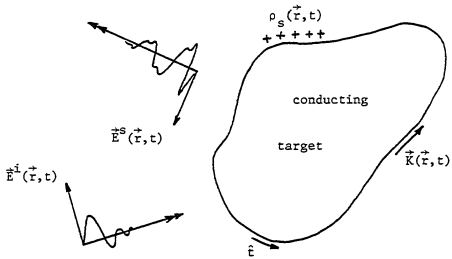

Figure 2.2.1. Transient excitation of a perfectly conducting scatterer.

$$F(s) = L\{f(t)\} = \int_0^\infty f(t)e^{-st}dt \qquad (2.2.2)$$

and the corresponding inverse transform is

$$f(t) = L^{-1}\{F(s)\} = \frac{1}{2\pi j}\int_{Br} F(s)e^{st}ds \qquad (2.2.3)$$

where the inversion integral is performed over the Bromwich contour, and f(t) is taken to be a time causal function. Substituting the time domain form of the surface current (2.2.1) into (2.2.2) results in the transform domain form of the surface current

$$\vec{K}(\vec{r},s) = \sum_{n=1}^{2N} a_n(s)\vec{K}_n(\vec{r})(s-s_n)^{-1} \qquad (2.2.4)$$

Thus, the late-time surface current is a sum of simple pole singularities in the complex frequency plane. For real conducting targets the natural frequencies occur in N complex conjugate pairs, and it is easily seen that application of the inverse transform (2.2.3) and Cauchy's residue theorem returns (2.2.4) to the time domain form (2.2.1). The amplitude and phase information of the n'th mode is contained in the aspect dependent "coupling coefficient" $a_n(s)$.

The fundamental assumption of SEM analysis is that (2.2.4) is a valid transform domain representation of the surface current during the late-time. That is, there exist no contributions due to higher order poles, essential singularities, entire functions, etc. It is important to stress, though, that this representation is valid in the

late-time only. Consensus holds that a simple pole series alone is not a sufficient representation during the early-time period (when the excitation field is interacting with the target), and an entire function must also be included (see [9] or [11] for example.)

Using retarded potential theory, the scattered electric field can be written as

$$\vec{E}^s(\vec{r},t) = -\nabla\phi^s(\vec{r},t) - \frac{\partial \vec{A}^s(\vec{r},t)}{\partial t} \qquad (2.2.5)$$

where the scalar potential is given in terms of electric surface charge density $\rho_s(\vec{r},t)$ as

$$\phi^s(\vec{r},t) = \frac{1}{4\pi\varepsilon_o}\int_S \frac{\rho_s(\vec{r}',t-R/c)}{R}\, dS' \qquad (2.2.6)$$

and the vector potential is given in terms of surface current density $\vec{K}(\vec{r},t)$ as

$$\vec{A}^s(\vec{r},t) = \frac{\mu_o}{4\pi}\int_S \frac{\vec{K}(\vec{r}',t-R/c)}{R}\, dS' \qquad (2.2.7)$$

Invoking the Laplace transform (2.2.2) and employing the continuity equation results in the transform domain expression for the scattered electric field maintained by the induced surface current

$$\vec{E}^s(\vec{r},s) = \frac{1}{s\varepsilon_o}\int_S \left\{ \nabla'\cdot\vec{K}(\vec{r}';s)\nabla - \gamma^2\vec{K}(\vec{r}';s) \right\} \frac{e^{-\gamma R}}{R}\, dS' \qquad (2.2.8)$$

where $R = |\vec{r}-\vec{r}'|$ and $\gamma = s/c$, c being the speed of light in free space.

At this point it becomes convenient to introduce the Green's dyadic notation. Denoting the electric Green's dyadic function as

$$\overleftrightarrow{G}_e(\vec{r}|\vec{r}';s) = (\overleftrightarrow{I} - \frac{\nabla\nabla}{\gamma^2})G(\vec{r}|\vec{r}';s) \qquad (2.2.9)$$

where

$$G(\vec{r}|\vec{r}';s) = \frac{e^{-\gamma R}}{R} \qquad (2.2.10)$$

With this notation and using (2.2.4) to represent surface current, the SEM transform domain representation of the scattered field can be written as

$$\vec{E}^s(\vec{r},s) = -s\mu_0 \sum_{n=1}^{2N} a_n(s)(s-s_n)^{-1} \int_S \overleftrightarrow{G}_e(\vec{r}|\vec{r}';s)\cdot\vec{K}_n(\vec{r}')dS' \qquad (2.2.11)$$

Finally, using (2.2.3) to invert (2.2.11) the SEM time domain representation of the scattered electric field is given by

$$\vec{E}^s(\vec{r},t) = -\mu_0 \sum_{n=1}^{2N} s_n a_n(s_n) e^{s_n t} \int_S \overleftrightarrow{G}_e(\vec{r}|\vec{r}';s_n)\cdot\vec{K}_n(\vec{r}')dS' \qquad (2.2.12)$$

2.3 Integral Equation for Surface Current

Before equation (2.2.12) can be employed to calculate the scattered electric field, the surface current established by the excitation field must be determined. This requires the calculation of the natural frequencies, coupling coefficients, and modal current distributions, all of which are included in the current representation (2.2.4). As stressed earlier, the natural frequencies and modal currents are determined from solutions to the unforced problem, and are functions of target geometry only. However, the coupling coefficients are strong functions of target excitation and contain all the information regarding target aspect.

The surface current is calculated through the solution to an electric field integral equation (EFIE). This integral equation is formulated by employing the boundary condition for the electric field on the surface of the perfectly conducting scatter

$$\hat{t}\cdot\vec{E}^{i}(\vec{r},s) = -\hat{t}\cdot\vec{E}^{s}(\vec{r},s) \qquad (2.3.1)$$

where $\vec{E}^{i}(\vec{r},s)$ is the excitation field incident upon the scatterer and $\hat{t}$ is the unit tangent vector. Writing the scattered field as in (2.2.11) yields the EFIE

$$\sum_{n=1}^{N} a_n(s)(s-s_n)^{-1}\int_S \hat{t}\cdot\vec{G}_e(\vec{r}|\vec{r}';s)\cdot\vec{K}_n(\vec{r}')dS' = \frac{\hat{t}\cdot\vec{E}^{i}(\vec{r},s)}{s\mu_0} \qquad (2.3.2)$$

which must hold for all points on the surface of the scatter: $\vec{r} \in S$.

When the excitation field is zero, the only possible solutions to the resulting homogeneous equation represent the natural oscillation modes of the target (i. e. there are solutions to the homogeneous EFIE only at discrete frequencies $s=s_n$.) Thus, the natural frequencies and the natural mode current distributions are determined by solving

$$\int_S \hat{t}\cdot\vec{G}_e(\vec{r}|\vec{r}';s)\cdot\vec{K}_n(\vec{r}')dS' = 0 \qquad \text{for all } \vec{r}\in S \qquad (2.3.3)$$

The coupling coefficients are determined from the EFIE (2.3.2) by replacing the tangential unit vector $\hat{t}$ with $\int_S d\vec{S}\vec{K}_m(\vec{r})$, where $\vec{K}_m(\vec{r})$ is the current distribution of the m'th mode. Employing the reciprocality of the Green's dyadic in $\vec{r}$ and $\vec{r}'$, taking the limit as $s_n \to s_m$ and using l'Hôpital's rule and (2.3.3) results in

$$a_m(s_m) = \frac{1}{s_m\mu_0 c_m}\int_S \vec{E}^i(\vec{r}',s_m)\cdot\vec{K}_m(\vec{r}')dS' \qquad (2.3.4)$$

where c_m is a normalization coefficient given by

$$c_m = \int_S d\vec{S}\vec{K}_m(\vec{r})\cdot\int_S \frac{\partial\vec{G}_e(\vec{r}|\vec{r}';s)}{\partial s}\bigg|_{s=s_m}\cdot\vec{K}_m(\vec{r}')dS' \qquad (2.3.5)$$

This is the so-called "class-1" coupling coefficient of Baum [8], which is applicable to late-time only, and is used in the time domain SEM representation of the scattered field (2.4.3). Replacing s_m by s yields the more controversial "class-2" coefficient

$$a_m(s) = \frac{1}{s\mu_0 c_m} \int_S \vec{E}^i(\vec{r}',s)\cdot\vec{K}_m(\vec{r}')dS' \qquad (2.3.6)$$

which is the late-time frequency domain equivelant to the class-1 coefficient; that is, its use in (2.2.11) along with Cauchy's residue theorem merely results in the identical class-1 $a_n(s_n)$ of equation (2.2.12). However, the class-2 coefficient is conjectured to apply to early-time as well [8]. In this case, $a_n(s)$ must be calculated explicitly, and a more rigorous inversion of (2.2.11) employed.

2.4 Time Domain Representation of Scattered Field

For the case of radar illumination, it can be assumed that the target is in the far field region of the transmitting antenna. Thus, the incident electric field is a component of a plane wave front, or

$$\vec{E}^i(\vec{r},t) = \hat{p}E_o e(t-r/c) \qquad (2.4.1)$$

where $\hat{p}$ determines the polarization of the electric field, and e(t) describes the temporal variation of the field. Transforming this to the frequency domain via (2.2.2) yields

$$\vec{E}^i(\vec{r},s) = \hat{p}E_o E(s)e^{-\gamma r} \qquad (2.4.2)$$

where E(s) is the transform of e(t). Substituting (2.4.2) into the class-1 coupling coefficient (2.3.4) and that result into (2.2.12) gives the time domain scattered field representation

$$\vec{E}^s(\vec{r},t) = -E_o \sum_{n=1}^{2N} \frac{E(s_n)}{c_n} e^{s_n t} \left(\int_S e^{-\gamma r_{\hat{p}} \cdot \vec{r}} \vec{K}_n(\vec{r}) dS \right) \times$$

$$\times \left(\int_S \vec{G}_e(\vec{r}|\vec{r}';s_n) \cdot \vec{K}_n(\vec{r}') dS' \right) \qquad (2.4.3)$$

Since the natural frequencies occur in complex conjugate pairs, the vector magnitude of this field can also be written as

$$E^s(\vec{r},t) = \sum_{n=1}^{N} A'_n(\vec{r}) e^{\sigma_n t} \cos(\omega_n t + \phi'_n(\vec{r})) \qquad (2.4.4)$$

revealing that the scattered electric field also varies, in the late-time, as a sum of damped sinusoidal functions.

It is this late-time behavior of the scattered field that will be utilized for radar target discrimination purposes in the following chapters.

CHAPTER 3

RADAR TARGET DISCRIMINATION AND IDENTIFICATION SCHEMES

3.1 Introduction

Radar target identification in its purest form is an inverse problem -- the reconstruction of the geometry and composition of a target from measurements of scattered electromagnetic radiation. The target can then be identified or discriminated from other targets or classes of targets by comparison to known shapes and compositions. In a less rigid sense, radar target discrimination involves the extraction of features from the measured scattered electromagnetic field which correspond uniquely to individual targets [29]. Discrimination (or identification) is then accomplished by a comparison of these features.

Radar target features for a conducting target are closely related to geometry, and can take advantage of all the information contained in the scattered field -- amplitude, phase, polarization, and frequency content. Whereas the solution of the true inverse problem requires an infinite amount of information (i. e. a measurement of the scattered field at all frequencies or all aspect angles) [30] only a few features may be required for the classification of a wide variety of targets. An example of a feature which is not unique is the classical radar cross section (RCS).

This chapter will conduct a short overview of some of the more recent methods conceived for radar target discrimination. It will be by no means exhaustive, but instead will try to place the proposed discrimination techniques of this thesis in proper perspective. The new scheme as suggested in this and later chapters will be shown to be an evolution of an attempt to overcome the two most fundamental problems of target discrimination -- noise and sensitivity to target aspect.

The discrimination schemes reviewed in this chapter can be divided into two fundamental groups. The first involves the use of the properties of the target scattering matrix. The second utilizes the frequency (or, equivalently, time) response of the target.

3.2 Polarization Techniques

In the case of time-harmonic excitation it is convenient to consider a radar target as a "polarization transformer" [31]. The vector electric field scattered from the perfectly conducting target can be related to the incident field through

$$\vec{E}^s = \overline{\overline{A}} \cdot \vec{E}^i \qquad (3.2.1)$$

where $\overline{\overline{A}}$ is the two dimensional scattering matrix. This matrix describes the changes in polarization between the incident and reflected waves and is a function of frequency and target aspect. The polarization states of these waves are often mapped onto the surface of a sphere (the Poincaré sphere.) Twice the orientation

angle of the elliptical polarization and twice the arctangent of the axial ratio define longitude and latitude, respectively, of a point on the sphere. Thus, the mapping is one to one and the equator of the sphere contains all linear polarizations [32].

Target classification by reconstructing the scattering matrix is impractical, since measurements would be required at an infinite number of polarization states. Rather, the polarization properties of any target can be characterized by its "null polarizations" -- the two states for which the backscattered wave is polarized orthogonal to the transmitting antenna (and for which the target is invisible to the radar.) These polarizations correspond to the eigenvectors of $\overline{\overline{A}}$. With this notation it is possible to make a general classification of radar targets based on their polarization properties. The null polarizations of linear targets (such as thin wires) coincide at a single point on the sphere. The null polarizations of an isotropic target (such as a homogeneous sphere) reside at opposite points on the sphere. A symmetric target has null points located along parallels of latitude equidistant from the linear polarization equator.

In addition to the null polarizations, each target has associated with it a maximal copolarization. Together, this set is referred to as the "optimum" polarizations [33]. The optimum polarizations fall on a great circle on the polarization sphere in a symmetrical arrangement referred to as the "Huynen fork." The Huynen fork is one of the most popular "polarization invarients" which can be used in target classification and discrimination. Although the fork rotates as the pitch angle of the target is changed (along the radar line of

sight), its relative orientation remains constant (thus the description "invarient".) Since each specific target has a specific huynen fork (at a given value of roll and yaw) the target can be conceivably discriminated regardless of the value of pitch angle.

The use of a polarization invarient such as the Huynen fork as the feature for target discrimination has a great appeal. Since only one frequency is needed this technique is easily adaptable to existing single frequency radar systems. It is only necessary that the radar be modified to be polarization sensitive. Unfortunately, the optimal polarizations have been shown to be extremely dependent upon the yaw and roll angle of the target [33]. Since the optimal polarizations describe the eigenvectors of the scattering matrix, any other polarization discriminant will also be highly sensitive to roll and yaw. This dependence upon changing aspect makes polarization invarients very difficult to use as target discrimination features for moving targets [33].

3.3 Frequency Response Techniques

Quite a large number of target discrimination schemes have been developed based on the frequency response of the target (or, equivalently, the impulse response, which is the inverse Fourier transform of the frequency response.) Several of these will be considered in this section.

3.3.1 Multiple Frequency Measurements

The component of backscattered field in the direction of the incident electric field a large distance from a conducting target can be written as [34]

$$E^s = \frac{e^{j(\omega t - kr)}}{2\sqrt{\pi}r} G(j\omega) E^i \qquad (3.3.1.1)$$

where k is the wave number and $G(j\omega)$ is the target's backscatter frequency response at a given aspect. (The magnitude squared of G corresponds to the RCS of the target.) Knowledge of $G(j\omega)$ uniquely determines the target and thus can be used for identification or discrimination. However, it is impractical to reconstruct $G(j\omega)$ since an infinite number of frequency measurements would be required. Rather, it is more plausible to approximate $G(j\omega)$ by making only a few measurements at carefully chosen frequencies. If the target response at these frequencies is uniquely dependent upon the target geometry, then the amplitude of the backscattered wave at these frequencies can be used as the set of target features.

It is important to decide over which frequency range the target is best characterized. The higher frequencies correspond to the fine detail of the target, while the lower frequencies characterize the target's bulk shape. This can be shown by letting $s = j\omega$ and expanding G(s) at small values of s, giving

$$G(s) = a_0 + a_1 s + a_2 s^2 + \ldots \qquad (3.3.1.2)$$

Here a_0 and a_1 are zero, while a_2, the Rayleigh coefficient, is approximately proportional to the volume of the object [35]. With this information, a discrimination scheme has been proposed utilizing the response of the target at discrete values of frequency in a range of wavelengths starting at about one half the maximum dimension of the target and increasing to about ten times this length [30]. This frequency range extends from the "Rayleigh" region up to the low resonance region and contains the essential information regarding overall target shape and composition.

By using the scattered field amplitudes measured at twelve equally spaced frequencies (in the range discussed above) as target features, it has been possible to classify a number of simple target shapes. Discrimination between the classes is accomplished using a linear discrimination procedure on the target feature vectors, at a given value of target aspect [35]. For more complex targets such as aircraft scale models, a more sophisticated "nearest neighbor" approach is required. With this technique it has been possible to discriminate between eight quite similar aircraft scale models, in the presence of moderate noise levels. Furthermore, it is possible to decrease the number of frequency measurements required to as few as two by employing the phase and the polarization of the scattered wave as additional target features [30].

The practical limitations of this method are threefold. The first is the expensive requirement for a multi-frequency radar. Because of this, great emphasis has been placed on minimizing the number of frequencies required for discrimination. Secondly, for true

aircraft targets, the radar would be required to operate at relatively low frequencies, down into the VHF band. Most importantly, though, the strong dependence of the frequency response $G(j\omega)$ on target aspect makes this technique quite cumbersome in actual situations. This problem can only be worsened if polarization is incorporated into the scheme, as shown by the last section. It has been suggested that the target attitude can be estimated to within 10° by using conventional radar [35]. However, it is questionable whether this represents sufficient accuracy in the case of complex target shapes.

3.3.2 Ramp Response Imaging

A very interesting radar target signature which uniquely describes the target is its response to an incident ramp waveform [3]. The frequency domain response to the time domain ramp signal can be written as

$$F(j\omega) = \left(\frac{1}{j\omega}\right)^2 G(j\omega) \qquad (3.3.2.1)$$

where $G(j\omega)$ is the response of the target at a frequency ω. By the properties of Fourier transforms, the time domain ramp response can also be written in terms of the second integral of the impulse response of the target.

As it is not possible to transmit a ramp or impulse waveform, it is necessary to approximate the ramp frequency response (3.3.2.1) of a target by using multiple frequency measurements. It has been found that measurements of the target response at ten discrete

frequencies in the upper Rayleigh to lower resonance range are adequate to approximate the ramp response of the target [36].

With the approximation to the ramp response it is possible to construct an image of the target. This image reflects the gross shape of the structure, since only low frequency measurements are involved. Target discrimination is then easily accomplished by a comparison to the shapes of known targets. However, the construction of an image is quite time consuming and requires the measurement of the (approximate) ramp response from three orthogonal look angles. Thus, it becomes more expedient to discriminate targets by a comparison of the ramp responses themselves. (That is, designating the ramp response as the target feature as opposed to the target image.) Such a comparison reverts to a technique nearly identical to that of the last section, except that the lower frequencies of the ramp response are accentuated by a $1/\omega^2$ factor. Therefore, comparison of ramp responses has all of the limitations of the previous method, especially the sensitivity to aspect angle.

3.3.3 Natural Resonance Based Ramp Response

The pressing problem of target aspect dependence can be overcome by incorporating target natural resonances into the ramp response comparison. The frequencies of the natural target oscillations are independent of the aspect of the target (only the amplitudes and phases of the natural modes are aspect dependent), as discussed in chapter 2.

It has been shown that the transient response of any linear system must obey the difference equation

$$f(t) = \sum_{n=1}^{N} (-1)^n A_{N,n} f(t-n\Delta t) \qquad (3.3.3.1)$$

where f(t) is the transient response and the difference coefficients $A_{N,n}$ are defined via an appropriate relationship involving the N natural frequencies of the system [37]. This allows the reconstruction of f(t) from N sampled values of the response.

Radar target discrimination is based upon the following scheme. The ramp response of an unknown target is approximated using M discrete frequency measurements via the Fourier synthesis

$$F_R(t) = K \sum_{m=1}^{M} \frac{G(m\omega_o)}{m^2} \cos\left(m\omega_o t + \phi(m\omega_o)\right) \qquad (3.3.3.2)$$

where K is a constant. Next, the natural frequencies of known targets are used to reconstruct the measured ramp response via equation (3.3.3.1). Here f(t) is taken to be the measured ramp response given by (3.3.3.2). Finally, a coefficient ρ' is defined as unity minus the normalized difference between the measured and reconstructed ramp responses. Equation (3.3.3.1) can be viewed as a predictor and the coefficient ρ' as a correlator. Ideally, when the natural frequencies of the measured target are used to reconstruct the measured ramp response, ρ' will be unity and the unknown target is identified. When the natural frequencies used to reconstruct the ramp response correspond to a target different than that measured, ρ' will be less than unity and the target is discriminated. In practice, the ramp response cannot be exactly reproduced, both because the ramp response is only approximate

and because only a finite number of natural frequencies can be used in the reconstruction. However, very good reconstruction has been accomplished using the dominant natural resonances of the targets (corresponding to the lower portion of the resonance range) [36].

Discrimination using this technique has been demonstrated for simple wire aircraft models. The dominant natural frequencies of the wire models are calculated theoretically using SEM analysis. A reaction integral equation is solved in the radiation mode for the case of zero driving voltage. This is equivalent to solving equation (2.3.3), and a search procedure is needed to locate the zeroes in the complex plane. With these natural frequencies, discrimination between straight and swept wing models has been accomplished for various target aspects and incident field polarizations, using ten frequency measurements.

Improved discrimination has been obtained by employing the following procedure. Instead of obtaining the natural resonances of the target model from the solution to a homogeneous integral equation, a less rigorous process is used. First, the frequency response of the aircraft model (at a specific aspect) is obtained numerically at the same ten frequencies as used in the measurements by a low frequency grid wire analysis [38]. This response is then used to calculate the approximate ramp response of the target model via equation (3.3.3.2). Lastly, Prony's method is used to extract the dominant natural frequencies from this time domain ramp response. Prony's method is a numerical technique for approximating a waveform using damped sinusoidal functions. It is discussed in depth in section 6.2. Using this process it is found that only the dominant few natural frequencies

match explicitly with the true frequencies found from solving the integral equation [39]. This is due in part to the approximations used to calculate the ramp response (only a finite number of frequencies used.) However, the discrimination does improve, because the Prony's method resonances provide a better fit to the approximate (measured) ramp response than do the true frequencies. It is difficult, though, to justify the use of resonances which do not in the least resemble those of the actual target.

This improved Prony's method ramp waveform discrimination has been successfully demonstrated for three quite complex aircraft models [39]. And although this technique has conquered the problem of target aspect sensitivity, it does have a few drawbacks. The predictor-correlator method is a fairly complicated procedure, and is sensitive to the choice of Δt in equation (3.3.3.1). Many values might need to be tried to provide adequate discrimination. Also, a multi-frequency radar system is still needed to measure the ramp response. Each of these problems is addressed by the method of the next section.

3.3.4 Natural Frequency Comparison

Perhaps the most straight forward way to utilize natural target resonances in a discrimination scheme is to use a direct comparison of the frequencies. The late-time time domain scattered field response of an unknown target can be analyzed in terms of its natural resonance modes and the natural frequencies determined. These can then be compared directly to a library of frequencies from known targets, and the target identified or discriminated. The benefits of this

technique are substantial. Besides being aspect independent, the technique does not require a low-frequency or multi-frequency radar. It is only necessary that a waveform be transmitted which has energy at the natural frequencies which uniquely determine the targets to be discriminated. Although a wideband pulse would be ideal, it may be possible to choose these frequency features to lie in a fairly narrow band at reasonably high frequency (describing some unique fine structure on the target.) Then, bandpass interrogation pulses can be used as the excitation waveform, which is compatible with existing radars [40]. Lastly, once the natural resonance frequencies of the unknown target have been chosen, the comparison is a simple problem in feature recognition. This is an area which is well developed, and has many rapid schemes for implementation.

In this scheme the problem of feature extraction reduces to extracting the natural resonance frequencies from the late-time portion of a target response. The most popular routine involves the use of Prony's method. It has been shown that Prony's method is capable of accurately identifying the natural frequencies in the responses of simple structures driven by transient sources [41]. A radar target discrimination concept based upon Prony's method has been investigated in depth both numerically [42] and experimentally [43].

Numerical simulation has resulted in the successful discrimination of differing natural frequency sets in the presence of noise levels as high as 0 dB signal to noise. The techniques used for feature recognition involved correlation based upon linear prediction, pole residues, pole values (i. e. natural frequency values), and

response waveforms. It is important to note that only linear prediction and pole values are independent of target aspect. The linear prediction scheme is identical to that outlined in the section on ramp responses, except that the measured time domain waveform is used instead of the approximate ramp response. For the two aspect independent techniques, a signal to noise level as low as 10 dB has still led to accurate discrimination.

Experimental results have not been quite as successful. A late-time signal to noise level of 15 to 20 dB is required for the accurate extraction of natural frequencies from a measured target response [44]. This sensitivity of Prony's method to the presence of noise is only one of the problems which restricts its use for discrimination purposes. Other difficulties have been detailed [45], [46]. They include error due to underestimating the number of modes in the response, aliasing, and under-use of sampled points (requiring "windowing" approaches.)

3.3.5 The K-pulse

The various problems associated with Prony's method have reduced the usefulness of a natural frequency comparison scheme. What is needed is a technique which includes all the benefits of frequency comparison (aspect independence, simplicity of implementation) but does not display Prony's method's sensitivity to noise. Such a method will be introduced in the next chapter (the E-pulse technique), and it has its roots in the so-called "K-pulse" concept introduced by Kennaugh [47].

A K-pulse is defined as a minimal duration, time limited waveform, which upon interaction with a radar target produces a time limited response. The response may be aspect dependent, but it is to be time limited for as large a range of aspect angles as possible. Kennaugh was able to construct approximate K-pulses (also called kill-pulses) for simple targets based upon geometric considerations. He used simple wave reflection arguments to approximate a K-pulse for a thin wire target, and the geometric theory of diffraction to approximate the K-pulse of a sphere. By employing a polynomial approximation to the Laplace transform of the K-pulse, he was also able to estimate the natural resonance frequencies of these structures by locating the zeroes of the polynomials.

The K-pulse technique can be implemented in target discrimination based on its unique correspondence to a particular target geometry. Its intention, though, is to approximate the resonances of a target using geometrical considerations. A more appropriate discrimination scheme would use the actual target resonance frequencies (determined from electromagnetic modeling, or scale model measurements) in the construction of the K-pulse, rather than vice-versa. It would be an aspect independent technique, and relatively insensitive to noise. Such a scheme, called the "E-pulse" technique, is the subject of the next chapter.

CHAPTER 4

THE EXTINCTION PULSE

4.1 Introduction

The natural resonance based target discrimination techniques of the previous chapter involved illuminating an unknown radar target with an arbitrary time varying waveform and analyzing the scattered electromagnetic field. No special care was given to the shape of the incident field waveform, other than demanding that it contain adequate frequency content to excite enough natural frequencies of the target to allow discrimination. In contrast, the K-pulse method investigated the possibility of constructing a special time-limited waveform which would result in a time-limited scattered field. This chapter will introduce a method to enhance radar target discrimination by combining the K-pulse concept with the aspect independence of natural frequencies.

An extinction-pulse (E-pulse) waveform is defined as a finite duration (i. e. time-limited) waveform which upon excitation of a particular radar target extinguishes a pre-specified portion of the target's natural mode spectrum. Since the target scattered field response is merely the convolution of the incident field waveform and the target scattered field impulse response, it is easy to show that the E-pulse need not actually be transmitted to affect discrimination.

Indeed, two views of the E-pulse will be considered. The first describes the effects of directly transmitting the E-pulse and uses a frequency domain approach. The second considers the more tractable scheme of convolving the E-pulse with the measured scattered field waveform and uses a time domain approach. Each approach will be shown to give equivalent results.

Preliminary treatment of the E-pulse technique has been carried out in [17] and [19]-[21].

4.2 Transmit Domain Discrimination

The motivation for shaping the incident field waveform can be found by examining the time domain scattered field representation (2.4.3). Each of the complex exponential terms in the scattered field natural mode series is multiplied by $E(s_n)$, where $E(s)$ is the Laplace transform of the incident field waveform $e(t)$, and s_n is the frequency of the n'th natural resonance mode of the scatterer. If N natural modes are excited by the finite frequency content of $e(t)$, then requiring

$$E(s_n) = 0 \tag{4.2.1}$$

$$E(s_n^*) = 0 \tag{4.2.2}$$

for all $1 \leq n \leq N$ (assuming that the natural frequencies occur in complex conjugate pairs) results in a null scattered field waveform in the late-time.

It is easy to envision target discrimination using E-pulse

waveforms. Since an E-pulse is based entirely on the natural frequencies of one particular target, and the natural frequencies of a scatterer are unique, each E-pulse will correspond uniquely to one target. Thus, if E-pulse (a) is designed to eliminate the natural frequencies of target (a), its interaction with a different target (b) will result in a scattered field that is non-zero in the late-time. In fact, equation (2.4.3) shows that the field scattered by target (b) will contain all the natural frequencies of (b) not common to (a). This allows discrimination between the two targets without any analysis of the late-time scattered field more difficult than recognizing a zero response.

The E-pulse concept can be broadened to allow further discrimination techniques. If equations (4.2.1) and (4.2.2) are enforced for all $1 \leq n \leq N$, $n \neq m$, then all the natural modes of the scattered field response except the m'th will be cancelled. Thus, the late-time scattered field will vary in time as a single damped sinusoid. This type of E-pulse waveform is termed a "single-mode excitation signal", "m-th mode excitation waveform", or an "E-m-pulse", since it excites only the single m'th mode (or, alternatively, eliminates all but the m'th mode.) The general term "E=pulse" will be taken to include these single mode excitation waveforms as well. Discrimination in this case requires differentiating between a single mode response (from the expected target) and a combination of many modes (from a different target.) This is a relatively simple task, since it is not necessary to decompose the waveforms into their natural mode constituents, as was required by the natural mode comparison techniques of chapter 3.

Perhaps the most important characteristic of the E-pulse is its

aspect independent nature. Although each term in the scattered field representation (2.4.3) depends upon the target aspect, the zero of E(s) demanded by (4.2.1) and (4.2.2) will nullify the term. This allows the use of one particular E-pulse regardless of the target's position with respect to the radar antenna.

4.3 Receive Domain Discrimination

The usefulness of transmit domain discrimination is limited by practical considerations. It is very difficult to transmit complicated time-varying waveforms, especially if they have a DC component. Thus, an alternative to transmitting the E-pulse waveforms must be considered.

An easily implemented technique involves utilizing the measured scattered field waveform. As in the natural resonance based techniques of chapter 3, any convenient waveform with adequate frequency content is used to illuminate the unknown target. But rather than analyzing the scattered field in terms of its natural mode composition, it is convolved with the E-pulse defined by equations (4.2.1) and (4.2.2). The results are analogous to actually transmitting the E-pulse and having it interact with the target. This is easily seen by calculating the convolution. Consider the Laplace transform of the time domain representation of the scattered field (2.4.4) which is given by

$$E^s(\vec{r},s) = \sum_{n=1}^{N} \frac{A'_n(\vec{r})}{2} \left\{ \frac{e^{j\phi'_n(\vec{r})}}{s-s_n} + \frac{e^{-j\phi'_n(\vec{r})}}{s-s_n^*} \right\} \qquad (4.3.1)$$

Convolution in the time domain is equivalent to multiplication in the frequency domain. Thus

$$L\{e(t)*E^s(\vec{r}_o,t)\} =$$

$$= \sum_{n=1}^{N} \frac{A'_n(\vec{r}_o)}{2} \left\{ \frac{e^{j\phi'_n(\vec{r}_o)}}{s-s_n} + \frac{e^{-j\phi'_n(\vec{r}_o)}}{s-s_n^*} \right\} E(s) \qquad (4.3.2)$$

Implementing the inversion integral (2.2.3) and invoking Cauchy's residue theorem results in the time domain convolved response

$$r(t) = e(t)*E^s(\vec{r}_o,t) = \qquad (4.3.3)$$

$$= \sum_{n=1}^{N} \frac{A'_n(\vec{r}_o)}{2} \left\{ E(s_n)e^{s_n t+j\phi'_n(\vec{r}_o)} + E(s_n^*)e^{s_n^* t-j\phi'_n(\vec{r}_o)} \right\}$$

But $E(s_n) = E(s_n^*) = 0$ by the definition of the E-pulse (4.2.1) and (4.2.2), so $r(t) = 0$ in the late-time. In other words, the E-pulse has extinguished the late-time measured scattered field.

It should be mentioned that receive domain discrimination is not identical to transmit domain discrimination. The response generated by convolving an E-pulse with an unexpected target is identical to (4.3.3). However, now the zeroes of E(s) do not correspond to the natural frequencies of the measured target. Using the fact that $E(s_n^*) = E^*(s_n)$ (as shown in the next section) equation (4.3.3) can be written as

$$r(t) = \sum_{n=1}^{N} A'_n(\vec{r}_o)|E(s_n)|e^{\sigma_n t}\cos(\omega_n t+\phi'_n(\vec{r}_o)+\beta_n) \qquad (4.3.4)$$

where

$$E_{rn} = \mathrm{Re}\{E(s_n)\} \qquad E_{in} = \mathrm{Im}\{E(s_n)\}$$

$$|E(s_n)| = \sqrt{E_{rn}^2 + E_{in}^2} \qquad \beta_n = \tan^{-1}\frac{E_{in}}{E_{rn}} \tag{4.3.5}$$

Thus, the time domain response r(t) is again a sum of natural modes, as is the measured scattered field in the transmit domain treatment. The difference is that the amplitude and phases will not necessarily be the same as those which would be measured if the E-pulse were transmitted directly. This may seem a trivial point, but it indicates that discrimination sensitivity to certain modes may be altered.

A second important point is that use of the E-pulse in the receive domain also gives aspect independent results. That is, the condition that r(t) be zero in equation (4.3.3) did not depend on the aspect dependent modal amplitudes and phases. Thus, convolution of the E-pulse with the measured scattered field from the expected target results in zero late-time response regardless of the position of the target when the measurements were made.

Single mode excitation waveforms can also be used in the receive domain. Using equation (4.3.4) and employing (4.2.1) and (4.2.2) for $1 \leq n \leq N$, $n \neq m$, results in the convolved response

$$r(t) = A_m'(\vec{r}_o)\,|E(s_m)|\,e^{\sigma_m t}\cos(\omega_m t + \phi_m'(\vec{r}_o) + \beta_m) \tag{4.3.6}$$

As expected, the result of convolving a single mode excitation waveform with the measured response of the expected target is a single

natural mode. Again, the amplitude and phase of this mode may not be the same as the amplitude and phase of the scattered field response if the waveform had actually been transmitted.

4.4 E-Pulse Synthesis

It is now necessary to find some convenient way to implement the defining E-pulse equations. For transmit domain discrimination equations (4.2.1) and (4.2.2) were taken as defining an E-pulse. For receive domain discrimination it is more appropriate to define an E-pulse via

$$r(t) = 0 \qquad t > T_E + T_e \tag{4.4.1}$$

where r(t) is given by

$$r(t) = e(t) * E^s(\vec{r}_o, t) \tag{4.4.2}$$

as in equation (4.3.3). Here T_E is the length of the early time period of the measured response determined by

$$T_E = T_w + 2T \tag{4.4.3}$$

where T is the maximal one way transit time of the target and T_w is the duration of the incident waveform. To this must be added T_e, the finite duration of the E-pulse waveform, to satisfy the requirements of the convolution. It is obvious that T_e must always be taken to be

finite, or else there would be no late-time period. It is also seen that receive domain discrimination has less late-time with which to work, since the duration of the excitation waveform must be added to early-time. This could be important if the target has rapidly decaying natural modes.

Both receive domain and transmit domain discrimination perspectives are now considered, and are shown to be equivalent.

4.4.1 Transmit Domain Perspective

This analysis may actually be termed a frequency domain analysis since it is the frequency domain representation of the excitation waveform which is utilized. The Laplace transform of the excitation waveform e(t) can be calculated using equation (2.2.2) as

$$E(s) = L\{e(t)\} = \int_0^{T_e} e(t)e^{-st}dt \qquad (4.4.1.1)$$

where T_e is the finite duration of the waveform. The transmit domain definition of the E-pulse (4.2.1) and (4.2.2) requires

$$E(s_n) = \int_0^{T_e} e(t)e^{-s_n t}dt = 0 \qquad 1 \leq n \leq N \qquad (4.4.1.2)$$

$$E(s_n^*) = \int_0^{T_e} e(t)e^{-s_n^* t}dt = 0 \qquad 1 \leq n \leq N \qquad (4.4.1.3)$$

Writing $s_n = \sigma_n + j\omega_n$ and expanding the exponential yields

$$E(s_n) = \int_o^{T_e} e(t)e^{-\sigma_n t}\left(\cos\omega_n t - j\sin\omega_n t\right)dt = 0 \quad 1\leq n\leq N \qquad (4.4.1.4)$$

$$E(s_n^*) = \int_o^{T_e} e(t)e^{-\sigma_n t}\left(\cos\omega_n t + j\sin\omega_n t\right)dt = 0 \quad 1\leq n\leq N \qquad (4.4.1.5)$$

Note that this shows that $E(s_n^*) = E^*(s_n)$. Both (4.4.1.4) and (4.4.1.5) hold simultaneously only if

$$\int_o^{T_e} e(t)e^{-\sigma_n t}\cos\omega_n t\,dt = 0 \quad 1\leq n\leq N \qquad (4.4.1.6)$$

$$\int_o^{T_e} e(t)e^{-\sigma_n t}\sin\omega_n t\,dt = 0 \quad 1\leq n\leq N \qquad (4.4.1.7)$$

These two equations will be used to calculate e(t) upon an appropriate mathematical representation.

4.4.2 Receive Domain Perspective

Just as section 4.4.1 was actually a frequency domain analysis, this section can more acurately be termed a time domain analysis since all calculations avoid the Laplace transform of e(t). Invoking the receive domain definition of the E-pulse (4.4.1) along with equation (4.4.2) and the scattered field representation (2.4.4) yields

$$r(t) = e(t) * \sum_{n=1}^{N} A_n'(\vec{r}_o)e^{\sigma_n t}\cos(\omega_n t + \phi_n'(\vec{r}_o)) = 0 \qquad (4.4.2.1)$$

Writing the convolution in integral form gives

$$r(t) = \int_0^{T_e} e(t') \sum_{n=1}^{N} A'_n(\vec{r}_o) e^{\sigma_n(t-t')} \times$$

$$\times \cos(\omega_n(t-t') + \phi'_n(\vec{r}_o))dt' = 0 \qquad (4.4.2.2)$$

which can be written more simply as

$$r(t) = \sum_{n=1}^{N} A'_n(\vec{r}_o) e^{\sigma_n t} \times$$

$$\times \left[a_n \cos(\omega_n t + \phi'_n(\vec{r}_o)) + b_n \sin(\omega_n t + \phi'_n(\vec{r}_o))\right] = 0 \qquad (4.4.2.3)$$

where

$$a_n = \int_0^{T_e} e(t') e^{-\sigma_n t'} \cos\omega_n t' dt' \qquad (4.4.2.4)$$

$$b_n = \int_0^{T_e} e(t') e^{-\sigma_n t'} \sin\omega_n t' dt' \qquad (4.4.2.5)$$

Now, since $\sin(\omega_n t + \phi_n)$ and $\cos(\omega_n t + \phi_n)$ are linearly independent, equation (4.4.2.2) can hold only if $a_n = b_n = 0$ for all $1 \leq n \leq N$. This requires

$$\int_0^{T_e} e(t') e^{-\sigma_n t'} \cos\omega_n t' dt' = 0 \qquad 1 \leq n \leq N \qquad (4.4.2.6)$$

$$\int_0^{T_e} e(t') e^{-\sigma_n t'} \sin\omega_n t' dt' = 0 \qquad 1 \leq n \leq N \qquad (4.4.2.7)$$

which are identical to (4.4.1.6) and (4.4.1.7) from the transmit domain analysis.

4.4.3 E-pulse Representation

To implement the 2N equations (4.4.1.6) and (4.4.1.7) the E-pulse waveform must be represented mathematically. It is necessary to have at least 2N variable parameters in the representation in order to satisfy the equations. The representation need not be linear in the unknown parameters, although that is essentially the simplest case. For example, it is easy to envision an E-pulse composed of 2N finite duration sinusoids, each of equal amplitude and duration, but with frequencies chosen to solve the defining equations. This results in 2N nonlinear equations in the 2N unknown frequency parameters.

The majority of the E-pulses to be considered can be represented as

$$e(t) = \sum_{m=1}^{M} \alpha_m f_m(t) \qquad (4.4.3.1)$$

where $f_m(t)$ is the m'th basis function from an appropriately chosen set and α_m is the amplitude of the basis function. The basis functions need not be similar to each other, and they may overlap or be sub-sectional. Substituting (4.4.3.1) into the E-pulse equations (4.4.1.6) and (4.4.1.7) yields

$$\sum_{m=1}^{M} \alpha_m \int_0^{T_e} f_m(t') e^{-\sigma_n t'} \cos\omega_n t' dt' = 0 \qquad 1 \leq n \leq N \qquad (4.4.3.2)$$

$$\sum_{m=1}^{M} \alpha_m \int_0^{T_e} f_m(t')e^{-\sigma_n t'} \sin\omega_n t' dt' \qquad 1 \leq n \leq N \qquad (4.4.3.3)$$

When some of the amplitude parameters represent all the unknown variables, these equations become simultaneous linear equations and can be written in matrix form as

$$\left[\begin{array}{c} M^c_{m,n} \\ \hline M^s_{m,n} \end{array}\right] \left[\begin{array}{c} \alpha_1 \\ \vdots \\ \alpha_M \end{array}\right] = \left[\begin{array}{c} 0 \\ \vdots \\ 0 \end{array}\right] \qquad (4.4.3.4)$$

where

$$M^c_{m,n} = \int_0^{T_e} f_m(t')e^{-\sigma_n t'} \cos\omega_n t' dt' \qquad (4.4.3.5)$$

$$M^s_{m,n} = \int_0^{T_e} f_m(t')e^{-\sigma_n t'} \sin\omega_n t' dt' \qquad (4.4.3.6)$$

The entries of the "M" matrix (4.4.3.4) are generally quite difficult to compute using (4.4.3.5) and (4.4.3.6). The amount of effort needed to calculate these entries in closed form (that is, using no numerical integration) can be reduced by using the transmit domain analysis of section 4.4.1. Comparison of equations (4.4.3.5) and (4.4.3.6) with (4.4.1.4) reveals that the matrix entries can also be written in terms of the Laplace transform of $f_m(t)$ as

$$M^c_{m,n} = \mathrm{Re}\{F_m(s_n)\} \qquad (4.4.3.7)$$

$$M^{s}_{m,n} = -\mathrm{Im}\{F_m(s_n)\} \qquad (4.4.3.8)$$

where $F_m(s)$ is the transform of $f_m(t)$. With few exceptions, the transform of $f_m(t)$ will be a much simpler function (albeit, complex) than those resulting from the computation of (4.4.3.5) and (4.4.3.6). The real and imaginary parts of $F_m(s_n)$ are easily separated after the transform has been numerically evaluated. The only drawback to this method is the need for complex arithmetic.

4.4.4 Forced and Natural E-pulses

When the amplitude coefficients in equation (4.4.3.1) represent all the unknown parameters, a special E-pulse can be constructed which has a helpful physical interpretation. The E-pulse waveform is augmented by a sub-sectional forcing function $e^{f}(t)$ extending from t=0 to $t=T_f$ which first interacts with the target. The remainder of the E-pulse, which extends from $t=T_f$ to $t=T_e$ as shown in Figure 4.4.4.1, is called the "extinction" component $e^{e}(t)$ and is viewed as extinguishing the response caused by $e^{f}(t)$.

Choosing a total of M=2N basis functions, equation (4.4.3.4) can then be written as

$$\begin{Bmatrix} M^{c}_{m,n} \\ \hline\hline M^{s}_{m,n} \end{Bmatrix} \begin{Bmatrix} \alpha_1 \\ \vdots \\ \alpha_{2N} \end{Bmatrix} = - \begin{Bmatrix} F^{c}_{n} \\ \hline\hline F^{s}_{n} \end{Bmatrix} \qquad (4.4.4.1)$$

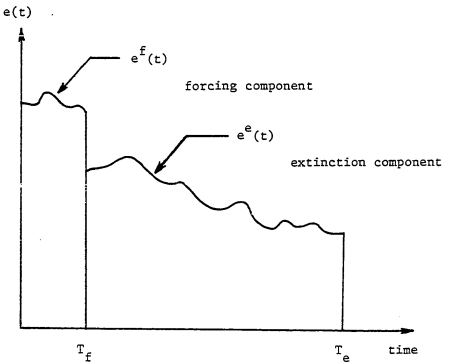

Figure 4.4.4.1. Decomposition of E-pulse waveform into forcing and extinction components.

where

$$F_n^c = \int_0^{T_f} e^f(t')e^{-\sigma_n t'}\cos\omega_n t'dt' \qquad (4.4.4.2)$$

$$F_n^s = \int_0^{T_f} e^f(t')e^{-\sigma_n t'}\sin\omega_n t'dt' \qquad (4.4.4.3)$$

This is a set of 2N linear equations in the 2N unknown amplitude parameters and can be solved easily by matrix methods.

It is now convenient to identify two fundamental types of E-pulses. When $T_f>0$ the forcing vector on the right hand side of equation (4.4.4.1) is non-zero and a solution for $e^e(t)$ exists for nearly any choice of T_e (excluding the case of a singular matrix.) This type of E-pulse has a non-zero forcing component and is called a "forced" E-pulse. In contrast, when $T_f=0$ the forcing vector vanishes and solutions for $e^e(t)$ exist only when the determinant of the coefficient matrix is zero. These solutions correspond to discrete eigenvalues for the E-pulse duration T_e and are found by solving

$$\det\left(\overline{\overline{M}}\right) = 0 \qquad (4.4.4.4)$$

where $\overline{\overline{M}}$ is the matrix in (4.4.4.1). Since there is no forcing component, this type of E-pulse is viewed as extinguishing itself and is termed a "natural" E-pulse.

The concept of the forced E-pulse can be broadened to involve a forcing function which is not a sub-sectional basis function. In particular, it can be of the type used to construct $e^e(t)$. In this

case the forcing vector components become merely

$$F_n^c = \alpha_{2N+1} \int_o^{T_e} f_{2N+1}(t') e^{-\sigma_n t'} \cos\omega_n t' dt' \qquad (4.4.4.5)$$

$$F_n^s = \alpha_{2N+1} \int_o^{T_e} f_{2N+1}(t') e^{-\sigma_n t'} \sin\omega_n t' dt' \qquad (4.4.4.6)$$

and α_{2N+1} is chosen to give the desired normalization of the E-pulse amplitude.

Note that a natural E-pulse requires only 2N basis functions, while a forced E-pulse requires 2N+1 (including the forcing function.)

4.4.5 DC E-pulse

The electric field scattered by a conducting target has been shown to take the form of equation (2.4.4). When this field is measured, however, it will show contamination in the form of various types of noise. Certain types of measurement systems (such as those utilizing digital sampling) will also introduce an artificial constant DC level. In this case, the measured scattered field will take the form

$$E^s(\vec{r}_o,t) = K + \sum_{n=1}^{N} A'_n(\vec{r}_o) e^{\sigma_n t} \cos(\omega_n t + \phi'_n(\vec{r}_o)) \qquad (4.4.5.1)$$

where K represents the constant DC level.

If an attempt is made to apply the E-pulse technique in the receive domain, the attempt will fail. The convolution will result in an added DC component which is not interpreted as zero. It thus becomes important to shape the extinction pulse so as to eliminate

the DC level in the measured response, as well as the natural modes.

Substituting (4.4.5.1) into the receive domain definition of the E-pulse (4.4.1) gives

$$r(t) = K' + \sum_{n=1}^{N} A'_n(\vec{r}_o)e^{\sigma_n t} \times$$

$$\times \left\{a_n \cos(\omega_n t+\phi'_n(\vec{r}_o)) + b_n \sin(\omega_n t+\phi'_n(\vec{r}_o))\right\} = 0 \quad (4.4.5.2)$$

where a_n and b_n are given by (4.4.2.4) and (4.4.2.5) and

$$K' = \int_o^{T_e} e(t')dt' \quad (4.4.5.3)$$

For (4.4.5.2) to hold requires

$$a_n = b_n = 0 \qquad 1 \leq n \leq N \quad (4.4.5.4)$$

and

$$K' = 0 \quad (4.4.5.5)$$

The first two requirements are exactly as previously determined for a non-DC E-pulse (4.4.2.6) and (4.4.2.7). The third requirement is equivalent to demanding that the area under the E-pulse be zero.

DC E-pulses can be constructed as forced or natural, exactly as in section 4.4.4. However, the added requirement from equation (4.4.5.5) necessitates the use of an additional basis function in the E-pulse

expansion (4.4.3.1). Thus, a forced DC E-pulse will consist of 2N+2 basis functions and a natural DC E-pulse will consist of 2N+1 basis functions. The E-pulse waveform itself is found by solving the matrix problem given by (4.4.4.1), with one additional row to implement (4.4.5.5).

Note that the requirement given by (4.4.5.5) can be interpreted in the frequency domain as requiring

$$E(s=0) = 0 \qquad (4.4.5.6)$$

This is easily seen by substituting s=0 into equation (4.4.1.1). The result is identical to (4.4.5.3). As with the other entries in the "M" matrix, calculating the spectra of the basis functions and using equation (4.4.5.6) is usually much simpler than calculating (4.4.5.3).

4.4.6 Convolutional E-pulse

A quite interesting and useful property of the E-pulse is that the convolution of an E-pulse synthesized to eliminate one group of natural modes with an E-pulse designed to eliminate a different group results in a single E-pulse which will eliminate both groups of modes. This is verified in the receive domain through equation (4.3.3) and the fact that convolution in the time domain is equivalent to multiplication in the frequency domain. If E(s) is taken as the product of several spectra, each with zeroes at various natural frequencies, then E(s) will also have zeroes at those frequencies. Thus, r(t) will have no natural mode content corresponding to those

frequencies. Identical reasoning applies to the transmit domain through equation (2.4.3).

Since a one mode E-pulse takes the minimum amount of effort to calculate, this method presents an alternative to solving large matrix problems of the form of (4.4.4.1). If N one mode E-pulses can be synthesized each to eliminate a different mode, then an N mode E-pulse is easily constructed by taking their convolution. This is especially simple when delta functions of equal spacing are used as the basis functions when calculating the one mode E-pulses [22].

The duration of the convolution of two finite duration waveforms is merely the sum of the two durations. Thus, the duration of the convolutional E-pulse may be written as

$$T_e = \sum_{i=1}^{M} T_{ei} \qquad (4.4.6.1)$$

where T_{ei} is the duration of the i'th E-pulse of the M used in the convolution. Note that this may be made as short as desired if forced E-pulses are used.

4.4.7 Single Mode Excitation Waveforms

The single mode excitation waveform was originally defined in section 4.2 as just a special case of the E-pulse where one mode was ignored during the synthesis. Although this type of E-pulse will certainly excite a single mode upon interaction with a target, the concept of single mode excitation can be expanded to include more specific information about the mode (in essence, phase.)

From the receive domain perspective, the convolution of a single mode excitation waveform and the measured scattered field is given by equation (4.3.4). The original definition of the E-m-pulse requires $a_n = b_n = 0$ for $1 \leq n \leq N$, $n \neq m$, resulting in the convolved response

$$r(t) = A'_m(\vec{r}_o)\,|E(s_m)|\,e^{\sigma_m t}\cos(\omega_m t + \phi'_m(\vec{r}_o) + \theta_m) \qquad (4.4.7.1)$$

The transmit domain analysis gives equivalent results through equation (2.4.4) and the measured scattered field would be merely

$$E^s(\vec{r}_o,t) = A'_m(\vec{r}_o)e^{\sigma_m t}\cos(\omega_m t + \phi'_m(\vec{r}_o)) \qquad (4.4.7.2)$$

Synthesis of this single mode excitation waveform proceeds exactly as with the E-pulse, via equation (4.4.3.1). If the amplitude coefficients are taken to be the unknown parameters, then both forced and natural single mode excitation waveforms can be constructed. Note that the natural waveform requires only 2N-2 basis functions (since one less mode is being eliminated) and the forced waveform requires only 2N-1. A matrix equation directly analogous to (4.4.4.1) now describes the problem, with 2N-2 entries rather than 2N.

Close examination of equation (4.4.2.3) reveals that a more specific E-m-pulse can be synthesized by requiring

$$a_n = b_n = 0 \qquad 1 \leq n \leq N \qquad n \neq m$$

$$a_m = 0 \qquad (4.4.7.3)$$

Then the convolved response becomes

$$r_s(t) = A'_m(\vec{r}_o)e^{\sigma_m t}b_{ms}\sin(\omega_m t+\phi'_m(\vec{r}_o)) \qquad (4.4.7.4)$$

where

$$b_{ms} = \int_o^{T_e} e_s(t')e^{-\sigma_m t'}\sin\omega_m t'dt' \qquad (4.4.7.5)$$

On the other hand, requiring

$$a_n = b_n = 0 \qquad 1\leq n\leq N \qquad n\neq m$$
$$b_m = 0 \qquad (4.4.7.6)$$

results in the convolved response

$$r_c(t) = A'_m(\vec{r}_o)e^{\sigma_m t}a_{mc}\cos(\omega_m t+\phi'_m(\vec{r}_o)) \qquad (4.4.7.7)$$

where

$$a_{mc} = \int_o^{T_e} e_c(t')e^{-\sigma_m t'}\cos\omega_m t'dt' \qquad (4.4.7.8)$$

The first of these E-m-pulses, $e_s(t)$, is called a sine m'th mode excitation waveform since the convolved response varies as $\sin(\omega_m t+\phi'_m)$ and the second, $e_c(t)$, a cosine m'th mode excitation waveform since the convolved response varies as $\cos(\omega_m t+\phi'_m)$.

By adding an additional constraint, the two E-pulses have been constructed to be exactly ninety degrees out of phase. The original E-pulse described by (4.4.7.1) is a combination of the sine and cosine waveforms and is termed a sin/cos m'th mode excitation waveform.

The utility of the sine and cosine E-m-pulses is made apparent through the following normalization scheme. Let $\tilde{e}_c(t) = K_c e_c(t)$ such that

$$\tilde{a}_{mc} = \int_0^{T_e} \tilde{e}_c(t')e^{-\sigma_m t'}\cos\omega_m t'dt' = 1 \qquad (4.4.7.9)$$

Then

$$\int_0^{T_e} K_c e_c(t')e^{-\sigma_m t'}\cos\omega_m t'dt' = 1 \qquad (4.4.7.10)$$

or

$$K_c = \frac{1}{\int_0^{T_e} e_c(t')e^{-\sigma_m t'}\cos\omega_m t'dt'} \qquad (4.4.7.11)$$

Thus

$$\tilde{e}_c(t) = \frac{e_c(t)}{\int_0^{T_e} e_c(t')e^{-\sigma_m t'}\cos\omega_m t'dt'} \qquad (4.4.7.12)$$

Likewise, choose the normalized $\tilde{e}_s(t)$ such that

$$\tilde{b}_{ms} = \int_0^{T_e} \tilde{e}_s(t')e^{-\sigma_m t'}\sin\omega_m t'dt' = 1 \qquad (4.4.7.13)$$

which results in

$$\tilde{e}_s(t) = \frac{e_s(t)}{\int_0^{T_e} e_s(t')e^{-\sigma_m t'}\sin\omega_m t'\,dt'} \qquad (4.4.7.14)$$

Now, equations (4.4.7.4) and (4.4.7.7) can be written in normalized form as

$$\tilde{r}_s(t) = A'_m(\vec{r}_o)e^{\sigma_m t}\tilde{b}_{ms}\sin(\omega_m t+\phi'_m(\vec{r}_o)) \qquad (4.4.7.15)$$

$$\tilde{r}_c(t) = A'_m(\vec{r}_o)e^{\sigma_m t}\tilde{a}_{mc}\cos(\omega_m t+\phi'_m(\vec{r}_o)) \qquad (4.4.7.16)$$

But $\tilde{a}_{mc} = \tilde{b}_{ms} = 1$ by the normalization just imposed, so

$$\omega_m t + \phi'_m(\vec{r}_o) = \tan^{-1}\frac{\tilde{r}_s(t)}{\tilde{r}_c(t)} \qquad (4.4.7.17)$$

$$\log\left(A'_m(\vec{r}_o)\right) + \sigma_m t = \tfrac{1}{2}\log\left(\tilde{r}_c^2(t) + \tilde{r}_s^2(t)\right) \qquad (4.4.7.18)$$

These equations provide a good graphical means of portraying target discrimination based on the sine and cosine single mode excitation waveforms. If the convolution is performed with the measured response of the expected target a single mode will result and equations (4.4.7.17) and (4.4.7.18) will produce straight lines in the late-time with slopes given by σ_m and ω_m, respectively. However, if the convolution is performed with the measured response of an unexpected target, the result will take the form of (4.4.2.3) where $a_n \neq 0$ and $b_n \neq 0$. Applying equations (4.4.7.17) and (4.4.7.18) then yields something

quite different than straight lines, easily distinguishable from the results due to the expected target.

It is interesting to investigate the transmit domain interpretation of the sine and cosine E-m-pulses. What requirements must be made of E(s) in equation (2.4.3) such that equation (4.4.7.4) or (4.4.7.7) is satisfied? The answer is obtained by working backwards, and examining the Laplace transform of the desired result. Taking the transform of (4.4.7.4) yields

$$L\{r_s(t)\} = \frac{A'_m(\vec{r}_o)b_{ms}}{2j}\left\{\frac{e^{j\phi'_m(\vec{r}_o)}}{s-s_m} - \frac{e^{-j\phi'_m(\vec{r}_o)}}{s-s^*_m}\right\} \qquad (4.4.7.19)$$

This suggests that

$$E(s_m) = -E(s^*_m) \qquad (4.4.7.20)$$

is necessary to synthesize a sine single mode excitation waveform. This translates to

$$\int_o^{T_e} e(t)e^{-s_m t}dt = -\int_o^{T_e} e(t)e^{-s^*_m t}dt \qquad (4.4.7.21)$$

or, expanding the exponentials

$$\int_o^{T_e} e(t)e^{-\sigma_m t}\cos\omega_m t\,dt - j\int_o^{T_e} e(t)e^{-\sigma_m t}\sin\omega_m t\,dt =$$

$$= -\int_o^{T_e} e(t)e^{-\sigma_m t}\cos\omega_m t\,dt - j\int_o^{T_e} e(t)e^{-\sigma_m t}\sin\omega_m t\,dt \qquad (4.4.7.22)$$

and thus

$$\int_0^{T_e} e(t)e^{-\sigma_m t}\cos\omega_m t\,dt = 0 \qquad (4.4.7.23)$$

This, together with the requirement that $E(s_n) = E(s_n^*) = 0$ (equivalent to $a_n = b_n = 0$, as shown earlier) for $1 \leq n \leq N$, $n \neq m$, is identical to the results from the receive domain analysis. Similarly, the transform of (4.4.7.7) gives

$$L\{r_c(t)\} = \frac{A'_m(\vec{r}_o)a_{mc}}{2}\left[\frac{e^{j\phi'_m(\vec{r}_o)}}{s-s_m} + \frac{e^{-j\phi'_m(\vec{r}_o)}}{s-s_m^*}\right] \qquad (4.4.7.24)$$

suggesting

$$E(s_m) = E(s_m^*) \qquad (4.4.7.25)$$

is required to construct a cosine single mode excitation waveform. This means

$$\int_0^{T_e} e(t)e^{-s_m t}dt = \int_0^{T_e} e(t)e^{-s_m^* t}dt \qquad (4.4.7.26)$$

or

$$\int_0^{T_e} e(t)e^{-\sigma_m t}\cos\omega_m t\,dt - j\int_0^{T_e} e(t)e^{-\sigma_m t}\sin\omega_m t\,dt =$$

$$= \int_0^{T_e} e(t)e^{-\sigma_m t}\cos\omega_m t\,dt + j\int_0^{T_e} e(t)e^{-\sigma_m t}\sin\omega_m t\,dt \qquad (4.4.7.27)$$

so

$$\int_0^{T_e} e(t)e^{-\sigma_m t}\sin\omega_m t\,dt = 0 \qquad (4.4.7.28)$$

which is the same as required by the receive domain analysis (4.4.7.6). For calculation purposes (analogous to (4.4.3.7) and (4.4.3.8)) equation (4.4.7.23) for the sine single mode can be written in terms of the transform of e(t) as

$$\mathrm{Re}\{E(s_m)\} = 0 \qquad (4.4.7.29)$$

and equation (4.4.7.28) for the cosine single mode as

$$\mathrm{Im}\{E(s_m)\} = 0 \qquad (4.4.7.30)$$

As with the E-pulse, both the sine and cosine E-m-pulses can be constructed as forced or natural waveforms. Due to the added constraint given by (4.4.7.29) or (4.4.7.30), the number of basis functions required in (4.4.3.1) for the synthesis is 2N-1 for the natural E-m-pulse and 2N for the forced waveform. They can also be synthesized as DC sine or cosine E-m-pulses by adding the requirement given by equation (4.4.5.6) and using one more basis function. The solution for any of these waveforms results from the solution to a matrix problem analogous to (4.4.4.1). In addition, convolutional sine and cosine single mode signals are easily created by convolving E-pulses to (jointly) eliminate all the modes in a response except the one to be excited.

One last method of sine and cosine single mode excitation waveform synthesis is worth mentioning. In equation (4.4.2.3) requiring

$$a_n = b_n = 0 \qquad 1 \leq n \leq N \qquad n \neq m$$
$$b_m = 0 \qquad a_m = 1 \tag{4.4.7.31}$$

will result in a cosine E-m-pulse with any selectable duration (except for those resulting in a singular coefficient matrix.) This requires 2N basis functions and has a solution given by the solution to the matrix problem

$$\begin{bmatrix} \\ M^c_{m,n} \\ \\ \hline \\ M^s_{m,n} \\ \\ \end{bmatrix} \begin{bmatrix} \alpha_1 \\ \\ \\ \\ \vdots \\ \\ \\ \\ \alpha_{2N} \end{bmatrix} = \begin{bmatrix} 0 \\ \vdots \\ 1 \\ \vdots \\ 0 \\ - \\ 0 \\ \vdots \\ 0 \end{bmatrix} \tag{4.4.7.32}$$

where $M^s_{m,n}$ and $M^c_{m,n}$ are given by equations (4.4.3.5) and (4.4.3.6). Thus, this is equivalent to a forced E-m-pulse in the spirit of the preceding anlysis. Likewise, requiring

$$a_n = b_n = 0 \qquad 1 \leq n \leq N \qquad n \neq m$$

$$a_m = 0 \qquad b_m = 1 \tag{4.4.7.33}$$

will result in a sine E-m-pulse with a solution determined by solving

$$\begin{bmatrix} & \\ M^c_{m,n} & \\ \text{------} & \\ & \\ M^s_{m,n} & \\ & \end{bmatrix} \begin{bmatrix} \alpha_1 \\ \vdots \\ \\ \\ \alpha_{2N} \end{bmatrix} = \begin{bmatrix} 0 \\ \vdots \\ 0 \\ - \\ 0 \\ \vdots \\ 1 \\ \vdots \\ 0 \end{bmatrix} \tag{4.4.7.34}$$

This waveform is equivalent to a forced sine E-m-pulse.

The benefit of this method is that because of the requirements on a_m and b_m in (4.4.7.31) and (4.4.7.33) the normalization previously required by (4.4.7.9) and (4.4.7.13) is automatically included.

4.5 E-pulse Basis Sets

It is possible to choose any number of basis sets to represent the E-pulse in (4.4.3.1). However, a judicious choice must take the following into consideration: simplicity of representation, simplicity of calculation, noise averaging quality, possibility of continuous waveform representation, completeness, and frequency domain shaping. A basis set consisting of very complicated functions would need to

display some important alternate quality to outweigh the first two considerations.

Five different E-pulse basis sets will be considered in this section and throughout the remainder of this thesis. Each has varying combinations of the above qualities. The required E-pulse matrix entries (4.4.3.5) and (4.4.3.6) will be derived for each basis set, as well as the E-pulse spectrum (4.4.1.1). To provide comparitive examples each basis set will then be used to construct various types of forced and natural E-pulses and single mode excitation waveforms.

4.5.1 Polynomial E-pulse

A quite simple set of E-pulse basis functions is given by

$$f_m(t) = t^{m-1} \tag{4.5.1.1}$$

so that

$$e(t) = \sum_{m=1}^{M} \alpha_m t^{m-1} \tag{4.5.1.2}$$

Thus, an N mode E-pulse is merely a polynomial of degree M-1, where M depends upon the number of basis functions needed (e. g. M-1 = 2N-1 for a natural E-pulse.)

The motivation behind choosing this set of basis functions is twofold. First, many types of polynomials (such as Chebyshev) have special properties which might be useful in constructing an E-pulse. The expansion (4.5.1.2) has a much simpler form than these, but it does

display the general behavior of a polynomial E-pulse. Second, this E-pulse has the benefit of being smooth and continuous. When the convolution process in (4.4.2) is performed all of the sampled points of the measured response will be used, averaging and thus reducing the noise level.

The matrix elements required to construct the polynomial E-pulse are given by (4.4.3.5) and (4.4.3.6) Substituting (4.5.1.1) yields

$$M^{c}_{m,n} = \int_{o}^{T_e} t^{m-1} e^{-\sigma_n t} \cos\omega_n t\, dt \qquad (4.5.1.3)$$

$$M^{s}_{m,n} = \int_{o}^{T_e} t^{m-1} e^{-\sigma_n t} \sin\omega_n t\, dt \qquad (4.5.1.4)$$

The integrations can be performed by using successive integration by parts [23], resulting in

$$M^{c}_{m,n} = \frac{m!}{\rho_n}\left(T_e^{m} e^{-\sigma_n T_e} \sum_{r=0}^{m} \frac{(-1)^r}{(m-r)!\,(\rho_n T_e)^r} \cos(\omega_n T_e - (r+1)\xi_n) - \right.$$

$$\left. - \frac{(-1)^m}{\rho_n^m} \cos(-(m+1)\xi_n)\right) \qquad (4.5.1.5)$$

$$M^{s}_{m,n} = \frac{m!}{\rho_n}\left(T_e^{m} e^{-\sigma_n T_e} \sum_{r=0}^{m} \frac{(-1)^r}{(m-r)!\,(\rho_n T_e)^r} \sin(\omega_n T_e - (r+1)\xi_n) - \right.$$

$$\left. - \frac{(-1)^m}{\rho_n^m} \sin(-(m+1)\xi_n)\right) \qquad (4.5.1.6)$$

where

$$\rho_n = \sqrt{\sigma_n^2 + \omega_n^2} \qquad (4.5.1.7)$$

and

$$\xi_n = \tan^{-1}\left(-\frac{\omega_n}{\sigma_n}\right) \qquad (4.5.1.8)$$

The required matrix elements are obviously quite complicated. It is easy now to see that simplicity of representation does not necessarily go hand in hand with simplicity of calculation.

The spectrum of the polynomial E-pulse is found by employing equation (4.4.1.1)

$$E(s) = \int_0^{T_e} \sum_{m=1}^{M} \alpha_m t^{m-1} e^{-st} dt \qquad (4.5.1.9)$$

Integrating yields

$$E(s) = -\sum_{m=1}^{M} \alpha_m \frac{m!}{s}\left\{ T_e^m e^{-sT_e} \sum_{r=0}^{m} \frac{1}{(m-r)!(sT_e)^r} - \frac{1}{s^m} \right\} \qquad (4.5.1.10)$$

It is necessary to know this frequency domain representation for use in equations such as (4.3.4). It also provides an alternative method for calculating the E-pulse matrix entries. A great simplicity over the entries (4.5.1.5) and (4.5.1.6) is obviously gained by using the E-pulse spectrum and equations (4.4.3.7) and (4.4.3.8). The penalty is that these entries are complex and thus complex matrix calculations are required to determine the E-pulse.

4.5.2 Damped Sinusoid E-pulse

A particularly important set of E-pulse basis functions is given by

$$f_m(t) = e^{\tilde{\sigma}_m t}\cos(\tilde{\omega}_m t + \tilde{\phi}_m) \qquad (4.5.2.1)$$

so that

$$e(t) = \sum_{m=1}^{M} \alpha_m e^{\tilde{\sigma}_m t}\cos(\tilde{\omega}_m t + \tilde{\phi}_m) \qquad (4.5.2.2)$$

The choice of complex frequencies $\tilde{s}_n = \tilde{\sigma}_n + j\tilde{\omega}_n$ and phases $\tilde{\phi}_n$ used in the expansion determines the usefulness of this E-pulse. Discussion of appropriate choices is given along with a more in depth analysis of the resulting frequency domain shaping in section 5.5.

Like the polynomial E-pulse, this E-pulse representation is smooth and continuous. As such, it also has the benefits of noise reduction through the averaging process introduced by the convolution integral.

The E-pulse matrix entries are found via (4.4.3.5) and (4.4.3.6) to be

$$M^c_{m,n} = \int_0^T e^{\tilde{\sigma}_m t}\cos(\tilde{\omega}_m t+\tilde{\phi}_m)e^{-\sigma_n t}\cos\omega_n t\,dt \qquad (4.5.2.3)$$

$$M^s_{m,n} = \int_0^T e^{\tilde{\sigma}_m t}\cos(\tilde{\omega}_m t+\tilde{\phi}_m)e^{-\sigma_n t}\sin\omega_n t\,dt \qquad (4.5.2.4)$$

Integrating gives

$$M^{C}_{m,n} = \left[I_1(T_e)-I_1(0)+I_2(T_e)-I_2(0)\right]\cos\tilde{\phi}_m - \left[I_3(T_e)-I_3(0)+I_4(T_e)-I_4(0)\right]\sin\tilde{\phi}_m \qquad (4.5.2.5)$$

$$M^{S}_{m,n} = \left[-I_3(T_e)+I_3(0)+I_4(T_e)-I_4(0)\right]\cos\tilde{\phi}_m - \left[I_1(T_e)-I_1(0)-I_2(T_e)+I_2(0)\right]\sin\tilde{\phi}_m \qquad (4.5.2.6)$$

where

$$\begin{aligned} I_1(t) &= \frac{e^{At}}{2(A^2+B^2)}\left(B\sin Bt + A\cos Bt\right) \\ I_2(t) &= \frac{e^{At}}{2(A^2+C^2)}\left(C\sin Ct + A\cos Ct\right) \\ I_3(t) &= \frac{e^{At}}{2(A^2+B^2)}\left(A\sin Bt - B\cos Bt\right) \\ I_4(t) &= \frac{e^{At}}{2(A^2+B^2)}\left(A\sin Ct - C\cos Ct\right) \end{aligned} \qquad (4.5.2.7)$$

where $A = \tilde{\sigma}_m-\sigma_n$, $B = \tilde{\omega}_m-\omega_n$, and $C = \tilde{\omega}_m+\omega_n$.

The E-pulse spectrum is found to be

$$E(s) = \int_0^{T_e}\sum_{m=1}^{M}\tilde{\alpha}_m e^{\tilde{\sigma}_m t}\cos(\tilde{\omega}_m t+\tilde{\phi}_m)e^{-st}dt \qquad (4.5.2.8)$$

or

$$E(s) = \frac{T_e}{2} \sum_{m=1}^{M} \alpha_m \left[e^{j\tilde{\phi}_m} e^{-(s-\tilde{s}_m)\frac{T_e}{2}} \operatorname{sinhc}\left((s-\tilde{s}_m)\frac{T_e}{2}\right) + \right.$$

$$\left. + e^{-j\tilde{\phi}_m} e^{-(s-\tilde{s}_m^*)\frac{T_e}{2}} \operatorname{sinhc}\left((s-\tilde{s}_m^*)\frac{T_e}{2}\right) \right] \quad (4.5.2.9)$$

where

$$\operatorname{sinhc} z \equiv \frac{\sinh(z)}{z} = \frac{e^z - e^{-z}}{2z} \quad (4.5.2.10)$$

Using the spectrum provides quite a sizable gain in simplicity over using (4.5.2.5) and (4.5.2.6) to calculate the E-pulse matrix entries.

4.5.3 Fourier Cosine E-pulse

A Fourier cosine basis set can be constructed from the functions

$$f_m(t) = \cos\left[(m-1)\frac{\pi t}{T_e} \right] \quad (4.5.3.1)$$

such that

$$e(t) = \sum_{m=1}^{M} \alpha_m \cos\left[(m-1)\frac{\pi t}{T_e}\right] \quad (4.5.3.2)$$

These functions are linearly independent and, in fact, form a complete set. Any arbitrary continuous waveform of finite duration T_e can be represented as a linear combination of Fourier cosines. This has particularly intriguing implications for E-pulse synthesis. While it is true that the measured response of any target contains only a finite

number of natural modes, it is difficult to tell exactly which modes will be present. An ideal E-pulse waveform would eliminate the entire infinite set of natural frequencies of the target. That is, the E-pulse would converge to a distinct waveform as the number of modes to be eliminated was taken to infinity. Such an E-pulse could only be constructed as an expansion over a complete set of basis functions.

The thought that a finite duration E-pulse could be constructed to eliminate an infinite number of natural modes is not as astounding as it might first seem. It can be shown quite easily that a rectangular pulse waveform of properly chosen duration is an E-pulse for a lossless transmission line. Applications to the more complicated thin wire scatterer will be addressed in section 5.6.

A Fourier cosine basis set has other important qualities besides the potential of representing an ideal E-pulse. It is smooth and continuous, and thus has the benefit of noise averaging in the convolution process.

Since the Fourier cosine basis set is merely a special case of the damped sinusoidal basis set with the implicit choice of complex frequencies and phases given by

$$\begin{aligned} \tilde{\sigma}_m &= 0 \\ \tilde{\omega}_m &= (m-1)\frac{\pi}{T_e} \\ \tilde{\phi}_m &= 0 \end{aligned} \qquad (4.5.3.3)$$

the matrix elements required to construct an E-pulse will not be repeated. The spectrum of the E-pulse is quite interesting, though,

and is found to be

$$E(s) = \int_0^{T_e} \sum_{m=1}^{M} \alpha_m \cos\left[(m-1)\frac{\pi t}{T_e}\right] e^{-st} dt \qquad (4.5.3.4)$$

or

$$E(s) = \frac{T_e}{2} e^{-s\frac{T_e}{2}} \sum_{m=1}^{M} \alpha_m \left\{ j^{m-1} \operatorname{sinhc}\left(s - j\frac{(m-1)\pi}{T_e}\right) + \right.$$

$$\left. + (-j)^{m-1} \operatorname{sinhc}\left(s + j\frac{(m-1)\pi}{T_e}\right) \right\} \qquad (4.5.3.5)$$

Of course, this can also be viewed as a special case of the damped sinusoidal E-pulse spectrum.

An interesting property of the Fourier cosine basis set arises from the fact that, except for m=1, each of the basis functions has no DC component. It is therefore possible to construct a DC E-pulse by using one fewer basis function (i. e. by eliminating the m=1 term.)

4.5.4 Pulse Function E-pulse

The most useful basis set, due in most part to its great simplicity, is one composed of sub-sectional pulse functions as

$$f_m(t) = \begin{cases} g(t-(m-1)\Delta) & (m-1)\Delta \leq t \leq m\Delta \\ 0 & \text{elsewhere} \end{cases} \qquad (4.5.4.1)$$

where g(t) is some arbitrary function and Δ is the pulse width given by

$$\Delta = \frac{T_e}{M} \tag{4.5.4.2}$$

The basis function representation can be simplified somewhat by defining

$$P_m(t) = \begin{cases} 1 & (m-1)\Delta \leq t \leq m\Delta \\ 0 & \text{elsewhere} \end{cases} \tag{4.5.4.3}$$

Then

$$f_m(t) = P_m(t)g(t-(m-1)\Delta) \tag{4.5.4.4}$$

and

$$e(t) = \sum_{m=1}^{M} \alpha_m P_m(t)g(t-(m-1)\Delta) \tag{4.5.4.5}$$

A simple example of a pulse function E-pulse is shown in Figure 4.5.4.1(a). In particular, g(t) could be defined as nonzero over only a portion of the pulse width Δ. Such an E-pulse is shown in Figure 4.5.4.1(b), with g(t) being in this case a unit step function.

The value of this type of E-pulse in reducing the noise introduced during target response measurements depends much upon the shape of the individual pulses. Obviously the narrower pulses of Figure 4.5.4.1(b) will do a much poorer job of averaging the noise than the wider pulses of Figure 4.5.4.1(a). Although the pulse function E-pulse is never smooth, it is piecewise continuous, and the numerical

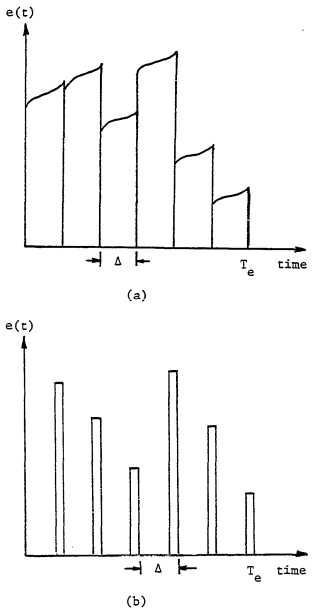

Figure 4.5.4.1. Typical pulse function E-pulse waveforms. (a) Using pulses of width Δ. (b) Using pulses of width less than Δ.

convolution can be performed without difficulty.

The E-pulse matrix elements are found using (4.4.3.5) and (4.4.3.6) to be

$$M^c_{m,n} = \int_0^{T_e} P_m(t)g(t-(m-1)\Delta)e^{-\sigma_n t}\cos\omega_n t\,dt \qquad (4.5.4.6)$$

$$M^s_{m,n} = \int_0^{T_e} P_m(t)g(t-(m-1)\Delta)e^{-\sigma_n t}\sin\omega_n t\,dt \qquad (4.5.4.7)$$

Using the definition of $P_m(t)$ gives

$$M^c_{m,n} = \int_{(m-1)\Delta}^{m\Delta} g(t-(m-1)\Delta)e^{-\sigma_n t}\cos\omega_n t\,dt \qquad (4.5.4.8)$$

$$M^s_{m,n} = \int_{(m-1)\Delta}^{m\Delta} g(t-(m-1)\Delta)e^{-\sigma_n t}\sin\omega_n t\,dt \qquad (4.5.4.9)$$

Now, using the substitution

$$u = t-(m-1)\Delta \qquad (4.5.4.10)$$

results finally in

$$M^c_{m,n} = e^{-\sigma_n(m-1)\Delta}\cos\omega_n(m-1)\Delta\int_0^{\Delta} g(u)e^{-\sigma_n u}\cos\omega_n u\,du - \\ - e^{-\sigma_n(m-1)\Delta}\sin\omega_n(m-1)\Delta\int_0^{\Delta} g(u)e^{-\sigma_n u}\sin\omega_n u\,du \qquad (4.5.4.11)$$

$$M^s_{m,n} = e^{-\sigma_n(m-1)\Delta}\cos\omega_n(m-1)\Delta\int_0^{\Delta} g(u)e^{-\sigma_n u}\sin\omega_n u\,du + \\ + e^{-\sigma_n(m-1)\Delta}\sin\omega_n(m-1)\Delta\int_0^{\Delta} g(u)e^{-\sigma_n u}\cos\omega_n u\,du \qquad (4.5.4.12)$$

The E-pulse spectrum is found using (4.4.1.1) to be

$$E(s) = \int_{o}^{T_e} \sum_{m=1}^{M} \alpha_m P_m(t) g(t-(m-1)\Delta) e^{-st} dt \qquad (4.5.4.13)$$

or

$$E(s) = \sum_{m=1}^{M} \alpha_m \int_{(m-1)\Delta}^{m\Delta} g(t-(m-1)\Delta) e^{-st} dt \qquad (4.5.4.14)$$

Using the substitution given in (4.5.4.10) results in

$$E(s) = \sum_{m=1}^{M} \alpha_m e^{-s(m-1)\Delta} \int_{o}^{\Delta} g(u) e^{-su} du \qquad (4.5.4.15)$$

which can also be written as

$$E(s) = F_1(s) e^{s\Delta} \sum_{m=1}^{M} \alpha_m e^{-sm\Delta} \qquad (4.5.4.16)$$

where $F_1(s)$ is the Laplace transform of the first pulse function

$$F_1(s) = L\{f_1(t)\} = \int_{o}^{\Delta} g(t) e^{-st} dt \qquad (4.5.4.17)$$

This is particularly simple in comparison to results for other basis sets such as (4.5.1.10) or (4.5.2.9).

The simplest and most useful choice for g(t) in equation (4.5.4.1) is

$$g(t) = 1 \qquad (4.5.4.18)$$

This merely represents a rectangular pulse basis set spanning T_e. The usefulness of the rectangular pulse is threefold: it is simple to use, it represents a uniform averaging of noise, and it forms a complete set of basis functions. The completeness condition puts it in the category with the Fourier cosine basis set as having the potential to represent an ideal E-pulse of infinite modal content.

The E-pulse matrix entries for the rectangular pulse function E-pulse are found by substituting (4.5.4.18) into (4.5.4.11) and (4.5.4.12) which results in

$$M^c_{m,n} = \frac{e^{-\sigma_n m\Delta}}{\sigma_n^2+\omega_n^2}\left(-\sigma_n \cos\omega_n m\Delta + \omega_n \sin\omega_n m\Delta\right) - \\ - \frac{e^{-\sigma_n (m-1)\Delta}}{\sigma_n^2+\omega_n^2}\left(-\sigma_n \cos\omega_n (m-1)\Delta + \omega_n \sin\omega_n (m-1)\Delta\right) \quad (4.5.4.19)$$

$$M^s_{m,n} = \frac{e^{-\sigma_n m\Delta}}{\sigma_n^2+\omega_n^2}\left(-\sigma_n \sin\omega_n m\Delta - \omega_n \cos\omega_n m\Delta\right) - \\ - \frac{e^{-\sigma_n (m-1)\Delta}}{\sigma_n^2+\omega_n^2}\left(-\sigma_n \sin\omega_n (m-1)\Delta - \omega_n \cos\omega_n (m-1)\Delta\right) \quad (4.5.4.20)$$

The spectrum is calculated in a similar manner. For a rectangular pulse equation (4.5.4.17) becomes

$$F_1(s) = \int_0^{\Delta} e^{-st}dt = \frac{\Delta}{2} e^{-s\frac{\Delta}{2}} \operatorname{sinhc}\left(s\frac{\Delta}{2}\right) \quad (4.5.4.21)$$

where sinhc(z) is defined in (4.5.2.10). Using (4.5.4.16) then results in

$$E(s) = \frac{\Delta}{2} e^{s\frac{\Delta}{2}} \operatorname{sinhc}\left(s\frac{\Delta}{2}\right) \sum_{m=1}^{M} \alpha_m e^{-sm\Delta} \qquad (4.5.4.22)$$

The pulse function basis set is so simple that it is possible to find an explicit formula for the expansion coefficients α_m. It is also possible to construct a different but very efficient algorithm for solving (4.4.4.1) for α_m without performing matrix inversion. These topics will be explored further in section 4.6.

4.5.5 Impulse Function E-pulse

Perhaps the simplest set of basis functions is defined by

$$f_m(t) = \delta(t-m\Delta) \qquad (4.5.5.1)$$

so that

$$e(t) = \sum_{m=1}^{M} \alpha_m \delta(t-m\Delta) \qquad (4.5.5.2)$$

Here $\delta(t)$ is the Dirac delta (impulse) function. This basis set can be viewed as a special case of the pulse function basis set with

$$g(t) = \delta(t-\Delta) \qquad (4.5.5.3)$$

This is the case shown in Figure 4.5.4.1(b) with the pulses taking on zero width but finite, nonzero area.

The delta function basis set is truly a poor choice if noise

level is an important consideration. Convolution will reduce to discrete, point by point integration which provides little averaging of random noise. Also, the delta function E-pulse is not continuous and does not have the potential of representing a unique E-pulse of infinite modal content (i. e. the impulse functions are not complete.)

The E-pulse matrix entries are found by substituting (4.5.5.3) into (4.5.4.11) and (4.5.4.12) and using the integral property of the delta function

$$\int_{o}^{x_1} \delta(x-x_o)f(x)dx = \begin{cases} 0 & 0 \leq x_1 < x_o \\ f(x_o) & x_1 \geq x_o \end{cases} \qquad (4.5.5.4)$$

which yields

$$M^c_{m,n} = e^{-\sigma_n(t-m\Delta)}\cos\omega_n(t-m\Delta) \qquad (4.5.5.5)$$

$$M^s_{m,n} = e^{-\sigma_n(t-m\Delta)}\sin\omega_n(t-m\Delta) \qquad (4.5.5.6)$$

The delta function E-pulse spectrum is particularly simple. Substituting (4.5.5.3) into (4.5.4.17) and using (4.5.5.4) results in

$$F_1(s) = e^{-s\Delta} \qquad (4.5.5.7)$$

and thus the spectrum is found from equation (4.5.4.16) to be

$$E(s) = \sum_{m=1}^{M} \alpha_m e^{-sm\Delta} \qquad (4.5.5.8)$$

The forced delta function E-pulse holds a very intriguing relationship with Prony's method. It is possible to obtain the expansion coefficients directly from a measured response by employing Prony's method as described in great detail in [22]. This procedure has the drawback, however, of being doubly sensitive to random noise. Not only is using Prony's method to obtain the E-pulse from a measured response highly sensitive to noise (as demonstrated in section 6.9), but using that E-pulse for discriminating a different target response provides little useful averaging of the noise in that response.

4.5.6 Examples of E-pulse Waveforms

It is possible to construct a multitude of natural/forced/DC E-pulse/m'th mode excitation waveforms based on a certain set of natural frequencies. This section will present a small number of these, characteristic of what might be constructed for a practical target. Thus, only E-pulses of short duration will be considered (in deference to maximum available late-time.)

The natural frequencies to be eliminated (or excited) are taken as the first ten (of the first layer) of the thin cylinder target as discussed in section 5.2. These are shown in Figure 5.2.1. E-pulses are constructed using various basis sets by solving equation (4.4.4.1).

The first group of E-pulses have been constructed using the pulse function basis set (and represented using rectangular pulses) and the Fourier cosine basis set. Figure 4.5.6.1 shows natural E-pulses of minimumduration plotted against time normalized by the length of the cylinder, L, and the speed of light, c. Construction of

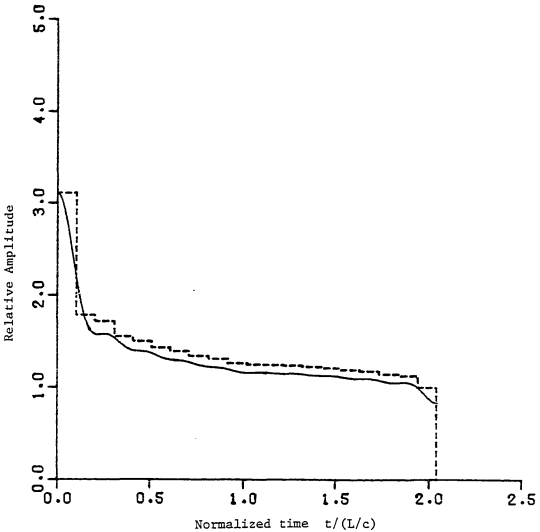

Figure 4.5.6.1. Natural E-pulses of minimum duration synthesized using pulse and Fourier cosine basis sets to eliminate first ten modes of thin cylinder.

these E-pulses requires a total of twenty basis functions. For the case of the pulse function E-pulse the minimum duration can be found explicitly from (4.6.1.24) and is calculated as

$$T_e = 20 \frac{\pi}{\omega_{10}} = 2.0407 \text{ L/c} \qquad (4.5.6.1)$$

For the Fourier cosine E-pulse the smallest duration is found via numerical computation to be $T_e = 2.0446$ L/c. Figure 4.5.6.2 shows natural E-pulses of the next largest duration. For the pulse function basis set this duration is

$$T_e = 20 \frac{\pi}{\omega_9} = 2.2708 \text{ L/c} \qquad (4.5.6.2)$$

whereas using the Fourier cosine basis set gives the next duration as $T_e = 2.2451$ L/c. Figure 4.5.6.3 displays the natural DC E-pulse of lowest duration. Now a total of 21 basis functions are required in the synthesis. The duration of the pulse function waveform is calculated as $T_e = 2.1427$ L/c while the duration of the Fourier cosine based waveform is found numerically to be $T_e = 2.1484$ L/c. Note that the area under each of these E-pulses is zero, as required by (4.4.5.5).

Forced E-pulses of duration shorter and longer than that of the minimum duration natural E-pulse are shown in Figures 4.5.6.4 and 4.5.6.5. Each requires a total of 21 basis functions. The first of these figures has E-pulses of duration chosen to be $T_e = 1.8$ L/c. These waveforms are seen to be very oscillatory and are not at all similar to the natural E-pulses. The second of these figures shows

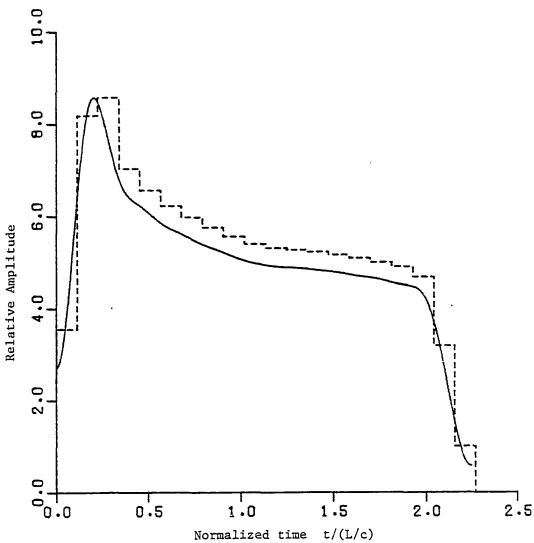

Figure 4.5.6.2. Natural E-pulses of second-smallest duration synthesized using pulse and Fourier cosine basis sets to eliminate first ten modes of thin cylinder.

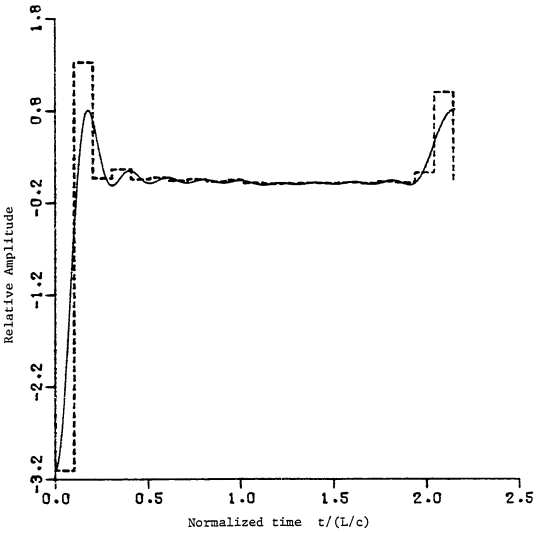

Figure 4.5.6.3. Natural DC E-pulses of minimum duration synthesized using pulse and Fourier cosine basis sets to eliminate first ten modes of thin cylinder.

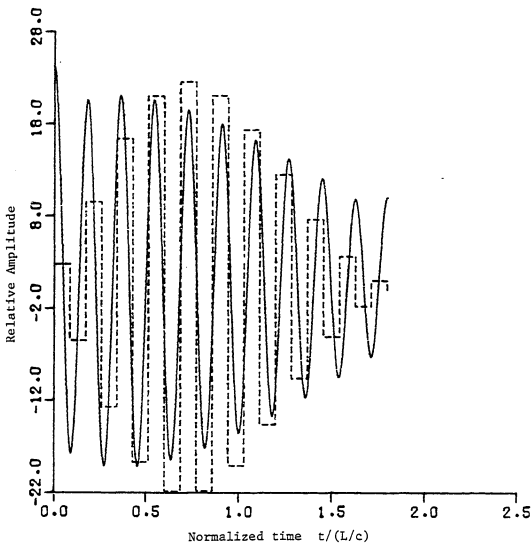

Figure 4.5.6.4. Forced E-pulses of duration T_e=1.8 L/c synthesized using pulse and Fourier cosine basis sets to eliminate first ten modes of thin cylinder.

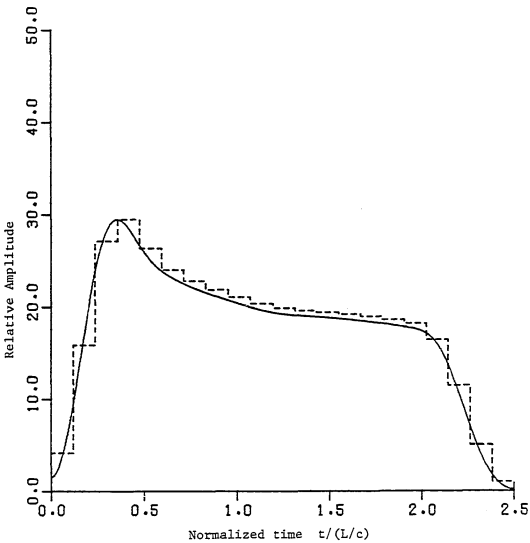

Figure 4.5.6.5. Forced E-pulses of duration T_e=2.5 L/c synthesized using pulse and Fourier cosine basis sets to eliminate first ten modes of thin cylinder.

E-pulses of duration chosen as T_e = 2.5 L/c. These waveforms are much smoother, and are actually quite similar to the natural E-pulses of Figure 4.5.6.2. Figure 4.5.6.6 displays forced DC E-pulses of duration chosen as T_e = 2.5 L/c. These E-pulses require 22 basis functions and are seen to be somewhat similar to the natural DC E-pulses of Figure 4.5.6.3. Note that they also have zero area.

Figure 4.5.6.7 shows natural sin/cos first mode excitation waveforms of minimum duration, each requiring a total of eighteen basis functions. The duration of the pulse function waveform is calculated as T_e = 1.8366 L/c, while the Fourier cosine waveform has a duration found numerically to be T_e = 1.8378 L/c.

Natural sine and cosine first mode excitation waveforms of minimum duration are displayed in Figures 4.5.6.8 and 4.5.6.9. Each requires a total of nineteen basis functions. The first of these figures shows the sine waveforms, with durations T_e = 1.9386 L/c and T_e = 1.9405 L/c for the pulse function and Fourier cosine basis sets, respectively. The second figure shows the cosine waveforms, with durations T_e = 1.9386 L/c and T_e = 1.9440 L/c for the pulse and Fourier cosine basis sets, respectively. Note that each waveform resembles quite closely a full period of the first natural mode of the target. The sine waveforms seem to approximate a sine wave of zero phase, while the cosine waveforms seem to approximate a cosine wave of zero phase. Figure 4.5.6.10 gives natural DC sine first mode excitation waveforms of minimum duration. Each requires a total of twenty basis functions. The duration of the pulse function waveform is calculated as T_e = 2.0407 L/c while the Fourier cosine waveform is found to have

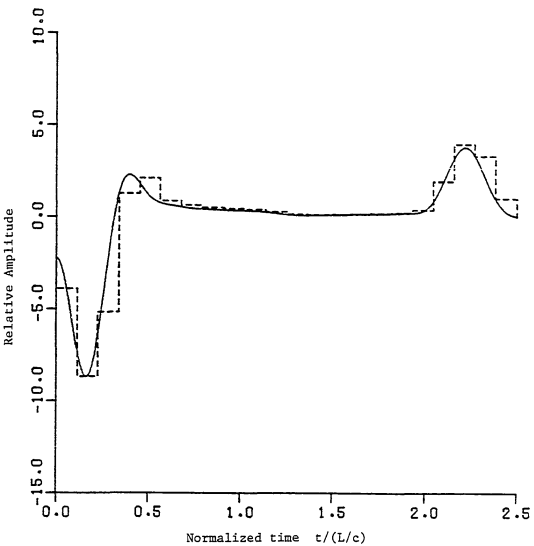

Figure 4.5.6.6. Forced DC E-pulses of duration T_E=2.5 L/c synthesized using pulse and Fourier cosine basis sets to eliminate first ten modes of thin cylinder.

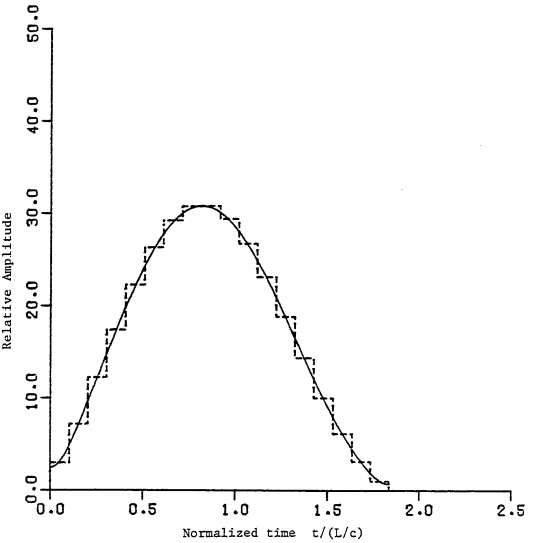

Figure 4.5.6.7. Natural sin/cos single mode excitation waveforms of minimum duration synthesized using pulse and Fourier cosine basis sets to excite the first mode of the thin cylinder, and eliminate modes two through ten.

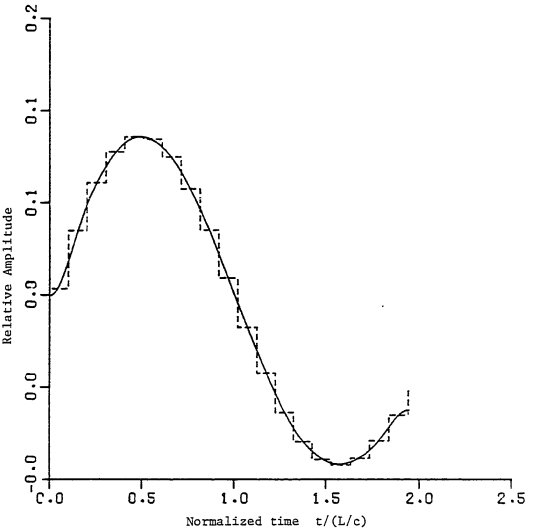

Figure 4.5.6.8. Natural sine single mode excitation waveforms of minimum duration synthesized using pulse and Fourier cosine basis sets to excite the first mode of the thin cylinder, and eliminate modes two through ten.

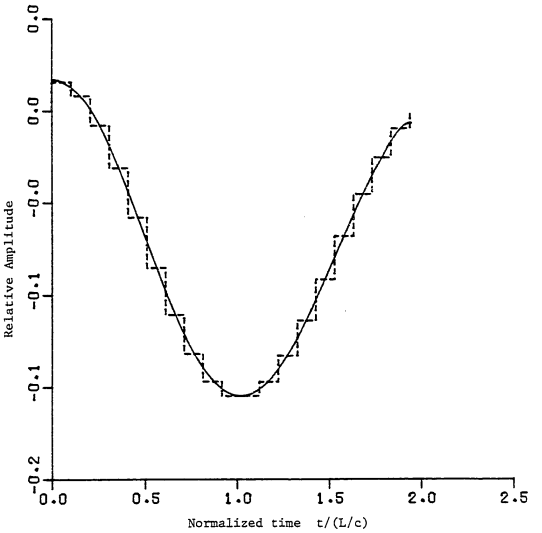

Figure 4.5.6.9. Natural cosine single mode excitation waveforms of minimum duration synthesized using pulse and Fourier cosine basis sets to excite the first mode of the thin cylinder, and eliminate modes two through ten.

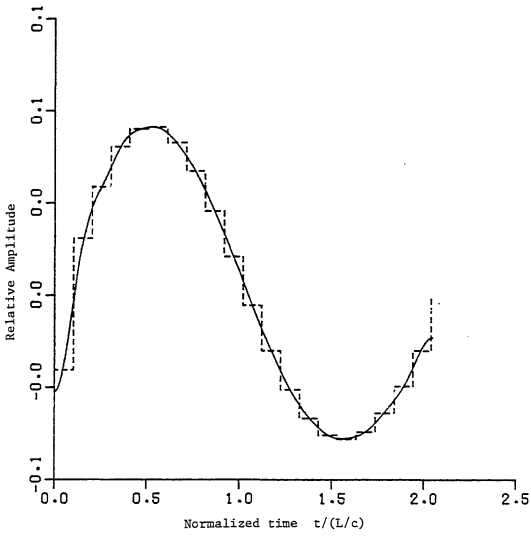

Figure 4.5.6.10. Natural DC sine single mode excitation waveforms of minimum duration synthesized using pulse and Fourier cosine basis sets to excite the first mode of the thin cylinder, and eliminate modes two through ten.

duration T_e = 2.0484 L/c. Each of these waveforms is also very similar to a sine wave of zero phase. Note also that each has zero area.

Figures 4.5.6.11 and 4.5.6.12 show natural third mode excitation waveforms of minimum duration, requiring nineteen basis functions. The first two excite a sine third mode and have duration T_e = 1.9386 L/c for the pulse basis and T_e = 1.9365 for the Fourier cosine basis. The second two excite a cosine third mode and have durations of T_e = 1.9386 L/c for the pulse basis and T_e = 1.9453 L/c for the Fourier cosine basis. This time the waveforms appear to be approximating three oscillations of the third mode.

Figure 4.5.6.13 displays forced sine first mode excitation waveforms of duration chosen as T_e = 2.5 L/c. Each again approximates one period of the first natural mode of the thin cylinder, and are quite similar in appearance, although not as similar as the corresponding natural waveforms. Figure 4.5.6.14 shows forced third mode excitation waveforms of duration chosen as T_e = 2.5 L/c. Each approximates three periods of the third natural target mode.

As a further comparison, the last three figures display forced E-pulses synthesized using the polynomial basis set of section 4.5.1 to eliminate the first five natural modes of the thin cylinder target (and thus require eleven basis functions.) Figure 4.5.6.15 shows a forced polynomial E-pulse of duration chosen to be T_e = 2.05 L/c, quite close to the durations of the natural E-pulses found using pulse and Fourier cosine basis functions. It is seen that the waveform is very similar to the natural E-pulse waveforms of Figure 4.5.6.1. Figure 4.5.6.16 shows a forced polynomial E-pulse of duration chosen

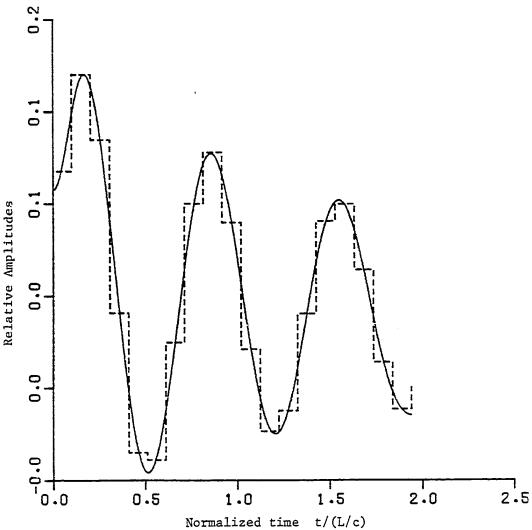

Figure 4.5.6.11. Natural sine single mode excitation waveforms of minimum duration synthesized using pulse and Fourier cosine basis sets to excite the third mode of the thin cylinder, and eliminate modes one, two, and four through ten.

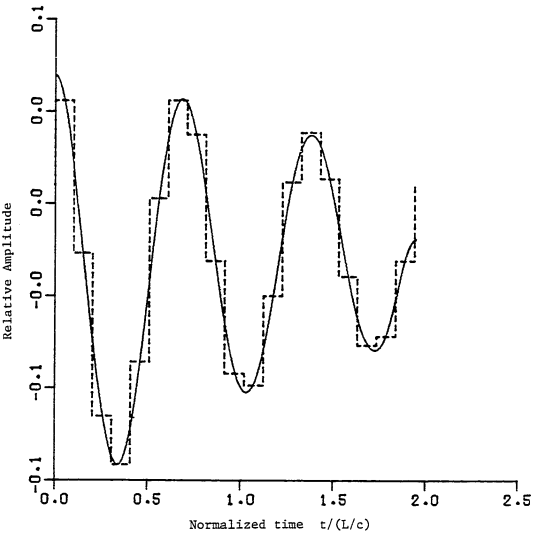

Figure 4.5.6.12. Natural cosine single mode excitation waveforms of minimum duration synthesized using pulse and Fourier cosine basis sets to excite the third mode of the thin cylinder, and eliminate modes one, two, and four through ten.

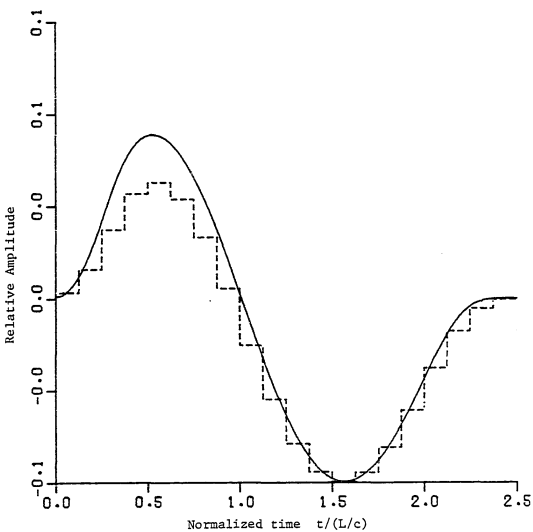

Figure 4.5.6.13. Forced sine single mode excitation waveforms of duration T_e=2.5 L/c synthesized using pulse and Fourier cosine basis sets to excite the first mode of the thin cylinder, and eliminate modes two through ten.

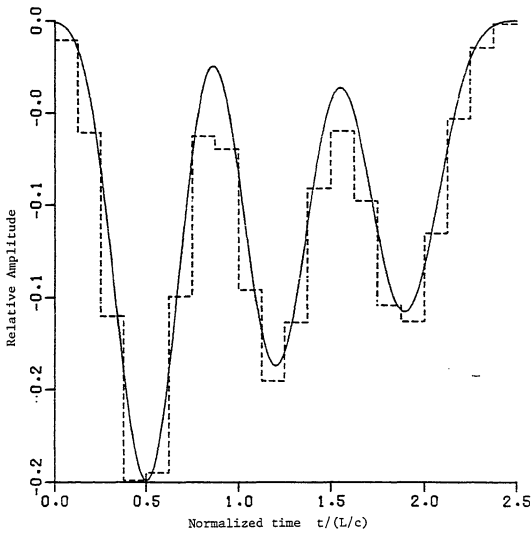

Figure 4.5.6.14. Forced sine single mode excitation waveforms of duration T_e=2.5 L/c synthesized using pulse and Fourier cosine basis sets to excite the third mode of the thin cylinder, and eliminate modes one, two, and four through ten.

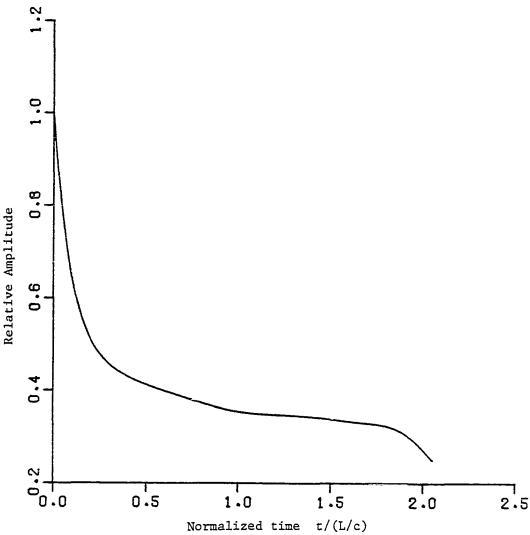

Figure 4.5.6.15. Forced E-pulse of duration T_E=2.05 L/c synthesized using polynomial basis set to eliminate first ten modes of the thin cylinder.

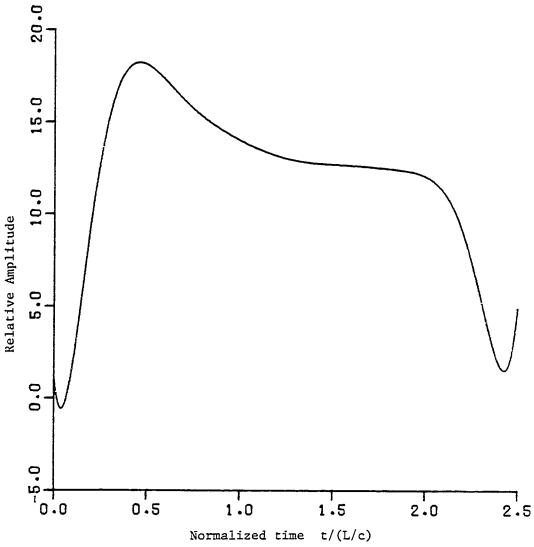

Figure 4.5.6.16. Forced E-pulse of duration T_e=2.5 L/c synthesized using polynomial basis set to eliminate first ten modes of the thin cylinder.

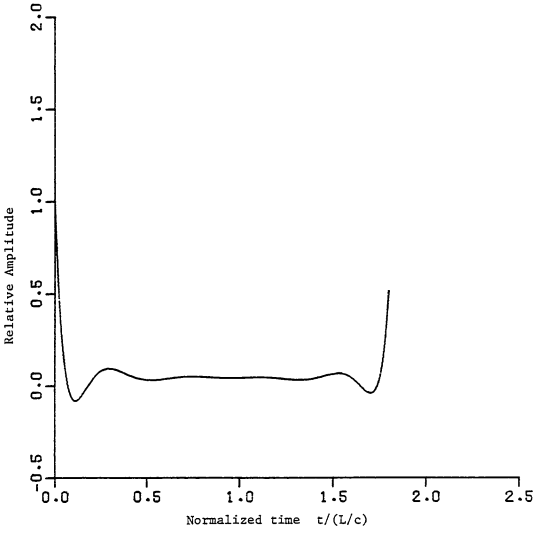

Figure 4.5.6.17. Forced E-pulse of duration T_E=1.8 L/c synthesized using polynomial basis set to eliminate first ten modes of the thin cylinder.

as T_e = 2.5 L/c. This time the resulting waveform is quite similar to the forced E-pulses of Figure 4.5.6.5 calculated using pulse and Fourier cosine functions. Lastly, Figure 4.5.6.17 gives a forced polynomial E-pulse of duration chosen to be T_e = 1.8 L/c. It is very interesting to note that this E-pulse is not oscillatory as were the forced Fourier cosine and pulse waveforms of identical duration.

The similarity between the waveforms constructed using the various basis sets is most intriguing. Especially fascinating are the natural waveforms which also have nearly identical durations. This seems to suggest that there may be an E-pulse unique to a particular target. The possibility of E-pulse uniqueness will be considered in more depth in chapter five.

4.6 The Pulse Function E-pulse

Because of its great simplicity and noise averaging qualities the rectangular pulse based E-pulse will be used extensively in the remainder of this thesis. It is of interest, then, to investigate the pulse function based E-pulse in greater depth.

Equation (4.5.4.16) demonstrates that the spectrum of the pulse function E-pulse is composed of the product of the spectrum of an individual pulse multiplied by a sum of exponential factors. The proper linear combination of the exponential factors results in the E-pulse spectrum being zero at the natural frequencies to be eliminated. Under many circumstances this simple relationship allows a closed form representation of the expansion coefficients α_m. It is also possible to create an efficient algorithm that, while not

specifying them directly, will calculate the expansion coefficients without inverting the E-pulse matrix. Each of these techniques provides the option of never keeping the E-pulse entries in computer memory, thus eliminating restrictions on storage.

The rectangular pulse function E-pulse and the delta function E-pulse also provide a simple means for investigating the use of free parameters other than the pulse function amplitudes. It is possible to use non-uniform pulse function widths as the parameters to be adjusted to satisfy the E-pulse equations. The resulting set of simultaneous nonlinear equations will be solved and the E-pulse will be placed in perspective with respect to the previous examples.

4.6.1 Expansion Coefficient Calculation

The transmit domain definition of the E-pulse requires the E-pulse spectrum to be zero at the natural frequencies to be eliminated. For the pulse function based E-pulse, equation (4.5.4.16) can be substituted into (4.2.1) and (4.2.2) to provide the requirements

$$F_1(s_n)e^{s_n\Delta}\sum_{m=1}^{M}\alpha_m e^{-s_n m\Delta} = 0 \qquad 1\leq n\leq N \qquad (4.6.1.1)$$

$$F_1(s_n^*)e^{s_n^*\Delta}\sum_{m=1}^{M}\alpha_m e^{-s_n^* m\Delta} = 0 \qquad 1\leq n\leq N \qquad (4.6.1.2)$$

Assuming that $F_1(s_n)\neq 0$ and $F_1(s_n^*)\neq 0$ these equations can be written more simply as

$$\sum_{m=1}^{M}\alpha_m e^{-s_n m\Delta} = 0 \qquad 1\leq n\leq N \qquad (4.6.1.3)$$

$$\sum_{m=1}^{M} \alpha_m e^{-s_n^* m\Delta} = 0 \qquad 1 \leq n \leq N \qquad (4.6.1.4)$$

which can be represented in matrix form as a simplification of equation (4.4.3.4). Defining

$$z_n = e^{-s_n \Delta} \qquad (4.6.1.5)$$

$$z_n^* = e^{-s_n^* \Delta} \qquad (4.6.1.6)$$

allows equations (4.6.1.3) and (4.6.1.4) to be written as

$$\sum_{m=1}^{M} \alpha_m z_n^m = 0 \qquad 1 \leq n \leq N \qquad (4.6.1.7)$$

$$\sum_{m=1}^{M} \alpha_m (z_n^*)^m = 0 \qquad 1 \leq n \leq N \qquad (4.6.1.8)$$

Now, since $z_n \neq 0$ and $z_n^* \neq 0$, one power of z and z* can be divided out to give

$$\sum_{m=0}^{M-1} \alpha_{m+1} z_n^m = 0 \qquad 1 \leq n \leq N \qquad (4.6.1.9)$$

$$\sum_{m=0}^{M-1} \alpha_{m+1} (z_n^*)^m = 0 \qquad 1 \leq n \leq N \qquad (4.6.1.10)$$

Analysis of these two equations proceeds along slightly different lines for the natural E-pulse and the generalized forced E-pulse. Thus, the two cases will be considered separately.

I. Natural E-pulse

For a natural E-pulse (which will be generalized to a natural single mode excitation waveform later) the number of basis functions required in the expansion is M = 2N. Thus, equations (4.6.1.9) and (4.6.1.10) become

$$\sum_{m=0}^{2N-1} \alpha_{m+1} z_n^m = 0 \qquad 1 \leq n \leq N \tag{4.6.1.11}$$

$$\sum_{m=0}^{2N-1} \alpha_{m+1} (z_n^*)^m = 0 \qquad 1 \leq n \leq N \tag{4.6.1.12}$$

Writing these in matrix form results in

$$\begin{pmatrix} 1 & z_1 & z_1^2 & \cdots & z_1^{2N-1} \\ 1 & z_1^* & z_1^{*2} & \cdots & z_1^{*2N-1} \\ 1 & z_2 & z_2^2 & \cdots & z_2^{2N-1} \\ \vdots & \vdots & \vdots & & \vdots \\ 1 & z_N^* & z_N^{*2} & & z_N^{*2N-1} \end{pmatrix} \begin{pmatrix} \alpha_1 \\ \alpha_2 \\ \\ \vdots \\ \alpha_{2N} \end{pmatrix} = \begin{pmatrix} 0 \\ 0 \\ \\ \vdots \\ 0 \end{pmatrix} \tag{4.6.1.13}$$

or

$$\underline{\underline{A}}\vec{\alpha} = \vec{0} \tag{4.6.1.14}$$

Note that the rows have been arranged in a slightly different manner than in equation (4.4.3.4). This is merely to provide a more convenient notation.

Since equation (4.6.1.14) represents a set of 2N homogeneous

linear equations in the 2N unknown expansion coefficients α, a solution is possible only if the matrix is singular. This requires

$$\det \left(\overline{\overline{A}} \right) = 0 \tag{4.6.1.15}$$

Close inspection of the matrix $\overline{\overline{A}}$ reveals that its determinant is one of a special group of determinants called "alternants" (determinants generated from alternating functions.) It is fairly common in mathematics and is sometimes referred to as the Vandermonde determinant [24]. Its value is given the notation $\zeta^{\frac{1}{2}}$ and can be expressed as the difference product [24]

$$\begin{aligned} \det \left(\overline{\overline{A}} \right) &= \zeta^{\frac{1}{2}}(z_1, z_1^*, \ \ldots \ , z_N, z_N^*) \\ &= \prod_{1 \leq i < j \leq 2N} (W_j - W_i) \end{aligned} \tag{4.6.1.16}$$

with the matrix entries ordered as

$$\begin{aligned} W_{2k-1} &= z_k \\ W_{2k} &= z_k^* \end{aligned} \tag{4.6.1.17}$$

A simple 4x4 example may clarify this notation

$$\begin{vmatrix} 1 & W_1 & W_1^2 & W_1^3 \\ 1 & W_2 & W_2^2 & W_2^3 \\ 1 & W_3 & W_3^2 & W_3^3 \\ 1 & W_4 & W_4^2 & W_4^3 \end{vmatrix} = \zeta^{\frac{1}{2}}(W_1, W_2, W_3, W_4)$$

$$= (W_4-W_3)(W_4-W_2)(W_4-W_1)(W_3-W_2)(W_3-W_1)(W_2-W_1) \qquad (4.6.1.18)$$

It is apparent from equation (4.6.1.16) and the above example that the matrix $\overline{\overline{A}}$ will be singular if and only if $(W_i - W_j) = 0$ for some i and j. Each of four possible combinations can be examined quite easily. Consider first the possibility $(z_n - z_m) = 0$, $m \neq n$. This implies

$$e^{-\sigma_m \Delta}(\cos\omega_m \Delta - j\sin\omega_m \Delta) = e^{-\sigma_n \Delta}(\cos\omega_n \Delta - j\sin\omega_n \Delta) \qquad (4.6.1.19)$$

Or, equating real and imaginary parts

$$\begin{aligned} e^{-\sigma_m \Delta}\cos\omega_m \Delta &= e^{-\sigma_n \Delta}\cos\omega_n \Delta \\ e^{-\sigma_m \Delta}\sin\omega_m \Delta &= e^{-\sigma_n \Delta}\sin\omega_n \Delta \end{aligned} \qquad (4.6.1.20)$$

Obviously both equations cannot hold simultaneously for arbitrary σ_n, σ_m, ω_n, and ω_m. Thus

$$z_m - z_n \neq 0 \qquad m \neq n \qquad (4.6.1.21)$$

Similar reasoning results in

$$z_m^* - z_n \neq 0 \qquad m \neq n$$

$$z_m - z_n^* \neq 0 \qquad m \neq n \tag{4.6.1.22}$$

Now consider $(z_m - z_m^*) = 0$. This implies

$$e^{-\sigma_m \Delta}\cos\omega_m \Delta = e^{-\sigma_m \Delta}\cos\omega_m \Delta$$

$$-e^{-\sigma_m \Delta}\sin\omega_m \Delta = e^{-\sigma_m \Delta}\sin\omega_m \Delta \tag{4.6.1.23}$$

which are satisfied if and only if

$$\Delta = \frac{p\pi}{\omega_m} \qquad p = 1,2,3,\ldots \qquad 1 \leq m \leq N \tag{4.6.1.24}$$

Note that this implies that the smallest possible duration of the natural pulse function E-pulse is

$$T_e = 2N \frac{\pi}{\omega_h} \tag{4.6.1.25}$$

where ω_h is the largest natural frequency (imaginary part) to be eliminated.

With Δ given by (4.6.1.24) the matrix $\overline{\overline{A}}$ becomes singular. The expansion coefficients can be solved for by letting $\alpha_{2N} = 1$ and eliminating the equation involving W_{2k} where

$$\Delta = \frac{p\pi}{\omega_k} \qquad \text{or} \qquad W_{2k} = e^{-s\overset{*}{\Delta}\Delta} \tag{4.6.1.26}$$

Bringing the last column of equation (4.6.1.13) to the right hand side results in the reduced matrix equation

$$\begin{Bmatrix} 1 & W_1 & W_1^2 & \cdots & W_1^{2N-2} \\ 1 & W_2 & W_2^2 & \cdots & W_2^{2N-2} \\ \vdots & \vdots & \vdots & & \vdots \\ 1 & W_{2k-1} & W_{2k-1}^2 & \cdots & W_{2k-1}^{2N-2} \\ 1 & W_{2k+1} & W_{2k+1}^2 & \cdots & W_{2k+1}^{2N-2} \\ \vdots & \vdots & \vdots & & \vdots \\ 1 & W_{2N} & W_{2N}^2 & \cdots & W_{2N}^{2N-2} \end{Bmatrix} \begin{Bmatrix} \alpha_1 \\ \alpha_2 \\ \\ \\ \vdots \\ \\ \\ \alpha_{2N-1} \end{Bmatrix} = - \begin{Bmatrix} W_1^{2N-1} \\ W_2^{2N-1} \\ \vdots \\ W_{2k-1}^{2N-1} \\ W_{2k+1}^{2N-1} \\ \vdots \\ W_{2N}^{2N-1} \end{Bmatrix} \tag{4.6.1.27}$$

This equation is now in a form which can be solved using standard matrix techniques. However, it is also in a form conducive to solution using Cramer's rule and a special theorem from alternants.

Cramer's rule is usually not employed to solve large systems of equations due to the tremendous number of arithmetic operations required to calculate the determinant ratios (as compared to Gaussian elimination, or similar methods.) In the case of equation (4.6.1.27), though, the determinant ratios take a special form which can be calculated quite quickly using the following identity from the theory of alternants [25]

$$\frac{\begin{vmatrix} 1 & a_1 & a_1^2 & \cdots & a_1^{i-1} & a_1^{i+1} & \cdots & a_1^n \\ 1 & a_2 & a_2^2 & \cdots & a_2^{i-1} & a_2^{i+1} & \cdots & a_2^n \\ 1 & a_3 & a_3^2 & \cdots & a_3^{i-1} & a_3^{i+1} & \cdots & a_3^n \\ \vdots & \vdots & \vdots & & \vdots & \vdots & & \vdots \\ 1 & a_n & a_n^2 & \cdots & a_n^{i-1} & a_n^{i+1} & \cdots & a_n^n \end{vmatrix}}{\zeta^{\frac{1}{2}}(a_1, a_2, \ldots a_n)} = P_{n-i} \qquad (4.6.1.28)$$

where P_{n-i} is the sum of the products n-i at a time, without repititions, of the quantities $a_1, \ldots, a_n$. For example

$$P_{4-2} = a_1a_2 + a_1a_3 + a_1a_4 + a_2a_3 + a_2a_4 + a_3a_4 \qquad (4.6.1.29)$$

Thus, P_{n-i} is the ratio of the difference product with the i'th power omitted to the original difference product.

Application of Cramer's rule to (4.6.1.27) results in the solution for the n'th expansion coefficient. This is accomplished by replacing the n'th column of the matrix with the column vector on the right hand side, and taking the ratio of the determinant of the resulting matrix to the determinant of the original. Thus

$$\alpha_n = -\frac{\begin{vmatrix} 1 & W_1 & \cdots & W_1^{n-2} & W_1^{2N-1} & W_1^{n} & \cdots & W_1^{2N-2} \\ 1 & W_2 & \cdots & W_2^{n-2} & W_2^{2N-1} & W_2^{n} & \cdots & W_2^{2N-2} \\ \vdots & \vdots & & \vdots & \vdots & \vdots & & \vdots \end{vmatrix}}{\begin{vmatrix} 1 & W_1 & & \cdots & & & & W_1^{2N-2} \\ 1 & W_2 & & \cdots & & & & W_2^{2N-2} \\ \vdots & \vdots & & & & & & \vdots \end{vmatrix}} \qquad (4.6.1.30)$$

with the minus sign being carried over from the right hand side vector. Now, the right hand side vector can be moved through the matrix so that it finally resides in the last column of the matrix by repeatedly swapping it with the column to its right. However, the theory of determinants requires the sign of the determinant to change whenever two columns are interchanged. Thus, (4.6.1.30) can also be written as

$$\alpha_n = (-1)^n \frac{\begin{vmatrix} 1 & W_1 & \cdots & W_1^{n-2} & W_1^{n} & \cdots & W_1^{2N-1} \\ 1 & W_2 & \cdots & W_2^{n-2} & W_2^{n} & \cdots & W_2^{2N-1} \\ \vdots & \vdots & & \vdots & \vdots & & \vdots \end{vmatrix}}{\begin{vmatrix} 1 & W_1 & & \cdots & & W_1^{2N-2} \\ 1 & W_2 & & \cdots & & W_2^{2N-2} \\ \vdots & \vdots & & & & \vdots \end{vmatrix}} \qquad (4.6.1.31)$$

This is exactly the form needed to employ equation (4.6.1.28). Thus, the n'th expansion coefficient can be written explicitly as

$$\alpha_n = (-1)^n P_{(2N-1)-(n-1)} \qquad (4.6.1.32)$$

where P involves the factors W_1, W_2, ... , W_{2k-1}, W_{2k+1}, ... , W_{2N}. It is not obvious at first that the sum of products of the complex factors W will result in a real value (as the pulse amplitudes must surely be), but grouping terms in complex conjugate pairs soon makes this apparent.

Besides providing an explicit formula for the expansion coefficients, equation (4.6.1.32) represents several improvements over solving (4.6.1.27) using standard matrix methods. First, it eliminates the necessity of having a large number of matrix elements in computer memory simultaneously, as required with Gaussian elimination. Second, only the 2N complex factors W_1, ... , W_{2N} need be calculated as opposed to the N^2 matrix elements. Lastly, equation (4.6.1.32) eliminates the error accumulated during Gaussian elimination due to repeated row operations.

A simple two mode E-pulse example should clarify the use of equation (4.6.1.31). For the case of two modes (4.6.1.14) becomes

$$\begin{pmatrix} 1 & W_1 & W_1^2 & W_1^3 \\ 1 & W_2 & W_2^2 & W_2^3 \\ 1 & W_3 & W_3^2 & W_3^3 \\ 1 & W_4 & W_4^2 & W_4^3 \end{pmatrix} \begin{pmatrix} \alpha_1 \\ \alpha_2 \\ \alpha_3 \\ \alpha_4 \end{pmatrix} = \begin{pmatrix} 0 \\ 0 \\ 0 \\ 0 \end{pmatrix} \qquad (4.6.1.33)$$

where

$$W_1 = z_1 = e^{-s_1\Delta} \qquad W_3 = z_2 = e^{-s_2\Delta}$$
$$W_2 = z_1^* = e^{-s_1^*\Delta} \qquad W_4 = z_2^* = e^{-s_2^*\Delta} \tag{4.6.1.34}$$

Now, choose the E-pulse duration using (4.6.1.24) as

$$\Delta = \frac{\pi}{\omega_2} \tag{4.6.1.35}$$

which corresponds to the smallest duration if $\omega_2 > \omega_1$. Reduction of the matrix yields

$$\begin{pmatrix} 1 & W_1 & W_1^2 \\ 1 & W_2 & W_2^2 \\ 1 & W_3 & W_3^2 \end{pmatrix} \begin{pmatrix} \alpha_1 \\ \alpha_2 \\ \alpha_3 \end{pmatrix} = - \begin{pmatrix} W_1^3 \\ W_2^3 \\ W_3^3 \end{pmatrix} \tag{4.6.1.36}$$

with α_4 set equal to 1. Applying (4.6.1.32) results in

$$\alpha_1 = - P_{3-0} = - W_1W_2W_3 = - z_1z_1^*z_2$$
$$= e^{-(2\sigma_1 + \sigma_2)\Delta} \tag{4.6.1.37}$$

$$\alpha_2 = P_{3-1} = W_1W_2 + W_1W_3 + W_2W_3 = z_1z_1^* + z_2(z_1 + z_1^*)$$
$$= e^{-\sigma_1\Delta}\left(e^{-\sigma_1\Delta} - 2e^{-\sigma_2\Delta}\cos\omega_1\Delta\right) \tag{4.6.1.38}$$

$$\alpha_3 = -P_{3-2} = -(W_1 + W_2 + W_3) = -z_2 - (z_1 + z_1^*)$$

$$= -2e^{-\sigma_1\Delta}\cos\omega_1\Delta + e^{-\sigma_2\Delta} \qquad (4.6.1.39)$$

In particular, if the first two natural frequencies of the thin wire target are used (as given in Figure 5.2.1), the expansion coefficients become

$$\alpha_1 = 1.602 \qquad \alpha_2 = 1.170$$
$$\alpha_3 = 1.104 \qquad \alpha_4 = 1 \qquad (4.6.1.40)$$

with the E-pulse duration

$$T_e = 4\Delta = 4\,\frac{\pi}{\omega_2}\,\frac{L}{c} = 2.092\,\frac{L}{c} \qquad (4.6.1.41)$$

It is important to remember that this analysis does not depend upon the individual pulse shapes. Thus, the results given by (4.6.1.40) could represent the amplitudes of triangle pulses, delta functions, or pulses of any desired shape.

It is interesting that, in particular, α_1 and α_{2N-1} are easily generalized for an N mode E-pulse

$$\alpha_1 = -P_{2N-1} = -(-1)^P e^{-\sigma_k\Delta} \prod_{\substack{i=1 \\ i\neq k}}^{N} (z_i z_i^*)$$

$$= -(-1)^P e^{+\sigma_k\Delta} \prod_{i=1}^{N} e^{-2\sigma_i\Delta} \qquad (4.6.1.42)$$

and

$$\alpha_{2N-1} = -P_1 = -(-1)^p e^{-\sigma_k \Delta} - \sum_{\substack{i=1 \\ i\neq k}}^{N} (z_i + z_i^*)$$

$$= (-1)^p e^{-\sigma_k \Delta} - 2 \sum_{i=1}^{N} e^{-\sigma_i \Delta} \cos\omega_i \Delta \qquad (4.6.1.43)$$

where $\Delta = p\pi/\omega_k$, p=1,2, ..., and $W_{2k-1} = (-1)^p e^{-\sigma_k \Delta}$. Thus, the first and last amplitudes (α_{2N} previously assumed as 1) of the minimum duration natural E-pulse (p=1) always have the same sign. Without knowing the specific values of the natural frequencies to be eliminated it is impossible to tell the sign of α_{2N-1}. It is also quite difficult to write out the algebraic expression for an arbitrary α when N is large. For example, the simplest remaing expansion coefficient to represent is α_2. By grouping terms properly this can be written as

$$\alpha_2 = W_{2k-1} \sum_{\substack{i=1 \\ i\neq k}}^{N} \Big((z_i + z_i^*) \prod_{\substack{j=1 \\ j\neq i \\ j\neq k}}^{N} z_j z_j^* \Big) + \prod_{\substack{j=1 \\ j\neq k}}^{N} z_j z_j^* \qquad (4.6.1.44)$$

$$= \Big(-(-1)^p e^{+\sigma_k \Delta} \prod_{j=1}^{N} e^{-2\sigma_j \Delta} \Big) \Big((-1)^p e^{\sigma_k \Delta} - 2 \sum_{i=1}^{N} e^{\sigma_i \Delta} \cos\omega_i \Delta \Big)$$

This latter form is the result of quite a bit of manipulation and is seen to be the product of two terms. The first is merely α_1 while the second is α_{2N-1} with $\sigma \to -\sigma$.

Extending the analysis to the case of sin/cos single mode

excitation is straight forward. The factors corresponding to the mode to be excited must be left out of P. Thus, the E-m-pulse expansion coefficients are given by

$$\alpha_n = (-1)^n P_{(2N-3)-(n-1)} \tag{4.6.1.45}$$

where P involves $W_1, \ldots, W_{2k-1}, W_{2k+1}, \ldots, W_{2N}$ but not W_{2m} or W_{2m-1}. Note that in $\Delta = p\pi/\omega_k$ the case k=m is not allowed.

It is also possible to extend this analysis to the DC E-pulse. A DC E-pulse requires one additional equation to satisfy (4.4.5.6). Using equation (4.5.4.16) results in

$$\sum_{m=0}^{2N} \alpha_m = 0 \tag{4.6.1.46}$$

where one additional basis function has been added to accommodate the additional constraint. With this, equation (4.6.1.13) becomes

$$\begin{pmatrix} 1 & z_1 & z_1^2 & \cdots & z_1^{2N} \\ 1 & z_1^* & z_1^{*2} & \cdots & z_1^{*2N} \\ 1 & z_2 & z_2^2 & \cdots & z_2^{2N} \\ \vdots & \vdots & \vdots & & \vdots \\ 1 & z_N^* & z_N^{*2} & \cdots & z_N^{*2N} \\ 1 & 1 & 1 & \cdots & 1 \end{pmatrix} \begin{pmatrix} \alpha_1 \\ \alpha_2 \\ \vdots \\ \alpha_{2N} \\ \alpha_{2N+1} \end{pmatrix} = \begin{pmatrix} 0 \\ 0 \\ \vdots \\ \\ 0 \end{pmatrix} \tag{4.6.1.47}$$

Using (4.6.1.16) the widths of the pulse functions are seen to be

unaltered from those of the non-DC E-pulse

$$\Delta = \frac{p\pi}{\omega_m} \qquad p = 1,2,3, \ldots \qquad 1 \leq m \leq N \tag{4.6.1.48}$$

but due to the extra basis function the duration of the E-pulse is slightly larger. The pulse function amplitudes can then be found as

$$\alpha_n = (-1)^{n+1} P_{2N-(n-1)} \tag{4.6.1.49}$$

where P involves the factors $W_1, W_2, \ldots, W_{2k-1}, W_{2k+1}, \ldots, W_{2N}, 1$.

II. Forced E-pulse

It is also possible to derive a relationship analogous to (4.6.1.32) for the forced E-pulse. For the derivation to work, however, this E-pulse must have a forcing component consisting of one identical pulse basis function. This allows equations (4.6.1.9) and (4.6.1.10) to be written as

$$\sum_{m=0}^{2N} \alpha_{m+1} z_n^m = 0 \qquad 1 \leq n \leq N \tag{4.6.1.50}$$

$$\sum_{m=0}^{2N} \alpha_{m+1} (z_n^*)^m = 0 \qquad 1 \leq n \leq N \tag{4.6.1.51}$$

where one more basis function has been used than in the natural E-pulse development. In matrix form these equations become

$$\begin{pmatrix} 1 & z_1 & z_1^2 & \cdots & z_1^{2N} \\ 1 & z_1^* & z_1^{*2} & \cdots & z_1^{*2N} \\ 1 & z_2 & z_2^2 & \cdots & z_2^{2N} \\ \vdots & \vdots & \vdots & & \vdots \\ 1 & z_N^* & z_N^{*2} & \cdots & z_N^{*2N} \end{pmatrix} \begin{pmatrix} \alpha_1 \\ \alpha_2 \\ \vdots \\ \alpha_{2N+1} \end{pmatrix} = \begin{pmatrix} 0 \\ 0 \\ \vdots \\ 0 \end{pmatrix} \qquad (4.6.1.52)$$

Since there is one more free parameter than there are equations, this matrix equation has no unique solution. It is necessary to specify one of the parameters and solve the resulting inhomogeneous system of equations. Letting $\alpha_{2N+1} = 1$ and moving the last column to the right hand side results in

$$\begin{pmatrix} 1 & W_1 & \cdots & W_1^{2N-1} \\ \vdots & \vdots & & \vdots \\ 1 & W_{2N} & \cdots & W_{2N}^{2N-1} \end{pmatrix} \begin{pmatrix} \alpha_1 \\ \vdots \\ \alpha_{2N} \end{pmatrix} = - \begin{pmatrix} W_1^{2N} \\ \vdots \\ W_{2N}^{2N} \end{pmatrix} \qquad (4.6.1.53)$$

where $W_1, \ldots, W_{2N}$ are given in (4.6.1.17). Again using successive applications of Cramer's rule and equation (4.6.1.28) yields the solution for the expansion coefficients as

$$\alpha_n = (-1)^{n-1} P_{2N-(n-1)} \qquad (4.6.1.54)$$

where P involves all the factors $W_1, \ldots, W_{2N}$.

A simple example involving a two mode E-pulse demonstrates the ease of using equation (4.6.1.54). Letting W_1, ... , W_4 be defined as in (4.6.1.34) the expansion coefficients become

$$\alpha_1 = P_{4-0} = W_1W_2W_3W_4 = (z_1z_1^*)(z_2z_2^*)$$

$$= e^{-2(\sigma_1+\sigma_2)\Delta} \qquad (4.6.1.55)$$

$$\alpha_2 = -P_{4-1} = -(W_1W_2W_3 + W_1W_2W_4 + W_1W_3W_4 + W_2W_3W_4)$$

$$= -(z_1z_1^*)(z_2+z_2^*) - (z_2z_2^*)(z_1+z_1^*) \qquad (4.6.1.56)$$

$$= -2e^{-(\sigma_1+\sigma_2)\Delta}\left(e^{-\sigma_1\Delta}\cos\omega_2\Delta + e^{-\sigma_2\Delta}\cos\omega_1\Delta\right)$$

$$\alpha_3 = P_{4-2} = W_1W_2 + W_1W_3 + W_1W_4 + W_2W_3 + W_2W_4 + W_3W_4$$

$$= (z_1+z_1^*)(z_2+z_2^*) + (z_1+z_1^*) + (z_2+z_2^*) \qquad (4.6.1.57)$$

$$= 4e^{-(\sigma_1+\sigma_2)\Delta}\cos\omega_1\Delta\cos\omega_2\Delta + 2e^{-\sigma_1\Delta}\cos\omega_1\Delta +$$

$$+ 2e^{-\sigma_2\Delta}\cos\omega_2\Delta$$

$$\alpha_4 = -P_{4-3} = -(W_1 + W_2 + W_3 + W_4) = -(z_1+z_1^*) - (z_2+z_2^*)$$

$$= -2e^{-\sigma_1\Delta}\cos\omega_1\Delta - 2e^{-\sigma_2\Delta}\cos\omega_2\Delta \qquad (4.6.1.58)$$

where α_5 has been set equal to 1. Note that Δ has not been specified in these equations. Any E-pulse duration that does not force the matrix in (4.6.1.53) to be singular can be used, and thus the E-pulse

can be made as short as desired. This was not the case with the natural pulse function E-pulse, which had a minimum duration given by (4.6.1.25).

In particular, α_1 and α_{2N} can be generalized as

$$\alpha_1 = P_{2N} = \prod_{i=1}^{N} (z_i z_i^*)$$

$$= \prod_{i=1}^{N} e^{-2\sigma_i \Delta} \qquad (4.6.1.59)$$

and

$$\alpha_{2N} = -P_{2N-(2N-1)} = -\sum_{i=1}^{N} (z_i + z_i^*)$$

$$= -2 \sum_{i=1}^{N} e^{-\sigma_i \Delta} \cos\omega_i \Delta \qquad (4.6.1.60)$$

Thus, the first and last pulse amplitudes (α_{2N+1} previously set equal to one) always have the same sign, exactly as with the natural E-pulse of minimum duration.

Extending this analysis for the case of sin/cos single mode excitation is quite easy. It requires only that the factors corresponding to the mode to be excited be left out of P. Thus, the expansion coefficients of the sin/cos E-m-pulse are given by

$$\alpha_n = (-1)^{n-1} P_{2N-2-(n-1)} \qquad (4.6.1.61)$$

where P involves $W_1, \ldots, W_{2N}$ but not W_{2m} or W_{2m-1}.

The forced DC E-pulse is also quite simple to analyze. The amplitudes are given by

$$\alpha_n = (-1)^n P_{2N+1-(n-1)} \tag{4.6.1.62}$$

where P involves $W_1, \ldots, W_{2N}, 1$.

Equations (4.6.1.32) and (4.6.1.54) have provided explicit formulas for calculating the expansion coefficients of a natural and a forced pulse function based E-pulse. However, their usefulness in actually computing the coefficients has only been demonstrated for a small number of modes (namely, two.) The question remains as to whether these simple representations are feasible when the number of modes to be eliminated is large.

The important parameter to calculate in reference to computer computation is the number of multiplications required to find $\alpha_1, \ldots, \alpha_{2N}$. If this number is excessively large in comparison to standard matrix solving routines then it does not represent a feasible method.

Let

$$\binom{n}{r} = C_r^n = \frac{n!}{r!(n-r)!} \tag{4.6.1.63}$$

which is the binomial coefficient corresponding to the combination of n things taken r at a time. With this, the total number of terms

added together to calculate all the α's for a natural E-pulse can be written as

$$T = \sum_{k=1}^{2N-1} \binom{2N-1}{k} \tag{4.6.1.64}$$

The total number of multiplications required is found by considering the number of multiplications involved in each term. This is just

$$M_{+} = \sum_{k=1}^{2N-1} (k-1)\binom{2N-1}{k} \tag{4.6.1.65}$$

By examining the form of P it is found that the number of multiplications required can be reduced considerably if intermediate results are stored in the computer's memory. Then each additional α adds only one additional multiplication per term. Using this procedure requires

$$m = T - (2N-1) \tag{4.6.1.66}$$

total multiplications. The additional storage needed by this method is

$$S = \max\left\{ \binom{2N-1}{k} \right\}_{k=1,2,\ldots,2N-1} = \frac{(2N-1)!}{N!(N-1)!} \tag{4.6.1.67}$$

complex terms stored.

M_{+}, T, and m can be calculated explicitly with the help of the following formulas [26]

$$1 + \binom{n}{2} + \binom{n}{4} + \cdots = 2^{n-1} \tag{4.6.1.68}$$

$$\left\{ {n \atop 1} \right\} + \left\{ {n \atop 3} \right\} + \left\{ {n \atop 5} \right\} + \cdots = 2^{n-1} \tag{4.6.1.69}$$

$$\sum_{k=0}^{n} (k+1) \left\{ {n \atop k} \right\} = 2^{n-1}(n+2) \tag{4.6.1.70}$$

Combining (4.6.1.68) and (4.6.1.69) gives

$$\sum_{k=1}^{n} \left\{ {n \atop k} \right\} = 2 \cdot 2^{n-1} - 1 = 2^{n} - 1 \tag{4.6.1.71}$$

and thus

$$T = 2^{2N-1} - 1 \tag{4.6.1.72}$$

which results in

$$m = 2^{2N-1} - 2N \tag{4.6.1.73}$$

Now, using (4.6.1.70) yields

$$\sum_{k=0}^{n} (k+1) \left\{ {n \atop k} \right\} = 1 + \sum_{k=1}^{n} (k+1) \left\{ {n \atop k} \right\}$$

$$= 2^{n-1}(n+2) + 1 \tag{4.6.1.74}$$

Thus

$$\sum_{k=1}^{n} (k-1) \left\{ {n \atop k} \right\} = 2^{n-1}(n-2) + 1 \tag{4.6.1.75}$$

which gives

$$M_+ = 2^{2N-2}(2N-3) + 1 \qquad (4.6.1.76)$$

It is informative to calculate M_+, S, and m for a three mode and a ten mode E-pulse. The results are

	3 modes	10 modes
M_+	49	3,932,161
m	26	524,268
S	10	92,378

(4.6.1.77)

Thus, a ten mode E-pulse requires nearly four million multiplications. This can be reduced to about half a million by saving intermediate results, but only at a cost of storing 92,000 complex numbers. Remembering that Gaussian elimination for n equations requires about $n^3/3$ multiplications (or about 2300 for a ten mode E-pulse) suggests that equations (4.6.1.32) and (4.6.1.54) are not feasible for calculating the expansion coefficients directly. This does not mean that those equations are worthless, however, for they provide a wealth of general information about the behavior of the pulse function amplitudes.

4.6.2 Natural Sine and Cosine E-m-pulse Duration

It would seem at first that the method of the preceeding section could be applied in a straight forward manner to construct natural sine or cosine single mode excitation waveforms. Unfortunately, the added requirement (4.4.7.20) or (4.4.7.25) for transmit domain synthesis results in an E-pulse matrix that is not amenable to solution using the techniques of section 4.6.1. It is possible, though, to solve explicitly for the discrete E-pulse durations. This is very helpful, since it eliminates the need for a search procedure.

The natural E-m-pulse durations are calculated by demanding that the determinant of the E-pulse matrix be zero. The matrix entries for a pulse function based E-pulse are found using the E-pulse spectrum (4.5.4.16), equations (4.4.7.20) and (4.4.7.25) and equations (4.2.1) and (4.2.2). The resulting matrix equation can be written as

$$\begin{Bmatrix} \beta_m z_m \pm \beta^* z^*_m & \beta_m z^2_m \pm \beta^* z^{*2}_m & \cdots & \beta_m z^{2N-1}_m \pm \beta^* z^{*2N-1}_m \\ 1 & W_1 & \cdots & W_1^{2N-2} \\ 1 & W_2 & \cdots & W_2^{2N-2} \\ \vdots & \vdots & & \vdots \\ 1 & W_{2m-2} & \cdots & W_{2m-2}^{2N-2} \\ 1 & W_{2m+1} & \cdots & W_{2m+1}^{2N-2} \\ \vdots & \vdots & & \vdots \\ 1 & W_{2N} & \cdots & W_{2N}^{2N-2} \end{Bmatrix} \begin{Bmatrix} \alpha_1 \\ \alpha_2 \\ \vdots \\ \alpha_{2N-1} \end{Bmatrix} = \begin{Bmatrix} 0 \\ 0 \\ \vdots \\ 0 \end{Bmatrix}$$

(4.6.2.1)

which is directly analogous to (4.6.1.13) from the previous section. In (4.6.2.1) the m'th mode is to be excited, the plus sign corresponds to a sine E-m-pulse and the minus sign to a cosine E-m-pulse, the W's are defined in equation (4.6.1.17), the z's are defined in (4.6.1.5) and (4.6.1.6), and

$$\beta_m = F_1(s_m)e^{s_m\Delta} \tag{4.6.2.2}$$

$$\beta^*_m = F_1(s^*_m)e^{s^*_m\Delta} \tag{4.6.2.3}$$

where $F_1(s)$ is defined in (4.5.4.17).

It is apparent that the above matrix equation cannot be put into a form to utilize (4.6.1.28) and so a solution for the expansion coefficients by the method of section 4.6.1 is not possible. However, it is possible to calculate the determinant explicitly, using the following rule [27]

$$\det \begin{pmatrix} a_{11}+a'_{11} & a_{12}+a'_{12} & \cdots & a_{1N}+a'_{1N} \\ a_{21} & a_{22} & & a_{2N} \\ \vdots & \vdots & & \vdots \\ a_{N1} & a_{N2} & & a_{NN} \end{pmatrix} =$$

$$= \det \begin{pmatrix} a_{11} & a_{12} & \cdots & a_{1N} \\ a_{21} & a_{22} & \cdots & a_{2N} \\ \vdots & \vdots & & \vdots \\ a_{N1} & a_{N2} & \cdots & a_{NN} \end{pmatrix} + \det \begin{pmatrix} a'_{11} & a'_{12} & \cdots & a'_{1N} \\ a_{21} & a_{22} & \cdots & a_{2N} \\ \vdots & \vdots & & \vdots \\ a_{N1} & a_{N2} & \cdots & a_{NN} \end{pmatrix} \tag{4.6.2.4}$$

Setting the determinant of the matrix in (4.6.2.1) equal to zero and employing (4.6.2.4) yields

$$\beta_m z_m \prod_{\substack{1\le i<j\le 2N \\ i\neq 2m}} (W_j - W_i) \pm \beta_m^* z_m^* \prod_{\substack{1\le i<j\le 2N \\ i\neq 2m-1}} (W_j - W_i) = 0 \qquad (4.6.2.5)$$

As with the E-pulse analysis this requires

$$z_k - z_k^* = 0 \qquad k\neq m \qquad (4.6.2.6)$$

for some k, or

$$\Delta = \frac{p\pi}{\omega_k} \qquad p=1,2,3,\ldots \qquad k\neq m \qquad (4.6.2.7)$$

Note that in this case $\Delta = p\pi/\omega_m$ is not allowed since equation (4.6.2.5) does not involve the term $(z_m - z_m^*)$.

4.6.3 Expansion Coefficient Calculation Algorithm

Section 4.6.1 presented a method for calculating the E-pulse expansion coefficients for a pulse function based E-pulse without using standard matrix solving routines. There was no excessive storage requirement, but the number of arithmetic operations needed was shown to be prohibitive. It is possible to take a different approach which allows the choice of one of two distinct advantages: 1) no storage requirement, but arithmetic complexity similar to Gaussian

elimination; or 2) storage equivalent to Gaussian elimination but a much smaller number of arithmetic calculations. Neither routine uses elementary row operations for reduction to triangular form, and thus are not as sensitive to matrix conditioning as Gaussian elimination. Each routine basically performs only the back substitution portion of the Gaussian method.

The algorithm is based on the following relationship [28]

$$\frac{\begin{vmatrix} 1 & W_1 & W_1^2 & \cdots & W_1^{M-2} & f_1 \\ 1 & W_2 & W_2^2 & \cdots & W_2^{M-2} & f_2 \\ 1 & W_3 & W_3^2 & \cdots & W_3^{M-2} & f_3 \\ \vdots & \vdots & \vdots & & \vdots & \vdots \\ 1 & W_M & W_M^2 & \cdots & W_M^{M-2} & f_M \end{vmatrix}}{\zeta^{\frac{1}{2}}(W_1, W_2, \ldots, W_M)} = \frac{f_1}{(W_1-W_2)(W_1-W_3)\cdots(W_1-W_M)} +$$

$$+ \frac{f_2}{(W_2-W_1)(W_2-W_3)\cdots(W_2-W_M)} + \cdots + \frac{f_M}{(W_M-W_1)(W_M-W_2)\cdots(W_M-W_{M-1})}$$

$$= \sum_{i=1}^{M} \frac{f_i}{\prod_{\substack{j=1 \\ j\neq i}}^{M} (W_i-W_j)} \qquad (4.6.3.1)$$

where $\zeta^{\frac{1}{2}}$ is given in (4.6.1.16). This identity is easily developed by expanding the determinant in the numerator in minors, each of which

is a Vandermonde determinant. It is a fundamental formula in the calculus of finite differences where it is used to calculate the M-1'th finite difference derivative.

The algorithm is slightly different for the natural and forced E-pulses, so each case will be considered separately.

I. Natural E-pulse

The matrix equation to be solved for the case of the natural pulse function based E-pulse is given in (4.6.1.27) where it has been assumed that the E-pulse duration is given by $\Delta = p\pi/\omega_k$. Thus, the row containing powers of W_{2k} has been eliminated. The general algorithm for calculating the expansion coefficients is then as follows:

1. Solve for α_{2N-1} by using Cramer's rule and (4.6.3.1).
2. With α_{2N-1} known, reduce the order of the matrix by multiplying the final column by α_{2N-1}, moving it to the right hand side, and eliminating the last equation.
3. Repeat until all the α's are computed.

Note that there is no need to create the matrix in (4.6.1.27) and thus very little computer storage is required.

If storage equivalent to that consumed by the matrix is allowed, an alternative, very efficient algorithm can be constructed. The expansion coefficients can then be solved for as follows:

1. Effectively eliminate the row containing W_{2k} by letting

for $1 \leq m \leq N$

$$W_{2m-1} = z_m \qquad W_{2m} = z^*_m \qquad \text{for } m \leq k$$

$$W_{2m-2} = z_m \qquad W_{2m-1} = z^*_m \qquad \text{for } m > k$$

with $W_{2k} = z_{k+1}$

where z_m and z^*_m are defined in (4.6.1.5) and (4.6.1.6).

2. Create an array D storing the required difference products. Its entries are given by

$$D_{11} = (W_1 - W_2)$$

$$D_{1j} = (W_j - W_1) \qquad \text{for } 2 \leq j \leq 2N-1$$

$$D_{ij} = \begin{cases} (W_j - W_i)D_{i-1,j} & i < j \\ (W_j - W_{i+1})D_{i-1,j} & i \geq j \end{cases}$$

$$\text{for } i = 2,3,\ldots,2N-2; \quad j = 1,2,\ldots,2N-1$$

3. Let $f_i = -W_i^{2N-1}$ for $1 \leq i \leq 2N-1$

4. Let $m = 2N-1$

5. Repeat until m=1

a) $\alpha_m = \sum_{i=1}^{m} \frac{f_i}{D_{m-1,i}}$ OR $\alpha_1 = f_1$

b) $f_i := f_i - \alpha_m w_i^{m-1}$ for $1 \leq i \leq m$

c) $m := m - 1$

Here := represents the replacement of the quantity on the left with the quantity on the right.

It is seen that for a given column each additional entry in the array D requires only one additional multiplication. Thus the number of multiplications needed to fill D is

$$M_D = (2N-1)(2N-2) \qquad (4.6.3.2)$$

Steps 5a and 5b require another

$$M_A = (2N-1)(2N-2) \qquad (4.6.3.3)$$

multiplications and divisions. Thus, the total number of important arithmetic operations required is

$$M_T = 2(2N-1)(2N-2) \approx 8N^2 \qquad (4.6.3.4)$$

On the other hand, Gaussian elimination requires

$$M_G \simeq \frac{1}{3}(2N-1)^3 \simeq \frac{8}{3}N^3 \qquad (4.6.3.5)$$

or, N/3 times as many multiplications and divisions. Note also that less multiplications of W are needed in step 5b than in filling up the matrix in (4.6.1.27) if an additional vector storing the m'th power of W_i is used. Then at each iteration W_i^{m-1} is calculated by merely dividing out one power of W_i.

II. Forced E-pulse

This method can be extended quite easily to the case of a forced E-pulse. It does not require the restriction, as did the analysis of section 4.6.1, that the forced E-pulse have a forcing component consisting of one identical pulse basis function.

Consider the E-pulse shown in Figure 4.4.4.1. It is composed of a forcing component $e^f(t)$ extending from t=0 to $t=T_f$ and an extinction component $e^e(t)$ made up of 2N pulse functions extending from $t=T_f$ to $t=T_e$. This can be written as

$$e(t) = e^f(t) + e^e(t) \qquad (4.6.3.6)$$

where

$$e^e(t) = \sum_{m=1}^{2N} \alpha_m P_m^f(t) g(t-(m-1)\Delta-T_f) \qquad (4.6.3.7)$$

with

$$P_m^f(t) = \begin{cases} 1 & T_f+(m-1)\Delta \le t \le T_f+m\Delta \\ 0 & \text{elsewhere} \end{cases} \qquad (4.6.3.8)$$

The spectrum of this E-pulse is found using (4.4.1.1) to be

$$E(s) = E^f(s) + E^e(s) \qquad (4.6.3.9)$$

where

$$E^f(s) = \int_0^{T_f} e^f(t)e^{-st}dt \qquad (4.6.3.10)$$

and

$$E^e(s) = \int_{T_f}^{T_e} e^e(t)e^{-st}dt$$

$$= \sum_{m=1}^{2N} \alpha_m \int_{T_f+(m-1)\Delta}^{T_f+m\Delta} g(t-(m-1)\Delta-T_f)e^{-st}dt \qquad (4.6.3.11)$$

The integral in (4.6.3.11) can be simplified using the substitution

$$u = t-(m-1)\Delta-T_f \qquad (4.6.3.12)$$

Then

$$E^e(s) = \sum_{m=1}^{2N} \alpha_m \int_0^{\Delta} g(u)e^{-su}e^{-s((m-1)\Delta-T_f)}du \qquad (4.6.3.13)$$

which can be written more simply as

$$E^e(s) = F_1(s)e^{s(\Delta+T_f)}\sum_{m=1}^{2N}\alpha_m e^{-sm\Delta} \qquad (4.6.3.14)$$

where $F_1(s)$ is given by (4.5.4.17). Invoking the transmit domain definition of the E-pulse (4.2.1) and (4.2.2) results in

$$E^f(s_n) + F_1(s_n)e^{s_n(\Delta+T_f)}\sum_{m=1}^{2N}\alpha_m e^{-s_n m\Delta} \qquad 1\leq n\leq N \qquad (4.6.3.15)$$

$$E^f(s_n^*) + F_1(s_n^*)e^{s_n^*(\Delta+T_f)}\sum_{m=1}^{2N}\alpha_m e^{-s_n^* m\Delta} \qquad 1\leq n\leq N \qquad (4.6.3.16)$$

Rearranging yields

$$\sum_{m=1}^{2N}\alpha_m e^{-s_n(m-1)\Delta} = -e^{-s_n T_f}\frac{E^f(s_n)}{F_1(s_n)} \qquad 1\leq n\leq N \qquad (4.6.3.17)$$

$$\sum_{m=1}^{2N}\alpha_m e^{-s_n^*(m-1)\Delta} = -e^{-s_n^* T_f}\frac{E^f(s_n^*)}{F_1(s_n^*)} \qquad 1\leq n\leq N \qquad (4.6.3.18)$$

Writing this in matrix form gives

$$\begin{pmatrix} 1 & W_1 & W_1^2 & \cdots & W_1^{2N-1} \\ 1 & W_2 & W_2^2 & \cdots & W_2^{2N-1} \\ 1 & W_3 & W_3^2 & \cdots & W_3^{2N-1} \\ \vdots & \vdots & \vdots & & \vdots \\ 1 & W_{2N} & W_{2N}^2 & \cdots & W_{2N}^{2N-1} \end{pmatrix} \begin{pmatrix} \alpha_1 \\ \alpha_2 \\ \vdots \\ \alpha_{2N} \end{pmatrix} = \begin{pmatrix} f_1 \\ f_2 \\ \vdots \\ f_{2N} \end{pmatrix} \qquad (4.6.3.19)$$

where

$$f_{2k-1} = -e^{-s_k T_f} \frac{E^f(s_k)}{F_1(s_k)} \qquad (4.6.3.20)$$

$$f_{2k} = -e^{-s_k^* T_f} \frac{E^f(s_k^*)}{F_1(s_k^*)} \qquad (4.6.3.21)$$

The expansion coefficients are now readily obtainable. Either of the algorithms discussed in this section can be used to solve equation (4.6.3.19).

4.7 Nonlinear E-pulse Calculation

The bulk of this chapter has considered E-pulses constructed from a linear combination of basis functions with the amplitudes of the functions representing all the free parameters. This is in essence a linear problem since the unknown amplitudes are described by a system of linear equations. It is also interesting, and informative, to investigate the behavior of E-pulses constructed using a group of free parameters not entirely composed of basis function amplitudes -- leading to a nonlinear problem for E-pulse solution.

The pulse function basis set provides an ideal vehicle for investigating nonlinear solutions. The durations of the pulses are easily incorporated as free parameters in solving (4.4.1.6) and (4.4.1.7). Also, because of the vast amount of pulse function analysis already undertaken in this chapter, there are ample results for comparison.

The very simplest example reveals an interesting connection

between nonlinear E-pulse analysis and the previously defined natural E-pulse. Consider an E-pulse consisting of two delta functions designed to eliminate a single natural mode, as shown in Figure 4.7.1. The first impulse is placed at t=0 and has an amplitude selected as unity. The two remaining parameters -- the height, A, and time position, T, of the second impulse -- are determined by solving the system of two nonlinear equations given through (4.4.1.6) and (4.4.1.7) as

$$1 + A\cos\omega T e^{-\sigma T} = 0 \qquad (4.7.1)$$

$$A\sin\omega T e^{-\sigma T} = 0 \qquad (4.7.2)$$

where $s = \sigma+j\omega$ is the natural frequency of the single mode to be eliminated. The solution is by inspection, and yields from equation (4.7.2)

$$T = \frac{p\pi}{\omega} \qquad p=1,2,\ldots \qquad (4.7.3)$$

and then from (4.2.3)

$$A = e^{\sigma T}(-1)^{p+1} \qquad (4.7.4)$$

This is recognized as merely a one mode natural E-pulse, with duration and amplitudes verified by using (4.6.1.24) and (4.6.1.32). Solving for the duration (the nonlinear variable) is essentially the same step

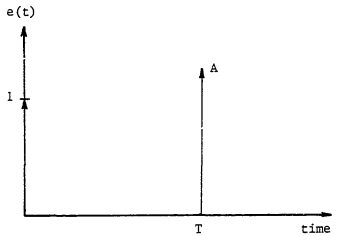

Figure 4.7.1. Two delta function E-pulse. Free parameters are position and amplitude of second impulse.

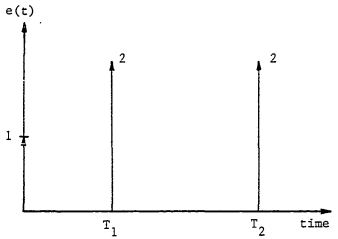

Figure 4.7.2. Three delat function E-pulse. Free parameters are positions of second and third impulses.

necessary to obtain a solution to any natural E-pulse problem (not just pulse function based.) Thus, natural E-pulses represent the solution to a combined linear/nonlinear problem, with the nonlinear problem involving only one variable (T_e), and the linear problem involving the remaining 2N-1 basis function amplitudes (where N is the number of modes to be eliminated) for a total of 2N free parameters, as required.

The next simplest example is to construct a three delta function E-pulse to eliminate one natural mode, as shown in Figure 4.7.2. The first impulse is placed at t=0, and the amplitudes of the impulses are chosen to be 1, 2, and 2, respectively. Equations (4.4.1.6) and (4.4.1.7) then require

$$\cos\omega T_1 e^{-\sigma T_1} + \cos\omega T_2 e^{-\sigma T_2} = -\frac{1}{2} \qquad (4.7.5)$$

$$\sin\omega T_1 e^{-\sigma T_1} + \sin\omega T_2 e^{-\sigma T_2} = 0 \qquad (4.7.6)$$

where T_1 and T_2 are the time position of the second and third impulses. This system of nonlinear equations can only be solved numerically. Depending on the values of σ and ω there may be one solution or more, or perhaps none at all. As an example let $\sigma = -0.1$ and $\omega = 1.0$. Equations (4.7.5) and (4.7.6) can then be solved individually and plotted as shown in Figure 4.7.3. The point where the two solutions intersect gives the solution to the system of two nonlinear equations: $T_1 = 3.76$, $T_2 = 0.90$, and an E-pulse with nonuniformly spaced impulses.

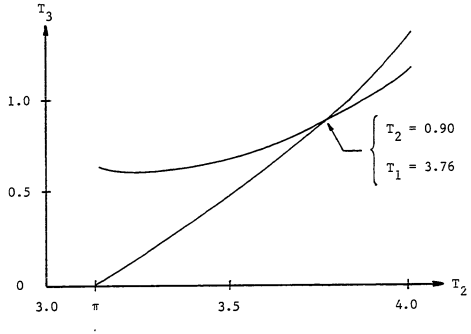

Figure 4.7.3. Graphical solution for impulse positions.

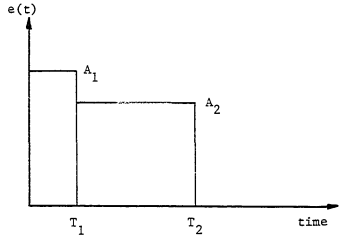

Figure 4.7.4. Two pulse function E-pulse. Free parameters are pulse widths.

A case similar to the first, but more interesting, can be constructed by using two rectangular pulses rather than delta functions. The E-pulse shown in Figure 4.7.4 is composed of two pulses of preselected amplitudes A_1 and A_2. Solving the system of two nonlinear equations described by (4.4.1.6) and (4.4.1.7) results in the durations T_1 and T_2. This is done graphically, as with the last case. To make the results more relevant assume $\sigma = -0.2601$ and $\omega = 2.906$, corresponding to the first (normalized) natural frequency of the thin wire scatterer. Then, letting $A_1 = 1$ and $A_2 = 0.75489$ results in $T_1 = 1.081$ and $T_2 = 2.162$, the results expected from working backwards from the solution for a natural E-pulse. Changing the pulse amplitudes results in different durations, as verified by letting $A_1 = 10$ and $A_2 = 1$, yielding $T_1 = 0.0488$ and $T_2 = 1.845$.

Increasing the amplitude of the first pulse in the two pulse example reveals an intriguing trend. As the amplitude is allowed to increase without bound, the resulting solution for the durations shows that the area under the first pulse and the total duration of the E-pulse waveform approach constants. That is, the E-pulse approaches a waveform consisting of a delta function followed by a singule rectangular pulse. This is shown in Figure 4.7.5. The product of the amplitude and duration of the first pulse is found to be asymptotic to 0.4622, while the duration of the second pulse approaches $T_2 = 1.8211$.

It is interesting to analyze exactly the waveform to which the E-pulse is converging. Consider a delta function followed by a rectangular pulse. Equations (4.4.1.6) and (4.4.1.7) demand

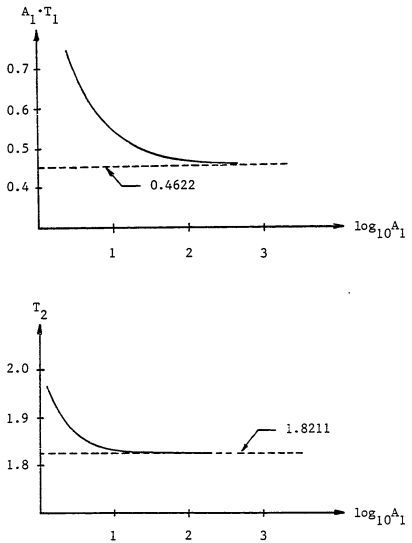

Figure 4.7.5. Convergence of the E-pulse duration, and convergence of the first pulse to an impulse.

$$A_1 + A_2\left\{\frac{e^{-\sigma T_e}}{\sigma^2+\omega^2}(-\sigma\cos\omega T_e + \omega\sin\omega T_e) + \frac{\sigma}{\sigma^2+\omega^2}\right\} = 0 \qquad (4.7.7)$$

$$A_2\left\{\frac{e^{-\sigma T_e}}{\sigma^2+\omega^2}(-\sigma\sin\omega T_e - \omega\cos\omega T_e) + \frac{\omega}{\sigma^2+\omega^2}\right\} = 0 \qquad (4.7.8)$$

where T_e is the duration of the waveform. Analyzing this as a natural E-pulse (that is, the amplitude of the impulse, A_1, and the amplitude of the rectangular pulse, A_2, are not prespecified) requires that the determinant of the matrix of coefficients be zero, resulting in

$$e^{-\sigma T_e}(-\sigma\sin\omega T_e - \omega\cos\omega T_e) + \omega = 0 \qquad (4.7.9)$$

Using the first natural frequency of the thin cylinder, the first two roots to this characteristic equation yield: $T_e = 1.82094$, $A_1/A_2 = 0.46225$, and $T_e = 2.48267$, $A_1/A_2 = -0.52698$. The first solution is recognized as the waveform to which the two pulse E-pulse appears to converge, verifying the earlier observations.

Solutions to more complex nonlinear E-pulse problems cannot be solved efficiently using the graphical method described earlier. It is necessary to employ a computer routine to solve the resulting system of nonlinear equations. A program has been developed which incorporates such a routine, allowing the specification of pulse amplitudes and solving for the pulse widths. As an example, consider the construction of a four pulse E-pulse designed to eliminate the first two natural modes of the thin cylinder. Specifying the amplitudes as $A_1 = 0.721$, $A_2 = 0.527$, $A_3 = 0.497$, and $A_4 = 0.45$ results in $T_1 = 0.523$,

$T_2 = 1.046$, $T_3 = 1.569$, and $T_4 = 2.092$. This is the expected solution obtained by working backwards from the solution to the natural E-pulse, and is plotted in Figure 4.7.6. However, choosing $A_1 = 1$, $A_2 = 0.58$, $A_3 = 0.49$, and $A_4 = 0.45$ results in the E-pulse shown in Figure 4.7.7, with duration $T_e = 2.0063$. Lastly, choosing $A_1 = 355$ and keeping $A_2 = 0.58$, $A_3 = 0.49$, and $A_4 = 0.45$ results in the E-pulse plotted in Figure 4.7.8 with duration 1.9353. Increasing A_1 further results again in the first pulse converging to a delta function, with the following pulse durations also converging to specific values. It is quite interesting to see how the last three pulses define a shape that changes very little as the first pulse amplitude is increased without bound. With their amplitudes fixed, the durations take on values which seem to mold the pulses to this particular shape. This phenomenon will be considered in more detail in chapter five when uniqueness of the thin cylinder E-pulse waveform is discussed.

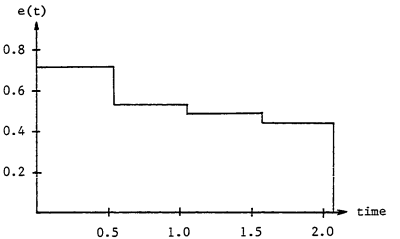

Figure 4.7.6. Two mode natural E-pulse reconstructed via nonlinear E-pulse analysis.

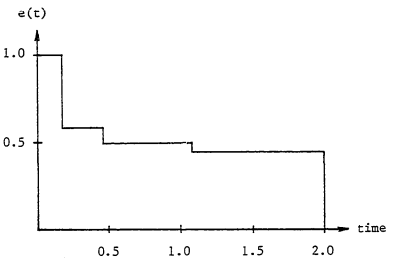

Figure 4.7.7. Two mode E-pulse synthesized via nonlinear E-pulse analysis.

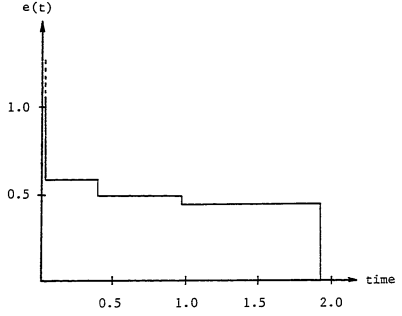

Figure 4.7.8. Two mode E-pulse synthesized via nonlinear E-pulse analysis.

CHAPTER 5

E-PULSE DISCRIMINATION

5.1 Introduction

The previous chapter considered the construction of various types of E-pulses using many different kinds of basis sets. This chapter will continue the investigation of the E-pulse concept, applying it to discrimination between differing theoretical targets.

E-pulses constructed from two different basis sets will be considered in detail. The first, the rectangular pulse basis set, is very easy to use, while the second, the damped sinusoid basis set (and its relative, the Fourier cosine basis set) has potentially useful frequency domain properties. They will be used to construct various E-pulses and single mode excitation waveforms which will in turn be convolved with theoretical thin cylinder target responses, and a comparison will be made between the results.

5.2 The Thin Cylinder Target

Verification of the E-pulse concept and experimentation with various E-pulse waveforms is most easily carried out using a theoretical response. The SEM analysis of a thin conducting cylinder has been carried out by various authors [14], [17] and its scattered field impulse response becomes an excellent guinea pig for testing E-pulse

merit.

The geometry of a thin circular cylindrical scatterer of radius 'a' and length L and its orientation with respect to a transient excitation field is shown in Figure 5.2.1. The angle θ represents the target aspect for the case of backscattered reception. Solving equation (2.3.3) results in the natural frequencies of this scatterer. These have been calculated by Tesche [14] within the bounds of the thin wire approximation (see chapter 7) and are found to occur in "layers" in the complex frequency plane. The lower portion of the first layer makes the most important contibution to the late-time response since it contains the frequencies with the smallest real parts. That is, the modes corresponding to this range of frequencies will damp the slowest. The values of the first ten of these first layer frequencies (one half of a set of complex conjugate pairs) are also shown in Figure 5.2.1, corresponding to L/a = 200. They are normalized by $\pi c/L$, where c is the speed of light in free space.

The backscattered field response of the thin cylinder target is calculated by determining the coupling coefficients (2.3.6). The result is, of course, dependent upon the aspect angle θ. Assuming plane wave excitation as in (2.4.1), the magnitude of the far zone backscattered electric field is found using (2.2.12) to be

$$E^{bs}(\vec{r},s) = E_o E(s) \frac{\sin^2\theta}{2\log(L/a)-1} \frac{L}{r} \sum_{n=1}^{N} \frac{1}{(n\pi)^2} \frac{sL}{c} \times$$

$$\times \left\{ \frac{1-(-1)^n e^{-sT}}{\left(\frac{sT}{n\pi}\right)^2 + 1} \right\}^2 \left\{ \frac{s/s_n}{s-s_n} + \frac{s/s_n^*}{s-s_n^*} \right\} \qquad (5.2.1)$$

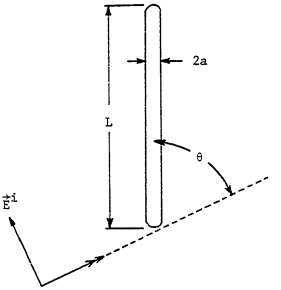

n	$s_n/(c\pi/L)$
1	-0.0828 + j0.9251
2	-0.1212 + j1.912
3	-0.1491 + j2.884
4	-0.1713 + j3.874
5	-0.1909 + j4.854
6	-0.2080 + j5.845
7	-0.2240 + j6.829
8	-0.2383 + j7.821
9	-0.2522 + j8.807
10	-0.2648 + j9.800

Figure 5.2.1. Orientation for thin cylinder excitation and first ten natural frequencies.

where $\vec{r}$ is the position vector measured in a coordinate system local to the target, $r = |\vec{r}|$, the one way transit time is

$$T = \frac{L}{c}\cos\theta \qquad (5.2.2)$$

and the class-2 coupling coefficients have been used (see [17]). Here also, E(s) is the Laplace transform of the incident field waveform e(t). In the late-time equation (5.2.1) can be written in the time domain as

$$E^{bs}(\vec{r},t) = E_o \frac{\sin^2\theta}{2\log(L/a)-1} \frac{L}{r} \sum_{n=1}^{N} \left\{ E(s_n)C_n(s_n)e^{s_n(t-r/c)} + \right.$$

$$\left. + E(s_n^*)C_n(s_n^*)e^{s_n^*(t-r/c)} \right\} \qquad (5.2.3)$$

where

$$C_n(s) = \frac{1}{(n\pi)^2} \frac{sL}{c} \left\{ \frac{1-(-1)^n e^{-sT}}{\left(\frac{sT}{n\pi}\right)^2 + 1} \right\}^2 \qquad (5.2.4)$$

Now, using

$$C_n(s_n^*) = C_n^*(s_n) \qquad E(s_n^*) = E^*(s_n) \qquad (5.2.5)$$

gives

$$E^{bs}(\vec{r},t) = E_o \frac{L}{r} \frac{\sin^2\theta}{2\log(L/a)-1} \sum_{n=1}^{N} 2|E(s_n)||C_n(s_n)| \times$$

$$\times e^{\sigma_n(t-r/c)}\cos\left(\omega_n(t-r/c) + \zeta_n\right) \qquad (5.2.6)$$

where

$$\zeta_n = \tan^{-1} \frac{\mathrm{Im}\{E(s_n)C_n(s_n)\}}{\mathrm{Re}\{E(s_n)C_n(s_n)\}} \qquad (5.2.7)$$

From equation (5.2.1) it is possible to identify the backscatter far zone transfer function of the thin wire target

$$H(s,\theta) = \sum_{n=1}^{N} \frac{1}{(n\pi)^2} \frac{sL}{c} \left(\frac{1-(-1)^n e^{-sT}}{\left(\frac{sT}{n\pi}\right)^2 + 1} \right)^2 \left(\frac{s/s_n}{s-s_n} + \frac{s/s_n^*}{s-s_n^*} \right) \qquad (5.2.8)$$

so that the time domain far zone backscattered field can be represented as

$$E^{bs}(\vec{r},t) = E_o \frac{\sin^2\theta}{2\log(L/a)-1} \frac{L}{r} e(t)*h(t,\theta) \qquad (5.2.9)$$

where

$$h(t,\theta) = L^{-1}\{H(s,\theta)\} \qquad (5.2.10)$$

is the impulse response of the target in the backscatter direction (i. e. the response to $e(t) = \delta(t)$.)

As expected, the impulse response is a function of target aspect, while the natural frequencies used to construct the response are not. Performing the Laplace inversion in (5.2.10) allows the calculation of the thin cylinder impulse response in both the early and late-time regions. Although the early-time response is probably incorrect (due to the questionable validity of the class-2 coupling

coefficients) it does provide a helpful indication of where late-time begins. (It is of course remembered that the early-time response was not used in the development of the E-pulse theory.)

5.3 Sampled Point Convolution

To demonstrate the validity of the E-pulse concept it is necessary to perform the time domain convolution given in (4.4.2). Since a measured response is sampled at discrete points in time it is tempting to use standard discrete point convolution. This corresponds to using rectangular rule integration, and although it might be well motivated in the presence of experimental noise, it does not represent sufficient accuracy when using theoretical data where "perfect" extinction is to be expected. It also neglects the fact that the E-pulse waveform is known explicitly.

More accurate convolution requires an interpolation between the points of the sampled response. Standard techniques make use of the sampling theorem which allows the exact reconstruction of a bandlimited signal from a finite sampling density. However, the natural mode response of a target is not bandlimited and, practically speaking, it is very difficult to estimate the highest frequency excited by the incident wave or passed by the measurement system. So, a different method of interpolation is needed.

A very common method of interpolation uses cubic splines. Here a cubic polynomial is passed between adjoining sample points in the measured response, and convolution reduces to Simpson's $\frac{3}{8}$ rule integration [48]. A much simpler routine involves replacing the cubic

by a straight line. Then the interpolation becomes linear, and convolution reduces to trapezoidal rule integration. The amount of increase in accuracy using trapezoidal rule integration over rectangular rule integration is quite substantial. There is another large jump in accuracy in going to Simpson's rule, but the complexity added does not justify its implementation. Thus, this section will consider only linear interpolation.

Two cases of trapezoidal rule convolution will be considered separately. For each it is first necessary to represent the measured response r(t) in terms of linear interpolation coefficients. This is done by letting

$$r(t) = m_i t + b_i \qquad t_i \leq t \leq t_{i+1} \tag{5.3.1}$$

where

$$m_i = \frac{r(t_{i+1}) - r(t_i)}{DT} \tag{5.3.2}$$

$$b_i = r(t_i) - m_i t_i \tag{5.3.3}$$

and

$$t_i = (i-1)DT \tag{5.3.4}$$

where DT is the time between sampled points.

Now consider the separate cases of the rectangular pulse

function based E-pulse and the damped sinusoid based E-pulse.

I. Rectangular Pulse Based E-pulse

The rectangular pulse based E-pulse waveform is given by

$$e(t) = \sum_{m=1}^{M} \alpha_m P_m(t) \tag{5.3.5}$$

where

$$P_m(t) = \begin{cases} 1 & (m-1)\Delta \leq t \leq m\Delta \\ 0 & \text{elsewhere} \end{cases} \tag{5.3.6}$$

Thus, the convolution of the E-pulse with the measured response is just

$$c(t) = e(t) * r(t) = \int_0^{T_e} \sum_{m=1}^{M} P_m(t')r(t-t')dt'$$

$$= \sum_{m=1}^{M} \alpha_m \int_{(m-1)\Delta}^{m\Delta} r(t-t')dt' \tag{5.3.7}$$

This is simplified by employing the change of variables

$$\tau = t - t' \tag{5.3.8}$$

Then

$$c(t) = \sum_{m=1}^{M} \alpha_m \int_{t-m\Delta}^{t-(m-1)\Delta} r(\tau)d\tau \tag{5.3.9}$$

By substituting the linear approximation for r(t) given by (5.3.1), the integral in (5.3.9) can also be written as

$$c(t) = \sum_{m=1}^{M} \alpha_m \left[I_{k_{1m}-1}(t-m\Delta, \tau_{k_{1m}}) + I_{k_{2m}}(\tau_{k_{2m}}, t-(m-1)\Delta) + \sum_{i=k_{1m}}^{k_{2m}-1} I_i(\tau_i, \tau_{i+1}) \right] \qquad (5.3.10)$$

where

$$I_i(\tau_1,\tau_2) = \int_{\tau_1}^{\tau_2} (m_i\tau + b_i)d\tau$$

$$= (\tau_2-\tau_1)\left(b_i + \frac{m_i}{2}(\tau_2+\tau_1)\right) \qquad (5.3.11)$$

The values of k_{1m} and k_{2m} used in the summation in (5.3.10) are given by

$$k_{1m} = 2 + \text{int}\left((t-m\Delta)/DT\right) \qquad (5.3.12)$$

$$k_{2m} = 1 + \text{int}\left((t-(m-1)\Delta)/DT\right) \qquad (5.3.13)$$

where int(x) represents the integer part of the real number x.

Two important notes are in order. First, it was assumed in this analysis that the first sampled point of r(t) occurs at t=0. If this is not the case it is merely necessary to shift the origin of the response. Second, if τ_1 or τ_2 are ever less than zero they should be set to zero to obtain the expected contribution from r(t).

II. Damped Sinusoid Based E-pulse

For this case the E-pulse waveform can be written as

$$e(t) = \sum_{m=1}^{M} \alpha_m e^{\tilde{\sigma}_m t} \cos(\tilde{\omega}_m t + \tilde{\phi}_m) \tag{5.3.14}$$

and so the convolution of the E-pulse with the measured response becomes

$$c(t) = e(t) * r(t) = \int_0^{T_e} \left(\sum_{m=1}^{M} \alpha_m e^{\tilde{\sigma}_m t'} \cos(\tilde{\omega}_m t' + \tilde{\phi}_m) \right) r(t-t')dt' \tag{5.3.15}$$

By the change of variables (5.3.8) this can be written as

$$c(t) = \sum_{m=1}^{M} \alpha_m \int_{t-T_e}^{t} e^{\tilde{\sigma}_m (t-\tau)} \cos(\tilde{\omega}_m (t-\tau) + \tilde{\phi}_m) r(\tau) d\tau \tag{5.3.16}$$

Substituting the linear approximation for r(t) results in

$$c(t) = \sum_{m=1}^{M} \alpha_m \left[I_{m,k_1-1}(t-T_e, \tau_{k_1}) + I_{m,k_2}(\tau_{k_2}, t) + \sum_{i=k_1}^{k_2-1} I_{m,i}(\tau_i, \tau_{i+1}) \right] \tag{5.3.17}$$

where

$$I_{m,i}(\tau_1, \tau_2) = \int_{\tau_1}^{\tau_2} (m_i \tau + b_i) e^{\tilde{\sigma}_m (t-\tau)} \cos(\tilde{\omega}_m (t-\tau) + \tilde{\phi}_m) d\tau \tag{5.3.18}$$

The integral in (5.3.18) is most easily calculated using complex

algebra

$$I_{n,i}(\tau_1,\tau_2) = \mathrm{Re}\{\int_{\tau_1}^{\tau_2}(m_i\tau+b_i)e^{\tilde{\sigma}_n(t-\tau)}e^{j(\tilde{\omega}_n(t-\tau)+\tilde{\phi}_n)}d\tau\}$$

$$= \mathrm{Re}\{e^{(\tilde{s}_n t+j\tilde{\phi}_n)}\left(I_1(\tau_2)+I_2(\tau_2)-I_1(\tau_1)-I_2(\tau_1)\right)\} \quad (5.3.19)$$

where $\tilde{s}_n = \tilde{\sigma}_n + j\tilde{\omega}_n$ and

$$I_1(\tau) = \begin{cases} \dfrac{e^{-\tilde{s}_n\tau}}{-\tilde{s}_n} & \tilde{s}_n \neq 0 \\ \tau & \tilde{s}_n = 0 \end{cases} \quad (5.3.20)$$

and

$$I_2(\tau) = \begin{cases} \dfrac{e^{-\tilde{s}_n\tau}}{\tilde{s}_n^2}(-\tilde{s}_n\tau - 1) & \tilde{s}_n \neq 0 \\ \dfrac{\tau^2}{2} & \tilde{s}_n = 0 \end{cases} \quad (5.3.21)$$

Also, the values of k_1 and k_2 used in equation (5.3.17) are given by

$$k_1 = 2 + \mathrm{int}\left((t-T_e)/DT\right) \quad (5.3.22)$$

$$k_2 = 1 + \mathrm{int}\left(t/DT\right) \quad (5.3.23)$$

Note that it is again assumed that the first sample occurs at t=0 and that τ_1 and τ_2 should not be allowed to be less than zero.

5.4 Quantifying E-pulse Discrimination

When using E-pulse waveforms it is usually quite difficult to tell when one waveform discriminates "better" than another. If the response data is experimental the decision must remain subjective. However, in the case of an artificially constructed response, it is possible to quantify discrimination explicitly.

Consider the case of the thin cylinder backscattered field response given in (5.2.6). If the incident field waveform e(t) is synthesized as an E-pulse for a particular thin cylinder target, the transform representation E(s) will be zero at the important natural frequencies of that target, and the time domain scattered field will be zero in the late-time. However, if the target is not the one expected it will have different natural frequencies than expected. These will be excited by e(t), and the backscattered field response will have nonzero late-time energy. Now, more than one E-pulse can be constructed to eliminate the natural frequencies of the expected target, and each will excite the modes of the unexpected target. The question is, how to decide which E-pulse leads to "best" discrimination between the targets?

A simple and informative measure of this discrimination is given by the value of the late-time energy of the scattered field response (or, equivalently, the convolved response.) In essence, the energy measures the "amount" of information that is available for analysis. If the target is the one expected the energy in the late-time response is zero. If the target is not the one expected then the energy will be nonzero (and finite.) The E-pulse which discriminates

best is then defined as the one which results in the greatest value of late-time energy.

In the spirit of the classical radar cross section, the discrimination area, D, can be defined as the ratio of the signal energy of the late-time far zone scattered field response waveform in a particular direction to the signal energy in the incident field waveform, multiplied by the distance to the target squared. The normalization is important since the value of the scattered field waveform signal energy is dependent upon the incident field waveform signal energy. Thus, backscatter discrimination area is given by

$$D_{bs} = 4\pi \lim_{r\to\infty} r^2 \frac{\int_{T_E+r/c}^{\infty} \frac{1}{E_o^2} |\vec{E}^{bs}(\vec{r},t)|^2 dt}{\int_0^{T_e} (e(t))^2 dt} = 4\pi \lim_{r\to\infty} r^2 \frac{\varepsilon_{bs}}{\varepsilon_e} \quad (5.4.1)$$

Note that D has dimension of area (as does radar cross section) and is an important function of target aspect and E-pulse waveform shape.

The discrimination area is easily calculated for the case of the thin cylinder target using the backscatter response given in (5.2.6). The late-time signal energy in this response waveform is given by

$$\varepsilon_{bs} = \frac{1}{E_o^2} \int_{T_E+r/c}^{\infty} |\vec{E}^{bs}(\vec{r},t)|^2 dt$$

$$= \frac{L^2}{r^2} \int_{T_E}^{\infty} \left\{ \frac{\sin^2\theta}{2\log(L/a)-1} \right\}^2 \left\{ \sum_{n=1}^{N} Q_n e^{\sigma_n t} \cos(\omega_n t+\zeta_n) \right\}^2 dt \quad (5.4.2)$$

where Q_n is defined as

$$Q_n = 2|E(s_n)||C_n(s_n)| \quad (5.4.3)$$

Multiplying out the square in (5.4.2) gives

$$e_{bs} = \frac{L^2}{r^2} \left\{ \frac{\sin^2\theta}{2\log(L/a)-1} \right\}^2 \sum_{i=1}^{N} \sum_{j=1}^{N} Q_i Q_j \{-I_{i,j}(T_E)\} \quad (5.4.4)$$

where

$$I_{i,j}(t) = \int_{T_E}^{\infty} \left(e^{\sigma_i t}\cos(\omega_i t+\zeta_i)\right)\left(e^{\sigma_j t}\cos(\omega_j t+\zeta_j)\right)dt \quad (5.4.5)$$

As in the convolution calculations of section 5.3, the integral $I_{i,j}$ is quite messy to calculate. A great deal of simplification is obtained again by using complex arithmetic. Expanding the damped cosine functions in terms of complex exponentials and integrating yields

$$I_{i,j}(t) = \tfrac{1}{2}\mathrm{Re}\begin{cases} e^{j(\zeta_i+\zeta_j)}\dfrac{e^{(s_i+s_j)t}}{s_i+s_j} + e^{j(\zeta_i-\zeta_j)}\dfrac{e^{(s_i+s_j^*)t}}{s_i+s_j^*} & s_i \neq 0 \text{ or } s_j \neq 0 \\ e^{j(\zeta_i+\zeta_j)}t + e^{j(\zeta_i-\zeta_j)}t & s_i = s_j = 0 \end{cases} \quad (5.4.6)$$

where $s_i = \sigma_i + j\omega_i$.

The signal energy in the incident E-pulse waveform is easily calculated. For the case of the rectangular pulse function based E-pulse this is just

$$\varepsilon_e = \int_0^{T_e} e^2(t)dt = \int_0^{T_e} \left[\sum_{m=1}^{M} \alpha_m P_m(t) \right]^2 dt \qquad (5.4.7)$$

or, simply

$$\varepsilon_e = \Delta \sum_{m=1}^{M} \alpha_m^2 \qquad (5.4.8)$$

where Δ is the pulse width.

For the case of the damped sinusoid based E-pulse, the signal energy is

$$\varepsilon_e = \int_0^{T_e} \left[\sum_{m=1}^{M} \alpha_m e^{\tilde{\sigma}_m t} \cos(\tilde{\omega}_m t + \tilde{\phi}_m) \right]^2 dt \qquad (5.4.9)$$

Integrating gives, analogous to (5.4.4)

$$\varepsilon_e = \sum_{i=1}^{M} \sum_{j=1}^{M} \alpha_i \alpha_j \left[I_{i,j}(T_e) - I_{i,j}(0) \right] \qquad (5.4.10)$$

where $I_{i,j}$ is given by equation (5.4.6) with $\zeta \to \tilde{\phi}$ and $s \to \tilde{s}$.

The discrimination area as defined is useful in measuring many things. As mentioned earlier, its major purpose is to measure the relative merit of E-pulses which, while eliminating the same set of

natural frequencies, have different waveform shapes. But it can also measure the sensitivity of E-pulse discrimination to target aspect, target size, and the actual number of modes present in the measured response.

5.5 Examples of E-pulse Discrimination

This section will investigate thin cylinder E-pulse discrimination under a variety of circumstances including the presence of random noise and spurious natural mode content. It will also consider single mode excitation and discrimination based on both the thin cylinder target and results from the measurement of a more complex aircraft target model. Lastly, application of frequency domain "shaping" for imroved single mode and E-pulse discrimination will be addressed.

5.5.1 E-pulse Discrimination

Verification of the E-pulse concept is easily accomplished by convolving an E-pulse synthesized to eliminate the natural modes of a thin cylinder target with the impulse response of the target. Figure 5.5.1.1 displays the impulse response of a thin cylinder of length L and radius a=L/200 oriented at $\theta=60^{o}$, constructed via equation (5.2.10) at 600 points in time using the first five natural frequencies of Figure 5.2.1. Note the expected early time region extending from t=0 to t=2T, where the one way transit time of the cylinder is $T=\cos(60^{o})$ L/c = 0.5 L/c. This forced period is followed immediately by the natural response.

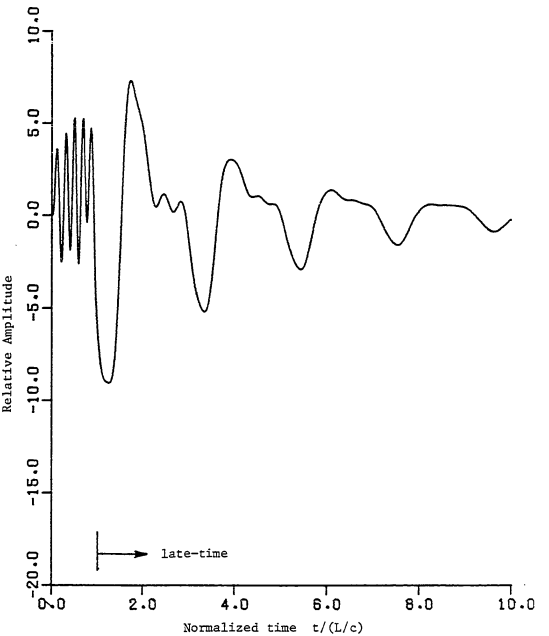

Figure 5.5.1.1. Impulse response of a thin cylinder oriented at $\theta=60^{\circ}$, constructed using first five natural frequencies.

Natural and forced rectangular pulse function based E-pulses have been synthesized using the analysis of section 4.6 to eliminate the first five natural modes of the thin cylinder response, and are shown in Figures 5.5.1.2 through 5.5.1.5. Figure 5.5.1.2 displays a natural E-pulse of minimum duration while Figure 5.5.1.3 shows a natural DC E-pulse of minimum duration. A forced E-pulse of duration T_e=2.5 L/c can be seen in Figure 5.5.1.4 and a forced E-pulse of duration T_e=1.8 L/c is shown in Figure 5.5.1.5. As observed in the previous chapter, all of these E-pulses are fairly smooth, except the shorter forced E-pulse which exhibits a highly oscillatory behavior. Also, each E-pulse has a DC component except the natural DC E-pulse.

The spectra of the four E-pulses are calculated using equation (4.5.4.22) and their magnitude is plotted in Figures 5.5.1.6 and 5.5.1.7 versus ω for σ=-0.2601 c/L. It is seen that each spectrum has the expected zero at the first natural frequency of the thin cylinder, s_1 = -0.2601+j2.906 c/L. It is also seen that while the spectra are not zero at the values of ω corresponding to the higher order modes of the cylinder, they are very small. This shows that the E-pulses are not terribly sensitive to the value of the real part of the natural frequencies, and should be more sensitive discriminators of ω as opposed to σ. It is also very interesting to note that due to the periodic nature of the spectra (a result of the "windowing" or finite duration requirement) there are minimum points at values of ω higher than the largest value of the imaginary part of the frequencies to be eliminated. This indicates that modes other than those intended may be (nearly) eliminated.

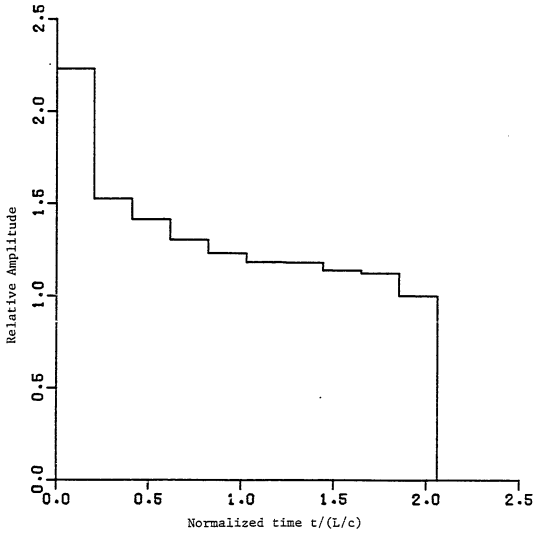

Figure 5.5.1.2. Natural E-pulse of minimum duration synthesized to eliminate the first five modes of the thin cylinder.

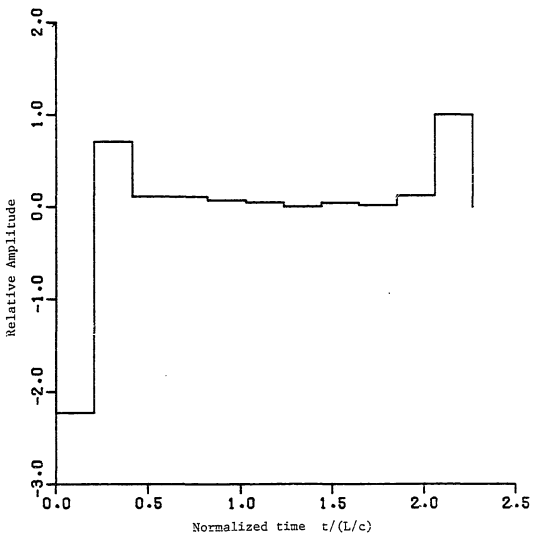

Figure 5.5.1.3. Natural DC E-pulse of minimum duration synthesized to eliminate the first five modes of the thin cylinder.

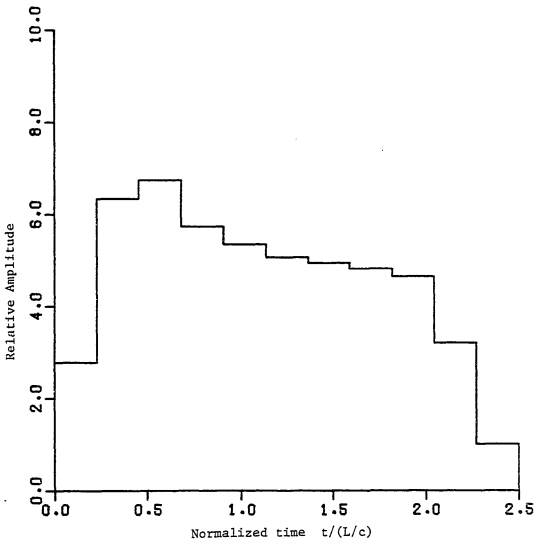

Figure 5.5.1.4. Forced E-pulse of duration T_e=2.5 L/c synthesized to eliminate the first five modes of the thin cylinder.

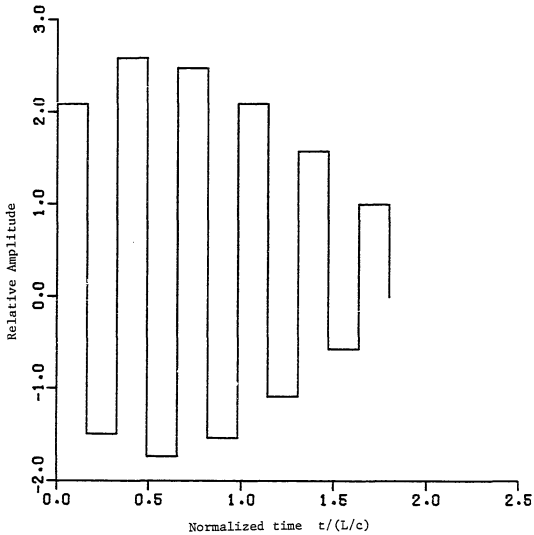

Figure 5.5.1.5. Forced E-pulse of duration T_e=1.8 L/c synthesized to eliminate the first five modes of the thin cylinder.

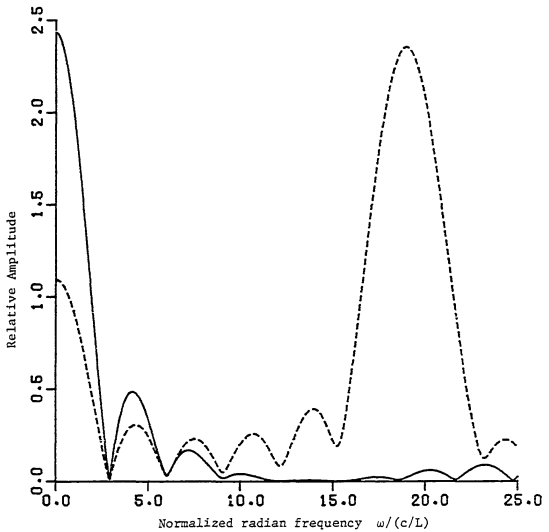

Figure 5.5.1.6. Spectra of forced E-pulses of duration T_e=2.5 L/c (solid line) and T_e=1.8 L/c (dotted line) for σ=-0.2601 c/L.

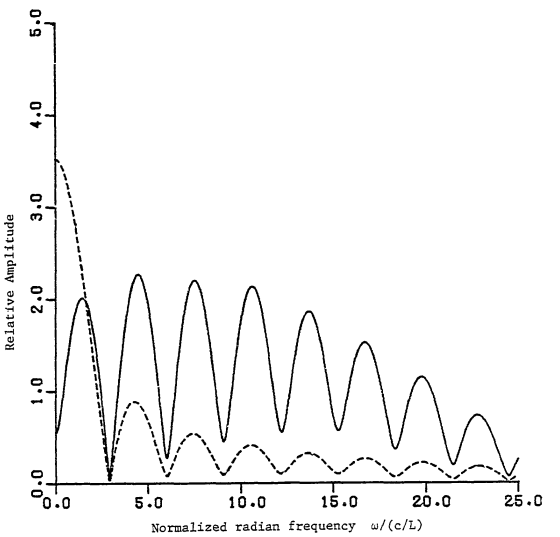

Figure 5.5.1.7. Spectra of natural E-pulse (dotted line) and natural DC E-pulse (solid line) for σ=-0.2601 c/L.

Perhaps the most important characteristic of the E-pulse spectra is the distribution of the peaks. The natural E-pulse and the forced E-pulse of longer duration both have a majority of their energy located near $\omega=0$. On the other hand, the forced E-pulse of shorter duration has most of its energy located at a frequency higher than the largest frequency to be eliminated. This is actually the frequency of oscillation of the E-pulse waveform. Experience has shown that as the duration of this E-pulse is reduced, the form of the oscillation remains the same -- that is, the pulse amplitudes alternate in sign. Thus, the frequency of oscillation increases and the peak moves farther up in frequency. Lastly, the spectrum of the natural DC E-pulse appears to have no large local peaks. Rather, there is an even spread of peaks and valleys. It will become apparent that this latter spectrum shape is the most desired for discrimination purposes.

Verification of the E-pulse concept is shown in Figure 5.5.1.8. The natural E-pulse of Figure 5.5.1.2 has been convolved (using the technique of section 5.3) with the thin cylinder impulse response of Figure 5.5.1.1. The result is seen to be composed of a nonzero early-time convolved response followed by a null late-time period. Thus, the E-pulse has succeeded in eliminating the five natural modes of the thin cylinder impulse response. Note that the late-time period begins at $t=T_e+2T$, as required by the convolution. The nonzero early-time convolved response period can be very useful by providing a comparison for determining the quality of the annulled portion of the response in the case of an imperfect "extinction" (due to noise, errors in the

natural frequencies, etc.)

Discrimination between differing thin cylinder targets is demonstrated by convolving the natural E-pulse of Figure 5.5.1.2 with the impulse response of a target 5% longer and a target 10% longer. The results are also shown in Figure 5.5.1.8. It is seen that while the late-time response of the expected target has been annulled, the responses of the differing targets are nonzero over the same period. Discrimination between the correct and incorrect targets is accomplished by differentiating between null and nonzero late-time convolved responses. Similar results are shown in Figures 5.5.1.9 and 5.5.1.10 for the forced E-pulses. Again, discrimination between the expected target and a target 5% longer is accomplished by a comparison of the annulled and nonzero late-time convolved responses. It appears that the natural E-pulse results in the greatest amount of late-time energy for the 5% longer target, and thus the greatest amount of discrimination.

Sensitivity of E-pulse performance to the presence of random noise is investigated by perturbing each point of the thin cylinder impulse response of Figure 5.5.1.1 by a random amount not exceeding 10% of the maximum value of the waveform (which is equivalent to adding a waveform consisting of uncorrelated random noise.) The result is shown in Figure 5.5.1.11. An attempt is then made to extinguish this noisy impulse response by convolving with it the forced and natural E-pulses discussed earlier. As expected, none of the resulting convolved responses as shown in Figures 5.5.1.12 through 5.5.1.14 reveals an identically zero late-time period. Instead, each results

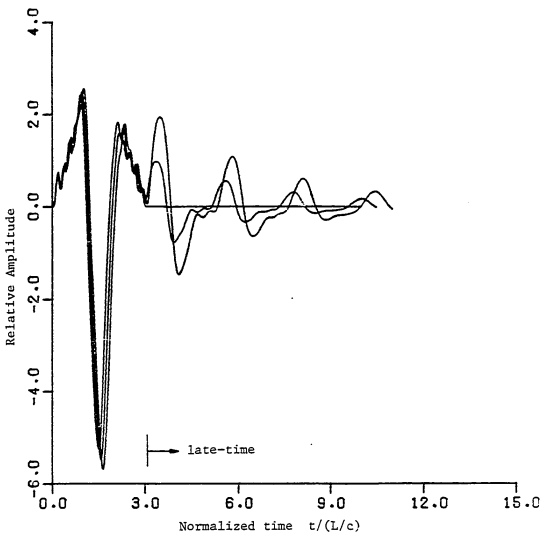

Figure 5.5.1.8. Convolution of natural E-pulse with impulse response of thin cylinder of expected length, and with impulse responses of cylinders 5% and 10% longer.

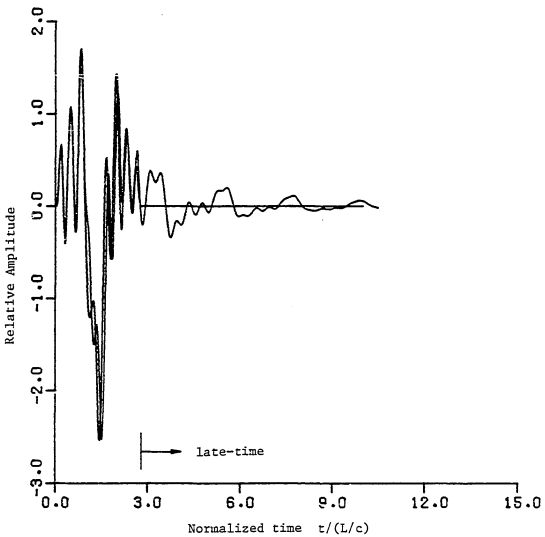

Figure 5.5.1.9. Convolution of forced E-pulse of duration T_E=1.8 L/c with impulse response of thin cylinder of expected length, and with impulse response of a cylinder 5% longer.

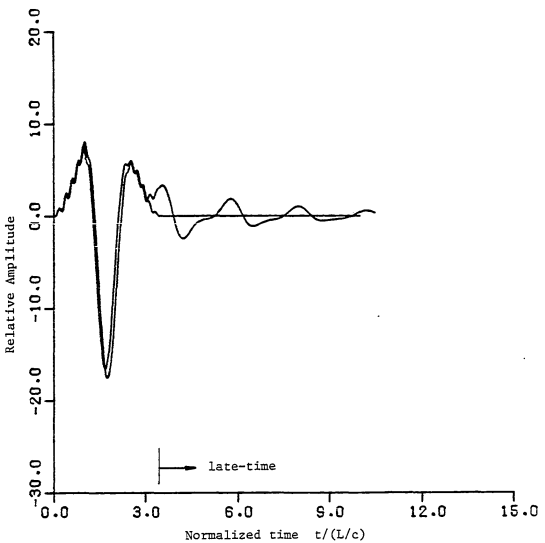

Figure 5.5.1.10. Convolution of forced E-pulse of duration T_e=2.5 L/c with impulse response of thin cylinder of expected length, and with impulse response of a cylinder 5% longer.

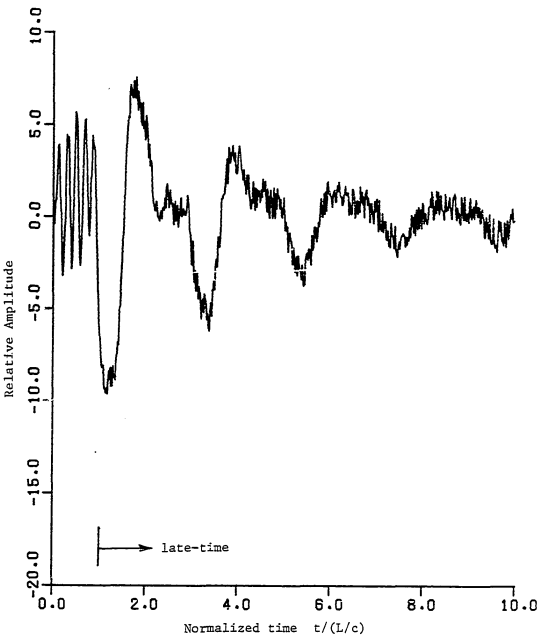

Figure 5.5.1.11. Five mode 60° thin cylinder impulse response with 10% random noise added.

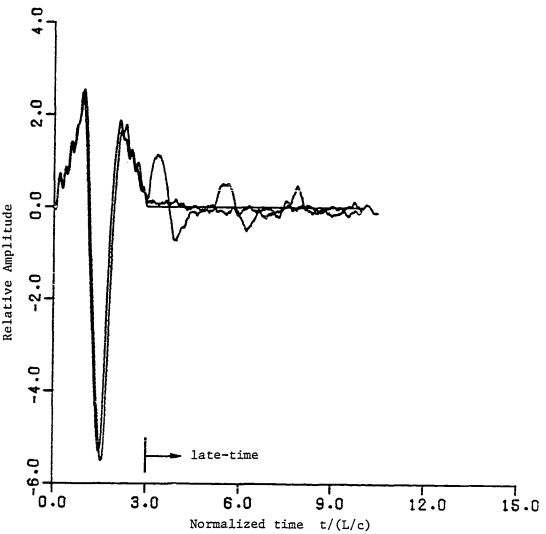

Figure 5.5.1.12. Convolution of natural E-pulse with noisy impulse response of thin cylinder of expected length, and with noisy impulse response of a cylinder 5% longer.

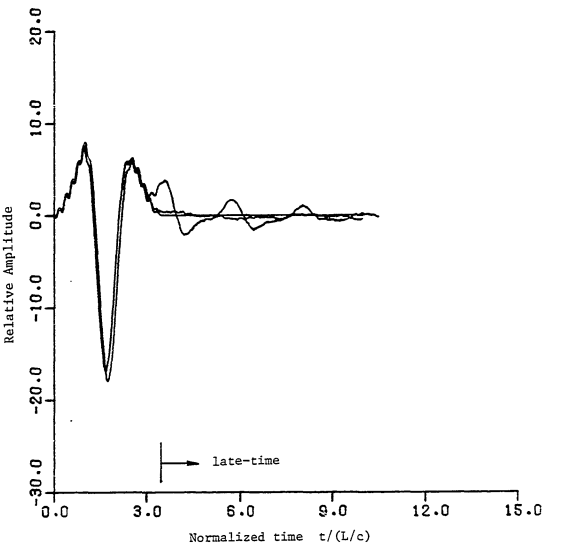

Figure 5.5.1.13. Convolution of forced E-pulse of duration T_e=2.5 L/c with noisy impulse response of thin cylinder of expected length, and with noisy impulse response of a cylinder 5% longer.

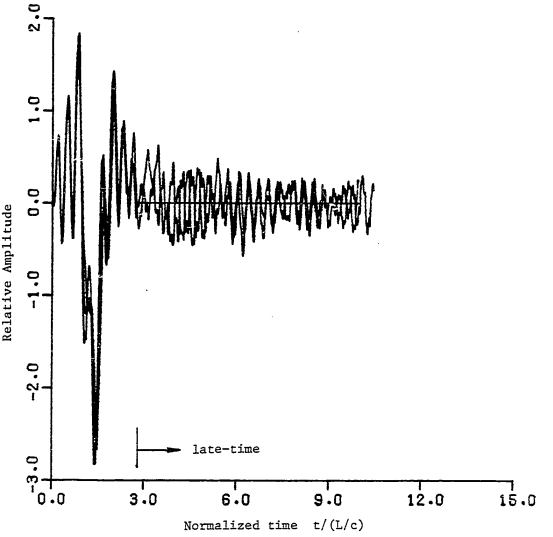

Figure 5.5.1.14. Convolution of forced F-pulse of duration T_e=1.8 L/c with noisy impulse response of thin cylinder of expected length, and with noisy impulse response of a cylinder 5% longer.

in a distribution of noise about the zero line. Using the early-time region for comparison, a relatively large amount of noise on the impulse response waveform appears to produce a much smaller amount on the convolved responses. This is not surprising since the convolution can be viewed as a smoothing process (as long as the E-pulse is relatively smooth), averaging and thus reducing the original noise content. Also plotted with these curves is the convolution of the E-pulses with a noisy impulse response of a 5% longer cylinder. For the case of the natural E-pulse and the forced E-pulse of longer duration, it is quite easy to separate the effects of noise and target length sensitivity, suggesting that random noise will not interfere with target discrimination. For the case of the shorter duration forced E-pulse, however, all potential target discrimination capability appears to be lost in the noise.

The behavior of the various convolved responses in the presence of random noise is easily explained by examining the spectra of the E-pulses. Adding noise to the impulse response of Figure 5.5.1.1 can be viewed as perturbing the values of the natural frequencies contained in the response. Since the natural E-pulse and the forced E-pulse of longer duration have their major spectral content at low frequencies, they will excite with greatest amplitude the smallest perturbed frequency in the noisy response upon convolution. This is indeed the behavior observed in Figures 5.5.1.12 and 5.5.1.13, where the noisy waveform oscillates with low frequency about the zero line. In contrast, the forced E-pulse of shorter duration has its greatest spectral content at a much higher frequency. This is reflected in

Figure 5.5.1.14, where the noise is observed to be rapidly oscillating about the zero line. The larger amplitude of this noise is due in part to the lack of smoothness of the E-pulse waveform, which prevents an effective averaging of the noise content.

It was mentioned earlier that the natural E-pulse appeared to result in the greatest amount of discrimination between the expected and longer target. This can be investigated in more depth by calculating the discrimination area D (as described in section 5.4) as a function of target length. Figure 5.5.1.15 shows normalized backscatter discrimination area D/L^2 (L = cylinder length) plotted against normalized target length for $\theta=60^{\circ}$, using the natural E-pulse and the forced E-pulse of shorter duration. For each case there is an expected zero at a normalized target length of 1.0. That is, each E-pulse extinguishes the response of the expected target. For longer and shorter targets the E-pulses do not extinguish the response, and there is a net energy content in the scattered field waveform, and thus a nonzero value of D/L^2. When the normalized target length is 1.05 (a 5% longer target) the backscatter discrimination area is much greater for the case of the natural E-pulse, verifying the more subjective assessment made earlier. It is apparent, however, that the natural E-pulse will discriminate larger targets better than smaller ones, since the value of D/L^2 is greater for longer targets. In contrast, the forced E-pulse of lesser duration will not discriminate targets well unless their normalized lengths are much smaller -- near 0.33 or 0.15 -- as indicated by the large values of D/L^2 at these lengths in Figure 5.5.1.15. Thus, this forced E-pulse is nearly

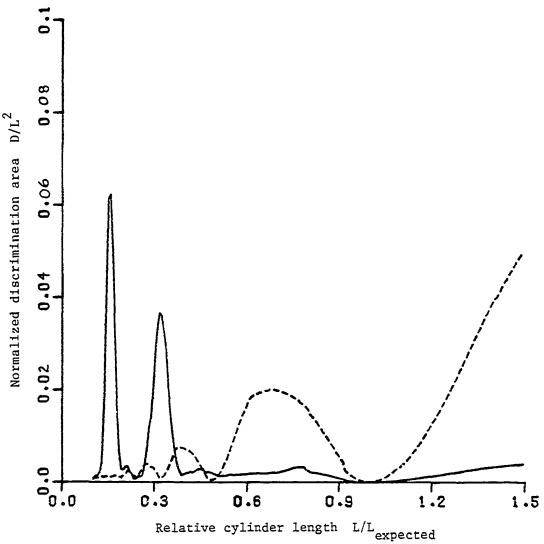

Figure 5.5.1.15. Discrimination area of 60° five mode thin cylinder excited by natural E-pulse (dotted line) and forced E-pulse of duration T_e=1.8 L/c (solid line).

useless for discriminating slight differences in target lengths.

The behavior of the discrimination area as a function of target length can be explained by examining the spectra of the two E-pulses. In essence, the natural frequencies of the thin cylinder target are inversely proportional to target length (as indicated in their normalization.) Thus, a longer target has lower natural frequencies. Since the natural E-pulse has a majority of its energy at lower frequencies, and since the smaller order natural frequencies have smaller damping coefficients (i.e. the lower order natural modes make the greatest contribution to the late-time scattered field response), the value of D/L^2 is greater for longer targets. On the other hand, the forced E-pulse of shorter duration has its energy concentrated at much higher frequencies. Thus, the discrimination area is small until the target length approaches a value at which the lower order natural frequencies coincide with the frequency of E-pulse energy concentration. Figure 5.5.1.15 shows this to occur near normalized lengths of 0.33 and 0.15.

The spectrum of the natural E-pulse also explains another intriguing anomaly seen in Figure 5.5.1.15. It is seen that the spectrum minima are spaced very evenly (due, of course, to the even spacing of the target natural frequencies to be eliminated) and that they repeat at higher frequencies. Thus, the responses of targets that have natural frequencies which are integral multiples of those to be eliminated are nearly extinguished as well. This is reflected in Figure 5.5.1.15 by minima at normalized lengths of 1/2, 1/3, 1/4, etc. In contrast, the large peak in the spectrum of the shorter duration

forced E-pulse prevents such minima in the discrimination area plot at these lengths.

The backscatter discrimination area has also been plotted versus length for the cases of the natural DC E-pulse and the forced E-pulse of longer duration. This is shown in Figure 5.5.1.16. The forced E-pulse is seen to discriminate longer targets much better than shorter targets, as did the natural E-pulse. This is not surprising, since the waveforms have very similar shapes. It is also seen that at normalized lengths smaller than 1/2, D/L^2 is nearly zero for the forced E-pulse, and discrimination is quite difficult. The reason for this is revealed by the E-pulse spectrum, which shows almost no energy at higher frequencies. In contrast, the natural DC E-pulse is seen to discriminate larger and smaller targets equally well. This is because the E-pulse energy is spread evenly across a wide band of frequencies. However, as with the natural E-pulse, there are minima at lengths of 1/2, 1/3, 1/4, etc., due to the extended periodic nature of the spectrum.

The backscatter discrimination area can also be plotted versus aspect angle and number of modes present in the response. Figures 5.5.1.17 and 5.5.1.18 show discrimination area versus aspect angle for the natural and forced E-pulses, at a normalized length of 1.05. As expected, there is no scattered field for end-on aspect, since the thin cylinder cannot be excited at this orientation. For the case of the natural E-pulse, D/L^2 increases fairly smoothly from end-on to normal aspect.

Figures 5.5.1.19 and 5.5.1.20 show discrimination area plotted

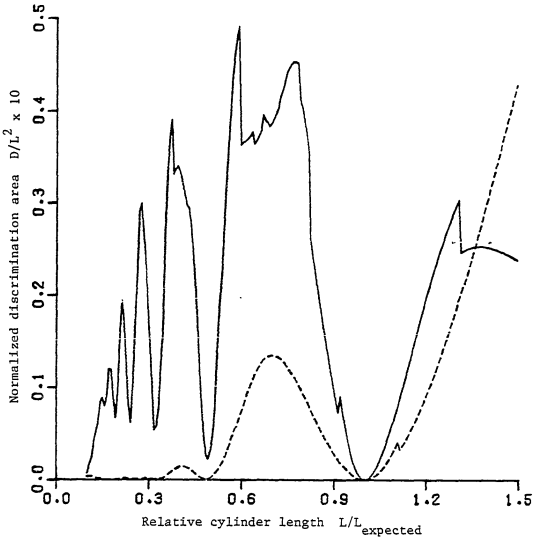

Figure 5.5.1.16. Discrimination area of 60° five mode thin cylinder excited by natural DC E-pulse (solid line) and forced E-pulse of duration T_e=2.5 L/c (dotted line).

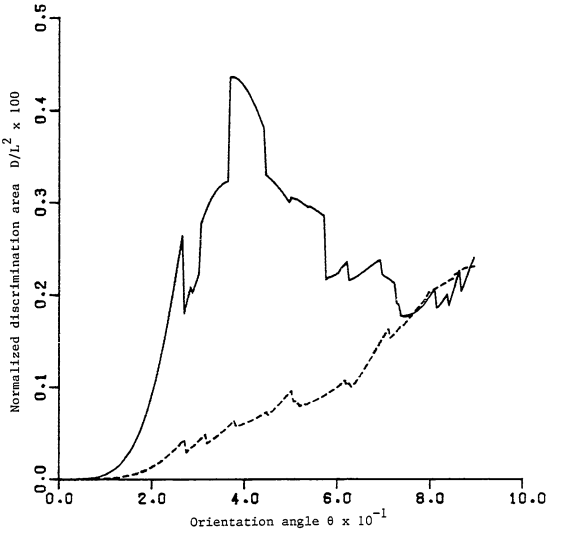

Figure 5.5.1.17. Discrimination area of a five mode thin cylinder of relative length 1.05 excited by natural E-pulse (dotted line) and natural DC E-pulse (solid line).

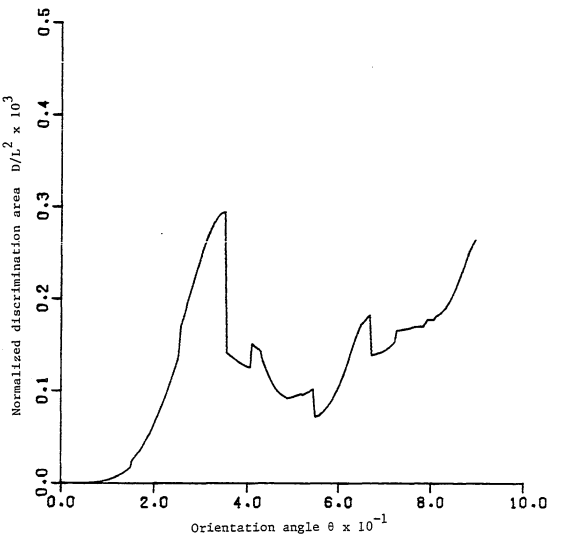

Figure 5.5.1.18. Discrimination area of a five mode thin cylinder of relative length 1.05 excited by forced E-pulse of duration T_e=1.8 L/c.

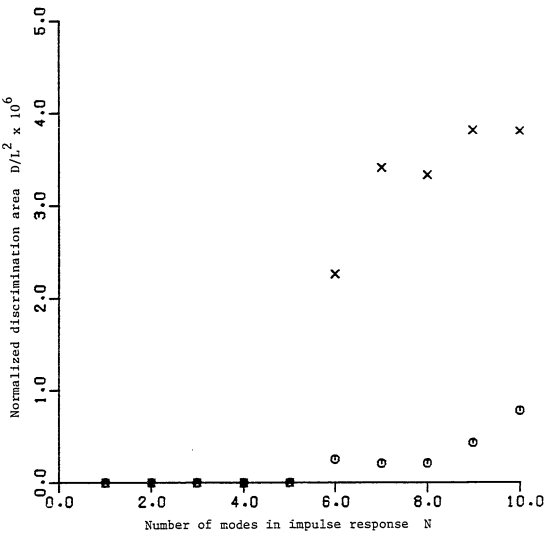

Figure 5.5.1.19. Discrimination area of 60° thin cylinder of relative length 1.0 excited by natural E-pulse (circles) and natural DC E-pulse (crosses).

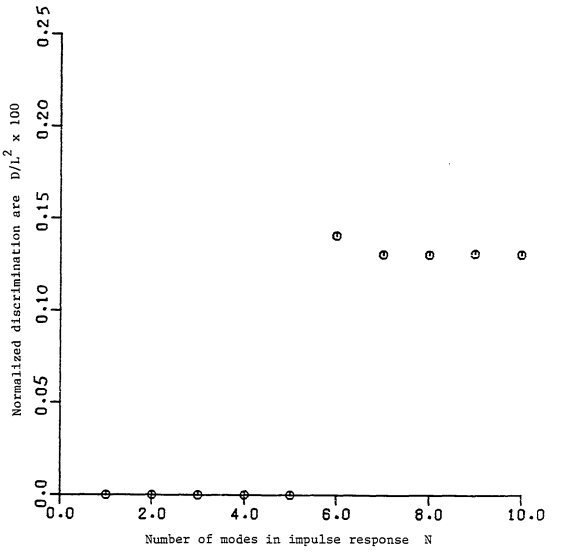

Figure 5.5.1.20. Discrimination area of 60° thin cylinder of relative length 1.0 excited by forced E-pulse of duration T_e=1.8 L/c.

versus the number, N, of natural frequencies used to construct the thin cylinder impulse response, for a normalized length of 1.0. Of course, when $N \leq 5$ the five mode E-pulses each extinguish the impulse response. However, for $N > 6$ the E-pulses excite the higher order modes, resulting in a nonzero late-time response. The discrimination area of the forced E-pulse of shorter duration is seen to be orders of magnitude larger than the discrimination area of the natural and the natural DC E-pulses. Examination of the E-pulse spectra explains the reason for this. Since the shorter duration forced E-pulse has a large amount of energy at higher frequencies, and the other spectra are much smaller at these frequencies, the higher order modes are excited most effectively by the shorter duration forced E-pulse.

Employing an E-pulse relatively insensitive to the exact number of natural modes present in a measured target response is potentially very important. As it is impossible to accurately determine all the natural modes of a complex target, only a finite number will be available for discrimination purposes, while an actual response may contain many more. Figures 5.5.1.19 and 5.5.1.20 indicate that an E-pulse should be constructed so as to not have a relatively large amount of energy in a region of the spectrum where the natural frequencies of the target are not accurately known. To this extent, the forced E-pulse of smaller duration is not a good choice for the use investigated in this section.

It becomes expedient at this point to ask the question: what is the form of the "best" E-pulse? The results of this section have shown that for acceptable performance in the presence of noise it is

important that the waveform be relatively smooth. The spectrum of the waveform should also take an ideal form. It should be zero over a small range of σ and ω around the natural frequencies to be eliminated. That way, if the natural frequencies of the target are not known with great precision, there is a little leeway available. The spectrum should then be constant at all complex frequencies in between, up to a range beyond which the natural frequencies of the target are not well known, and zero everywhere outside this range. With this type of spectrum, each of the known natural frequencies would be eliminated, while those of an unknown target would each be excited with similar amplitudes. For the very simple case of a target with equal damping coefficients, the spectrum might appear as in Figure 5.5.1.21.

The spectrum shown in Figure 5.5.1.21 does not, of course, correspond to a finite duration waveform, since it is frequency limited [72]. The question then becomes whether it is possible to arrive at a finite duration E-pulse with a spectrum at all similar to the ideal. For the thin cylinder target, a good approximation to this spectrum has already been identified. Figure 5.5.1.7, it is remembered, displays the spectrum of the natural DC E-pulse. This spectrum has zeroes at the natural frequencies to be eliminated, and has a fairly constant amplitude at frequencies in between. Also, it is seen to taper off at higher frequencies where undetermined natural frequencies might lie. Thus, the natural DC E-pulse appears to be the best choice for thin cylinder discrimination.

For more complex targets, the natural DC E-pulse may not have the desired spectral form. Also, the natural E-pulses may have a

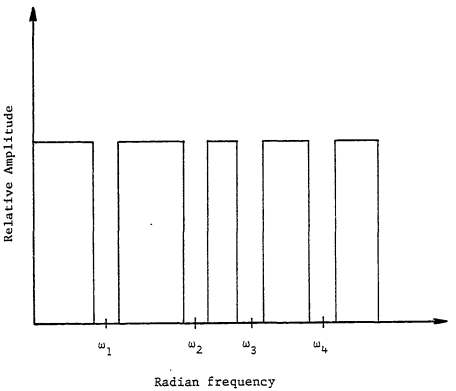

Figure 5.5.1.21. "Ideal" spectrum for E-pulse designed to eliminate four target modes which have equal damping coefficients.

minimum duration larger than that desired. It might still be possible in these cases to construct E-pulses with spectra similar to the ideal. The key lies in using a different basis set.

The spectrum of the damped sinusoid based E-pulse is given by equation (4.5.2.9). The transform of a single damped sinusoid is merely a pair of poles of the form $1/(s-s_0)$. When multiplied by a rectangular windowing function to truncate the waveform to finite duration, the spectrum is convolved in the complex frequency plane with a function of the type sinh(s)/s (see [18]). Alone, the sinh(s)/s function has a peak along the ω axis at ω=0. When convolved with the poles of the damped sinusoid spectrum, the peak shifts to a point nearer the position of the poles (a result of employing Cauchy's residue theorem in the complex plane convolution.) Thus, by proper choice of the complex frequencies of the damped sinusoids, the spectrum of the E-pulse can be peaked at various prechosen points along the ω axis.

As an example of this type of spectrum shaping, consider a one mode natural damped sinusoid E-pulse synthesized to eliminate the first mode of the thin cylinder target: $s_1 = -0.2601+j2.906$ c/L. The damped sinusoid functions are constructed using the frequencies and phases

$$\begin{aligned} \frac{L}{c}\sigma_1 &= -0.2601 \quad \frac{L}{c}\omega_1 = 2.406 \quad \phi_1 = 0 \\ \frac{L}{c}\sigma_2 &= -0.2601 \quad \frac{L}{c}\omega_2 = 3.406 \quad \phi_2 = \frac{\pi}{2} \end{aligned} \tag{5.5.1.1}$$

and the resulting E-pulse is shown in Figure 5.5.1.22. The spectrum of this E-pulse is shown in Figure 5.5.1.23. The complex frequencies

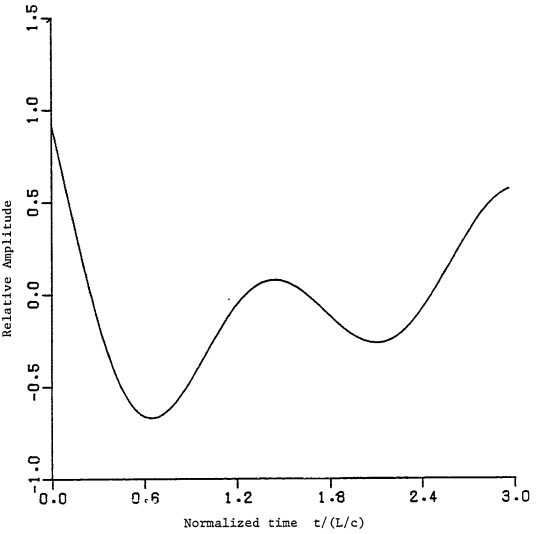

Figure 5.5.1.22 Natural E-pulse of minimum duration synthesized using damped sinusoid basis functions to eliminate the first mode of the thin cylinder.

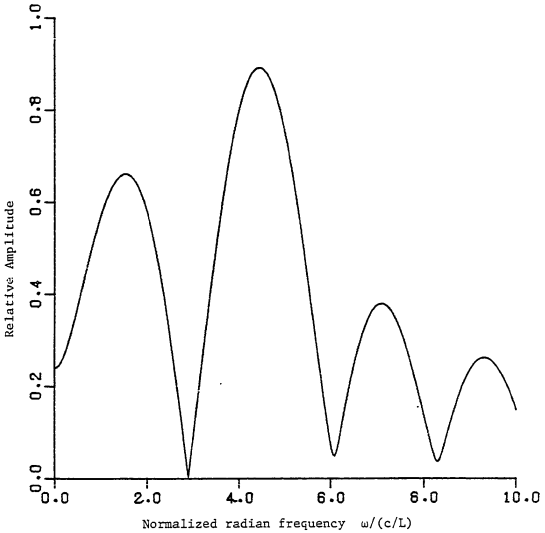

Figure 5.5.1.23. Spectrum of one mode damped sinuscid based E-pulse for σ=-0.2601 c/L.

used to construct the E-pulse have been chosen so that their imaginary parts are just to the right and just to the left of the imaginary part of the natural frequency to be eliminated. It is hoped that this will result in peaks of the spectrum on each side of the frequency to be eliminated, and more closely simulate the previously discussed "ideal". Figure 5.5.1.23 shows that this attempt has succeeded.

Extending this technique to the case of a multimode E-pulse is not straight forward. One is tempted merely to put peaks in between the frequencies to be eliminated. However, it is not obvious that the amplitudes of the basis functions determined by applying the E-pulse equations (4.4.1.2) and (4.4.1.3) will result in a spectrum that has relatively constant amplitude between the zeroes. A different approach can be tried, though, which might achieve a fairly even distribution between the zeroes.

It is known from the discussion of section 4.4.6 that a multimode E-pulse can be constructed from the convolution of many single mode E-pulses. This corresponds to multiplying the E-pulse spectra in the complex frequency domain. If a single mode E-pulse could be constructed so that its spectrum was fairly constant except at the frequency of the mode to be eliminated (where there would be a zero) it could be convolved with similar E-pulses designed to eliminate other modes, resulting in an overall spectrum near the "ideal". This could be accomplished using forced damped sinusoid E-pulses of short duration. Since the widths of the $\sin(x)/x$ lobes along the ω axis are inversely proportional to the individual E-pulse durations, making the durations short results in a spreading of the E-pulse energy across the

spectrum -- a more "constant" distribution. It is also necessary to keep the durations of the individual E-pulses small since the total duration of the convolved E-pulse is equal to the sum of the individual durations.

5.5.2 Single Mode Discrimination

Radar target discrimination can also be based upon the difference in target responses to single mode excitation signals. A single mode signal created to excite one mode of a specific target will excite many modes of a different target, resulting in very dissimilar late-time responses. (Or, alternatively, the single mode signal will eliminate all but one mode of the expected target, while exciting many modes of a different target.) Figures 5.5.2.1 and 5.5.2.2 show minimum duration natural sine and cosine single mode excitation waveforms synthesized using the rectangular pulse function basis set via the analysis of section 4.6 to excite the first and third modes of the thin cylinder target, respectively. The first five natural frequencies tabulated in Figure 5.2.1 have been used in the construction. Note that the first mode excitation waveforms have the approximate shape of one period of the first natural mode of the thin cylinder, while the third mode excitation signals appear to consist of approximately three cycles of the third natural mode.

The shapes of the single mode excitation waveforms are reflected in their spectra, as shown in Figure 5.5.2.3. This figure shows the spectrum of the sine first mode signal, at a value of σ=-0.2601 c/L, and also the spectrum of the sine third mode signal, at a value of

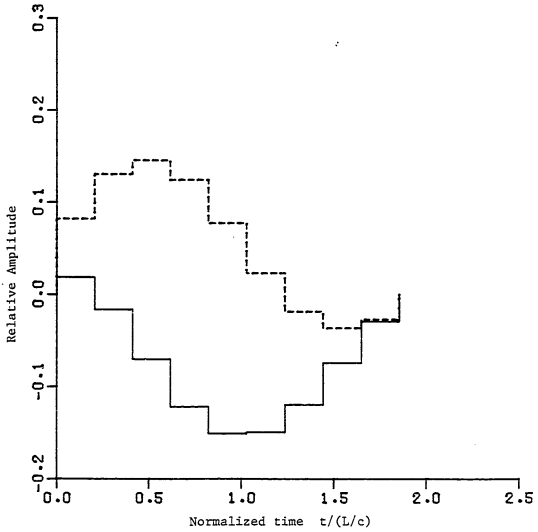

Figure 5.5.2.1. Natural sine (dotted line) and cosine (solid line) first mode excitation signals of minimum duration for five mode thin cylinder.

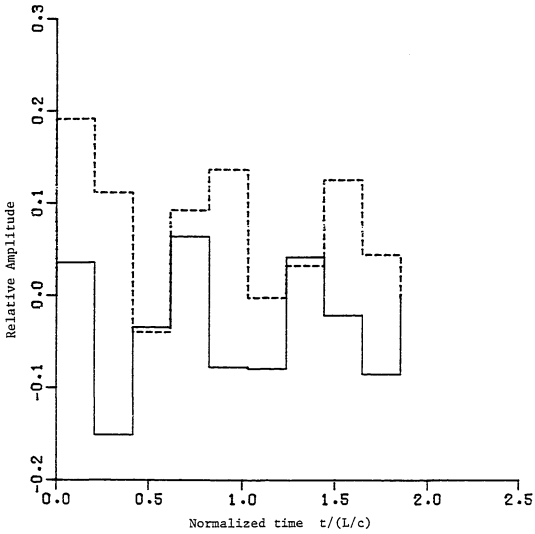

Figure 5.5.2.2. Natural sine (dotted line) and cosine (solid line) third mode excitation signals of minimum duration for five mode thin cylinder.

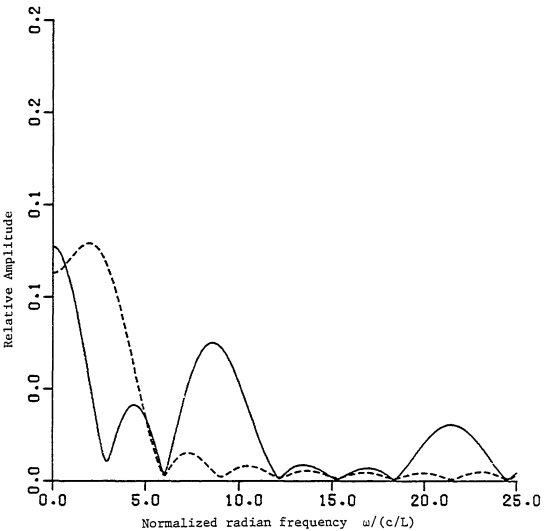

Figure 5.5.2.3. Spectra of first (dotted line) and third (solid line) mode thin cylinder excitation signals for σ=-0.2601 c/L.

σ=-0.4684 c/L. It is seen that there is a peak in each of the spectra at a value of ω corresponding to the ω of the natural frequency to be excited. This automatic concentration of energy seems to be unique to the natural single mode excitation signals. It will be seen that such a frequency distribution results in optimum discrimination, and attempts will be made to duplicate it artificially, using the damped simusoid basis set, later in this section.

Verification of the single mode excitation signals is accomplished by convolving the single mode F-pulses of Figures 5.5.2.1 and 5.5.2.2 with the thin cylinder impulse response of Figure 5.5.1.1. The results are shown in Figures 5.5.2.4 and 5.5.2.5. It is easily seen that the convolved responses are indeed single damped sinusoids oscillating at the frequencies of the first and third modes of the thin cylinder. It is also seen that the sine and cosine responses are exactly 90^{o} out of phase, as requested. The most striking difference between the first and third mode responses is due to the difference in the damping coefficients (real parts of the natural frequencies.) The larger (negative) damping coefficient of the third mode drives the magnitude of its response to near zero by the end of the display, while the first mode response is still quite large. This makes the higher order single mode responses less practical for discrimination purposes, which is unfortunate, since it will be seen that the higher order responses are actually the most sensitive discriminants.

There are many ways to interpret the convolved responses shown in Figures 5.5.2.4 and 5.5.2.5. Perhaps the most dramatic is to use the technique described in section 4.4.7. The single mode excitation

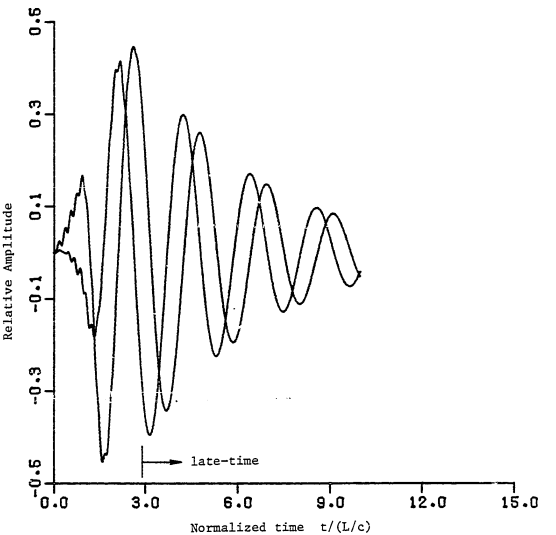

Figure 5.5.2.4. Convolution of first mode sine and cosine excitation signals with five mode 60° thin cylinder impulse response.

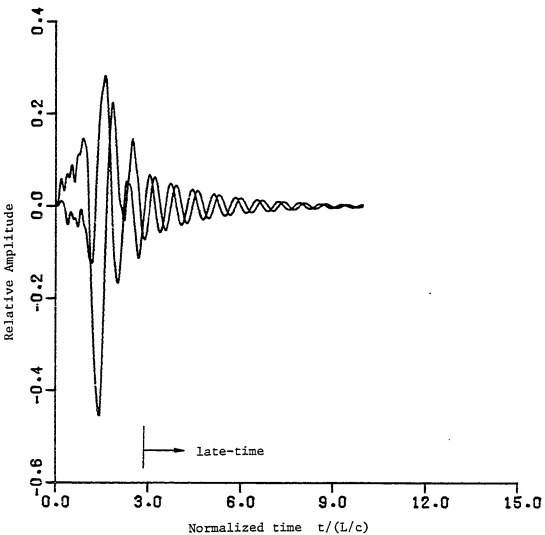

Figure 5.5.2.5. Convolution of third mode sine and cosine excitation signals with five mode 60° thin cylinder impulse response.

signals shown in Figures 5.5.2.1 and 5.5.2.2 have been normalized according to equations (4.4.7.12) and (4.4.7.14), and thus the convolved sine and cosine responses can be combined to provide a plot of the damping coefficient and the oscillation frequency. These are shown in Figures 5.5.2.6 through 5.5.2.9. If the responses are pure damped sinusoids, these plots should produce straight lines, the slopes of which correspond to frequency (real or imaginary part.) This is indeed seen to be the case, as each of the plots does produce a straight line in late-time. (Note that this also provides a good graphical indication of the beginning of the late-time period -- the point where the response becomes a pure damped sinusoid.)

To implement a discrimination scheme, the slopes of the frequency plots must be compared with the natural frequencies of the expected target. If the two match, the target has been identified. If the two are dissimilar, the target is discriminated from the expected target. The simplest way to implement discrimination is to use a visual comparison. This has been provided in each of the Figures 5.5.2.6 through 5.5.2.9, where the slope of the expected target frequencies has been plotted next to the frequency plots. It is apparent that the two lines are parallel in the late-time for each of the figures, and thus the target is identified as that expected. A less subjective comparison can be provided by computing a linear regression for the late-time portion of the frequency plots. This provides a more global measure of the frequency content of the convolved response (and results in a single number), as opposed to the local description provided by the plot itself. Application of linear regression gives values of

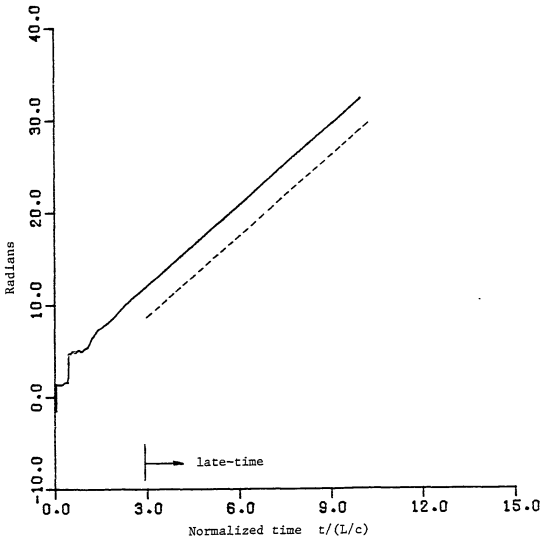

Figure 5.5.2.6. Radian frequency plot from first mode excitation signal convolutions. Dotted line is radian frequency plot of expected first mode.

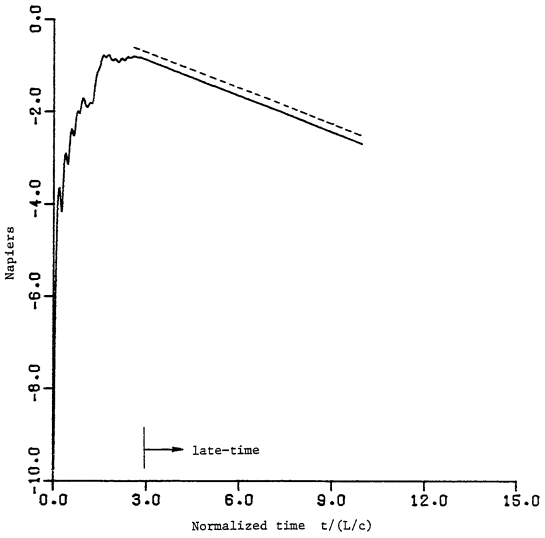

Figure 5.5.2.7. Damping coefficient plot from first mode excitation signal convolutions. Dotted line is damping coefficient plot of expected first mode.

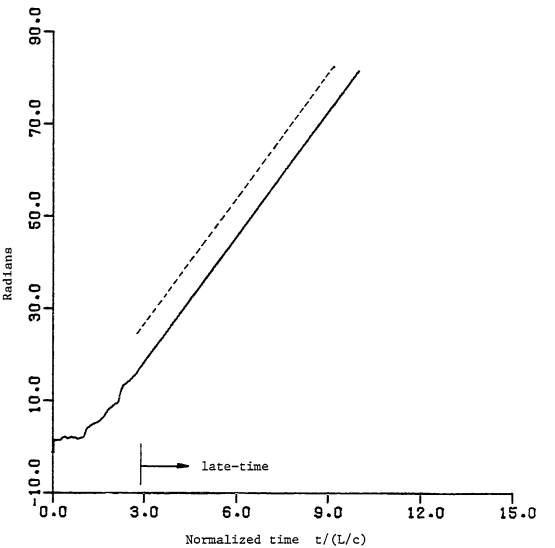

Figure 5.5.2.8. Radian frequency plot from third mode excitation signal convolutions. Dotted line is radian frequency plot of expected third mode.

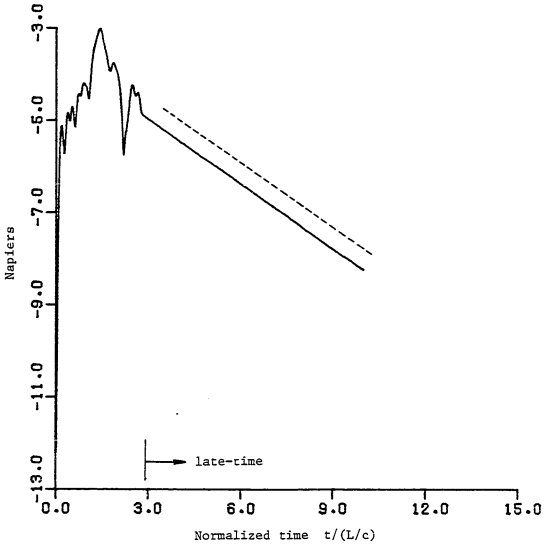

Figure 5.5.2.9. Damping coefficient plot from third mode excitation signal convolutions. Dotted line is damping coefficient plot of expected third mode.

σ=-0.2601 c/L and ω=2.906 c/L for the first mode response, and σ=-0.4684 c/L and ω=9.058 c/L for the third mode response. These compare extremely well with the exact frequencies of the expected target. Any slight discrepancies in the last decimal place is probably due to inaccuracies in the convolution technique discussed in section 5.3.

The construction of frequency plots requires the use of both sine and cosine single mode excitation signals. The complexity of the discrimination process can be reduced by a factor of two if only one of the two waveforms need be used. This requires a different interpretation of the convolved responses. One quite simple method is to employ one of the natural mode extraction schemes (as described in chapter 6) to the late-time portion of either the sine or cosine response (or a sin/cos response.) This approach involves extracting just a single mode. If the target is the expected one, the extracted values of σ and ω will match those anticipated. If the target is not that expected, the extracted values will not match. As an example, the continuation method has been applied to the sine responses of Figures 5.5.2.4 and 5.5.2.5. For the first mode response, the extracted values are found to be σ=-0.2601 c/L and ω=2.906 c/L, while the third mode sine response yields σ=-0.4674 c/L and ω=9.058 c/L. Again, these are extremely close to the expected results. Note that this technique also describes a global rather than a local behavior.

A third way of interpreting the convolved responses combines both a local and a global description, and involves only one of either the sine or cosine responses. This method involves fitting a

one mode damped sinusoidal waveform to the late-time portion of the convolved response. The expected natural frequency is held constant and the amplitude and phase of the waveform which best fits the late-time response are calculated. This is a linear least-squares problem and is described explicitly in section 6.4. To provide a graphical presentation of the results, this best fit is then subtracted from the convolved response. The resulting waveform is then much like the output from an E-pulse convolution. If the target is that expected, the waveform is identically zero in the late-time (since the best fit exactly fits the convolved response in the late-time.) If the target is not the one expected, then the late-time portion will be nonzero. Figures 5.5.2.10 and 5.5.2.11 show the results for the first and third mode sine responses. As anticipated, the waveforms are zero in the late-time.

It is important to realize that the latter two methods of interpreting the convolved responses require a knowledge (or at least an estimate) of the beginning of the late-time period. This was not needed to construct the frequency plots of the first method. However, comparing the frequency plots with the expected slopes does require knowing the point to begin the comparison. And performing linear regression on the frequency lines also requires the knowledge of the beginning of the late-time region. This is identical with the interpretation of the E-pulse convolutions, since it is necessary to know the point beyond which a null response it to be expected.

Discrimination between differing thin cylinder targets is investigated by convolving the single mode excitation waveforms with

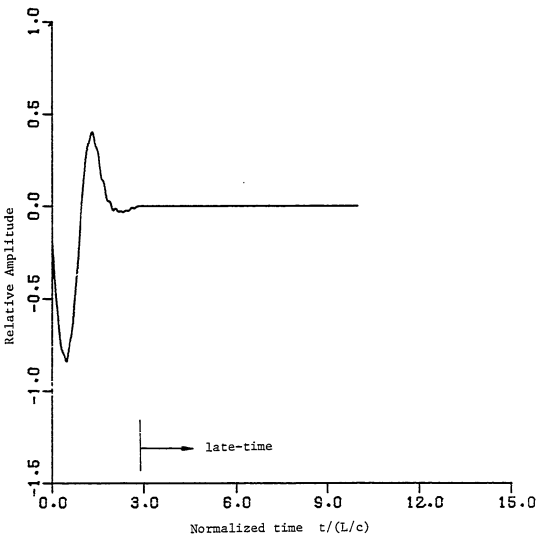

Figure 5.5.2.10. Best fit difference plot for sine first mode convolution.

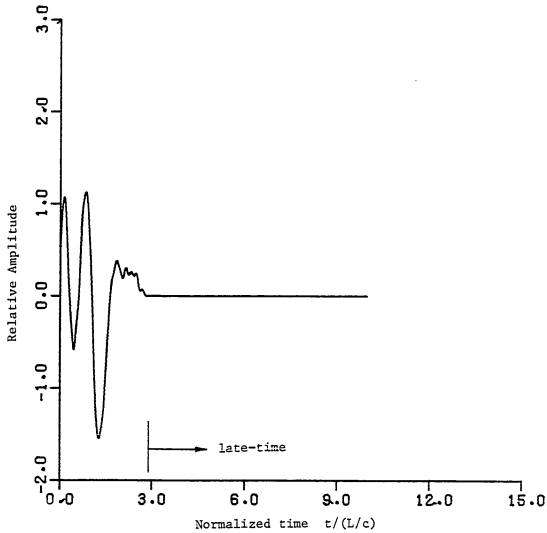

Figure 5.5.2.11. Best fit difference plot for sine third mode convolucion.

a target 10% longer. The convolved responses for the first mode signals are shown in Figure 5.5.2.12 while those for the third mode signals are shown in Figure 5.5.2.13. It is somewhat difficult to tell that the first mode sine and cosine responses are not identical to those of the correct cylinder shown in Figure 5.5.2.4, but a close examination reveals that the periods are longer for the longer target. It is much more obvious that the third mode convolved responses are not merely the single damped sinusoids expected.

The reason for the difference between the trends seen in the first and third mode responses is threefold. First, the amplitude of the first mode in both the expected and longer targets is greater than that of the third mode. Second, the smaller damping coefficient of the first mode allows it to come through much stronger. In the case of the response of the longer target to the first mode excitation signal, the excited first mode dominates the excited third mode (and, of course, the other modes.) In the case of the response of the longer target to the third mode excitation signal, both the excited first and second modes make important contributions. Lastly, the spectra of the excitation signals reveal that for the first mode signal there is little energy at the frequency of the third mode (of the longer target), while for the third mode excitation signal there is quite a lot of energy at the frequency of the first mode (of the longer target.)

Discrimination between the expected and the longer target is based on the difference between the late-time convolved responses. If the convolved response is a pure damped sinusoid with the expected frequency then the target has been identified. If it is not a pure

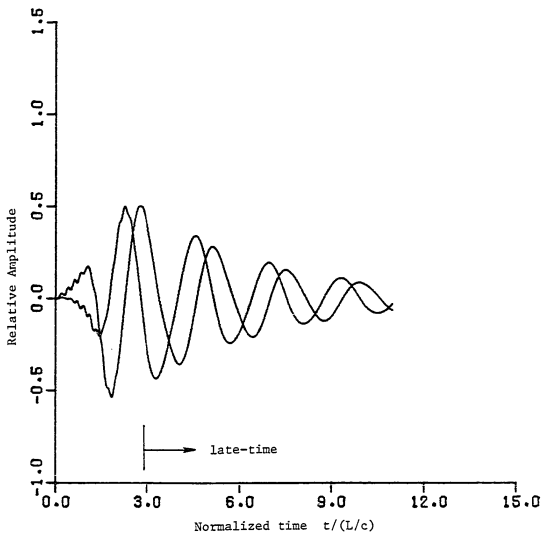

Figure 5.5.2.12. Convolution of first mode sine and cosine excitation signals with five mode impulse response of 60^{o} thin cylinder which is 10% longer than expected.

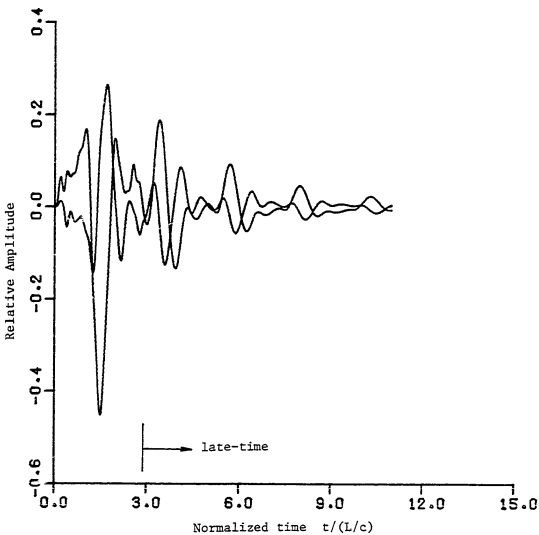

Figure 5.5.2.13. Convolution of third mode sine and cosine excitation signals with five mode impulse response of 60° thin cylinder which is 10% longer than expected.

sinusoid, or if it has a frequency other than that expected, the target is discriminated from the expected target. Employing the three interpretations of the convolved responses provides a firm basis for this discrimination. Figures 5.5.2.14 through 5.5.2.17 show the frequency plots for each response. It is apparent that none of these exactly parallels the expected slope. Application of linear regression to the late-time portion of these curves yields values of σ=-0.2395 c/L and ω=2.635 c/L for the first mode and σ=-0.1884 c/L and ω= 3.662 c/L for the third mode, all of which are quite a bit different from the expected values. The third mode response provides the greatest amount of discrimination, for the three reasons discussed above. Using the continuation method on the late-time portions of the convolved sine responses results in best fit values of σ=-0.2402 c/L and ω=2.632 c/L for the first mode and σ=-0.5713 c/L and ω=4.274 c/L for the third mode. Again, all of these are different from the expected values, and the longer target is discriminated from the expected target. Lastly, the late-time portion of the sine responses have been best fit and the result subtracted from the original waveforms. Figures 5.5.2.18 and 5.5.2.19 show the resulting waveforms. Here the nonzero late-time portion of the waveforms discriminate the longer target from the target expected, in a manner analogous to the E-pulse discrimination of the last section.

Sensitivity of single mode discrimination to the presence of random noise is investigated by convolving the first and third mode sine and cosine excitation signals with the noisy thin cylinder impulse response of Figure 5.5.1.11. The resulting convolved responses

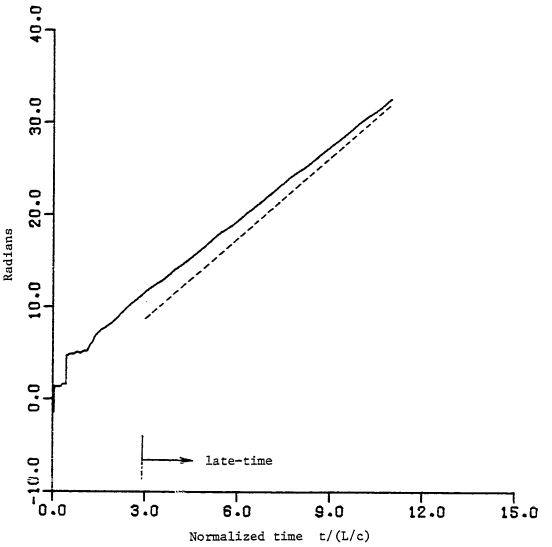

Figure 5.5.2.14. Radian frequency plot from 10% longer cylinder, first mode excitation signal convolutions. Dotted line is radian frequency plot of expected first mode.

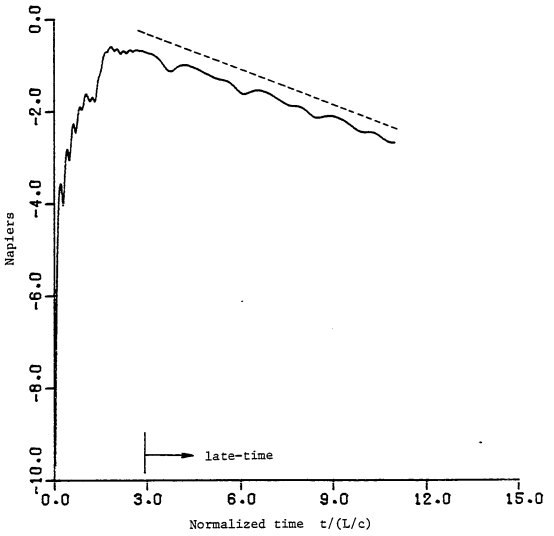

Figure 5.5.2.15. Damping coefficient plot from 10% longer cylinder, first mode excitation signal convolutions. Dotted line is damping coefficient plot of expected first mode.

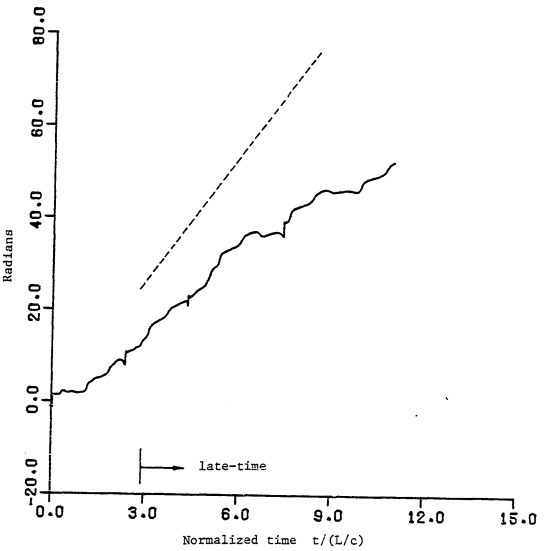

Figure 5.5.2.16. Radian frequency plot from 10% longer cylinder, third mode excitation signal convolutions. Dotted line is radian frequency plot of expected third mode.

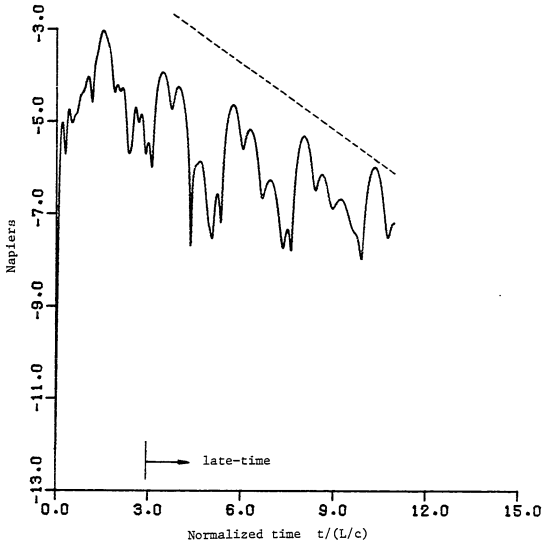

Figure 5.5.2.17. Damping coefficient plot from 10% longer cylinder, third mode excitation signal convolutions. Dotted line is damping coefficient plot of expected third mode.

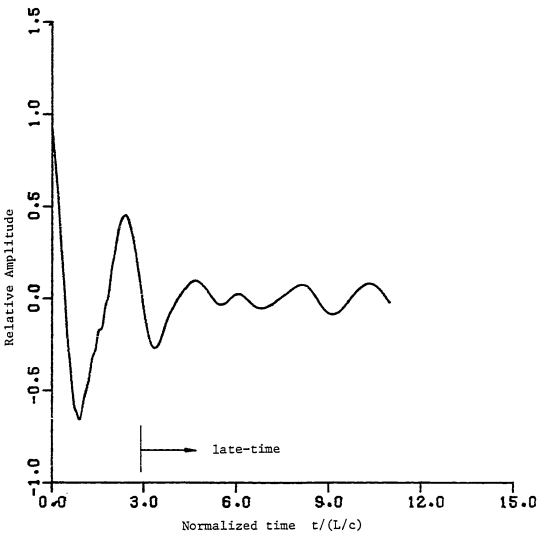

Figure 5.5.2.18. Best fit difference plot for sine first mode, 10% longer cylinder convolution.

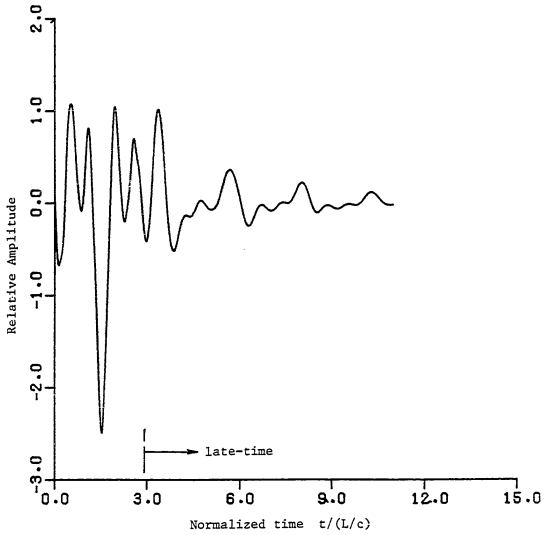

Figure 5.5.2.19. Best fit difference plot for sine third mode, 10% longer cylinder convolution.

are shown in Figures 5.5.2.20 and 5.5.2.21. It is apparent that the first mode convolved responses have been effected very little by the presence of random noise while the third mode responses have been effected substantially. This might be due in part to the more oscillatory nature of the third mode excitation signal, resulting in less noise averaging. The frequency plots, shown in Figures 5.5.2.22 through 5.5.2.25 also reflect this difference. Whereas the first mode frequency plots are nearly identical to the expected slopes, the third mode plots are much noisier, especially the plot of σt. Note that the third mode response is effected most greatly at later times, when it has damped down to a very small magnitude.

Linear regression of the late-time portion of the frequency plots in Figures 5.5.2.22 through 5.5.2.25 gives values of σ=-0.2745 c/L and ω=2.915 c/L for the first mode responses and σ=-0.1931 c/L and ω=10.65 c/L for the third mode responses. Application of the continuation method to the late-time portion of the sine responses results in σ=-0.2590 c/L and ω=2.909 c/L for the first mode and σ=-0.4938 c/L and ω=8.981 c/L for the third mode. Note that the values calculated using the continuation method are quite close to the expected values, even for the third mode response. This allows a separation of the effects of random noise and target length sensitivity. Lastly, Figures 5.5.2.26 and 5.5.2.27 show the results of best fitting the late-time regions of the sine responses and subtracting. Although neither late-time region of the resulting waveforms is identically zero, each is quite small. In fact, a quick comparison shows that they are much smaller than the corresponding regions of the

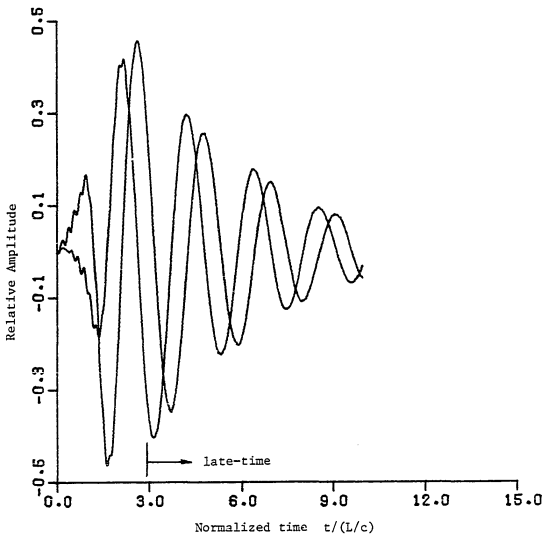

Figure 5.5.2.20. Convolution of first mode sine and cosine excitation signals with noisy five mode 60° thin cylinder impulse response.

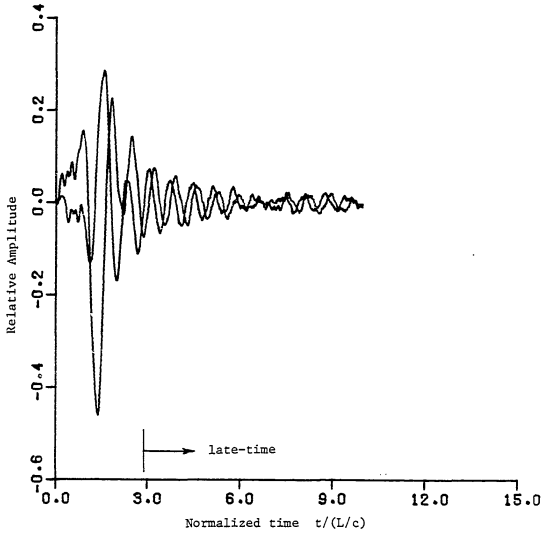

Figure 5.5.2.21. Convolution of third mode sine and cosine excitation signals with noisy five mode 60° thin cylinder impulse response.

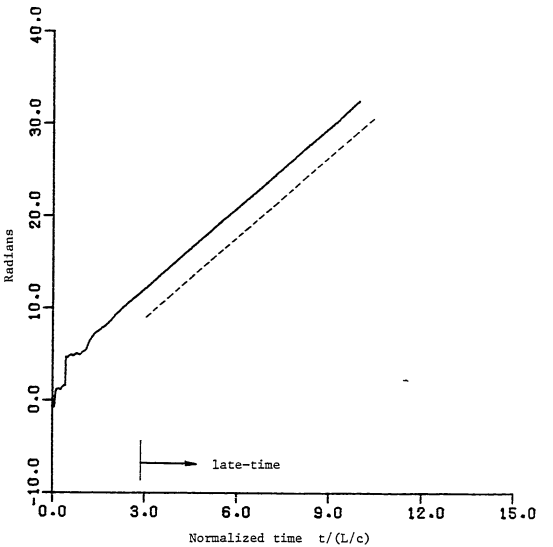

Figure 5.5.2.22. Radian frequency plot from first mode excitation signal, noisy impulse response convolutions. Dotted line is radian frequency plot of expected first mode.

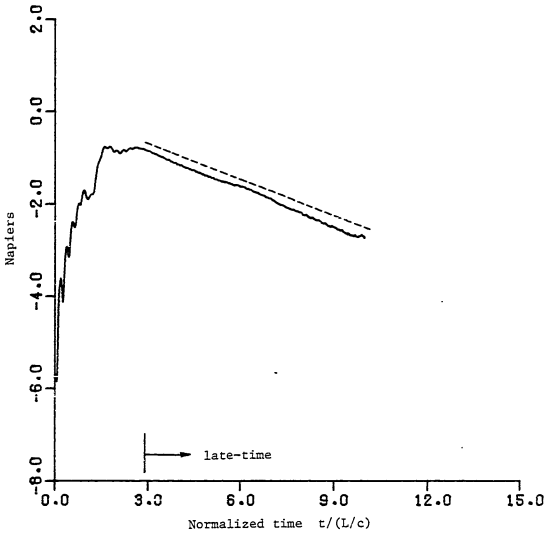

Figure 5.5.2.23. Damping coefficient plot from first mode excitation signal, noisy impulse response convolutions. Dotted line is damping coefficient plot of expected first mode.

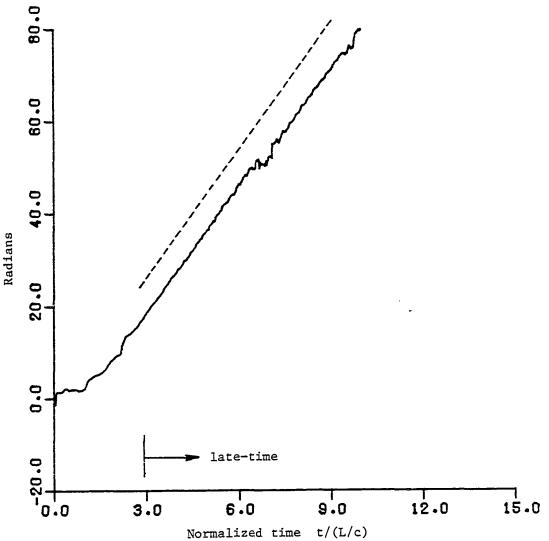

Figure 5.5.2.24. Radian frequency plot from third mode excitation signal, noisy impulse response convolutions. Dotted line is radian frequency plot of expected third mode.

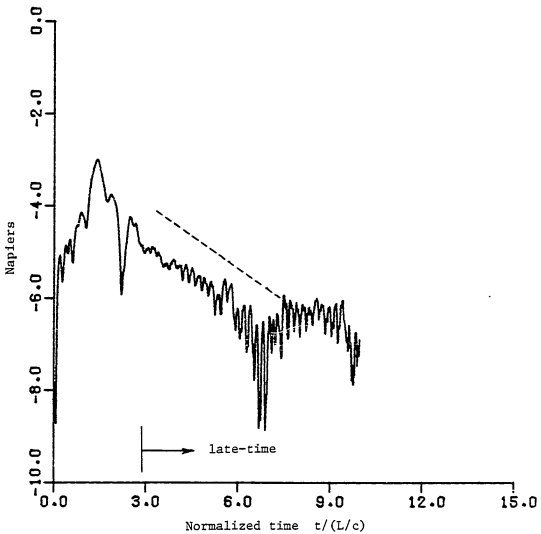

Figure 5.5.2.25. Damping coefficient plot from third mode excitation signal, noisy impulse response convolutions. Dotted line is damping coefficient plot of expected third mode.

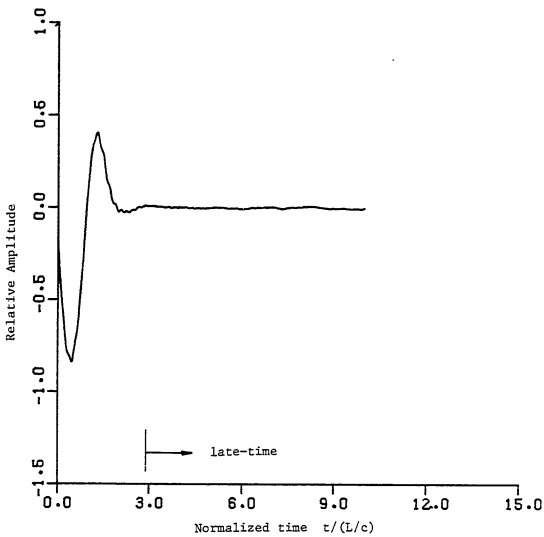

Figure 5.5.2.26. Best fit difference plot for sine first mode, noisy impulse response convolution.

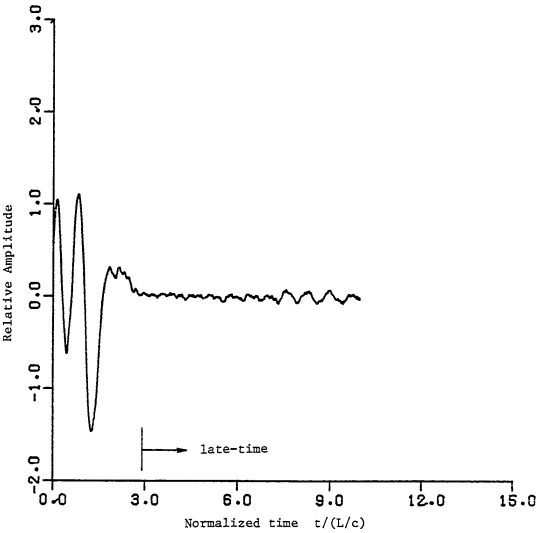

Figure 5.5.2.27. Best fit difference plot for sine third mode, noisy impulse response convolution.

figures generated from the longer target. Again, this allows a separation of the effects of random noise and target length sensitivity.

It is appropriate at this point to inquire, as was done with the E-pulse, as to what might be the behavior of an "ideal" single mode excitation signal. The answer is somewhat different from that given for the E-pulse. It is most important for the spectrum of a single mode excitation waveform to have a large magnitude at the frequency of the mode to be excited, in comparison to that at the frequencies to be eliminated. This is due to the practical problem of the presence of errors in the measured natural frequencies used to construct the single mode excitation signals. Because of this error, the modes which should be eliminated will actually be excited. The amplitudes of these modes are, of course, determined by the amount of energy in the excitation signal spectrum at the modal frequencies. Now, if there is a relatively small amount of energy at the frequency to be excited, these extraneous modes may make a relatively large contribution to the late-time portion of the convolved response, so that the expected target might not be properly identified. This is especially troublesome for the case of higher mode excitation, where the smaller damping coefficients of the lower order modes to be eliminated allow them to dominate the expected higher order mode in the latter part of the late-time region.

The spectra of the natural first and third mode thin cylinder excitation signals presented earlier in Figure 5.5.2.3 revealed that peaks were created automatically near the frequencies of the modes to be excited. This behavior is probably due to the equally spaced nature

of the thin cylinder natural frequencies, and shouldn't be expected in the case of more complex targets. For these cases, though, it might be possible to artificially induce a peak in the excitation signal spectrum at a desired frequency by using the damped sinusoid basis set. This is accomplished by using complex frequencies near the natural frequency to be excited. As an example, consider the first three measured natural frequencies of a McDonnel Douglas F-18 aircraft scale model (as discussed in chapter 8)

$$s_1 = -0.26 + j3.29 \quad x10^9$$

$$s_2 = -0.13 + j7.32 \quad x10^9 \qquad (5.5.2.1)$$

$$s_3 = -0.44 + j9.89 \quad x10^9$$

Figure 5.5.2.28 shows single mode excitation waveforms constructed to excite the second of these three modes. The dotted curve is a forced sin/cos waveform synthesized using the rectangular pulse function basis set. The solid curve is a forced sin/cos waveform of identical duration synthesized using the damped sinusoid basis set with the phases and complex frequencies

$$\tilde{s}_1 = -0.13 + j7.32 \quad x10^9 \qquad \tilde{\phi}_1 = 0$$

$$\tilde{s}_2 = -0.13 + j7.32 \quad x10^9 \qquad \tilde{\phi}_2 = -\pi$$

$$\tilde{s}_3 = \ 0.13 + j7.32 \quad x10^9 \qquad \tilde{\phi}_3 = 0 \qquad (5.5.2.2)$$

$$\tilde{s}_4 = \ 0.13 + j7.32 \quad x10^9 \qquad \tilde{\phi}_4 = -\pi$$

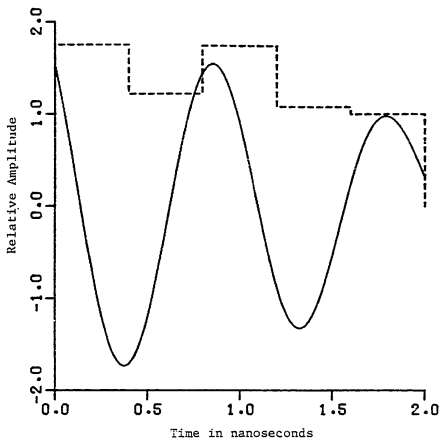

Figure 5.5.2.28. Forced sin/cos single mode excitation signals of duration T_e=2.0 ns synthesized using pulse functions (dotted line) and damped sinusoids (solid line) to excite the second mode of the F-18 aircraft model.

$$\tilde{s}_5 = 0. \quad + j7.32 \quad x10^9 \qquad \tilde{\phi}_5 = -\frac{\pi}{2}$$

Note that the complex frequencies are chosen to be quite close to the natural frequency of the mode to be excited. Figure 5.5.2.29 displays the spectra of the two excitation signals. It is seen that while the pulse function signal has only a small portion of its energy at the frequency of the mode to be excited, the damped sinusoid signal has a majority of its energy at this frequency. By proper choice of the complex frequencies, the spectrum has been shaped for improved single mode performance.

A similar frequency domain shaping can be accomplished using the Fourier cosine basis set as

$$e(t) = \sum_{m=I}^{5} \alpha_m \cos\left(\frac{m\pi}{T_e}\right) t \qquad (5.5.2.3)$$

The duration of this second mode forced sin/cos excitation signal is chosen so that the largest expansion frequency is equal to the imaginary part of the frequency of the mode to be excited. Using $T_e = 2.14159\ x10^{-9}$ results in the expansion frequencies

$$\tilde{\omega}_1 = 1.464 \quad x10^9$$

$$\tilde{\omega}_2 = 2.928 \quad x10^9$$

$$\tilde{\omega}_3 = 4.392 \quad x10^9 \qquad (5.5.2.4)$$

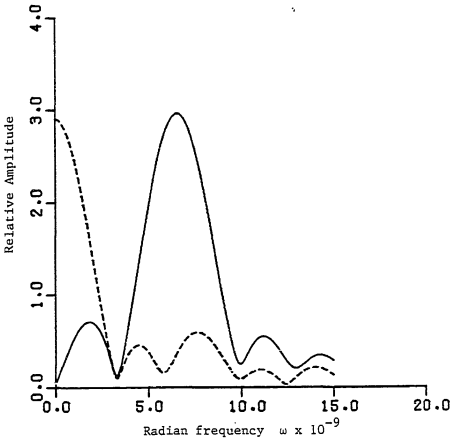

Figure 5.5.2.29. Spectra of pulse function (dotted line) and damped sinusoid (solid line) F-18 second mode excitation signals for σ=-0.13 x 10^9.

$$\tilde{\omega}_4 = 5.856 \times 10^9$$

$$\tilde{\omega}_5 = 7.320 \times 10^9$$

Note that (5.5.2.3) is a DC E-pulse waveform, since the m=0 component has not been used. This is important, since further numerical experimentation has shown that if the m=0 term is included a majority of the excitation signal energy is forced to reside near ω=0.

The excitation signal generated by (5.5.2.3) using (5.5.2.4) is shown in Figure 5.5.2.30 while its spectrum is displayed in Figure 5.5.2.31. The spectrum is seen to take the desired shape, with the largest peak at the frequency of the mode to be excited. The only problem foreseen using this synthesis technique is that the duration needed to place the largest expansion frequency at the imaginary part of the frequency of the mode to be excited may be too large to be practical (due to a limited amount of available late-time response.)

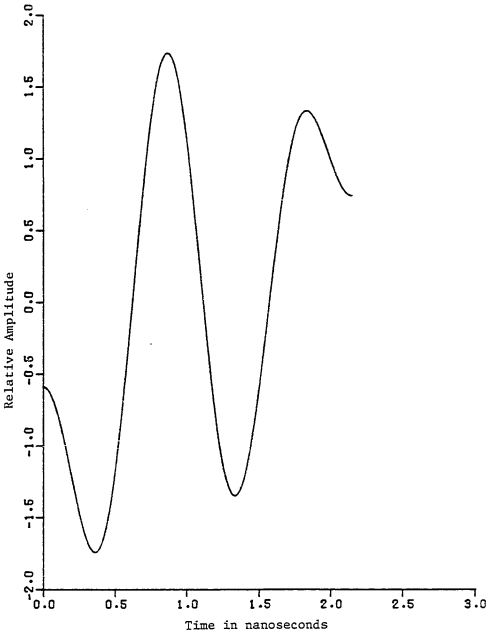

Figure 5.5.2.30. Forced sin/cos single mode excitation waveform of duration T_e=2.14 ns synthesized using Fourier cosine basis functions to excite the second mode of the F-18 aircraft model.

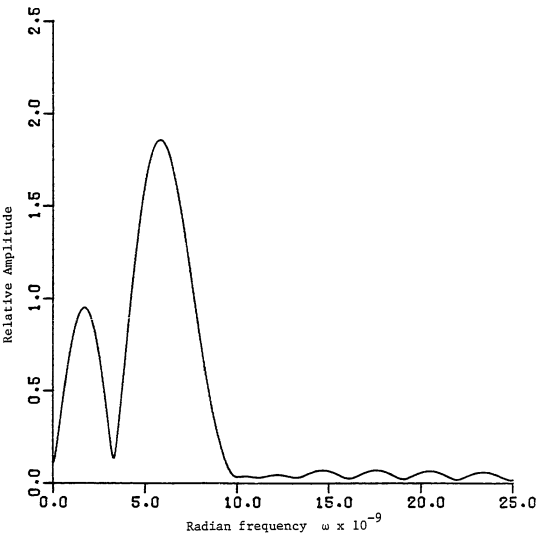

Figure 5.5.2.31. Spectrum of F-18 Fourier cosine second mode excitation signal at σ=-0.13 x 10^9.

5.6 E-pulse Uniqueness

A very important topic to consider is whether there exists a "perfect" E-pulse unique to a particular target. That is, for a given target can a finite duration waveform be constructed which eliminates all the target's natural frequencies? Figures 5.6.1 and 5.6.2 and the analysis of section 4.7 suggest that such a waveform might exist for the case of the thin cylinder target. This section will explore that possibility a little more fully.

Figures 5.6.1 and 5.6.2 display natural E-pulses of minimum duration designed to eliminate various numbers of natural modes of the thin cylinder target using both rectangular pulse and Fourier cosine basis sets. It appears that for each basis set the waveform is converging to the same unique E-pulse as the number of modes to be eliminated is increased. And since these E-pulses involve the first "layer" of thin cylinder natural resonances, it seems that this unique, basis-independent waveform may eliminate all the frequencies of the first layer. If this is indeed true, it would be plausible to extend the assumption to the elimination of all the layers. It is important to note that if the perfect E-pulse does exist it must be a specific natural E-pulse. For any given number of modes to be eliminated, the forced E-pulse is not well defined, since almost any duration may be chosen. Despite the existance of an infinite number of natural E-pulses, this section will concentrate only on the natural E-pulse of minimum duration.

To prove that this E-pulse is convergent is quite difficult. It requires that all the natural frequencies of the thin cylinder

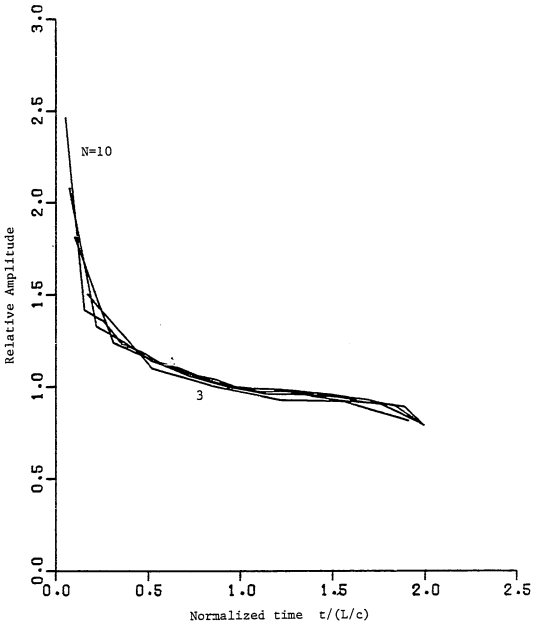

Figure 5.6.1. Natural E-pulses of minimum duration synthesized using pulse functions to eliminate 3, 5, 7, and 10 modes of the thin cylinder.

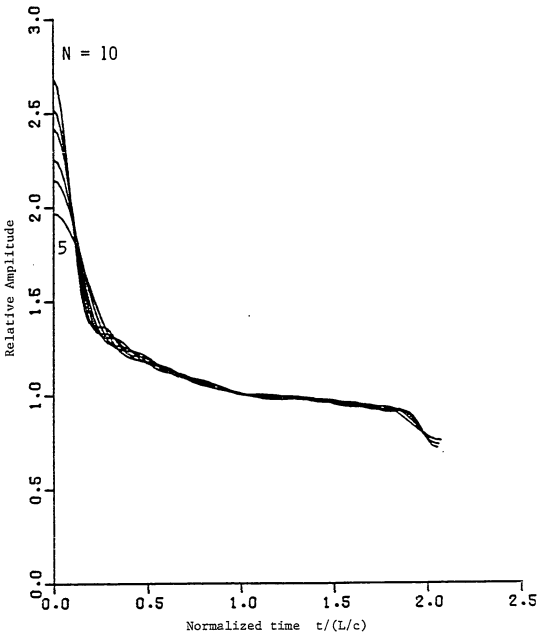

Figure 5.6.2. Natural E-pulses of minimum duration synthesized using Fourier cosine basis functions to eliminate the first 5, 6, 7, 8, 9, and 10 modes of the thin cylinder.

be known (or, at least those of the first layer), and it requires that the E-pulse waveform be calculated for increasingly larger numbers of natural frequencies. Neither of these are practical, of course, but it is interesting to explore a few aspects of E-pulse convergence using the pulse function basis set.

If the E-pulse is truly unique, then it should be independent of the basis set chosen to represent it (in the infinte limit), as long as the basis set is complete. However, it is possible to represent explicitly the E-pulse waveform using rectangular pulse functions and the analysis of section 4.6.1. This is not possible with the other complete basis sets. (At least, not at this time.) Without the explicit representation, it is quite difficult to compare the waveforms as N, the number of frequencies to be eliminated, is taken to infinity.

The most apparent requirement for E-pulse uniqueness is that the duration converge to a specific value. Even if this happens, though, it does not insure that the corresponding waveform will converge. However, if the duration does not converge, the waveform cannot possibly converge. Equation 4.6.1.24 reveals that the duration is dependent only upon the imaginary part of one of the natural frequencies of the target. For the natural E-pulse of minimum duration, this becomes

$$T_e = 2N \frac{\pi}{\omega_h} \qquad (5.6.1)$$

where ω_h is the largest imaginary frequency component to be eliminated.

Thus, for the duration to converge to a certain value, ω_h must be directly proportional to N in the limit that $N \to \infty$. For the case of the thin cylinder, the imaginary part of the k'th natural frequency can be represented as

$$\omega_k = \pi\left(k - \delta(k)\right) \frac{c}{L} \tag{5.6.2}$$

where

$$\lim_{k\to\infty} \frac{\delta(k)}{k} = 0 \tag{5.6.3}$$

This is in accordance with the observed behavior of the first layer of natural frequencies, and is shown quite clearly in Table 5.6.1 and Figure 5.6.3. With this, the minimum duration converges to

$$(T_e)_{min} = \lim_{N\to\infty} 2N \frac{\pi}{\pi\left(N-\delta(N)\right)} \frac{L}{c} \tag{5.6.4}$$

$$= 2\frac{L}{c}$$

demonstrating the uniqueness of the E-pulse duration.

With the duration shown to converge to a unique value it becomes necessary to verify that the corresponding waveform converges to a unique shape. This is quite difficult, since it requires the construction of an increasingly large number of pulse function amplitudes. Indeed, it would be much easier to prove the opposite -- that the waveform does not converge. Figure 5.6.1 shows why this might be a

Table 5.6.1 Thin cylinder natural frequencies and approximations.

n	$\sigma_n(L/c)$	$\frac{\sigma_n}{\sigma_{n-1}} \frac{\log(n)}{\log(n+1)}$	$-.3409\log(n+1)$	$\frac{\omega_n(L/c)}{n\pi}$
1	-0.2601		-0.2362	0.9250
2	-0.3808	0.9237	-0.3745	0.9560
3	-0.4684	0.9105	-0.4726	0.9613
4	-0.5382	0.9897	-0.5487	0.9685
5	-0.5997	1.001	-0.6108	0.9708
6	-0.6535	1.003	-0.6634	0.9740
7	-0.7037	1.008	-0.7089	0.9754
8	-0.7486	1.007	-0.7490	0.9776
9	-0.7923	1.010	-0.7850	0.9786
10	-0.8319	1.008	-0.8174	0.9800

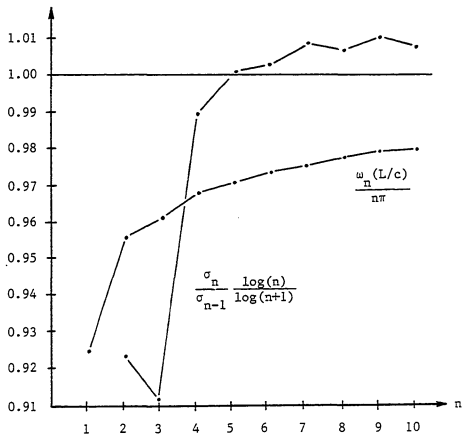

Figure 5.6.3. Thin cylinder natural frequency behavior.

worry. As N is increased, the leading portion of the E-pulse waveform appears to increase without bound. It is important to examine this behavior more closely.

Equation 4.6.1.42 states that the relative amplitude of the first pulse function is always positive and is determined only by the E-pulse duration and by the real parts of the natural frequencies to be eliminated. It is given by

$$\tilde{\alpha}_1 = \frac{\alpha_1}{\alpha_{2N}} = e^{\sigma_N \Delta} \prod_{n=1}^{N} e^{-2\sigma_n \Delta} \qquad (5.6.5)$$

where Δ is the width of each pulse, α_1 is the amplitude of the first pulse function, and α_{2N} is the amplitude of the last pulse function. By knowing all the σ's it would be possible to calculate the relative amplitude of the first pulse. There are three possible values it can take as $N \to \infty$. It might diverge (i.e. $\tilde{\alpha}_1 \to \infty$ or $\tilde{\alpha}_1 \neq$ single value), it might converge to zero, or it might converge to a number $\neq 0$. It would be hoped that the amplitude would converge to a nonzero value. If $\tilde{\alpha}_1$ does approach infinity, it doesn't necessarily mean that the E-pulse doesn't converge, since this could also indicate that $\alpha_{2N}=0$ (and thus $e(T_e)=0$.)

Of greatest interest is $\Delta\alpha_1$ which describes the area of the first pulse function. If the E-pulse is converging to a continuous waveform, then $\Delta\alpha$ will converge to zero, for each α. However, the nonlinear E-pulse analysis of section 4.7 suggested the possibility that the first pulse function might actually converge to

an impulse. In that case, its area would approach a constant. This requires that $\tilde{\alpha}_1$ be inversely proportional to the width of a pulse, for N very large. That is, if the width of the pulses is decreased by one half, the relative amplitude of the first pulse must double.

To examine the behavior of the first pulse function amplitude, it is convenient to rewrite (5.6.5), replacing the product of exponentials with the exponential of a sum

$$\tilde{\alpha}_1 = e^{\sigma_N \Delta} \exp\{-2\Delta \sum_{n=1}^{N} \sigma_n\} \tag{5.6.6}$$

This pulse function amplitude will converge to a specific nonzero value only if

$$\lim_{N\to\infty} \left(\sigma_N \Delta - 2\Delta \sum_{n=1}^{N} \sigma_n\right) \tag{5.6.7}$$

exists. As the duration $T_e = 2N\Delta$ is converging to a unique value as $N \to \infty$, (5.6.7) can be written as

$$\lim_{N\to\infty} \frac{T_e}{N}\left(\frac{\sigma_N}{2} - \sum_{n=1}^{N} \sigma_n\right) \tag{5.6.8}$$

On the other hand, the first pulse will converge to an impulse if

$$\lim_{N\to\infty} \Delta e^{\sigma_N \Delta} \exp\{-2\Delta \sum_{n=1}^{N} \sigma_n\} \tag{5.6.9}$$

exists and is not zero. This requires

$$\lim_{N\to\infty} \frac{1}{N}\left(\frac{\sigma_N}{2} - \sum_{n=1}^{N} \sigma_n - N\log N\right) = K \qquad (5.6.10)$$

where K is some constant.

Rather than calculating the amplitude of the first pulse function based upon a knowledge of all the natural frequencies, it is more expedient to examine its behavior using an empirical relationship for σ_n. Examination of the first layer of the natural frequencies of the thin cylinder target reveals that the real parts are negative and monotonically increasing (negatively.) Using the first ten natural frequencies it is possible to deduce that the σ's obey an approximate relationship given by

$$\sigma_n = A\log(n+1)\,\frac{c}{L} \qquad (5.6.11)$$

where A<0. This is shown quite clearly in Table 5.6.1 and in Figure 5.6.3, which plots $\left(\sigma(n)/\sigma(n-1)\right)\cdot\left(\log(n)/\log(n+1)\right)$. If the relationship were exact, this would yield unity. It is not exact, but it is quite close. The value of the constant A is determined by performing a least squares fit of the σ's

$$A = \frac{\sum_n \sigma_n \log(n+1)}{\sum_n \left(\log(n+1)\right)^2} \qquad (5.6.12)$$

Substituting the values for σ_n from Table 5.6.1 gives A=-0.3409. The

values of σ_n generated using this value of A and (5.6.11) are also shown in Table 5.6.1.

Using (5.6.11) in the formula for the relative amplitude of the first pulse function, along with the relationship for the duration for large N

$$\Delta = \frac{\pi}{\omega_N} \simeq \frac{1}{N}\frac{L}{c} \tag{5.6.13}$$

results in

$$\tilde{\alpha}_1 = \exp\{\frac{A}{N}\log(N+1)\} \prod_{n=1}^{N} \exp\{-2A\frac{1}{N}\log(n+1)\} \tag{5.6.14}$$

or

$$\tilde{\alpha}_1 = (N+1)^{A/N} \prod_{n=1}^{N} (n+1)^{-2A/N}$$

$$= (N+1)^{A/N}\{(N+1)!\}^{-2A/N} \tag{5.6.15}$$

For large N, Stirling's approximation for the factorial function [70]

$$n! \simeq (n/e)^n\sqrt{2\pi n} \tag{5.6.16}$$

can be applied to yield

$$\tilde{\alpha}_1 \approx (N+1)^{A/N}\left(\frac{N+1}{e}\right)^{N+1}\sqrt{2\pi(N+1)}\Bigg)^{-2A/N}$$

$$\approx (2\pi)^{-A/N}\left(\frac{N+1}{e}\right)^{-2A(N+1)/N} \qquad (5.6.17)$$

$$\to (N/e)^{-2A} \qquad \text{as } N \to \infty$$

Thus, since A<0, $\tilde{\alpha}_1$ does not converge. This agrees with the trend seen in Figure 5.6.1, where the relative amplitude of the first pulse seems to grow as N increases. Now, the relative area of the first pulse goes to

$$\Delta\tilde{\alpha}_1 \to \frac{L}{c}\, e^{2A}\, N^{-2A-1} \qquad (5.6.18)$$

Thus

$$\Delta\tilde{\alpha}_1 \to \begin{cases} 0 & A > -\tfrac{1}{2} \\ \infty & A < -\tfrac{1}{2} \\ \frac{L}{c}\, e^{-1} & A = -\tfrac{1}{2} \end{cases} \qquad (5.6.19)$$

Since A=-0.3409, the relative area of the first pulse converges tc zero. This implies that while the amplitude increases in an unbounded manner as $N \to \infty$, the area behaves as does the area of a bounded pulse.

This section has not proved or disproved the convergence of the thin cylinder E-pulse waveform. However, it has provided some insight into the difficulty such a proof might entail.

CHAPTER 6

EXTRACTION OF NATURAL FREQUENCIES FROM A MEASURED RESPONSE

6.1 Introduction

The most obvious requirement for the implementation of a radar target discrimination scheme based on natural target resonances is the accurate knowledge of the natural frequencies of a wide variety of targets. For most realistic targets, theoretical determination of the natural frequencies is impractical. Thus it becomes necessary, in some manner, to determine the natural frequencies from a measurement of the response of a scale model target.

This chapter presents a variety of methods for extracting the natural frequencies of a target from its measured response. Basically, the methods can be divided into four categories. The first involves Prony's method, which is well known and was discussed in chapter 3. It has many disadvantages, including a high sensitivity to noise, which prompts the investigation into the other methods presented in this chapter. In the second group, methods are developed which employ least squares parameter estimation, including a technique for regularizing the usually ill-conditioned problem. The last two groups utilize the E-pulse concept, solving first for an E-pulse and then extracting the natural frequencies from the E-pulse waveform. The first of these two groups involves minimizing the norm of the late-time convolution of

the measured response and the E-pulse waveform. The second involves using the method of moments to solve the integral equation obtained by setting this convolution equal to zero.

Each of these techniques will be examined in detail. Their performance under various circumstances, including the presence of random noise, will be examined for artificially constructed responses.

6.2 Prony's Method

Prony's method is an old and well respected technique for approximating a known function using a finite sum of complex exponentials [49]. If the function is taken as the measured response of a target then the complex frequencies used to construct the curve which passes through all the measured data points (or a selected subset) can be taken as an estimate of the natural frequencies in the response.

Let r(t) represent the response of a conducting target, and assume that the response is sampled at a finite number of points in time. Then $\{r_i\} = \{r(t_i)\}$ becomes the discrete representation of the measured response, where t_i is the time of the i'th sample

$$t_i = (i-1)\Delta \tag{6.2.1}$$

and Δ is the constant sampling interval. Prony's method attempts to find a function of the form

$$f(t) = \sum_{m=1}^{M} c_m e^{s_m t} \tag{6.2.2}$$

which has the same values as r(t) at the sampled times. Here s_m and c_m are complex quantities. Equation (6.2.2) can also be written as

$$f(t) = \sum_{m=1}^{M} c_m z_m^t \qquad (6.2.3)$$

where

$$z_m = e^{s_m} \qquad (6.2.4)$$

The function f(t) is a good model for r(t) if r(t) is composed of a sum of damped sinusoids (as expected in the late-time response of a target.) Since r(t) is necessarily real, c_m and s_m will occur only only in complex conjugate pairs.

For f(t) to be calculated uniquely, there must be at least 2M sampled response points. Then f(t) can be made to fit exactly through those points. If fewer points are used the resulting values of the complex frequencies will not be a good estimate of the natural frequencies in the response. It is thus necessary to have a good guess at the number of complex exponentials needed to accurately model the measured response (i. e. to know how many modes are present in the response.)

Since the sampling density Δ is assumed to be constant, equating the sampled response and the model f(t) demands that the following difference equation be satisfied

$$r_M - \sum_{i=1}^{M} a_i r_{M-i} = \sum_{i=1}^{M} c_i \left((z_i^{\Delta})^M - \sum_{j=1}^{M} a_j (z_i^{\Delta})^{M-j} \right) \qquad (6.2.5)$$

In essence, this requires that the model fit exactly through the sampled response points. Now, let z_i^{Δ} be the complex roots of the polynomial equation

$$z^M - \sum_{i=1}^{M} a_i z^{M-i} = 0 \qquad (6.2.6)$$

Using this, the right hand side of (6.2.5) reduces to zero and the equation becomes

$$\sum_{i=1}^{M} a_i r_{M-i} = r_M \qquad (6.2.7)$$

The coefficients of the polynomial can be determined by choosing $K \geq M$ sampled response values to use in the right hand side of (6.2.7). This results in

$$\sum_{i=1}^{M} a_i r_{M+k-i} = r_{M+k} \qquad k=1,2,\ldots,K \qquad (6.2.8)$$

Equation (6.2.8) is a matrix equation which can be solved quite easily using standard techniques. If K>M it can be solved approximately using the method of least squares. Once the a's are determined, the roots z_i^{Δ} are found by solving (6.2.6), and estimates for the natural frequencies in the measured response are given via (6.2.4) as

$$s_m = \frac{1}{\Delta} \log(Z_m) \qquad (6.2.9)$$

Lastly, with s_i known, the complex amplitudes c_i can be determined by solving

$$f(t_i) = r(t_i) \qquad i=1,2,\ldots,K \qquad (6.2.10)$$

by the method of least squares.

Prony's method is extremely simple to use. Except for (6.2.6) all equations are linear and can be solved using standard matrix algebra. Several standard numerical techniques also exist for solving the large polynomial equation (6.2.6). However, Prony's method has many shortcomings which greatly reduce its usefulness under practical circumstances. The worst of these is its extreme sensitivity to random noise, which will almost certainly be present in the measured response. Hildebrand [50] gives a clasic example of sensitivity to errors in the data, indicating that Prony's method is inherently an ill-conditioned algorithm, and averaging of results over different groups of samples or using linear least squares in (6.2.8) can only give marginally improved results. Examples of the performance of Prony's method in the presence of random noise, and an additional suggestion for improvement, are presented in section 6.9.

A second important drawback to Prony's method is the necessity of knowing the number of modes present in the measured response waveform. If M/2 modes are actually present, using fewer than M

exponentials in (6.2.2) results in very inaccurate estimates of the natural frequencies. This is especially misleading since the approximation f(t) calculated using the smaller number of exponentials will still pass exactly through the sampled points, and will probably be a good approximation elsewhere (again, see the example in Hildebrand.)

Lastly, although it is not of great consideration with most measurement systems, Prony's method is the only technique of this chapter that requires a constant sampling density.

These practical difficulties have prompted the need for improved natural frequency extraction techniques. Five such methods are considered in the following sections.

6.3 Least Squares Curve Fitting

Let $\{r_i\} = \{r(t_i)\}$ represent the measured response of a conducting target, sampled at times t_i. Assuming that the response is composed of a finite number of natural modes (plus possibly a DC level), an estimate of the natural frequencies contained in r(t) can be determined by finding the function of the form

$$F(A_1,\ldots,\psi_N,K,t) = K + \sum_{n=1}^{N} A_n e^{\hat{\sigma}_n t}\cos(\hat{\omega}_n t + \psi_n) \qquad (6.3.1)$$

which "best fits" in some way the measured data. With a best fit, the extracted natural frequencies are given by $(\hat{\sigma}_n + j\hat{\omega}_n)$.

The most common means of determining a best fit is to minimize the squared error between the fitting function and the measured data.

In terms of multivariable calculus, let $\vec{F}(\vec{x})$ be a nonlinear vector valued function of the vector $\vec{x}$, where $\vec{F}$ has the form given in (6.3.1) with i'th component $F(A_1,\ldots,\psi_N,K,t_i)$ and $\vec{x}$ is given by

$$\vec{x} = (A_1,\sigma_1,\ldots,\omega_N,\psi_N,K)^T \tag{6.3.2}$$

where T denotes matrix transpose. Now, define $\vec{R}(\vec{x})$ as the difference between the measured data and the fitting function

$$R_i(\vec{x}) = F_i(\vec{x}) - r_i \tag{6.3.3}$$

where

$$\begin{aligned} F_i(\vec{x}) &= F(\vec{x},t_i) \\ R_i(\vec{x}) &= R(\vec{x},t_i) \end{aligned} \tag{6.3.4}$$

Then, least squares analysis requires the minimization of [51]

$$E(\vec{x}) = |\vec{R}(\vec{x})|_2^2 = \sum_{i=1}^{M} R_i^2(\vec{x}) \tag{6.3.5}$$

with respect to the vector $\vec{x}$, where M is the number of data points to be used and the subscript 2 on the absolute value sign designates L_2 norm (vector magnitude.) In vector notation, equation (6.3.5) can also be written as

$$E(\vec{x}) = \vec{R}(\vec{x})^T\vec{R}(\vec{x}) \tag{6.3.6}$$

Minimization of the quantity (6.3.5) is accomplished by setting the partial derivatives of $E(\vec{x})$ with respect to each of the components of $\vec{x}$ equal to zero. This is merely the gradient of E, so

$$\vec{f}(\vec{x}) = \nabla_{\vec{x}} E(\vec{x}) = \sum_{i=1}^{M} \nabla_{\vec{x}} R_i(\vec{x}) R_i(\vec{x}) = 0 \qquad (6.3.7)$$

which can be written in matrix notation as

$$\vec{f}(\vec{x}) = \overline{\overline{J}}_R(\vec{x})^T \vec{R}(\vec{x}) = 0 \qquad (6.3.8)$$

where $\overline{\overline{J}}_R(\vec{x})$ is the Jacobian matrix of $\vec{R}(\vec{x})$, with entries

$$\left(\overline{\overline{J}}_R(\vec{x})\right)_{i,j} = \frac{\partial R_i(\vec{x})}{\partial x_j} \qquad (6.3.9)$$

The vector valued function $\vec{f}(\vec{x})$ in (6.3.8) represents a system of 4N+1 nonlinear equations in the 4N+1 unknown variables of $\vec{x}$. There are many ways of solving such a system, but the most widely used is straight forward Newton's method.

Newton's method for solving (6.3.8) is developed by expanding $\vec{f}(\vec{x})$ in a Taylor series about a point $\vec{x}=\vec{x}_o$

$$\vec{f}(\vec{x}) = \vec{f}(\vec{x}_o) + \nabla_{\vec{x}} \vec{f}(\vec{x}_o)^T (\vec{x}-\vec{x}_o) + \tfrac{1}{2}(\vec{x}-\vec{x}_o)^T \nabla_{\vec{x}}^2 f(\vec{x}_o)(\vec{x}-\vec{x}_o) + \ldots \qquad (6.3.10)$$

Keeping only the first two terms on the right hand side of (6.3.10) and using $\vec{f}(\vec{x})=0$ gives the approximation

$$\vec{x} = \vec{x}_o - \left(\nabla_{\vec{x}}\vec{f}(\vec{x}_o)\right)^{-1}\vec{f}(\vec{x}) \qquad (6.3.11)$$

This equation is then used in an iterative scheme to converge from some initial guess for $\vec{x}$ to the solution of (6.3.8).

The gradient of $\vec{f}(\vec{x})$ in (6.3.11) can be expanded as

$$\nabla_{\vec{x}}\vec{f}(\vec{x}) = \nabla^2_{\vec{x}}E(\vec{x}) = \nabla_{\vec{x}}\left(\sum_{i=1}^{M}\nabla_{\vec{x}}R_i(\vec{x})R_i(\vec{x})\right)$$

$$= \bar{\bar{J}}_R(\vec{x})^T\bar{\bar{J}}_R(\vec{x}) + \bar{\bar{S}}_R(\vec{x}) \qquad (6.3.12)$$

where $\bar{\bar{S}}_R(\vec{x})$ is the 2N+1 by 2N+1 matrix

$$\bar{\bar{S}}_R(\vec{x}) = \sum_{i=1}^{M} R_i(\vec{x})\nabla^2_{\vec{x}}R_i(\vec{x}) \qquad (6.3.13)$$

and

$$\bar{\bar{J}}_R(\vec{x})^T\bar{\bar{J}}_R(\vec{x}) = \sum_{i=1}^{M}\nabla_{\vec{x}}R_i(\vec{x})\nabla_{\vec{x}}R_i(\vec{x})^T \qquad (6.3.14)$$

Here $\nabla^2_{\vec{x}}R_i(\vec{x})$ is sometimes called the "Hessian" of $R_i(\vec{x})$, and has the entries

$$\left(\nabla^2_{\vec{x}}R_i(\vec{x})\right)_{m,n} = \frac{\partial^2 R_i(\vec{x})}{\partial x_m \partial x_n} \qquad (6.3.15)$$

Thus, equation (6.3.11) can be written as

$$\vec{x} \simeq \vec{x}_o - \left(\overline{\overline{J}}_R(\vec{x}_o)^T \overline{\overline{J}}_R(\vec{x}_o) + \overline{\overline{S}}_R(\vec{x}_o)\right)^{-1} \overline{\overline{J}}_R(\vec{x}_o)^T \vec{R}(\vec{x}_o) \qquad (6.3.16)$$

It is obvious that a great deal of calculation is necessary to compute each value of $\vec{x}$ in (6.3.16). If $\vec{R}(\vec{x})$ was a more complicated function than (6.3.3) many of the derivatives involved would have to be approximated using finite differences. Such approximation usually leads to a reduction in the region of convergence of Newton's method. Fortunately, for this application the derivatives can be calculated analytically. The Jacobian requires the first partials of $R_i(\vec{x})$ and the Hessian the second partials. For the sake of completeness, these derivatives are given below. They are written in terms of the original variables in (6.3.1) with the required substitution given by (6.3.2) as

$$\begin{aligned} x_{4n-3} &= A_n & x_{4n-1} &= \hat{\omega}_n & x_{4N+1} &= K \\ x_{4n-2} &= \hat{\sigma}_n & x_{4n} &= \psi_n \end{aligned} \qquad (6.3.17)$$

Using these, the derivatives are

$$\frac{\partial R_i}{\partial A_j} = e^{\hat{\sigma}_j t_i} \cos(\hat{\omega}_j t_i + \psi_j)$$

$$\frac{\partial R_i}{\partial \hat{\sigma}_j} = t_i A_j e^{\hat{\sigma}_j t_i} \cos(\hat{\omega}_j t_i + \psi_j)$$

$$\frac{\partial R_i}{\partial \hat{\omega}_j} = -t_i A_j e^{\hat{\sigma}_j t_i} \sin(\hat{\omega}_j t_i + \psi_j)$$

$$\frac{\partial R_i}{\partial \psi_j} = -A_j e^{\hat{\sigma}_j t_i} \sin(\hat{\omega}_j t_i + \psi_j)$$

$$\frac{\partial R_i}{\partial K} = 1$$

$$\frac{\partial}{\partial A_k}\frac{\partial R_i}{\partial A_j} = 0$$

$$\frac{\partial}{\partial \hat{\sigma}_k}\frac{\partial R_i}{\partial A_j} = \delta_{jk} t_i e^{\hat{\sigma}_j t_i} \cos(\hat{\omega}_j t_i + \psi_j)$$

$$\frac{\partial}{\partial \hat{\omega}_k}\frac{\partial R_i}{\partial A_j} = -\delta_{jk} t_i e^{\hat{\sigma}_j t_i} \sin(\hat{\omega}_j t_i + \psi_j)$$

$$\frac{\partial}{\partial \psi_k}\frac{\partial R_i}{\partial A_j} = -\delta_{jk} e^{\hat{\sigma}_j t_i} \sin(\hat{\omega}_j t_i + \psi_j)$$

$$\frac{\partial}{\partial K}\frac{\partial R_i}{\partial A_j} = 0$$

$$\frac{\partial}{\partial \hat{\sigma}_k}\frac{\partial R_i}{\partial \hat{\sigma}_j} = \delta_{jk} t_i^2 A_j e^{\hat{\sigma}_j t_i} \cos(\hat{\omega}_j t_i + \psi_j)$$

$$\frac{\partial}{\partial \hat{\omega}_k}\frac{\partial R_i}{\partial \hat{\sigma}_j} = -\delta_{jk} t_i^2 A_j e^{\hat{\sigma}_j t_i} \sin(\hat{\omega}_j t_i + \psi_j)$$

$$\frac{\partial}{\partial \psi_k}\frac{\partial R_i}{\partial \hat{\sigma}_j} = -\delta_{jk} t_i A_j e^{\hat{\sigma}_j t_i} \sin(\hat{\omega}_j t_i + \psi_j)$$

$$\frac{\partial}{\partial K}\frac{\partial R_i}{\partial \hat{\sigma}_j} = 0$$

$$\frac{\partial}{\partial \hat{\omega}_k}\frac{\partial R_i}{\partial \hat{\omega}_j} = -\delta_{jk} t_i^2 A_j e^{\hat{\sigma}_j t_i} \cos(\hat{\omega}_j t_i + \psi_j)$$

$$\frac{\partial}{\partial \psi_k}\frac{\partial R_i}{\partial \hat{\omega}_j} = -\delta_{jk} t_i A_j e^{\hat{\sigma}_j t_i} \cos(\hat{\omega}_j t_i + \psi_j)$$

$$\frac{\partial}{\partial K}\frac{\partial R_i}{\partial \hat{\omega}_j} = 0$$

$$\frac{\partial}{\partial \psi_k}\frac{\partial R_i}{\partial \psi_j} = -\delta_{jk} A_j e^{\hat{\sigma}_j t_i} \cos(\hat{\omega}_j t_i + \psi_j)$$

$$\frac{\partial}{\partial K}\frac{\partial R_i}{\partial \psi_j} = 0 \qquad (6.3.18)$$

$$\frac{\partial}{\partial K}\frac{\partial R_i}{\partial K} = 0$$

where

$$\delta_{jk} = \begin{cases} 1 & j=k \\ 0 & j\neq k \end{cases} \qquad (6.3.19)$$

There are two difficulties encountered when directly applying Newton's method via (6.3.16). First, Newton's method is only locally convergent. Obtaining a meaningful solution is highly dependent upon the initial guess for $\vec{x}$ [52]. In general, it will be possible to estimate the natural frequencies by using other techniques (such as the Fourier transform), but the amplitudes and phases of the individual

modes will be quite difficult to approximate. Second, nonlinear least squares analyses are usually ill-conditioned problems. This is transferred into poor conditioning of the matrices in (6.3.16). The first of these problems, the effect of poor initial guesses, is addressed by the method of section 6.4. Both problems are attacked by the continuation method techniques of section 6.5.

6.4 Linear/Nonlinear Iteration

The least squares problem as introduced in equation (6.3.5) is actually a combined linear/nonlinear problem. The fitting function (6.3.1) is linear in amplitude and phase (and DC level) but nonlinear in complex frequency. It might seem that this type of problem could be separated into two problems, one requiring linear least squares and the other requiring nonlinear least squares. This is indeed the case, and a general technique for solving combined linear/nonlinear least squares problems has been introduced by various authors [53] - [56]. The benefit gained by this separation approach is twofold. First, it eliminates the need to provide initial guesses for the amplitudes and phases which, it has been pointed out, is quite difficult. Second, it reduces the size of the nonlinear problem to be solved by ½. However, this technique is considerably more complicated than taking the problem as totally nonlinear and using Newton's method. This section presents an alternative to the separation of the linear and the nonlinear problems, keeping the benefits of that approach, but eliminating the complexity.

The algorithm to be introduced is termed "linear/nonlinear

iteration" (hereafter referred to as l/n iteration.) The vector difference between the fitting function and the measured data can be written with its linear component separated out by expanding the cosine in (6.3.1) as

$$A_n\cos(\hat{\omega}_n t + \psi_n) = a_n\cos\hat{\omega}_n t + b_n\sin\hat{\omega}_n t \qquad (6.4.1)$$

where

$$a_n = A_n\cos\psi_n \qquad b_n = -A_n\sin\psi_n \qquad (6.4.2)$$

Note that the phase-amplitude form (6.3.1) is easily regained through

$$A_n = (a_n^2 + b_n^2)^{\frac{1}{2}}$$

$$\psi_n = \tan^{-1}\left(-\frac{b_n}{a_n}\right) + \begin{cases} \pi & a_n<0 \\ 0 & a_n>0 \end{cases} \qquad (6.4.3)$$

Now, define two new vectors, one containing the linear variables and one containing the nonlinear variables, as

$$\vec{y} = (a_1, b_1, \ldots, a_N, b_N, K)^T$$

$$\vec{z} = (\hat{\sigma}_1, \hat{\omega}_1, \ldots, \hat{\sigma}_N, \hat{\omega}_N)^T \qquad (6.4.4)$$

Using these allows the vector difference between the fitting function and the measured data to be written as

$$\vec{R}(\vec{x}) = \bar{\bar{A}}(\vec{z})\vec{y} - \vec{r} \tag{6.4.5}$$

where $r_i = r(t_i)$ and $\bar{\bar{A}}$ is an M by 2N+1 matrix with the entries

$$\left(\bar{\bar{A}}\right)_{n,m} = \begin{cases} e^{\hat{\sigma}_m t_k}\cos\hat{\omega}_m t_k & k = \frac{n+1}{2}\ ; \quad n \text{ odd} \\ e^{\hat{\sigma}_m t_k}\sin\hat{\omega}_m t_k & k = \frac{n}{2} \qquad n \text{ even} \end{cases} \tag{6.4.6}$$

$$\left(\bar{\bar{A}}\right)_{2N+1,m} = 1$$

If the vector $\vec{z}$ in (6.4.5) is taken as constant, then the least squares problem given by minimizing (6.3.5) becomes purely linear, involving only the vector $\vec{y}$. The solution to this problem is well known and requires no searching algorithm. The vector $\vec{y}^*$ which minimizes the squared difference is the solution to the normal equation

$$\left[\bar{\bar{A}}(\vec{z})^T\bar{\bar{A}}(\vec{z})\right]\vec{y} = \bar{\bar{A}}(\vec{z})^T\vec{r} \tag{6.4.7}$$

which is

$$\vec{y}^* = \left[\bar{\bar{A}}(\vec{z})^T\bar{\bar{A}}(\vec{z})\right]^{-1}\bar{\bar{A}}^T\vec{r} \tag{6.4.8}$$

Writing (6.4.7) more simply as

$$\overline{\overline{B}}(\vec{z})\vec{y} = \vec{b} \tag{6.4.9}$$

allows the solution to be written as

$$\vec{y}^{*} = \overline{\overline{B}}(\vec{z})^{-1}\vec{b} \tag{6.4.10}$$

The entries in $\overline{\overline{B}}$ and $\vec{b}$ are easily calculated as

1. n odd, k = (n+1)/2

$$\left(\overline{\overline{B}} \right)_{n,2N+1} = \sum_{i=1}^{M} e^{\hat{\sigma}_k t_i} \cos\hat{\omega}_k t_i$$

2. n even, k = n/2

$$\left(\overline{\overline{B}} \right)_{n,2N+1} = \sum_{i=1}^{M} e^{\hat{\sigma}_k t_i} \sin\hat{\omega}_k t_i$$

3. n odd, k = (n+1)/2; m odd, q = (m+1)/2

$$\left(\overline{\overline{B}} \right)_{n,m} = \sum_{i=1}^{M} e^{\hat{\sigma}_k t_i} \cos\hat{\omega}_k t_i \; e^{\hat{\sigma}_q t_i} \cos\hat{\omega}_q t_i$$

4. n odd, k = (n+1)/2; m even, q = m/2

$$\left(\overline{\overline{B}} \right)_{n,m} = \sum_{i=1}^{M} e^{\hat{\sigma}_k t_i} \cos\hat{\omega}_k t_i \; e^{\hat{\sigma}_q t_i} \sin\hat{\omega}_q t_i$$

5. n even, k = n/2; m odd, q = (m+1)/2

$$\left[\bar{\bar{B}}\right]_{n,m} = \sum_{i=1}^{M} e^{\hat{\sigma}_k t_i} \sin\hat{\omega}_k t_i \; e^{\hat{\sigma}_q t_i} \cos\hat{\omega}_q t_i$$

6. n even, k = n/2; m even, q = m/2

$$\left[\bar{\bar{B}}\right]_{n,m} = \sum_{i=1}^{M} e^{\hat{\sigma}_k t_i} \sin\hat{\omega}_k t_i \; e^{\hat{\sigma}_q t_i} \sin\hat{\omega}_q t_i$$

7. m odd, q = (m+1)/2

$$\left[\bar{\bar{B}}\right]_{2N+1,m} = \sum_{i=1}^{M} e^{\hat{\sigma}_q t_i} \cos\hat{\omega}_q t_i$$

8. m even, q = m/2 (6.4.11)

$$\left[\bar{\bar{B}}\right]_{2N+1,m} = \sum_{i=1}^{M} e^{\hat{\sigma}_q t_i} \sin\hat{\omega}_q t_i$$

9.

$$\left[\bar{\bar{B}}\right]_{2N+1,2N+1} = M$$

10. n odd, k = (n+1)/2

$$b_n = \sum_{i=1}^{M} r_i e^{\hat{\sigma}_k t_i} \cos\hat{\omega}_k t_i$$

11. n even, k = n/2

$$b_n = \sum_{i=1}^{M} r_i e^{\hat{\sigma}_k t_i} \sin \hat{\omega}_k t_i$$

12.

$$b_{2N+1} = \sum_{i=1}^{M} r_i$$

If the vector $\vec{y}$ in (6.4.5) is taken as constant, then the least squares problem given by minimizing (6.3.5) becomes completely nonlinear, involving only the vector $\vec{z}$. This problem must be solved by some searching algorithm, such as the Newton's method of section 6.3, and requires initial guesses for the components of $\vec{z}$. However, the number of variables involved in the minimization is reduced by ½ over the original combined linear/nonlinear problem.

The 1/n iteration algorithm alternates between the solutions to the linear and nonlinear problems outlined above. A simplified flowchart for the algorithm is shown in Figure 6.4.1. At the outset an initial guess is made for the natural frequencies in the measured response and the linear problem is solved with the vector $\vec{z}$ assumed constant as the initial guesses. Then, with the vector $\vec{y}$ assumed constant as the solution $\vec{y}^*$ to the linear problem, the nonlinear problem is solved for an updated vector $\vec{z}$ using Newton's method (6.3.16) to a specified accuracy. With $\vec{z}$ held constant, a new vector $\vec{y}^*$ is calculated and the process is repeated, iterating between the linear and nonlinear problems, until sufficient accuracy in both $\vec{y}$ and $\vec{z}$ are

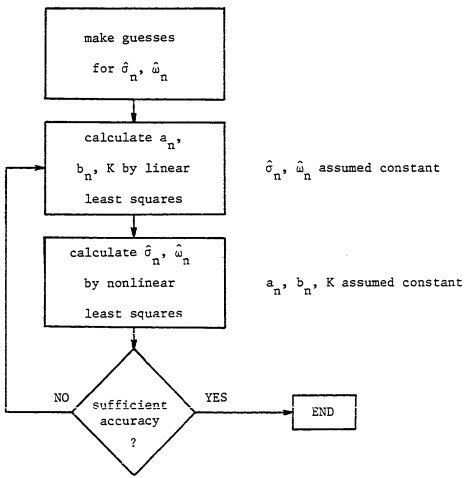

Figure 6.4.1. Simplified flowchart for linear/nonlinear iteration.

obtained.

The success of the 1/n iteration scheme is contingent upon the solutions to the linear and the nonlinear problems being different. That this is so is not obvious. Furthermore, the author knows of no previous algorithm of this type, and thus knows of no analysis of its convergence properties (and none will be attempted.) Although there is no guarantee that this method will converge at all, numerical experimentation shows that under many circumstances it does, and that its region of convergence is surprisingly large.

As a simple example, consider a theoretical response consisting of one mode, constructed as

$$r(t) = 0.1 + 1e^{-0.2t}\cos(2t + 1) \qquad (6.4.12)$$

Now, as a measurement simulation, this response is sampled at 100 points between t=0 and t=10, with a constant sampling interval of t=0.1. An attempt is then made to recover $\sigma = -0.2$ and $\omega = 2.0$ by means of the 1/n iteration algorithm. An initial guess of $\hat{\sigma} = 0$ and $\omega = 1.6$ is assumed, and Figure 6.4.2 shows the results. Each of the components of $\vec{y}$ and $\vec{z}$ (normalized to the actual values in the constructed response) have been plotted versus the iteration number. Iteration 0 represents the initial guesses for $\hat{\sigma}$ and $\hat{\omega}$ and the initial linear solution for A, ψ, and K. Each additional iteration represents one solution to both the linear and nonlinear problems. It can be seen that the different variables converge at quite different rates. While $\hat{\omega}$ has converged to within a percent of its actual value by the

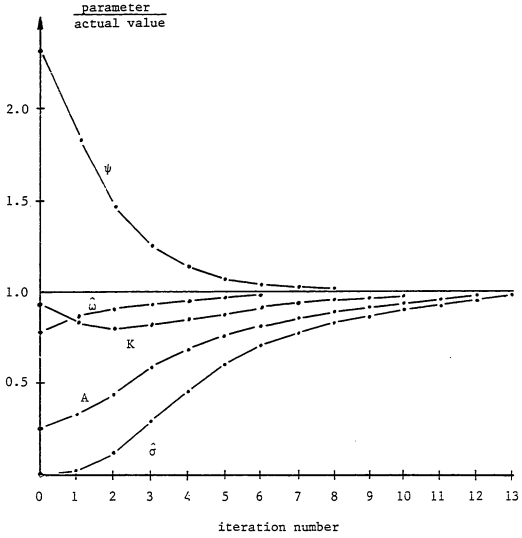

Figure 6.4.2. Convergence of the linear/nonlinear iteration method.

sixth iteration, it takes nearly eleven iterations before K has converged to within the same accuracy, even though the "initial guess" guess for K (from the first solution to the linear problem -- iteration 0) is much closer to the actual value.

6.5 The Continuation Method

The 1/n iteration method of section 6.4 attempted to alleviate the problem of needing good initial guesses for the implementation of Newton's method to solve (6.3.8), but it did not address the fact [57] that the nonlinear least squares problem is ill-conditioned. When a problem is ill-conditioned no algorithm can be depended upon to produce truly accurate results under most circumstances. "Regularization" is a technique for solving such a problem by transforming it into a related well-conditioned problem with a solution that is a good approximation to the elusive solution of the original problem [58], [59]. An easily applicable choice for a regularization scheme for the nonlinear least squares problem is the well-known "continuation method" [60], [61]. This technique is discussed in general terms in Allgower and Georg [62].

Instead of minimizing the norm of the vector distance between the fitting function and the measured data as in (6.3.5) consider the minimization of the quantity

$$G_\tau(\vec{x}) = \tau|\vec{R}(\vec{x})|_2^2 + (1-\tau)|\vec{W}(\vec{x})|_2^2 \qquad (6.5.1)$$

where $\vec{R}(\vec{x})$ is given in (6.3.3), the subscript 2 on the absolute value

sign designates L_2 norm, and the i'th component of the vector $\vec{W}(\vec{x})$ is given by

$$W_i(\vec{x}) = \frac{x_i}{x_{oi}} - 1 \qquad (6.5.2)$$

where $\vec{x}_o$ contains a set of initial guesses for the components of $\vec{x}$. $\vec{W}(\vec{x})$ is sometimes referred to as a "penalty term" and is designed to keep $\vec{x}$ from wandering too far from the initial guesses, as well as improving the conditioning of the problem.

Minimization of $G_\tau(\vec{x})$ with respect to the parameters in $\vec{x}$ requires

$$\vec{H}(\vec{x},\tau) = \nabla_{\vec{x}} G_\tau(\vec{x}) = \tau \bar{\bar{J}}_R(\vec{x})^T \vec{R}(\vec{x}) + (1-\tau)\bar{\bar{J}}_W(\vec{x})^T \vec{W}(\vec{x}) = 0 \qquad (6.5.3)$$

analogous to (6.3.8). The second term in $\vec{H}(\vec{x},\tau)$ is quite simple. Using

$$\left(\bar{\bar{J}}_W(\vec{x}) \right)_{i,j} = \frac{\partial W_i(\vec{x})}{\partial x_j} = \frac{1}{x_{oi}} \delta_{ij} \qquad (6.5.4)$$

gives

$$\left(\bar{\bar{J}}_W(\vec{x})^T \vec{W}(\vec{x}) \right)_i = \frac{W_i}{x_{oi}} \qquad (6.5.5)$$

It is seen that with $\tau=1$ (6.5.3) represents the original ill-conditioned nonlinear least squares problem (6.3.8). However, with $\tau=0$ equation (6.5.3) reduces to the well-conditioned problem

$$\bar{\bar{J}}_W(\vec{x})^T \vec{W}(\vec{x}) = 0 \qquad (6.5.6)$$

which has the obvious solution

$$\vec{x} = \vec{x}_o \qquad (6.5.7)$$

The continuation method is an iterative procedure, beginning with $\tau_o=0$ and with $\vec{x}_o$ as a set of initial guesses. At each successive iteration τ_i is replaced by $\tau_{i+1} = \tau_i + \Delta\tau$ and the problem (6.5.3) is solved using the Newton's method analysis of section 6.3. As τ increases at each step, more of the original ill-conditioned problem is added onto the well-conditioned problem (6.5.6). Assuming that $\Delta\tau$ is small enough to insure convergence, the procedure continues until $\tau = \tau_f$. If $\tau_f=1$ then the original problem is solved. However, it might be necessary to stop at $\tau_f<1$ if the problem (6.5.3) becomes too ill-conditioned. It is hoped that at this value of τ the solution to (6.5.3) is a good approximation to the solution to (6.3.8).

The continuation method as outlined above has been implemented using the standard IMSL routine "ZSCNT" [63] to solve (6.5.3) with very promising results. However, this particular version will not converge under many circumstances. Fixing the step size $\Delta\tau$ and always requiring τ to increase is overly restrictive, as it may actually become necessary to reduce τ at certain points to insure convergence.

It is possible to develop an alternative scheme which works well in practice and seems to be less sensitive to the initial guesses by

assuming that (6.5.3) determines a simple path in $(\vec{x},\tau)$ space leading from $(\vec{x}_o,0)$ to $(\vec{x}_f,\tau_f)$ as shown in Figure 6.5.1. The path leads from a set of initial guesses to the best approximation for the desired solution to (6.3.8). Locating the solution thus reduces to merely following this path until $\tau=1$ or the problem becomes too ill-conditioned.

It is convenient to parameterize the path by arc length s. Then, if the chain rule is applied, the derivative of equation (6.5.3) can be written as

$$\frac{d}{ds}\vec{H}(\vec{x}(s),\tau(s)) = \left(\nabla_{\vec{x}}\vec{H}\right)\cdot\frac{d\vec{x}}{ds} + \frac{d\vec{H}}{d\tau}\frac{d\tau}{ds} = 0 \qquad (6.5.8)$$

This can be viewed as a differential equation

$$\begin{pmatrix} \dfrac{d\vec{x}}{ds} \\ \\ \dfrac{d\tau}{ds} \end{pmatrix} = \vec{v} \qquad (6.5.9)$$

where $\vec{v}$ is the normalized solution to the homogeneous equation

$$\left(\nabla_{\vec{x}}\vec{H},\ \frac{d\vec{H}}{d\tau}\right)\vec{v} = 0 \qquad (6.5.10)$$

Here "normalized" indicates that the solution to (6.5.10) should be replaced by the unit vector $\vec{v}/|\vec{v}|$ before being used in (6.5.9).

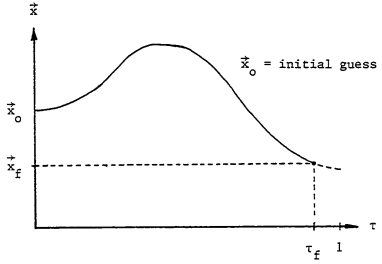

Figure 6.5.1. Typical path for continuation method in $(\vec{x},\tau)$ space.

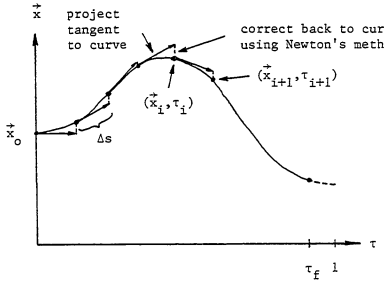

Figure 6.5.2. Typical succession of predictions and corrections in continuation method.

If it is assumed that at each point on the curve

$$\text{a)} \quad \left(\nabla_{\vec{x}} H,\ \frac{d\vec{H}}{d\tau}\right) \quad \text{has full rank}$$

$$\text{b)} \quad \bar{\bar{A}}(s) = \begin{pmatrix} \left(\frac{d\vec{x}}{d\tau}\right)^T, & \frac{d\tau}{ds} \\ \nabla_{\vec{x}}\vec{H}, & \frac{d\vec{H}}{d\tau} \end{pmatrix} \quad \text{is nonsingular} \tag{6.5.11}$$

then equation (6.5.9) can be solved using a standard ordinary differential equation follower, leading to the desired solution at $\tau=\tau_f$.

It is also possible to construct a "predictor-corrector" follower to step along the path until the final point $(\vec{x}_f,\tau_f)$ is reached, either at $\tau_f=1$ or when the problem becomes too ill-conditioned. The predictor step (Euler) is to solve (6.5.10) for $(\Delta x,\Delta\tau)$ using a preselected value of arc length Δs. The sign of $\det(\bar{\bar{A}}(s))$ is used to choose the correct sign of $\vec{v}$, to continue moving in the same direction along the curve. Problems can occur if $\det(\bar{\bar{A}}(s))=0$, which indicates that the path crosses itself at that point or that the path bifurcates. These problems can be overcome, and are addressed in [64]. It is also possible to incorporate a variable step size Δs which increases at points of small curvature and decreases when the path makes sharp turns. This is discussed in [62].

Correction back to the curve uses Newton's method as described in section 6.3, with τ held constant

$$\vec{x}_{i+1} = \vec{x}_i - \left(\nabla_{\vec{x}}\vec{H}(\vec{x}_i,\tau_p)\right)^{-1}\vec{H}(\vec{x}_i,\tau_p) \qquad (6.5.12)$$

where τ_p is the predicted value of τ. At each iteration in Newton's method the condition number of the matrix

$$\nabla_{\vec{x}}\vec{H}(\vec{x}_i,\tau_p) \qquad (6.5.13)$$

is checked to determine if the problem is becoming too ill-conditioned and whether the algorithm should be terminated. The condition number is calculated using singular value decomposition or estimated using Linpack routine "SGECO" [65]. Termination is demanded when the log (base ten) of the condition number becomes larger than the difference between the number of digits carried by the computer and the number of digits of accuracy estimated to be present in the measured data. If termination is not required the algorithm continues to follow the curve. Figure 6.5.2 shows a typical succession of predictions and corrections, and Figure 6.5.3 presents a structured flowchart for the implementation of the predictor-corrector algorithm. Theorems concerning sufficient conditions for the convergence of this form of the continuation method are discussed in [64] and [66].

It would seem that initial guesses must still be made for the amplitudes and phases of the modes at the beginning of the algorithm. Although this requirement is true, it can be side-stepped somewhat by making guesses only for the natural frequencies and then calculating the amplitudes, phases, and DC level by using the linear least squares

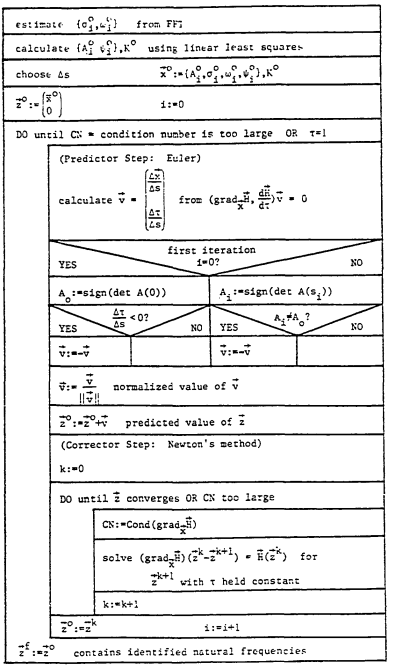

Figure 6.5.3. Structured flowchart for continuation method.

analysis of equation (6.4.8).

An improvement upon the correction step can be made by including τ as a free variable in Newton's method, and demanding that correction be made normal to the prediction vector. This requirement demands

$$\hat{u}^T(\vec{x}_i,\tau_i) = 0 \qquad (6.5.14)$$

where $\hat{u}$ is a unit tangent vector to the curve at the point of prediction, and the multiplication is the vector dot product. Such a change would allow the predictor-corrector follower to "turn the corner" better if the path was to fold back along τ. However, this change has not been implemented. A further improvement, which has been tried, is to use linear least squares at the end of each prediction step, to give the Newton's method correction step a better starting point. Results have been favorable, but perhaps not quite worth the additional computational expense.

As a simple example, consider the constructed response given by (6.4.12) and sampled as discussed in section 6.4. A step size of $\Delta s=0.05$ is chosen and an attempt is made to recover the natural frequencies via initial guesses of $K=0.17$, $A=1.5$, $\hat{\sigma}=0$, $\hat{\omega}=1.6$, and $\psi=2.0$. The results are shown in Figure 6.5.4. The parameters are plotted (normalized to the actual values in the constructed response) against τ on a logarithmic scale. Each of the parameters is seen to converge at a different rate: ω converges quite rapidly while σ does not even begin to converge until τ is quite close to 1. The logarithmic scale cloaks somewhat the large amount of change occurring in many

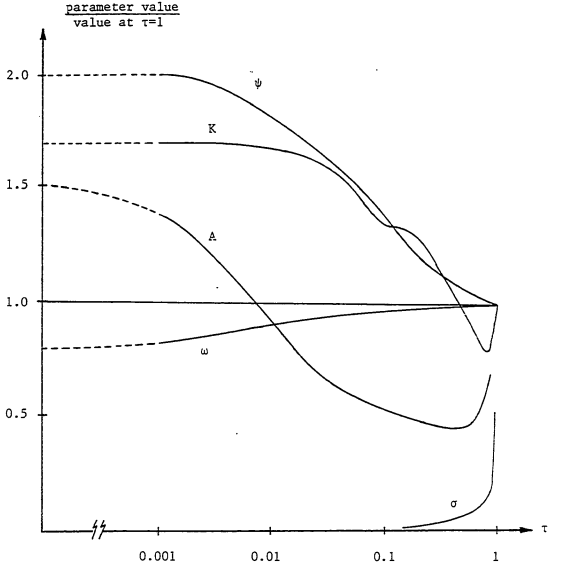

Figure 6.5.4. Example solution using the continuation method.

of the parameters for small values of τ. Note also that there is no "folding back" of the path -- the curve is single valued in τ for this case.

It is somewhat disconcerting to see the amount of correction occurring near τ=0 and near τ=1. This is due in great part to the form of the penalty term $\vec{W}(\vec{x})$ in equation (6.5.1). As τ varies from 0 to 1, the transition between the solution to

$$\overline{\overline{J}}_W(\vec{x})^T\vec{W}(\vec{x}) = 0 \qquad (6.5.15)$$

and the solution to

$$\overline{\overline{J}}_R(\vec{x})^T\vec{R}(\vec{x}) = 0 \qquad (6.5.16)$$

is not very smooth, because of the dissimilar natures of $\vec{W}(\vec{x})$ and $\vec{R}(\vec{x})$. Thus, a much smaller step size Δs is required than would be necessary if the transition were more direct, in order to allow the sharp corners to be negotiated. It is very important to note that a rapid convergence is not desired with this method. Rather, the ideal relationship would be to have a linear transition between τ=0 and τ=1, requiring the least amount of correction after each prediction step. If $\vec{W}(\vec{x})$ were a function more similar to $\vec{R}(\vec{x})$ this transition might be made much smoother.

Instead of minimizing $G_\tau(\vec{x})$ as given in (6.5.1) consider the minimization of the quantity

$$\tilde{G}_\tau(\vec{x}) = \tau|\vec{R}(\vec{x})|_2^2 + A(1-\tau)|\vec{R}^o(\vec{x})|_2^2 + B(1-\tau)|\vec{W}(\vec{x})|_2^2 \qquad (6.5.17)$$

where

$$R_i^o(\vec{x}) = F_i(\vec{x}) - r_i^o \qquad (6.5.18)$$

Here $\{r_i^o\}$ represents the curve generated by the initial guesses and is given by

$$r_i^o = F_i(\vec{x}_o) \qquad (6.5.19)$$

The constants A and B are chosen to make the transition between the solutions at τ=0 and τ=1 as smooth as possible. Since $\vec{R}^o(\vec{x})$ and $\vec{R}(\vec{x})$ are nearly identical in nature, the transition when A is relatively large and B relatively small should be more direct. Note that the original problem is easily regained by letting A=0 and B=1 in (6.5.17).

As an example of the improvement allowed by this modification, consider the simple one mode example solved earlier using (6.5.1), as shown in Figure 6.5.4. Using A=1, B=0, and the same set of initial guesses for $\hat{\sigma}$ and $\hat{\omega}$ (and linear least squares for the amplitude and phase), the natural frequencies are extracted via (6.5.17). The results are plotted in Figure 6.5.5 on a linear scale, and the transition is seen to be substantially smoother. There is no longer the behavior of rapid correction near τ=0 and τ=1, and so a much

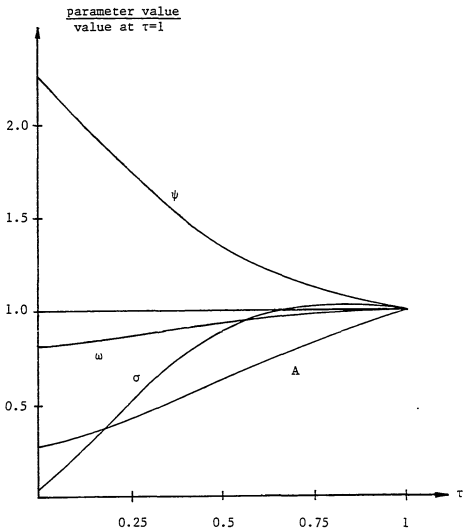

Figure 6.5.5. Example solution using the continuation method with modified penalty term.

larger step size is allowed. Although this solution represents the case of no penalty term $\vec{W}(\vec{x})$, more complex problems should include a nonzero value for B to insure proper conditioning and to keep $\vec{x}$ from wandering too far from the initial guesses.

The modification of equation (6.5.1) given by (6.5.17) is quite easy to implement, and because of the sizable improvement in the smoothness of the path its use is highly reccmmended.

6.6 E-pulse Method

A very interesting method for natural frequency extraction can be constructed using the E-pulse concept introduced in chapter 4. If the measured response is indeed a pure sum of natural modes (plus, perhaps, a constant DC level) then there should exist a whole spectrum of E-pulses which when convolved with this response result in a zero late-time period. As the response will actually be contaminated by various types of noise, application of an E-pulse would yield a small, but nonzero response. The E-pulse method is an iterative procedure which searches for the natural frequencies which may be used to construct an E-pulse which results in a minimum late-time convolved response.

Let r(t) represent the measured response of a particular target. (Actually, this will be a set of discrete sampled data points.) Then, the convolution of an excitation signal e(t) and this response can be written as

$$q(t) = e(t)*r(t) = \int_0^{T_e} e(t')r(t-t')dt' \qquad t>T_E \qquad (6.6.1)$$

The natural frequencies embedded in r(t) can be extracted by constructing e(t) as an E-pulse (via (4.4.3.4)) and minimizing the norm of the late-time convolved response

$$|q(t)|_2^2 = \sum_{i=1}^{M} (q(t_i))^2 \qquad (6.6.2)$$

with respect to the parameters $\sigma_1,\ldots,\omega_N$, where M discrete points are chosen at which to evaluate the norm. As mentioned above, if r(t) is a pure sum of natural modes, and if a sufficient number of natural frequencies are used to construct e(t), then the minimum of (6.6.2) would be zero, and the routine would work perfectly. Since the response will actually be contaminated by noise, the natural frequencies used to construct the E-pulse will only be an estimate of the frequencies in the response.

It is not worthwhile to attempt to construct a Newton's method minimization scheme as was done in section 6.5, since it is impossible to calculate analytically the derivatives of the norm of the late-time convolved response with respect to the natural frequencies. Rather, it is necessary to calculate these using finite differences. There is a wealth of prepackaged computer routines to perform a minimization when the derivatives are not supplied, and the IMSL routine "ZXMIN" was chosen [63].

As with the minimization employed in section 6.5, ZXMIN requires initial guesses as a starting point for iteration. The main benefit of the E-pulse method over the continuation method is that no guesses for the phases and amplitudes of the modes are required, since

they are not used in the construction of the E-pulse. This also means that the number of variables in the minimization will be half that used in the continuation method. If the amplitudes and phases are needed for some reason they can be calculated as a final step using linear least squares via (6.4.8) with the natural frequencies held constant.

The major problem in employing this scheme is deciding which type of E-pulse to use in the convolution. The E-pulse should be as stable as possible, so that as the natural frequencies are varied in the minimization process the response waveform q(t) does not change wildly, making the local minimum difficult to find. From the results of chapter 5, this suggests using a natural E-pulse. Also, since the minimization is an iterative process, it is necessary to make the construction of the E-pulse and the convolution with the measured response as rapid as possible. Thus, the logical choice is to construct e(t) as a rectangular pulse function based natural E-pulse. Section 4.6 provides a very quick algorithm for its calculation, and sampled data convolution can be performed rapidly and accurately using the trapezoidal method of section 5.3.

As a simple example consider a one mode response constructed as

$$r(t) = 1e^{-0.2t}\cos(2t + 1) \qquad (6.6.3)$$

This response is then sampled at 500 points between t=0 and t=10, with a constant sampling interval. Using initial guesses of σ=-0.1 and ω=1.9 and minimizing the norm of the late-time convolved response at a

total of 25 discrete points equally spaced between the beginning of late-time and t=10, an attempt is made to recover the natural frequencies. Requesting three digits of accuarcy from routine ZXMIN results in σ=-0.200 and ω=2.00, and the routine has obviously been successful.

As a second example, consider the response given by (6.6.3) with a very small DC level of 0.01 added. The same set of sampling conditions and initial guesses then results in σ=-0.208 and ω=1.98. It is seen that the presence of a DC level adversely affects the performance of the E-pulse technique. This suggests that a DC E-pulse should be used in the convolution (6.6.1). Using a DC E-pulse, results for the above example (with DC=0.01) become σ=-0.200 and ω=2.00. Thus, the DC level has been adequately accommodated.

There is one unfortunate difficulty involved in implementing the E-pulse method, and it resides in using the natural E-pulse. Since the E-pulse duration is a function of the natural frequencies used in its construction, each iteration of the routine will have a different beginning to late-time. It thus becomes necessary to estimate the range over which the late-time region will vary, so that no points in the early-time are used in calculating the norm (6.6.2). This is quite difficult since it is hard to tell beforehand in what direction the natural frequencies will move. The best approach is to always use the natural E-pulse of minimum duration (which results in the greatest amount of late-time convolved response) and attempt to accurately estimate the frequency (imaginary part) of the highest mode present.

No experimentation has been undertaken employing forced

E-pulses in the convolution. As this would eliminate the above problem, such an approach should be considered an important topic for future study.

6.7 Late-time Minimization Method

This method is very similar to that of section 6.6 in that it also requires the minimization of the late-time convolved response of an E-pulse and a measured response. However, here the minimization is not done with respect to the natural frequencies, but with respect to the amplitudes of the basis functions used to construct the E-pulse. The benefit over the E-pulse method is that an E-pulse need not be constructed at each step, and thus execution time should be reduced.

The result of the minimization in this method is the amplitudes of the basis functions forming an E-pulse. As a final step it is necessary to determine the complex frequencies that the E-pulse eliminates, and they are taken as an estimate of the natural frequencies in the measured response. The amplitudes and phases can be calculated, if desired, using linear least squares with the frequencies held constant. As with the E-pulse method, if the measured response is a pure set of natural modes and the right number of modes are used in the minimization of the convolved response, this method should work perfectly.

It is quite possible, in principle, to extract the natural frequencies from the E-pulse waveform, since equation (4.4.1.2) states that the Laplace transform of the E-pulse waveform should have zeroes

at the complex frequencies that the E-pulse eliminates. However, if the E-pulse spectrum is quite complicated there must be a search through the complex plane for these frequencies, and this could be computationally difficult. It is therefore prudent to use an E-pulse with a spectrum that has easily determinable zeroes.

The most convenient E-pulse is that based upon rectangular pulse functions. Sampled data convolution can be performed rapidly using the trapezoidal rule integration method of section 5.3, and the complex frequencies that the E-pulse eliminates can be extracted as follows.

The spectrum of an arbitrary pulse function based E-pulse is given by equation (4.5.4.16). Thus, at the frequencies that the E-pulse eliminates

$$\sum_{\ell=1}^{L} \alpha_\ell e^{-s\ell\Delta} = 0 \tag{6.7.1}$$

where Δ is the pulse width, α_ℓ is the amplitude of the ℓ'th pulse function determined by the minimization process, and the complex frequencies to be determined reside at $s=s_k$. Now, letting

$$z = e^{-s\Delta} \tag{6.7.2}$$

then (6.7.1) can be written as

$$\sum_{\ell=1}^{L} \alpha_\ell z^\ell = 0 \tag{6.7.3}$$

or, from complex algebra

$$\prod_{k=1}^{L-1} (z-z_k) = 0 \tag{6.7.4}$$

This indicates that there are exactly L-1 solutions to (6.7.4) for z_k. The values of z_k are determined from (6.7.3) by using a standard complex polynomial root solving routine. Finally, the complex frequencies which solve (6.7.1) are given by

$$s_k = -\frac{1}{\Delta} \log(z_k) \tag{6.7.5}$$

For a natural E-pulse the number of pulse functions used is L=2N, where N is the number of modes to be extinguished. Thus, there appears to be only 2N-1 roots to (6.7.4). However, this does not mean that only 2N-1 natural frequencies are eliminated (obviously, since the E-pulse was constructed to eliminate 2N frequencies -- the set of s_k plus their complex conjugates.) Equation (6.7.4) only gives values of z_k. The natural frequencies, as determined from (6.7.5), will be infinite in number since the log is a multivalued function. The frequencies of interest are the principle values of (6.7.5), plus one other which is temporarily hiding (since there are only 2N-1 principle value frequencies.) The missing frequency is discovered numerically to be

$$s = \pm s_j^* \tag{6.7.6}$$

where s_j is the frequency used to calculate the E-pulse duration via (4.6.1.24) and the sign depends on the specific problem. To recover this frequency write (6.7.1) as

$$\sum_{\ell=1}^{L} \alpha_\ell e^{-\ell\sigma\Delta}\left[\cos(\omega\ell\Delta) - j\sin(\omega\ell\Delta)\right] = 0 \qquad (6.7.7)$$

Then it is obvious that $(\tilde{\sigma},\omega=\pm\pi/\Delta)$ is a root if $\tilde{\sigma}$ obeys

$$\sum_{\ell=1}^{L} \alpha_\ell (-1)^\ell e^{-\tilde{\sigma}\ell\Delta} = 0 \qquad (6.7.8)$$

It is important now to remember exactly the condition that led to the natural E-pulse solution. Demanding that (4.6.1.15) hold led to discrete values of the E-pulse duration, given through

$$\Delta = \frac{p\pi}{\omega_j} \qquad p=1,2,... \qquad (6.7.9)$$

where ω_j is any one of the frequencies of the modes to be eliminated. But this root also requires (6.7.8) via (4.4.3.4). Thus, $s=\sigma_j \pm j\omega_j$ are both zeroes of (6.7.1), and the set of 2N principle value frequencies is complete.

The convolution of the E-pulse waveform and a measured response r(t) is given by (6.6.1). An estimate of the values of the natural frequencies embedded in r(t) is determined by first minimizing the norm of the late time convolved response (6.6.2) with respect to the amplitudes of the pulse functions and perhaps the duration $T_e=L\Delta$. Then the frequencies are extracted from the amplitude values by

locating the zeroes of (6.7.1).

Minimization of (6.6.2) is carried out as in the E-pulse technique by using a standard computer library routine. This routine requires initial guesses for the free parameters -- the amplitudes of the pulse functions and perhaps the duration. However, it is very difficult to estimate the heights of the pulses in an E-pulse waveform from the response it is to extinguish. This problem can be circumvented by constructing an E-pulse at the first iteration based on guesses for the natural frequencies in the response. The amplitudes of the pulses in this E-pulse then become the initial guesses in the minimization routine.

It is remembered from chapter 4 that there exist an infinite number of E-pulses that eliminate the same finite set of natural modes. Thus, this technique could lead to a wide variety of E-pulse shapes. The factor restricting the shape is the initial guess. If the initial guesses for the amplitudes are obtained by constructing a natural E-pulse based on guesses for the natural frequencies in the measured response, then chances are the waveform will converge to a natural E-pulse based on the actual frequencies in the response. For a natural E-pulse, 2N pulse amplitudes and the duration are used as free parameters in the minimization, where the response is assumed to contain N modes. For a forced E-pulse, the duration is chosen (and fixed) and 2N+1 pulse amplitudes are used in the minimization. Either way, there are 2N+1 variables involved. To date the technique has only been implemented using natural E-pulses of minimum duration. Note that longer duration natural E-pulses could be utilized, but the length

of the late-time period of the convolved response is reduced.

As a simple example, consider the response constructed as in (6.6.3). This response is sampled at 500 equally spaced points between t=0 and t=10. Using initial guesses of σ=-0.1 and ω=2.2 and minimizing the late-time convolved response at a total of 25 points equally spaced between the beginning of late-time and t=10, an attempt is made to recover the natural frequencies. With two pulses and a request for three digits of accuracy from IMSL routine ZXMIN, the results are α_1=1.265, α_2=0.924, and T_e=3.142. The natural frequencies are extracted using (6.7.1) and are found to be σ=-0.200 and ω=2.00, and the routine has succeeded.

As a second example, consider the response in (6.6.3) with a small DC level of 0.02 added. The same conditions and initial guesses as above result in α_1=0.706, α_2=0.547, and T_e=3.146. The natural frequencies are then calculated to be σ=-0.162 and ω=1.99. Obviously, the presence of this small DC level has had a deleterious effect on the accuracy of σ. This is easily overcome by using three pulses in the minimization and constructing a natural DC E-pulse as an initial guess. With this, the above example results in the amplitudes and duration α_1=-3.61, α_2=0.973, α_3=2.64, T_e=4.71, and the natural frequencies σ_1=0, ω_1=0, σ_2=-0.200, and ω_2=2.00. Again the technique has succeeded. Note the expected frequency at s=0 necessary to eliminate the DC component.

As in section 6.6 there remains the difficulty involving the variability of the beginning of late-time. Future studies should include modifying this technique to use forced E-pulses.

6.8 Moment Method Approach

The previous section obtained the natural frequencies from a measured response by first creating an E-pulse through late-time convolved response minimization and then extracting the frequencies from the E-pulse. This section also presents a two step method, first calcularing an E-pulse using the method of moments to solve the integral equation created by setting the late-time convolved response to zero, and then extracting the frequencies from the E-pulse.

The convolution of an excitation signal e(t) and a measured response r(t) is given by equation (6.6.1). If r(t) is a pure sum of natural modes then e(t) can be constructed as an E-pulse, resulting in a null late-time convolved response. Thus, solving

$$q(t) = \int_0^{T_e} e(t')r(t-t')dt' = 0 \qquad t>T_E \tag{6.8.1}$$

for e(t) results in a waveform that approximates an E-pulse (for r(t) contaminated by noise), and the frequencies that it eliminates can be taken as an estimate for the natural frequencies contained in r(t).

Equation (6.8.1) is an integral equation for the unknown waveform e(t), and it can be solved using the standard method of moments technique. The unknown waveform e(t) is first expanded in an appropriately chosen set of basis functions

$$e(t) = \sum_{\ell=1}^{L} \alpha_\ell f_\ell(t) \tag{6.8.2}$$

Then, rather than forcing (6.8.1) to be satisfied for all time, it is multiplied by a set of M weighting functions $w_m(t)$ and the moments are taken [67]

$$\left\langle w_m(t) \ , \ \sum_{\ell=1}^{L} \alpha_\ell \int_0^{T_e} f_\ell(t')r(t-t')dt' \right\rangle = 0 \quad m=1,2,\ldots,M \qquad (6.8.3)$$

where the angle brackets represent the usual inner product

$$\left\langle f(t) \ , \ g(t) \right\rangle = \int f(t)g(t)dt \qquad (6.8.4)$$

The integral equation (6.8.1) has now been reduced to a matrix equation (6.8.3). This is the main benefit of this method over the methods of the two preceeding sections. A matrix equation is much easier to solve than the minimization problem of (6.6.2). If the number of weighting functions is chosen to be equal to the number of basis functions, as is usually done, then a search must be made to find a zero of the determinant. But since only one parameter is involved (the E-pulse duration), the computation needed is still much less than that in the minimization scheme.

The proper selection of basis functions is determined as in section 6.7 by the need to make the extraction of the complex frequencies from the E-pulse as easy as possible. The choice of weighting functions is controlled by the desire to simplify the calculation of the moments (6.8.3). All told, three separate cases will be considered.

I. Impulse basis functions, point matching

An E-pulse waveform constructed using impulse functions can be written similar to (4.5.5.2) as

$$e(t) = \sum_{\ell=0}^{2N-1} \alpha_\ell \delta(t-\ell\Delta) \tag{6.8.4}$$

where N modes are assumed to be in r(t). Thus, e(t) represents a natural E-pulse. In theory it would be allowable to use more than 2N basis functions, but this leads to matrix conditioning problems if only N modes are actually present in r(t) (see [60]). Using impulse functions for weighting

$$w_m(t) = \delta(t-m\Delta) \tag{6.8.5}$$

is equivalent in (6.8.3) to point matching at times $t=m\Delta$. That is, the integral equation is forced to be satisfied at discrete values of time which are spaced the same as the impulse functions in e(t). This allows (6.8.3) to be written as

$$\begin{aligned}
&\alpha_0 r_{N-1} + \alpha_1 r_{N-2} + \alpha_2 r_{N-3} + \cdots + \alpha_{2N-1} r_0 = 0 \\
&\alpha_0 r_N + \alpha_1 r_{N-1} + \alpha_2 r_{N-2} + \cdots + \alpha_{2N-1} r_1 = 0 \\
&\alpha_0 r_{N+1} + \cdots + \alpha_{2N-1} r_2 = 0 \qquad (6.8.6) \\
&\vdots \qquad\qquad\qquad\qquad\qquad\qquad \vdots \\
&\alpha_0 r_{N+M-2} + \cdots + \alpha_{2N-1} r_{M-1} = 0
\end{aligned}$$

where

$$r_\ell = r(t=\ell\Delta) \qquad (6.8.7)$$

Equation (6.8.6) can also be written in matrix form as

$$\overline{\overline{R}}\,\vec{\alpha} = 0 \qquad (6.8.8)$$

with the matrix entries

$$\left(\overline{\overline{R}} \right)_{i,j} = r_{N+i-j-1} \qquad i=1,2,\ldots,M \qquad j=1,2,\ldots 2N \qquad (6.8.9)$$

Proper application of the moment method requires that the same number of weighting functions as basis functions be used. This results in a homogeneous matrix equation, a solution of which can only

occur when

$$\det \left\{ \overline{\overline{R}} \right\} = 0 \qquad (6.8.10)$$

resulting in discrete, characteristic values of Δ. With Δ determined, the matrix is reduced and then inverted to give the pulse amplitudes, which describe a natural E-pulse. The complex frequencies eliminated by the E-pulse are calculated by solving (6.7.1) and they are taken as an estimate of the natural frequencies in r(t).

Since r(t) will be available only as a sampled waveform, there are two simple ways to calculate the matrix entries in (6.8.8). Either r(t) can be interpolated between sampled points, or Δ can be fixed and discrete convolution used. With Δ fixed, though, it is doubtful that (6.8.10) will be satisfied. Discrete convolution can also be employed if one more basis function than matching point and one more sample point from the measured response are used. Then e(t) becomes a forced E-pulse, Δ can be fixed at the sampling interval, and (6.8.8) can be solved as an inhomogeneous matrix problem. Although this approach is not properly motivated from the point of view of the moment method, the results are most interesting. The matrix equation given by (6.8.3) now becomes

$$\overline{\overline{R}}\vec{\alpha} = \vec{\beta} \qquad (6.8.11)$$

where

$$\beta_i = -r_{N+i-1}\alpha_{-1} \tag{6.8.12}$$

With the amplitude coefficients determined by solving (6.8.11), the complex frequencies eliminated by e(t) are found by calculating the roots to

$$\sum_{\ell=0}^{2N} \alpha_{\ell-1} z^{\ell} = 0 \tag{6.8.13}$$

where z is given in equation (6.7.2). An astounding fact is now revealed. These are exactly the same two steps used in Prony's method as described in section 6.2. Thus, moment method solution using impulse basis and weighting functions is identical to Prony's method, if one extra basis function is allowed. Since Prony's method has already been discussed, no numerical results will be presented.

II. Rectangular pulse function basis, point matching

Expanding e(t) according to

$$e(t) = \sum_{\ell=1}^{L} \alpha_{\ell} P_{\ell}(t) \tag{6.8.14}$$

where $P_{\ell}(t)$ is given in (4.5.4.3), and point matching at times $t=t_m$ allows (6.8.3) to be written in the matrix form

$$\overline{\overline{P}}\,\overline{\alpha} = 0 \tag{6.8.15}$$

with the entries

$$\left(\overline{\overline{P}} \right)_{m,n} = \int_0^{T_e} P_n(t')r(t_m - t')dt' \qquad (6.8.16)$$

Calculating these entries is identical to performing the sampled data convolution discussed in section 5.3. Since this involves interpolating on r(t), there is no restriction on the pulse width Δ. Thus, a natural E-pulse can be used and, with L=2N, the requirement

$$\det \left(\overline{\overline{P}} \right) = 0 \qquad (6.8.17)$$

can be satisfied in the true spirit of the moment method. Then, solutions to (6.8.15) can be found, corresponding to discrete values for the duration of the E-pulse, and the complex frequencies can be extracted from the resulting E-pulse waveform by solving (6.7.1).

III. Rectangular pulse basis, rectangular pulse weighting

In this case, the excitation signal is expanded according to (6.8.14) while the weighting functions are given by

$$w_m(t) = \tilde{P}_m(t) \qquad (6.8.18)$$

where

$$\tilde{P}_m(t) = \begin{cases} 1 & (m-1)\tilde{\Delta} \leq t \leq m\tilde{\Delta} \\ 0 & \text{elsewhere} \end{cases} \qquad (6.8.19)$$

and $\tilde{\Delta}$ is chosen in such a way that the weighting functions cover the entire late-time period. Whereas point matching forces the convolved response to be exactly zero at discrete points, using pulse weighting functions corresponds to forcing an average of the convolved response to be zero. When r(t) is contaminated by noise, employing an average of the convolved response should be a more stable approach.

Writing (6.8.3) in the matrix form (6.8.15) leads to the matrix entries

$$\left(\overline{\overline{P}} \right)_{m,n} = \left\langle \tilde{P}_m(t) \, , \int_o^{T_e} P_n(t')r(t-t')dt' \right\rangle \qquad (6.8.20)$$

The double integration required by the inner product of the pulse and the convolution can be calculated quite simply by using rectangular rule integration

$$\left(\overline{\overline{P}} \right)_{m,n} \simeq \frac{\tilde{\Delta}}{K} \sum_{k=1}^{K} \int_o^{T_e} P_n(t')r(t_{m,k}-t')dt' \qquad (6.8.21)$$

where the double subscript on $t_{m,k}$ indicates the k'th value of t out of a total of K values equally distributed over the m'th weighting function interval. The remaining integral in (6.8.21) is of the type calculated in the pulse function basis, point matching analysis. Thus, the matrix elements are merely sums of elements of the type used for that technique, and solutions for the natural frequencies embedded in r(t) proceed identically.

As a simple example consider a response constructed as in (6.6.3). This response is sampled at 500 points in time, equally distributed between t=0 and t=10. An attempt is then made to recover the complex frequency in r(t) by using the moment method, first with impulse and then pulse weighting. Using two pulse functions for expansion, and matching at two points (at the beginning and end of late-time) results in a root to the determinental equation (6.8.17) being found at T_e=3.14159. The corresponding pulse function amplitudes are found to be α_1=1.369 and α_2=1, while the complex frequency found by solving (6.7.1) is σ=-0.200, ω=2.00. Using two pulse functions for expansion and two pulse functions for weighting results in a root of (6.8.17) at T_e=3.14159, pulse function amplitudes of α_1=1.369 and α_2=1, and the complex frequency σ=-0.200, ω=2.00. Thus, the moment method technique has been successful for both types of weighting functions.

As a second example, consider the response in (6.6.3) with a small DC level of 0.02 added. Sampling under the same conditions as above and using two pulse functions for expansion and two impulse functions for weighting results in a root to (6.8.17) being found at T_e=3.199. The corresponding pulse amplitudes are α_1=1.278 and α_2=1, while the extracted frequency is σ=-0.153, ω=1.964. Using two pulse functions for expansion and two pulse functions for weighting results in a root to (6.8.17) at T_e=3.113 and the corresponding pulse amplitudes and frequency α_1=0.9172, α_2=1, and σ=0.0555, ω=2.018. Obviously, the presence of the DC component has had a harmful effect on the accuracy of the extracted frequency, both for impulse and for pulse function weighting.

The DC level in the previous example can be accommodated by expanding in three pulse functions, resulting in the creation of a natural DC E-pulse. Using three impulse functions for weighting gives a root to (6.8.17) at T_e=4.712, with the corresponding pulse amplitudes and frequencies α_1=-1.369, α_2=0.369, α_3=1 and σ_1=0, ω_1=0, σ_2=-0.200, and ω_2=2.00. Using three pulse functions for weighting results in a root to (6.8.17) at T_e=4.712 as well, with amplitudes and frequencies identical to those found with impulse weighting. Thus, the moment method technique has succeeded in extracting both the expected frequency at σ=-0.2, ω=2 and also the frequency at s=0 necessary to eliminate the DC component.

The moment method technique seems uncomfortably similar to Prony's method, and case I showed the reason for concern. However, the problems afflicting Prony's method in the presence of random noise are well handled by expanding the E-pulse in pulse functions as opposed to impulse functions. With pulse expansion functions, the convolution integral in (6.8.3) incorporates all of the points in the measured response, resulting in an averaging of the noise. With impulse functions the convolution only involves roughly 4N points. For the simple one mode example discussed earlier, this meant using only 1% of the total of 500 points available. In the presence of noise, no averaging can be expected using Prony's method and only five points.

As in sections 6.6 and 6.7, there exists the problem of the beginning of late-time changing. However, this is a much less serious problem here, since T_e is the only parameter that is varied in

searching for the solution to (6.8.17).

6.9 Comparison of the Methods

Six methods for extracting the natural frequencies of a radar target from a measured response have been presented in this chapter, of which only one, Prony's method, is not original. The sensitivity of Prony's method to random noise has been noted as the motivation behind introducing the new methods. In this section, a comparison will be made between the various methods, and justification for using the new techniques will be sought.

It has been shown that each of the new extraction routines is successful in the simple case of a one mode response, while Prony's method is also known to work well under ideal circumstances. In addition, the new methods have been extended to multimode responses without difficulty. However, there are three important practical circumstances under which the natural frequency extraction schemes must be able to perform. The first is performance in the presence of random noise, which will undoubtedly be introduced at many points in the measuring process. The second is the ability to discriminate between nearly degenerate modes -- that is, between modes with natural frequencies which are quite closely spaced compared to the separation between other frequencies. The last is the ability to work well when the number of modes present in the measured response is underestimated.

The last requirement leads to a particularly useful technique. Since the number of modes present in the measured response will not be

known a priori, one would like to begin by assuming a small number (usually one) and slowly increasing it. For the methods which need initial guesses, the results from the solution with a small number of modes assumed can be used as guesses when a larger number is assumed. This is only possible, of course, if the routine works well when the number of modes in the measured response is underestimated. The importance of each additional mode is determined either by the amount that it reduces the residual (the value of the minimized quantity) for the methods which use minimization, or by the amount of energy the mode contains. (Amplitude alone is a poor description of the relevance of a mode; the damping factor may reduce the amplitude rapidly.)

This technique of underestimating the number of natural modes has proven quite useful when the continuation and moment method schemes are employed. In the continuation method, assuming a single mode rarely fails to extract the dominant mode in the response (as long as the initial guess is reasonably close.) In the moment method technique, the E-pulse duration obtained remains a good approximation when the number of modes assumed to be in the response is increased, since a root to (4.6.15) remains a root even in the presence of more modes.

To test the various requirements, consider the three mode response (with DC) given by

$$r(t) = 0.1 + 1e^{-0.2601t}\cos(2.906t+1) + 0.5e^{-0.3808t}\cos(6.007t+2)$$

$$+ 0.3e^{-0.4684t}\cos(9.060t+3) \qquad (6.9.1)$$

Here, the complex frequencies used to construct r(t) are the first three natural frequencies of the thin wire target (with factors of 10^9 suppressed, see section 5.2) and the amplitudes have been chosen to accentuate the lower frequency modes. This response is then sampled at 500 equally spaced points between t=0 and t=10.

The sensitivity of each of the routines to the presence of random noise can be tested by perturbing each point in the response by a random number, the value of which is bounded by a certain percentage of the maximum (absolute value) of the response. Table 6.9.1 shows the results of using each method with various levels of noise. In the continuation method and the 1/n iteration method only 100 of the 500 points have been used. Using more points would have given an increase in accuracy, but would have required more computer time. A total of fifteen iterations were allowed in the 1/n iteration method. In the late-time minimization method, the norm has been calculated at a total of 25 points. For the moment method, results are shown for both impulse and pulse function expansion. For the single case of Prony's method, the DC level in (6.9.1) has been omitted, since the version of Prony's method used is unable to accommodate a DC level (although modification for such is possible.) Lastly, results for the E-pulse method have not been included due to the similarity between the

Table 6.9.1. Performance of various natural frequency extraction methods in the presence of random noise.

5% NOISE

	σ_1	ω_1	σ_2	ω_2	σ_3	ω_3
VALUE	-.2601	2.906	-.3808	6.007	-.4684	9.060
PM	-.4593	2.783	.0179	3.491	-.3043	.7620
L/N	-.2575	2.899	-.3964	6.055	-.4711	9.149
LTM	-.2614	2.909	-.3976	6.005	-.5229	8.959
MMPF	-.2584	2.903	-.4294	6.032	-.0414	8.961
MMIF	-.2697	2.936	-.3847	6.031	-.2284	8.924
CM	-.2575	2.899	-.3964	6.056	-.4717	9.149

10% NOISE

	σ_1	ω_1	σ_2	ω_2	σ_3	ω_3
VALUE	-.2601	2.906	-.3808	6.007	-.4684	9.060
PM	-.3533	2.694	.1410	2.981	-.1717	.6729
L/N	-.2539	2.892	-.4099	6.111	-.4825	9.224
LTM	-.2729	2.912	-.3910	5.955	-.4708	8.973
MMPF	-.2537	2.899	-.4788	6.075	.0332	9.211
MMIF	-.2781	2.957	-.3838	6.022	-.0878	8.907
CM	-.2538	2.892	-.4099	6.112	-.4845	9.225

Table 6.9.1 (cont'd.)

25% NOISE

	σ_1	ω_1	σ_2	ω_2	σ_3	ω_3
VALUE	-.2601	2.906	-.3808	6.007	-.4684	9.060
PM	-.3917	2.775	.0614	2.117	.2330	.8231
L/N	-.2348	2.863	-.4053	6.321	-.5911	9.521
LTM	-.2574	2.933	-.3393	5.996	1.272	8.541
MMPF	-.2419	2.882	-.4999	6.208	.3077	9.312
MMIF	-.2961	3.009	-.4344	5.946	.0990	8.899
CM	-.2343	2.862	-.4036	6.322	-.5936	9.527

KEY:

VALUE	Actual frequency value in response
PM	Prony's method (no DC)
L/N	Linear/nonlinear iteration (15 iterations)
LTM	Late-time minimization method
MMPF	Moment method -- pulse function weighting
MMIF	Moment method -- impulse function weighting
CM	Continuation method

E-pulse and late-time minimization techniques.

Table 6.9.1 reveals that each of the new techniques works reasonably well in the presence of random noise, with the continuation method and 1/n iteration working the best. It is seen that the results for these two methods are nearly identical. This is not surprising, since each technique minimizes the same quantity. It is reassuring, though, to see that the two quite different approaches give the same results. The slight discrepancy is due to an insufficient number of iterations in the 1/n iteration method. For 10% random noise, the maximum error is 1.8% on ω_3 and 6% on σ_2 when using the continuation method.

Most importantly, Table 6.9.1 shows that with the possible exception of the first mode, Prony's method fails miserably in the presence of random noise. Results could be improved somewhat by averaging or using least squares, as discussed in section 6.2, but only marginally. Results can also be improved by overestimating the number of modes present in the response. This is considered later, when Prony's method and the continuation method are considered in greater detail.

To test their performance when the number of modes in the response is underestimated, each of the methods is applied as described above, assuming first one mode and then two modes are present. The results are shown in Table 6.9.2. Again, each of the new methods works quite well, with the late-time minimization method working the best (remarkably so when two modes are assumed present.) Prony's method, on the other hand, cannot possibly work without using a sufficient number of modes. This means that it is essential to

Table 6.9.2. Performance of various natural frequency extraction methods when number of modes is underestimated.

ONE MODE EXPECTED

	σ_1	ω_1
VALUE	-.2601	2.906
PM	-.0468	.4251
L/N	-.2171	2.848
LTM	-.2589	2.897
MMPF	-.2460	2.909
MMIF	-.2606	2.896
CM	-.2171	2.848

TWO MODES EXPECTED

	σ_1	ω_1	σ_2	ω_2
VALUE	-.2601	2.906	-.3808	6.007
PM	-.3649	1.883	-.6549	.8467
L/N	-.2486	2.889	-.3524	5.882
LTM	-.2603	2.907	-.3803	6.009
MMPF	-.2598	2.905	-.3312	6.007
MMIF	-.2977	2.914	-.3781	6.056
CM	-.2486	2.889	-.3523	5.882

See key in Table 6.9.1 for explanation of terms

accurately determine the number of modes in the response when using Prony's method, or to always radically overestimate.

To see if the methods can discriminate between nearly degenerate modes, ω=6.007 is changed to ω=3.1 in the second term of (6.9.1) so that the first and second frequencies are quite close. Each method is then used to extract the complex frequencies and, as expected, each succeeds. It is difficult to assess the relative ability of each method to separate the modes, but Prony's method, the moment method and the continuation method seem to work the best. Prony's method needs no initial guesses and an exact answer is easily obtained when there is no noise. The moment method also works quite well since there is only the E-pulse duration to be determined. The continuation method works the best of the methods which need initial guesses in that it converges for even bad guesses. For example, the continuation method converges rapidly for guesses of σ_1=-0.1, σ_2=-0.1, σ_3=-0.1 and ω_1=2.5, ω_2=2.6, ω_3=8.6.

It is seen from the above tests that Prony's method is the least practical of all the techniques considered, even though it is the quickest and easiest to use. Of the remaining methods, the moment method technique is the most efficient since it is also quick and only needs a guess for the duration. However, it does have drawbacks. On many occasions extraneous roots will be found corresponding to non-existent modes. The trustworthiness of a root must be estimated by changing the late-time region over which the weighting functions are used. A true root shouldn't vary by much when this is done. In the presence of noise there may be no root at all, but sometimes it can

be teased out by using the same trick.

The most reliable method under the widest variety of circumstances is the continuation method. As one last, more realistic simulation, Figure 6.9.1 shows a 30^{o} thin cylinder impulse response constructed using the first eight natural frequencies. This represents what might be a typical measured response. Figure 6.9.2 shows the same response with 10% (of the maximum response value) random noise added. An attempt is made to extract the eight natural frequencies from the noisy response using both the continuation method and Prony's method.

Figure 6.9.3 shows the result of using straightforward Prony's method. As can be seen, except for the first and fourth modes the results are quite disappointing. Improvement can be gained by assuming that sixteen modes rather than eight are present in the response. The results for this case are also shown in Figure 6.9.3. The accuracy has indeed improved for many frequencies, as is expected since more of the sampled points have been included in the analysis. However, an additional problem arises. It is very difficult to determine which of the sixteen frequencies are actually present in the response. Although some of the corresponding amplitudes are quite low, others belonging to nonexistent modes are of substantial magnitude. Without the a priori knowledge of the true frequency values, it would be quite difficult to categorize the results.

In contrast, Figure 6.9.4 shows the frequencies extracted using the continuation method with eight modes assumed present. The accuracy is quite remarkable. Even though it would not have been known to

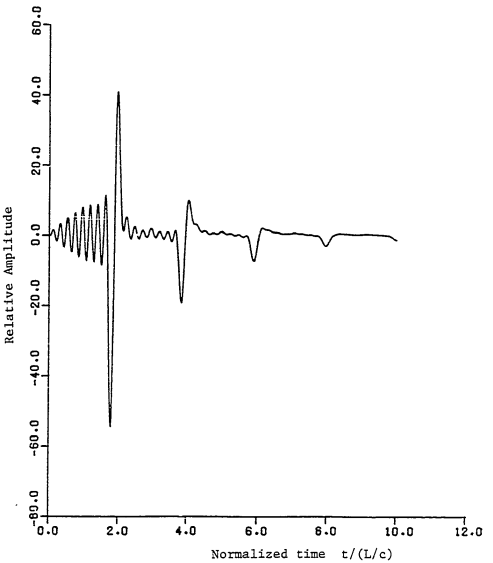

Figure 6.9.1. Impulse response of a thin cylinder oriented at $\theta=30^{\circ}$, constructed using first eight natural modes.

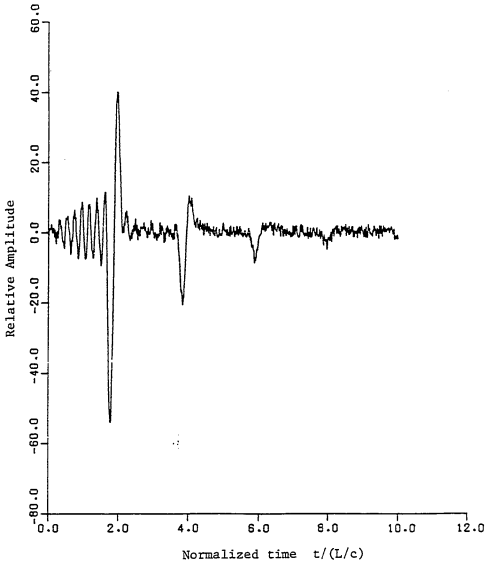

Figure 6.9.2. Eight mode 30° thin cylinder impulse response with 10% random noise added.

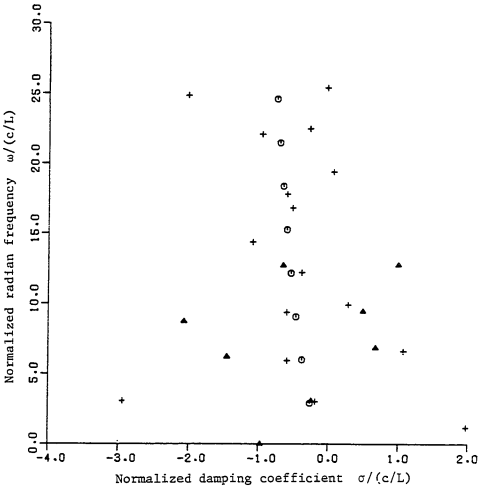

Figure 6.9.3. Natural frequencies extracted from noisy impulse response using Prony's method with eight modes assumed (Δ) and sixteen modes assumed (+). Circles represent frequencies used to construct noise free impulse response.

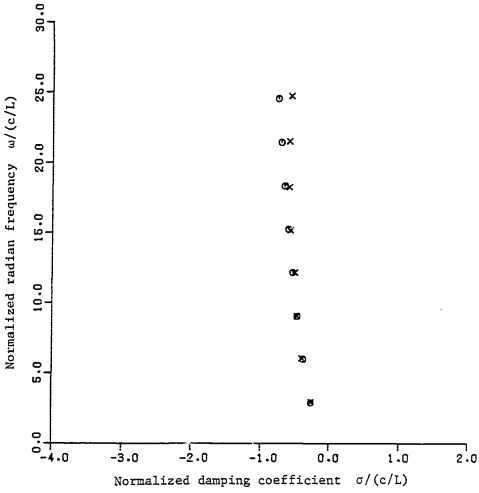

Figure 6.9.4. Natural frequencies extracted from noisy impulse response using continuation method with eight modes assumed (×). Circles represent frequencies used to construct noise free impulse response.

expect eight modes, the residual generated using nine or more would not have been significantly smaller than when using eight. The "underestimating" technique would have said to stop at eight.

CHAPTER 7

THIN WIRE ELLIPTICAL LOOP SCATTERER

7.1 Introduction

The natural frequencies of a perfectly conducting body can be obtained theoretically through the solution to the electric field integral equation given by (2.3.3). As this equation contains only variables of position, it is easy to see that the natural frequencies depend only on the geometry of the scatterer, and not upon excitation. However, since the natural mode expansion of current given in (2.2.4) may not be complete, it becomes prudent to verify the expansion experimentally. This can be accomplished by comparing the natural frequencies extracted from the measured response of a target with those determined through a theoretical analysis, and by demonstrating their aspect independence.

An appropriate target for experimental investigation must be simple to analyze theoretically, and yet possess enough complexity to allow an efficient method for varying its aspect dependent interaction with respect to the transmitting and receiving antennas. Thus the sphere, while allowing a simple theoretical analysis, is useless for aspect dependence checks. The thin cylinder target provides a good check on the values of analytically determined natural frequencies, but since the present experiment involves transmission over a

conducting ground screen (see chapter 8), only normal incidence is allowed, and aspect dependence checks are again unavailable.

It is well known that a thin wire loop antenna is highly directive. This suggests that a wire loop would be a good choice for an aspect sensitive target. If the loop is planar, experimental verification of natural frequency aspect independence would be quite simple. Measurements of scattered field or surface currents could be made with the plane of the loop normal to the ground screen, and the loop could be rotated to provide a change of aspect. Note that this requires defining a loop geometry that is symmetric, to include the imaging effect of the ground screen.

This chapter will conduct a theoretical analysis of an elliptically shaped thin wire loop scatterer. Such a loop conforms with the above description and should provide a good check of the values and aspect independence of its natural frequencies. The simple mathematical description of an elliptical boundary allows the formulation of a precise electric field integral equation (within the approximations allowed by a thin wire analysis), avoiding the messy boundary conditions required by a segmental representation of more odd shapes (such as a rectangle.) This integral equation will be solved numerically using the moment method, and the natural frequencies determined.

It is interesting to point out the special cases allowed by the analysis of the elliptical loop. When the eccentricity is zero the ellipse becomes a circle. Analysis of a circular loop is particularly simple, and is carried out as a preliminary in

section 7.3. When the eccentricity approaches unity, the elliptical scatterer approaches a parallel wire transmission line, with each end shorted. Such a transmission line should not radiate and thus determination of its natural frequencies is trivial.

7.2 Thin Wire Electric Field Integral Equation

The natural frequencies and modal surface current densities for an arbitrarily shaped conducting body can be found through equation (2.3.3). Specializing the target to be a thin circular wire and employing a number of approximations results in many simplifications.

It is more convenient at this point to return to the notation used in equation (2.2.8). With this, equation (2.3.3) can be written as

$$\int_S \left(\nabla' \cdot \vec{K}(\vec{r}',s)(\hat{t}\cdot\nabla) - \gamma^2 \hat{t}\cdot\vec{K}(\vec{r}',s) \right) \frac{e^{-\gamma R}}{4\pi R} \, dS' = 0 \qquad (7.2.1)$$

$$\text{for all } r \in S$$

Now assume that the target is a thin wire with constant circular cross section of radius 'a'. This allows any point on the wire surface to be described by (u,ψ), where u is the distance along the axis from some convenient origin of axial coordinates, and ψ describes the angular position on the periphery of the wire cross section.

Further assumptions follow along the lines of the classic "thin wire approximation" of antenna theory. It is assumed that the surface current $\vec{K}(\vec{r})$ has only an axial component and that it can be written as

the product of an axial current I(u) and a constant function f=1/2πa. This corresponds to zero transverse variation of $\vec{K}(\vec{r})$, and allows the surface integral to be written as the product of two line integrals, one along the axis and the other around the periphery. Furthermore, R, which represents the distance between a field point and a source point on the surface of the wire, is approximated as the distance $\bar{R}$ between the axial location of the field point and the source point on the surface. Lastly, the line integral around the periphery is replaced by the average value of the integrand multiplied by the total angle of traversal, 2π.

With these approximations, equation (7.2.1) reduces to

$$\int_{\Gamma}\left\{ \frac{\partial I(u',s)}{\partial u'} \frac{\partial}{\partial u} - \gamma^2(\hat{u}\cdot\hat{u}')I(u',s) \right\} \bar{g}(u|u';s)du' = 0 \qquad (7.2.2)$$

for all $u \in \Gamma$

where

$$\bar{g}(u|u';s) = \frac{e^{-\gamma\bar{R}}}{4\pi\bar{R}} \qquad (7.2.3)$$

and

$$\bar{R}(u|u') = \left(d^2+a^2\right)^{\frac{1}{2}} \qquad (7.2.4)$$

Here d is the distance between axial points u and u' on the outer periphery of the wire, $\hat{u}$ is a unit vector in the axial direction at

position u, and Γ represents the axial path of integration. This is the thin wire electric field integral equation which will be employed in the following sections.

7.3 Circular Loop Scatterer

A thin wire shaped into a circle forms the basis for the classic loop antenna, and has been analyzed in depth [68], [69]. An antenna analysis using the singularity expansion method has also been examined [16]. As this shape forms a special case for the elliptically shaped loop, the natural frequencies will be calculated here using a similar analysis.

The integral equation describing the natural frequencies of the circular loop based on the thin wire approximation can be obtained by using equation (7.2.2). Employing the geometry of the loop shown in Figure 7.3.1, the axial position is given by

$$u = b\phi \tag{7.3.1}$$

while the dot product of the unit vectors in the primed and unprimed coordinate systems is

$$\hat{u}\cdot\hat{u}' = \cos(\phi-\phi') \tag{7.3.2}$$

and the distance between a point on the axis of the wire and a point on the outer surface is given using (7.2.4) as

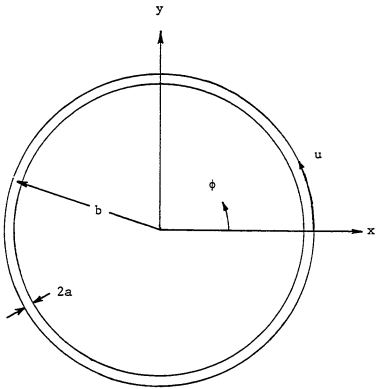

Figure 7.3.1. Geometry of thin wire circular loop scatterer.

$$\bar{R}(\phi|\phi') = \bar{R}(\phi-\phi') = \left(4b^2\sin^2\left(\frac{\phi-\phi'}{2}\right) + a^2\right)^{\frac{1}{2}} \qquad (7.3.3)$$

In these equations ϕ is the usual angular variable in polar coordinates, b is the outer radius of the loop, and 'a' is the wire radius. With these, equation (7.2.2) can be written as

$$\int_{-\pi}^{\pi} \left(\frac{\partial I(\phi',s)}{\partial \phi'} \frac{\partial}{\partial \phi} - (\gamma b)^2 \cos(\phi-\phi') I(\phi',s) \right) \bar{g}(\phi|\phi';s)\, d\phi' = 0 \qquad (7.3.4)$$

$$\text{for all } -\pi \leq \phi \leq \pi$$

where

$$\bar{g}(\phi|\phi';s) = \bar{g}(\phi-\phi') = \frac{e^{-\gamma \bar{R}(\phi-\phi')}}{4\pi \bar{R}(\phi-\phi')} \qquad (7.3.5)$$

A solution to (7.3.4) could be achieved directly by using a numerical technique such as the method of moments. However, the special symmetry of the problem allows a more insightful solution.

Equation (7.3.4) can be simplified somewhat by integrating the first term by parts

$$\int_{-\pi}^{\pi} \frac{\partial I(\phi',s)}{\partial \phi'} \frac{\partial \bar{g}(\phi-\phi';s)}{\partial \phi}\, d\phi' = I(\phi',s) \left.\frac{\partial \bar{g}(\phi-\phi';s)}{\partial \phi}\right|_{\phi'=-\pi}^{\pi} -$$

$$-\int_{-\pi}^{\pi} I(\phi',s)\,\frac{\partial^2 \bar{g}(\phi-\phi';s)}{\partial\phi\partial\phi'}\,d\phi'$$

$$=\int_{-\pi}^{\pi} I(\phi',s)\,\frac{\partial^2 \bar{g}(\phi-\phi';s)}{\partial\phi^2}\,d\phi' \qquad (7.3.6)$$

The integral equation then reduces to

$$\int_{-\pi}^{\pi} K(\phi-\phi';s)I(\phi',s)d\phi' = 0 \qquad \text{for all } -\pi\leq\phi\leq\pi \qquad (7.3.7)$$

where

$$K(\phi-\phi';s) = \left[\frac{\partial^2}{\partial\phi^2} - (\gamma b)^2\cos(\phi-\phi')\right]\bar{g}(\phi-\phi';s) \qquad (7.3.8)$$

Because of its dependence only on the difference between the angles ϕ and ϕ', the kernel of the integral equation can be expanded in a Fourier series as

$$K(\phi-\phi';s) = \sum_{n=-\infty}^{\infty} a_n(s)e^{-jn(\phi-\phi')} \qquad (7.3.9)$$

where

$$a_n(s) = a_{-n}(s) = -\frac{j\gamma b}{2}\left[K_{n+1}(s) + K_{n-1}(s)\right] - \frac{jn^2}{\gamma b}K_n(s) \qquad (7.3.10)$$

and

$$K_n(s) = \frac{b}{2\pi} \int_{-\pi}^{\pi} \frac{e^{jn\theta} e^{-\gamma \bar{R}(\theta)}}{\bar{R}(\theta)} d\theta \tag{7.3.11}$$

The current can also be expanded in a Fourier series

$$I(\phi,s) = \sum_{m=-\infty}^{\infty} I_m(s) e^{-jm\phi} \tag{7.3.12}$$

where the modal current coefficients $I_m(s)$ depend upon the particular form of excitation. Substituting the expansions (7.3.9) and (7.3.12) into the integral equation (7.3.7) results in

$$\int_{-\pi}^{\pi} \sum_m \sum_n a_n(s) I_m(s) e^{-jn\phi} e^{j(n-m)\phi'} d\phi' = 0 \tag{7.3.13}$$

$$\text{for all } -\pi \leq \phi \leq \pi$$

or

$$\sum_m \sum_n a_n(s) I_m(s) e^{-jn\phi} \int_{-\pi}^{\pi} e^{j(n-m)\phi'} d\phi' = 0 \tag{7.3.14}$$

$$\text{for all } -\pi \leq \phi \leq \pi$$

The integral merely results in the Kronecker delta and thus (7.3.14) reduces to

$$\sum_n a_n(s)I_n(s)e^{-jn\phi} = 0 \qquad \text{for all } -\pi \leq \phi \leq \pi \tag{7.3.15}$$

Employing the orthogonality of the exponentials gives the required characteristic equation for the natural frequencies of the circular loop

$$a_n(s) = 0 \tag{7.3.16}$$

Roots to the above equation occur at $s=s_{ni}$, where the i refers to the i'th root at a given value of n.

The integral representation for the modal kernels $K_n(s)$ can be simplified by identifying even and odd components. First write

$$e^{-(\gamma b)\tilde{r}}e^{jn\theta} = e^{-(\sigma b)\tilde{r}/c}\left(\cos(n\theta-\omega b\tilde{r}/c) + j\sin(n\theta-\omega b\tilde{r}/c)\right) \tag{7.3.17}$$

where $\tilde{r}$ is the normalized distance

$$\tilde{r}(\theta) = \frac{\bar{R}(\theta)}{b} \tag{7.3.18}$$

Here also, $s=\sigma+j\omega$, and c is the speed of light. Next, let

$$K_n(s) = \frac{1}{2\pi}\left\{ K_{nr}(s) + jK_{ni}(s) \right\} \tag{7.3.19}$$

Then

$$K_{nr}(s) = \int_{-\pi}^{\pi} \frac{e^{-\sigma b\tilde{r}/c}\cos n\theta\cos(\omega b\tilde{r}/c)}{\tilde{r}}d\theta + \int_{-\pi}^{\pi} \frac{e^{-\sigma b\tilde{r}/c}\sin n\theta\sin(\omega b\tilde{r}/c)}{\tilde{r}}d\theta$$

$$= 2\int_{0}^{\pi} \frac{e^{-\sigma b\tilde{r}/c}\cos n\theta\cos(\omega b\tilde{r}/c)}{\tilde{r}}\,d\theta \qquad (7.3.20)$$

and

$$K_{ni}(s) = \int_{-\pi}^{\pi} \frac{e^{-\sigma b\tilde{r}/c}\sin n\theta\cos(\omega b\tilde{r}/c)}{\tilde{r}}d\theta - \int_{-\pi}^{\pi} \frac{e^{-\sigma b\tilde{r}/c}\cos n\theta\sin(\omega b\tilde{r}/c)}{\tilde{r}}d\theta$$

$$= -2\int_{0}^{\pi} \frac{e^{-\sigma b\tilde{r}/c}\cos n\theta\sin(\omega b\tilde{r}/c)}{\tilde{r}}\,d\theta \qquad (7.3.21)$$

Note that the integrand of $K_{nr}(s)$ has a large peak at $\theta=0$ while the integrand of $K_{ni}(s)$ does not. This suggests that special attention is required in performing the numerical integration in (7.3.20). Experience has shown that the integral converges quite quickly if the domain is split into two portions: $(0,\bar{\Delta})$ and $(\bar{\Delta},\pi)$, where $\bar{\Delta}$ is given by the point where $1/\tilde{r}$ becomes one tenth its maximum value. This occurs at approximately

$$\bar{\Delta} \approx 10\,\frac{a}{b} \qquad (7.3.22)$$

Finally, it is convenient to write the characteristic equation for

the natural frequencies in the normalized form

$$(\gamma b)^2 \left[K_{n+1}(s) + K_{n-1}(s) \right] + 2n^2 K_n(s) = 0 \qquad (7.3.23)$$

7.4 Elliptical Loop Scatterer Integral Equation

The natural frequencies of a thin wire formed into an ellipse can be determined by the thin wire analysis of section 7.2. A proper specialization of the thin wire electric field integral equation (7.2.2) can be obtained based on the geometry of this scatterer, as given in Figure 7.4.1.

A standard system of elliptical coordinates [70] is established according to

$$\begin{aligned} x &= q\cosh\xi\cos\eta \\ y &= q\sinh\xi\sin\eta \end{aligned} \qquad (7.4.1)$$

where ξ and η are measured in radians. Thus, a point on the outer periphery of the wire is given by constant values of q and ξ. Defining the distance from the origin of (x,y) coordinates to the outer edge of the loop along the x-axis as A and the distance along the y-axis as B, a point on the outer periphery of the loop can also be written as

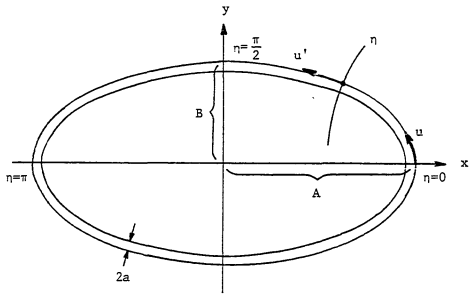

Figure 7.4.1. Geometry of thin wire elliptical loop scatterer.

$$x = A\cos\eta$$
$$y = B\sin\eta \qquad (7.4.2)$$

Therefore, the distance between two points on the outer periphery of the loop is given by

$$d(\eta|\eta') = A\left[(\cos\eta-\cos\eta')^2 + \frac{B^2}{A^2}(\sin\eta-\sin\eta')^2\right]^{\frac{1}{2}} \qquad (7.4.3)$$

The distance along the outer edge of the loop from the origin of the η coordinate at the x-axis is given by the corresponding arc length of the ellipse

$$u(\eta) = A\int_0^{\eta}\left[\left(\frac{dx}{d\eta'}\right)^2 + \left(\frac{dy}{d\eta'}\right)^2\right]^{\frac{1}{2}}d\eta' \qquad (7.4.4)$$

Using

$$\frac{dx}{d\eta'} = -A\sin\eta' \qquad \frac{dy}{d\eta'} = B\cos\eta' \qquad (7.4.5)$$

the arc length becomes

$$u(\eta) = A\int_0^{\eta}\left[\sin^2\eta' + \frac{B^2}{A^2}\cos^2\eta'\right]^{\frac{1}{2}}d\eta' \qquad (7.4.6)$$

and the differential arc length is

$$du = \frac{d\eta}{W(\eta)} \tag{7.4.7}$$

where

$$\frac{1}{W(\eta)} = A \left(\sin^2\eta + \frac{B^2}{A^2} \cos^2\eta \right)^{\frac{1}{2}} \tag{7.4.8}$$

Using this, the partial derivative with respect to the arc length can be written as

$$\frac{\partial}{\partial u} = \frac{\partial}{\partial \eta} \frac{d\eta}{du} = W(\eta) \frac{\partial}{\partial \eta} \tag{7.4.9}$$

Lastly, it is necessary to calculate the form of a unit vector $\hat{u}$ tangent to the surface of the wire. The slope of the ellipse at a point u on the outer edge of the ellipse is given by

$$S_u = \frac{dy}{dx} = -\frac{x}{y} \frac{B^2}{A^2} = -\frac{B}{A} \cot\eta \tag{7.4.10}$$

and thus the unit vector $\hat{u}$ becomes

$$\hat{u} = -\frac{S_u \hat{y} + \hat{x}}{(S_u^2 + 1)^{\frac{1}{2}}} \Sigma \tag{7.4.11}$$

where $\Sigma = \text{sign}(\eta)$, $-\pi \leq \eta \leq \pi$. This is used to obtain the product of the

unit vectors at u and u' as

$$\hat{u}\cdot\hat{u}' = U(\eta|\eta') = \frac{\sin\eta\sin\eta' + \frac{B^2}{A^2}\cos\eta\cos\eta'}{\left(\sin^2\eta + \frac{B^2}{A^2}\cos^2\eta\right)^{\frac{1}{2}}\left(\sin^2\eta' + \frac{B^2}{A^2}\cos^2\eta'\right)^{\frac{1}{2}}} \tag{7.4.12}$$

With these relationships, the integral equation (7.2.2) takes the form

$$\int_{-\pi}^{\pi}\left(W(\eta)W(\eta')\frac{\partial I(\eta',s)}{\partial\eta'}\frac{\partial}{\partial\eta} - \gamma^2 U(\eta|\eta')I(\eta',s)\right)\bar{g}(\eta|\eta';s)\frac{d\eta'}{W(\eta')} = 0$$

$$\text{for all } -\pi\leq\eta\leq\pi \tag{7.4.13}$$

which can also be written as

$$\int_{-\pi}^{\pi}\left(\frac{\partial I(\eta',s)}{\partial\eta'}\frac{\partial}{\partial\eta} - \gamma^2 S(\eta|\eta')I(\eta',s)\right)\bar{g}(\eta|\eta';s)d\eta' = 0$$

$$\text{for all } -\pi\leq\eta\leq\pi \tag{7.4.14}$$

where

$$S(\eta|\eta') = A^2\left(\sin\eta\sin\eta' + \frac{B^2}{A^2}\cos\eta\cos\eta'\right) \tag{7.4.15}$$

Note that unless A=B, $S(\eta|\eta') \neq S(\eta-\eta')$ and $\bar{g}(\eta|\eta') \neq g(\eta-\eta')$, and

thus a Fourier series type solution is not possible.

The integral equation (7.4.14) can also be written in the more convenient normalized form

$$\int_{-\pi}^{\pi} \left(\frac{\partial I(\eta',s)}{\partial \eta'} \frac{\partial}{\partial \eta} - (\gamma A)^2 \tilde{S}(\eta|\eta') I(\eta',s) \right) \bar{g}(\eta|\eta';s) d\eta' = 0$$

$$\text{for all } -\pi \leq \eta \leq \pi \qquad (7.4.16)$$

where

$$\tilde{S}(\eta|\eta') = \frac{S(\eta|\eta')}{A} \qquad \tilde{d}(\eta|\eta') = \frac{d(\eta|\eta')}{A} \qquad (7.4.17)$$

and

$$\bar{g}(\eta|\eta';s) = \frac{e^{-(\gamma A)\tilde{R}}}{(\gamma A)\tilde{R}} \qquad (7.4.18)$$

where

$$\tilde{R} = \left(\tilde{d}^2 + \left(\frac{a}{A}\right)^2 \right)^{\frac{1}{2}} \qquad (7.4.19)$$

An important check on the validity of the integral equation can be performed by letting A→B. This gives

$$S \rightarrow A^2 \cos(\eta - \eta') \qquad (7.4.20)$$

and

$$d \to A\left[(\cos\eta-\cos\eta')^2+(\sin\eta-\sin\eta')^2\right]^{\frac{1}{2}}$$

$$\to 2A\sin\left(\frac{\eta-\eta'}{2}\right) \qquad (7.4.21)$$

Using this, along with the fact that the coordinate variable η becomes the polar coordinate variable ϕ, the elliptical loop integral equation reduces to the circular loop integral equation (7.3.7), as expected.

7.5 Moment Method Solution to Electric Field Integral Equation

The elliptical loop electric field integral equation can be solved by using the standard method of moments technique [67]. Before a solution is attempted, however, the symmetry of the elliptical loop can be used to simplify equation (7.4.16) considerably. There are in fact only four possible manners in which the current can be distributed around the loop. These are numbered one to four as shown in Figure 7.5.1. The sign indicated in each quadrant of the ellipse corresponds to the relative sign of the current in that quadrant (referred to the sign in quadrant I, which is chosen as positive in each case.) With these, the current in any quadrant can be written in terms of the current in quadrant I as

$$\begin{aligned} I(\pi-\eta) &= Q_{2j}I(\eta) \\ I(\eta-\pi) &= Q_{3j}I(\eta) \qquad 0\leq\eta\leq\frac{\pi}{2} \\ I(-\eta) &= Q_{4j}I(\eta) \end{aligned} \qquad (7.5.1)$$

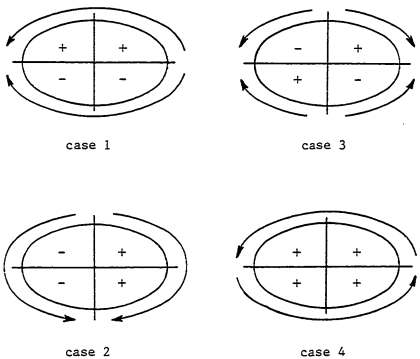

Figure 7.5.1. Symmetry cases for current on elliptical loop scatterer.

Here Q_{ij} represents the sign of the current in quadrant i for symmetry case j, referred to the first quadrant. Thus, Q_{ij} is given by the sign table

CASE	Q_{1j}	Q_{2j}	Q_{3j}	Q_{4j}
j=1	+	+	-	-
j=2	+	-	-	+
j=3	+	-	+	-
j=4	+	+	+	+

(7.5.2)

The ellipse symmetry can be utilized by splitting up the integral equation into four parts

$$\int_{0}^{\pi/2} f(\eta|\eta';s)d\eta' + \int_{\pi/2}^{\pi} f(\eta|\eta';s)d\eta' + \int_{-\pi}^{-\pi/2} f(\eta|\eta';s)d\eta' + \int_{-\pi/2}^{0} f(\eta|\eta';s)d\eta' = 0$$

$$\text{for all } -\pi \leq \eta \leq \pi \qquad (7.5.3)$$

where

$$f(\eta|\eta';s) = \left\{ \frac{\partial I(\eta',s)}{\partial \eta'} \frac{\partial}{\partial \eta} - (\gamma A)^2 \tilde{S}(\eta|\eta') I(\eta',s) \right\} \tilde{g}(\eta|\eta';s) \qquad (7.5.4)$$

Numbering these integrals as one through four, each can be considered individually. First consider

$$I_2 = \int_{\pi/2}^{\pi} f(\eta|\eta';s)d\eta' \qquad (7.5.5)$$

Using the change of variables

$$x = \pi - \eta' \tag{7.5.6}$$

yields

$$I_2 = \int_0^{\pi/2} \left\{ \frac{\partial I(\pi-x,s)}{\partial(\pi-x)} \frac{\partial}{\partial \eta} - (\gamma A)^2 \tilde{S}(\eta|\pi-x) I(\pi-x,s) \right\} \bar{g}(\eta|\pi-x;s)dx \tag{7.5.7}$$

The partial derivative is calculated as

$$\frac{\partial I(\pi-x,s)}{\partial(\pi-x)} = \frac{\partial I(\pi-x,s)}{\partial x} \frac{\partial x}{\partial(\pi-x)} = \frac{\partial I(\pi-x,s)}{\partial x} \left(\frac{1}{\frac{\partial(\pi-x)}{\partial x}} \right)$$

$$= - \frac{\partial I(\pi-x,s)}{\partial x} \tag{7.5.8}$$

Employing this and the symmetry relationship from (7.5.1) gives

$$I_2 = Q_{2j} \int_0^{\pi/2} \left\{ - \frac{\partial I(x,s)}{\partial x} \frac{\partial}{\partial \eta} - (\gamma A)^2 \tilde{S}(\eta|\pi-x) I(x,s) \right\} \bar{g}(\eta|\pi-x;s)dx \tag{7.5.9}$$

Similarly, the remaining two integrals can be shown to be

$$I_3 = \int_{-\pi}^{-\pi/2} f(\eta|\eta';s)d\eta'$$

$$= Q_{3j} \int_0^{\pi/2} \left\{ \frac{\partial I(x,s)}{\partial x} \frac{\partial}{\partial \eta} - (\gamma A)^2 \tilde{S}(\eta|x-\pi) I(x,s) \right\} \bar{g}(\eta|x-\pi;s)dx \tag{7.5.10}$$

and

$$I_4 = \int_{-\pi/2}^{0} f(\eta|\eta';s)d\eta'$$

$$= Q_{4j} \int_{0}^{\pi/2} \left\{ -\frac{\partial I(x,s)}{\partial x}\frac{\partial}{\partial \eta} - (\gamma A)^2 \tilde{S}(\eta|-x)I(x,s) \right\} \bar{g}(\eta|-x;s)dx \tag{7.5.11}$$

Thus, the integral equation (7.4.16) can be written as

$$\int_{0}^{\pi/2} \left\{ Q_{1j} \left\{ \frac{\partial I(\eta',s)}{\partial \eta'}\frac{\partial}{\partial \eta} - (\gamma A)^2 \tilde{S}_1(\eta|\eta')I(\eta',s) \right\} \bar{g}_1(\eta|\eta';s) - \right.$$

$$- Q_{2j} \left\{ \frac{\partial I(\eta',s)}{\partial \eta'}\frac{\partial}{\partial \eta} + (\gamma A)^2 \tilde{S}_2(\eta|\eta')I(\eta',s) \right\} \bar{g}_2(\eta|\eta';s) +$$

$$+ Q_{3j} \left\{ \frac{\partial I(\eta',s)}{\partial \eta'}\frac{\partial}{\partial \eta} - (\gamma A)^2 \tilde{S}_3(\eta|\eta')I(\eta',s) \right\} \bar{g}_3(\eta|\eta';s) -$$

$$\left. - Q_{4j} \left\{ \frac{\partial I(\eta',s)}{\partial \eta'}\frac{\partial}{\partial \eta} + (\gamma A)^2 \tilde{S}_4(\eta|\eta')I(\eta',s) \right\} \bar{g}_4(\eta|\eta';s) \right\} d\eta' = 0$$

$$\text{for all } 0 \leq \eta \leq \frac{\pi}{2} \tag{7.5.12}$$

where the condition of zero tangential field need be forced only over $0 \leq \eta \leq \frac{\pi}{2}$ due to the corresponding symmetry of the electric field. Here

$$\tilde{S}_1(\eta|\eta') = \tilde{S}(\eta|\eta') = \sin\eta\sin\eta' + \frac{B^2}{A^2}\cos\eta\cos\eta'$$

$$\tilde{S}_2(\eta|\eta') = \tilde{S}(\eta|\pi-\eta') = \sin\eta\sin\eta' - \frac{B^2}{A^2}\cos\eta\cos\eta'$$

$$\tilde{S}_3(\eta|\eta') = \tilde{S}(\eta|\eta'-\pi) = -\sin\eta\sin\eta' - \frac{B^2}{A^2}\cos\eta\cos\eta' \qquad (7.5.13)$$

$$\tilde{S}_4(\eta|\eta') = \tilde{S}(\eta|-\eta') = -\sin\eta\sin\eta' + \frac{B^2}{A^2}\cos\eta\cos\eta'$$

and

$$\tilde{g}_i(\eta|\eta';s) = \frac{e^{-(\gamma A)\tilde{R}_i}}{(\gamma A)\tilde{R}_i} \qquad i=1,2,3,4 \qquad (7.5.14)$$

where

$$\tilde{R}_i(\eta|\eta') = \left(\tilde{d}_i^2 + \frac{a^2}{A^2} \right)^{\frac{1}{2}} \qquad (7.5.15)$$

with

$$\tilde{d}_1(\eta|\eta') = \tilde{d}(\eta|\eta') = \left[(\cos\eta-\cos\eta')^2 + \frac{B^2}{A^2}(\sin\eta-\sin\eta')^2 \right]^{\frac{1}{2}}$$

$$\tilde{d}_2(\eta|\eta') = \tilde{d}(\eta|\pi-\eta') = \left[(\cos\eta+\cos\eta')^2 + \frac{B^2}{A^2}(\sin\eta-\sin\eta')^2 \right]^{\frac{1}{2}}$$

$$\tilde{d}_3(\eta|\eta') = \tilde{d}(\eta|\eta'-\pi) = \left[(\cos\eta+\cos\eta')^2 + \frac{B^2}{A^2}(\sin\eta+\sin\eta')^2 \right]^{\frac{1}{2}}$$

$$\tilde{d}_4(\eta|\eta') = \tilde{d}(\eta|-\eta') = \left[(\cos\eta-\cos\eta')^2 + \frac{B^2}{A^2}(\sin\eta+\sin\eta')^2 \right]^{\frac{1}{2}} \qquad (7.5.16)$$

Close examination of the signs involved in the above relations allows them to be written more simply as

$$\tilde{S}_i(\eta|\eta') = s_{si}\sin\eta\sin\eta' + s_{ci}\frac{B^2}{A^2}\cos\eta\cos\eta' \qquad (7.5.17)$$

and

$$\tilde{d}_i(\eta|\eta') = \left[(\cos\eta - s_{ci}\cos\eta')^2 + \frac{B^2}{A^2}(\sin\eta - s_{si}\sin\eta')^2\right]^{\frac{1}{2}} \qquad (7.5.18)$$

where s_{si} and s_{ci} represent the signs on the sine and cosine terms, and are given by

i	s_{ci}	s_{si}
1	+	+
2	+	-
3	-	-
4	-	+

(7.5.19)

With this notation, the integral equation (7.5.12) can be written more simply as

$$\int_0^{\pi/2} \frac{\partial I(\eta',s)}{\partial \eta'} \sum_{i=1}^{4} (-1)^{i-1} Q_{ij} \frac{\partial \bar{g}_i(\eta|\eta';s)}{\partial \eta} d\eta' -$$

$$- (\gamma A)^2 \int_0^{\pi/2} I(\eta',s) \sum_{i=1}^{4} Q_{ij} \tilde{S}_i(\eta|\eta') \bar{g}_i(\eta|\eta';s) d\eta' = 0$$

$$\text{for all } 0 \leq \eta \leq \frac{\pi}{2} \qquad (7.5.20)$$

where the condition

$$\left\{ \frac{\partial \bar{g}(\eta|\eta';s)}{\partial \eta} \right\}_i = \frac{\partial \bar{g}_i(\eta|\eta';s)}{\partial \eta} \qquad (7.5.21)$$

has been used.

Finally, the derivative of the Green's function $\bar{g}$ is calculated as

$$\frac{\partial \bar{g}_i(\eta|\eta';s)}{\partial \eta} = \frac{\partial}{\partial \eta} \frac{e^{-(\gamma A)\tilde{R}_i}}{(\gamma A)\tilde{R}_i} = - \frac{e^{-(\gamma A)\tilde{R}_i}}{(\gamma A)\tilde{R}_i^2} \left((\gamma A)\tilde{R}_i + 1\right) \frac{\partial \tilde{R}_i}{\partial \eta} \qquad (7.5.22)$$

where

$$\frac{\partial \tilde{R}_i}{\partial \eta} = \frac{\tilde{d}_i}{\tilde{R}_i} \frac{\partial \tilde{d}_i}{\partial \eta} \qquad (7.5.23)$$

with

$$\frac{\partial \tilde{d}_i}{\partial \eta} = -\frac{(\cos\eta - s_{ci}\cos\eta')\sin\eta - \frac{B^2}{A^2}(\sin\eta - s_{si}\sin\eta')\cos\eta}{\tilde{d}_i} \qquad (7.5.24)$$

Combining these yields

$$\frac{\partial \bar{g}_i(\eta|\eta';s)}{\partial \eta} = \frac{e^{-(\gamma A)\tilde{R}_i}}{(\gamma A)\tilde{R}_i^3}\left\{ (\gamma A)\tilde{R}_i + 1 \right\} \times$$

$$\times \left\{ (\cos\eta - s_{ci}\cos\eta')\sin\eta - \frac{B^2}{A^2}(\sin\eta - s_{si}\sin\eta')\cos\eta \right\} \qquad (7.5.25)$$

It is important to note that

$$\left.\frac{\partial \bar{g}_i(\eta|\eta';s)}{\partial \eta}\right|_{\eta=\eta'} = 0 \qquad (7.5.26)$$

The electric field integral equation has now been presented in a form that is quite amenable to solution by the method of moments. The current on the wire can be expanded in terms of a rectangular pulse function basis set as

$$I(\eta,s) = \sum_{n=1}^{N} \alpha_n P_n(\eta) \qquad (7.5.27)$$

where

$$(n-1)\Delta \leq \eta \leq n\Delta$$

$$P_n(\eta) = \begin{cases} 1 & (n-1)\Delta \leq \eta \leq n\Delta \\ 0 & \text{elsewhere} \end{cases} \qquad (7.5.28)$$

and

$$\Delta = \frac{\pi}{2N} \tag{7.5.29}$$

Here the discretization reflects basis functions of equal angular width Δ. Note that the region of expansion of the current has been reduced to the domain of the integral $(0,\frac{\pi}{2})$, requiring fewer basis functions than the original integral equation (7.4.16). Using the fact that the derivative of a unit step function is a positive impulse, the derivative of the current in (7.5.20) becomes

$$\frac{\partial I(\eta',s)}{\partial \eta'} = \sum_{n=1}^{N} \alpha_n \frac{\partial}{\partial \eta'} P_n(\eta') = \sum_{n=1}^{N} \alpha_n \left[\delta(\eta'-(n-1)\Delta) - \delta(\eta'-n\Delta)\right] \tag{7.5.30}$$

where $\delta(x)$ is the Dirac delta, or impulse function. Using the integral property of the impulse function then yields

$$\int_0^{\pi/2} \frac{\partial I(\eta',s)}{\partial \eta'} \sum_{i=1}^{4} (-1)^{i-1} Q_{ij} \frac{\partial \bar{g}_i(\eta|\eta';s)}{\partial \eta} d\eta' =$$

$$= \sum_{n=1}^{N} \alpha_n \left\{ \sum_{i=1}^{4} (-1)^{j-1} Q_{ij} \left[\bar{g}_i'(\eta|(n-1)\Delta;s) - \bar{g}_i'(\eta|n\Delta;s)\right] \right\} \tag{7.5.31}$$

where

$$\bar{g}_i'(\eta|\eta';s) = \frac{\partial \bar{g}_i(\eta|\eta';s)}{\partial \eta} \tag{7.5.32}$$

The integral equation (7.5.20) then becomes

$$\sum_{n=1}^{N} \alpha_n \left\{ \sum_{i=1}^{4} Q_{ij} (-1)^{i-1} \left[\bar{g}_i'(\eta|(n-1)\Delta;s) - \bar{g}_i'(\eta|n\Delta;s) \right] \right\} -$$

$$- (\gamma A)^2 \sum_{n=1}^{N} \alpha_n \left\{ \sum_{i=1}^{4} Q_{ij} \int_{(n-1)\Delta}^{n\Delta} \tilde{s}_i(\eta|\eta') \bar{g}_i(\eta|\eta';s) d\eta' \right\} = 0$$

$$\text{for all } 0 \leq \eta \leq \frac{\pi}{2} \qquad (7.5.33)$$

Instead of forcing the integral equation (7.5.33) to be satisfied at all points $0 \leq \eta \leq \frac{\pi}{2}$, it is more convenient to match this condition only at N discrete points $\eta=\eta_m$. This is accomplished by multiplying the integral equation by $\delta(\eta-\eta_m)$ and integrating, which yields

$$\sum_{n=1}^{N} \alpha_n \left\{ \sum_{i=1}^{4} Q_{ij} (-1)^{i-1} \left[\bar{g}_i'(\eta_m|(n-1)\Delta;s) - \bar{g}_i'(\eta_m|n\Delta;s) \right] \right\} -$$

$$- (\gamma A)^2 \sum_{n=1}^{N} \alpha_n \left\{ \sum_{i=1}^{4} Q_{ij} \int_{(n-1)\Delta}^{n\Delta} \tilde{s}_i(\eta_m|\eta') \bar{g}_i(\eta_m|\eta';s) d\eta' \right\} = 0$$

$$m=1,2,\ldots,N \qquad (7.5.34)$$

It is most appropriate to choose matching points in the center of a pulse interval. Thus

$$\eta_m = (m-\tfrac{1}{2})\Delta \qquad (7.5.35)$$

The integral in (7.5.34) can be approximated quite simply by

using rectangular rule integration

$$\int_{(n-1)\Delta}^{n\Delta} \tilde{S}_i(\eta_m|\eta')\bar{g}_i(\eta_m|\eta';s)d\eta' \simeq \left(\tilde{S}_i(\eta_m|\eta_n)\bar{g}_i(\eta_m|\eta_n;s)\right)\Delta \qquad (7.5.36)$$

where the integrand has been evaluated at the midpoint of the domain of the integral

$$\eta_n = (n-\tfrac{1}{2})\Delta \qquad (7.5.37)$$

This approximation will not be accurate when i=1 and η' and η_m are in the same partition (i.e., $\eta_n=\eta_m$, or, n=m). In this case it becomes necessary to approximate the integral more carefully.

Approximation of the integral can be accomplished by appropriate approximation of the integrand. Expanding $\tilde{S}_1$ in a Taylor series about the point $\eta'=\eta_m$ gives

$$\tilde{S}_1(\eta_m|\eta') = \tilde{S}_1(\eta_m|\eta_m) + (\eta'-\eta_m)\left.\frac{d\tilde{S}_1(\eta_m|\eta')}{d\eta'}\right|_{\eta'=\eta_m} + \cdots \qquad (7.5.38)$$

where

$$\frac{d\tilde{S}_1}{d\eta'} = \sin\eta_m\cos\eta' - \frac{B^2}{A^2}\cos\eta_m\sin\eta' \qquad (7.5.39)$$

Thus

$$\left.\frac{d\tilde{S}_1}{d\eta'}\right|_{\eta'=\eta_m} = \sin\eta_m\cos\eta_m - \frac{B^2}{A^2}\cos\eta_m\sin\eta_m \qquad (7.5.40)$$

and

$$\tilde{S}_1(\eta_m|\eta') \approx C_{1m} + C_{2m}(\eta'-\eta_m) \tag{7.5.41}$$

where

$$\begin{aligned} C_{1m} &= \sin^2\eta_m + \frac{B^2}{A^2}\cos^2\eta_m \\ C_{2m} &= \sin\eta_m\cos\eta_m\left(1 - \frac{B^2}{A^2}\right) \end{aligned} \tag{7.5.42}$$

Expanding $\tilde{d}_1$ about the same point results in

$$\tilde{d}_1(\eta_m|\eta') = \tilde{d}_1(\eta_m|\eta_m) + (\eta'-\eta_m)\left.\frac{d\tilde{d}_1}{d\eta'}\right|_{\eta'=\eta_m} + \cdots \tag{7.5.43}$$

where

$$\tilde{d}_1(\eta_m|\eta_m) = 0 \tag{7.5.44}$$

and

$$\frac{d\tilde{d}_1}{d\eta'} = \frac{(\cos\eta_m-\cos\eta')\sin\eta' - \frac{B^2}{A^2}(\sin\eta_m-\sin\eta')\cos\eta'}{\left\{(\cos\eta_m-\cos\eta')^2 + \frac{B^2}{A^2}(\sin\eta_m-\sin\eta')^2\right\}^{\frac{1}{2}}} \tag{7.5.45}$$

Evaluation of the derivative of $\tilde{d}_1$ is simplified by using the expansions [23]

$$\cos\eta_m - \cos\eta' = -2\sin\tfrac{1}{2}(\eta_m+\eta')\sin\tfrac{1}{2}(\eta_m-\eta')$$

$$\sin\eta_m - \sin\eta' = 2\cos\tfrac{1}{2}(\eta_m+\eta')\sin\tfrac{1}{2}(\eta_m-\eta') \tag{7.5.46}$$

then

$$\frac{d\tilde{d}_1}{d\eta'} = \pm\frac{-\sin\tfrac{1}{2}(\eta_m+\eta')\sin\eta' - \frac{B^2}{A^2}\cos\tfrac{1}{2}(\eta_m+\eta')\cos\eta'}{\left(\sin^2\tfrac{1}{2}(\eta_m+\eta') + \frac{B^2}{A^2}\cos^2\tfrac{1}{2}(\eta_m+\eta')\right)^{\frac{1}{2}}} \tag{7.5.47}$$

and

$$\left.\frac{d\tilde{d}_1}{d\eta'}\right|_{\eta'=\eta_m} = \pm\left(\sin^2\eta_m + \frac{B^2}{A^2}\cos^2\eta_m\right)^{\frac{1}{2}} \tag{7.5.48}$$

Thus, $\tilde{d}_1$ is approximated as

$$\tilde{d}_1(\eta_m|\eta') \simeq |\eta'-\eta_m|C_{3m} \tag{7.5.49}$$

where

$$C_{3m} = \sqrt{C_{1m}} \tag{7.5.50}$$

And so $\tilde{R}_1$ is given by

$$\tilde{R}_1 \simeq \left((\eta'-\eta_m)^2C_{3m}^2 + \frac{a^2}{A^2}\right)^{\frac{1}{2}} \tag{7.5.51}$$

Lastly, it is necessary to expand the exponential as

$$\frac{e^{-(\gamma A)\tilde{R}_1}}{(\gamma A)\tilde{R}_1} \simeq \frac{1}{(\gamma A)\tilde{R}_1} - 1 \qquad \text{for } \tilde{R}_1 << \frac{1}{\gamma A} \tag{7.5.52}$$

With these approximations, the integral in (7.5.34) becomes

$$\int_{(n-1)\Delta}^{n\Delta} \tilde{S}_1(\eta_m|\eta')\tilde{g}_1(\eta_m|\eta';s)d\eta' \simeq$$

$$\simeq \int_{\eta_m-\Delta/2}^{\eta_m+\Delta/2} (C_{1m}+C_{2m}(\eta'-\eta_m))\left\{(\gamma A)^{-1}\left[(\eta'-\eta_m)^2C_{3m}^2 + \frac{a^2}{A^2}\right]^{-\frac{1}{2}} - 1\right\}d\eta'$$

$$\text{for } n=m \tag{7.5.53}$$

which can be split up into the following four separate integrals

$$I_1 = -\Delta C_{1m} \tag{7.5.54}$$

$$I_2 = -C_{2m}\tfrac{1}{2}(\eta'-\eta_m)^2 \Big|_{\eta_m-\Delta/2}^{\eta_m+\Delta/2} = 0 \tag{7.5.55}$$

$$I_3 = \frac{C_{1m}}{\gamma A}\int_{\eta_m-\Delta/2}^{\eta_m+\Delta/2} \left[(\eta'-\eta_m)^2C_{3m}^2 + \frac{a^2}{A^2}\right]^{-\frac{1}{2}}d\eta' \tag{7.5.56}$$

$$I_4 = \frac{C_{2m}}{\gamma A}\int_{\eta_m-\Delta/2}^{\eta_m+\Delta/2} \left[(\eta'-\eta_m)^2C_{3m}^2 + \frac{a^2}{A^2}\right]^{-\frac{1}{2}}(\eta'-\eta_m)d\eta' \tag{7.5.57}$$

$$= 0$$

Note that I_2 and I_4 are zero due to the integrands being odd functions about $\eta=\eta_m$. I_3 can be calculated by a simple change of variables as

$$I_3 = 2\frac{C_{1m}}{C_{3m}}\frac{1}{\gamma A}\log\left\{ C_{3m}\frac{\Delta}{2}\frac{A}{a} + \left\{ 1 + \left(C_{3m}\frac{\Delta}{2}\frac{A}{a}\right)^2 \right\}^{\frac{1}{2}} \right\} \qquad (7.5.58)$$

The partitioned electric field integral equation (7.5.34) represents a system of N simultaneous linear equations in the N unknown current expansion coefficients α. It can be written in matrix form as

$$\overline{\overline{A}}\vec{\alpha} = 0 \qquad (7.5.59)$$

where the matrix entries are found using (7.5.36) and (7.5.53) and are given in Table 7.5.1. Since this is a homogeneous system, it will have a solution only when the determinant of the coefficient matrix is zero. The frequencies which cause this to occur result in (7.5.34) being satisfied, and are thus taken as the natural frequencies of the thin wire elliptical loop scatterer.

7.6 Alternative Moment Method Solution

In the previous section the current on the elliptical loop scatterer was expanded in terms of a rectangular pulse function basis set where the pulse functions had equal angular width. For reasons to be discussed later in this section, it is sometimes advantageous to choose pulse functions that have unequal angular widths. This does not change the form of the integral equation to be solved (7.5.20),

Table 7.5.1. Entries in moment method matrix for elliptical loop scatterer.

a) $m \neq n$

$$A_{mn} = \sum_{i=1}^{4} (-1)^{i-1} Q_{ij} \left\{ \bar{g}_i'(\eta_m | (n-1)\Delta; s) - \bar{g}_i'(\eta_m | n\Delta; s) \right\} -$$

$$- (\gamma A)^2 \Delta \sum_{i=1}^{4} Q_{ij} \left(\bar{S}_i(\eta_m | \eta_n) \bar{g}_i(\eta_m | \eta_n; s) \right)$$

b) $m = n$

$$A_{mn} = \sum_{i=1}^{4} (-1)^{i-1} Q_{ij} \left\{ \bar{g}_i'(\eta_m | (m-1)\Delta; s) - \bar{g}_i'(\eta_m | m\Delta; s) \right\} -$$

$$- (\gamma A)^2 \Delta \sum_{i=2}^{4} Q_{ij} \left(\bar{S}_i(\eta_m | \eta_m) \bar{g}_i(\eta_m | \eta_m; s) \right) -$$

$$- (\gamma A)^2 Q_{1j} \left\{ -\Delta C_{1m} + \frac{2C_{3m}}{\gamma A} \times \right.$$

$$\left. \times \log \left\{ C_{3m} \frac{\Delta}{2} \frac{A}{a} + \left\{ 1 + \left(C_{3m} \frac{\Delta}{2} \frac{A}{a} \right)^2 \right\}^{\frac{1}{2}} \right\} \right\}$$

but it does result in different entries for the moment method matrix (7.5.59).

Let the current expansion take the form

$$I(\eta,s) = \sum_{n=1}^{N} \alpha_n \bar{P}_n(\eta) \tag{7.6.1}$$

where

$$\bar{P}_n(\eta) = \begin{cases} 1 & \eta_{n-1} \leq \eta \leq \eta_n \\ 0 & \text{elsewhere} \end{cases} \tag{7.6.2}$$

and the pulse widths $\eta_n - \eta_{n-1}$ are left as a free choice. Using this expansion, the integral in (7.5.31) takes the form

$$\int_0^{\pi/2} \frac{\partial I(\eta',s)}{\partial \eta'} \sum_{i=1}^{4} (-1)^{i-1} Q_{ij} \frac{\partial \bar{g}_i(\eta|\eta';s)}{\partial \eta} d\eta' =$$

$$= \sum_{n=1}^{N} \alpha_n \left\{ \sum_{i=1}^{4} (-1)^{i-1} Q_{ij} \left(\bar{g}_i'(\eta|\eta_{n-1};s) - \bar{g}_i'(\eta|\eta_n;s) \right) \right\} \tag{7.6.3}$$

and the integral equation (7.5.20) becomes

$$\sum_{n=1}^{N} \alpha_n \left\{ \sum_{i=1}^{4} (-1)^{i-1} Q_{ij} \left(\bar{g}_i'(\eta|\eta_{n-1};s) - \bar{g}_i'(\eta|\eta_n;s) \right) \right\} -$$

$$- (\gamma A)^2 \sum_{n=1}^{N} \alpha_n \left\{ \sum_{i=1}^{4} Q_{ij} \int_{\eta_{n-1}}^{\eta_n} \tilde{S}_i(\eta|\eta') \bar{g}_i(\eta|\eta';s) d\eta' \right\} = 0 \tag{7.6.4}$$

for all $0 \leq \eta \leq \frac{\pi}{2}$. This equation can be point matched at arbitrary angles ζ_m by multiplying by $\delta(\eta-\zeta_m)$ and integrating, giving

$$\sum_{n=1}^{N} \alpha_n \left\{ \sum_{i=1}^{4} (-1)^{i-1} Q_{ij} \left(\bar{g}_i'(\zeta_m|\eta_{n-1};s) - \bar{g}_i'(\zeta_m|\eta_n;s) \right) \right\} -$$

$$- (\gamma A)^2 \sum_{n=1}^{N} \alpha_n \left\{ \sum_{i=1}^{4} Q_{ij} \int_{\eta_{n-1}}^{\eta_n} \tilde{S}_i(\zeta_m|\eta') \bar{g}_i(\zeta_m|\eta';s) d\eta' \right\} = 0$$

$$m=1,2,3,\ldots,N \qquad (7.6.5)$$

Unless i=1 and η' and ζ_m are in the same partition, the integral in (7.6.5) can be approximated using rectangular rule integration as

$$\int_{\eta_{n-1}}^{\eta_n} \tilde{S}_i(\zeta_m|\eta') \bar{g}_i(\zeta_m|\eta';s) d\eta' \approx \left(\tilde{S}_i(\zeta_m|\kappa_n) \bar{g}_i(\zeta_m|\kappa_n;s) \right) \Delta_n \qquad (7.6.6)$$

where

$$\eta_{n-i} \leq \kappa_n \leq \eta_n \qquad (7.6.7)$$

and

$$\Delta_n = \eta_n - \eta_{n-1} \qquad (7.6.8)$$

Here κ_n represents the arbitrary angles at which the integrand is to be evaluated. It is sensible to demand that they lie within the domain of integration.

When i=1 and η' and ζ_m are in the same partition, the integral must be calculated more carefully. Expanding in a Taylor series about $\eta'=\zeta_m$ gives

$$\tilde{S}_1(\zeta_m|\eta') \simeq \bar{C}_{1m} + \bar{C}_{2m}(\eta'-\zeta_m) \tag{7.6.9}$$

where

$$\begin{aligned} \bar{C}_{1m} &= \sin^2\zeta_m + \frac{B^2}{A^2}\cos^2\zeta_m \\ \bar{C}_{2m} &= \sin\zeta_m\cos\zeta_m\left(1 - \frac{B^2}{A^2}\right) \end{aligned} \tag{7.6.10}$$

and

$$\tilde{d}_1(\zeta_m|\eta') \simeq |\eta'-\zeta_m|\bar{C}_{3m} \tag{7.6.11}$$

where

$$\bar{C}_{3m} = (\bar{C}_{1m})^{1/2} \tag{7.6.12}$$

Thus

$$\tilde{R}_1 \simeq \left((\eta'-\zeta_m)^2\bar{C}_{3m}^2 + \frac{a^2}{A^2} \right)^{1/2} \tag{7.6.13}$$

Also

$$\frac{e^{-(\gamma A)\tilde{R}_1}}{(\gamma A)\tilde{R}_1} \approx \frac{1}{(\gamma A)\tilde{R}_1} - 1 \qquad \text{for } \tilde{R}_1 << \frac{1}{\gamma A} \tag{7.6.14}$$

Thus, the integral is approximated as

$$\int_{\eta_{n-1}}^{\eta_n} \tilde{S}_i(\zeta_m|\eta')\tilde{g}_i(\zeta_m|\eta';s)d\eta' \approx$$

$$\approx \int_{\eta_{n-1}}^{\eta_n} (\bar{C}_{1m}+\bar{C}_{2m}(\eta'-\zeta_m)) \left\{(\gamma A)^{-1}\left[(\eta'-\zeta_m)^2\bar{C}_{3m}^2 + \frac{a^2}{A^2}\right]^{-\frac{1}{2}} - 1\right\} d\eta'$$

$$\text{for } n=m \tag{7.6.15}$$

Splitting this up into four integrals gives

$$I_1 = -\bar{C}_{1m}(\eta_n-\eta_{n-1}) = -\bar{C}_{1m}\Delta_n \tag{7.6.16}$$

$$I_2 = -\frac{\bar{C}_{2m}}{2}\left((\eta_n-\zeta_m)^2 - (\eta_{n-1}-\zeta_m)^2\right) \tag{7.6.17}$$

$$I_3 = \frac{\bar{C}_{1m}}{\gamma A}\int_{\eta_{n-1}}^{\eta_n}\left[(\eta'-\zeta_m)^2\bar{C}_{3m}^2 + \frac{a^2}{A^2}\right]^{-\frac{1}{2}} d\eta' \tag{7.6.18}$$

$$I_4 = \frac{\bar{C}_{2m}}{\gamma A}\int_{\eta_{n-1}}^{\eta_n}\left[(\eta'-\zeta_m)^2\bar{C}_{3m}^2 + \frac{a^2}{A^2}\right]^{-\frac{1}{2}} (\eta'-\zeta_m)d\eta' \tag{7.6.19}$$

Note that I_2 and I_4 are no longer zero, since the integrands are not necessarily odd functions about the midpoint of integration. Integrals I_3 and I_4 can be calculated in closed form as

$$I_3 = \frac{\bar{C}_{1m}}{\bar{C}_{3m}} \frac{1}{\gamma A} \log \left(\frac{(\eta_n - \zeta_m) + \left[(\eta_n - \zeta_m)^2 + \left[(a/A)/\bar{C}_{3m} \right]^2 \right]^{\frac{1}{2}}}{(\eta_{n-1} - \zeta_m) + \left[(\eta_{n-1} - \zeta_m)^2 + \left[(a/A)/\bar{C}_{3m} \right]^2 \right]^{\frac{1}{2}}} \right) \tag{7.6.20}$$

$$I_4 = \frac{\bar{C}_{2m}}{\bar{C}_{3m}} \frac{1}{\gamma A} \left(\left[(\eta_n - \zeta_m)^2 + \left[(a/A)/\bar{C}_{3m} \right]^2 \right]^{\frac{1}{2}} - \right.$$

$$\left. - \left[(\eta_{n-1} - \zeta_m)^2 + \left[(a/A)/\bar{C}_{3m} \right]^2 \right]^{\frac{1}{2}} \right) \tag{7.6.21}$$

Using these, the resulting moment method matrix (7.5.59) entries can be calculated, and are given in Table 7.6.1.

The proper choice of basis function widths can be made by using a little intuition. Making the widths equal in angular size results in the partitions being shorter in arc length near $\eta=0$ than near $\eta=\pi/2$. For example, with B/A=0.1 and N=18, the partitions are nine times larger at $\eta=\pi/2$ than at $\eta=0$. It also means that the matching points and integral evaluation points are not at the arc length center of the partition. It seems much more sensible to choose η_n such that the pulse widths are equal in arc length. Then the matching points

Table 7.6.1. Alternative entries in moment method matrix for elliptical loop scatterer.

a) $m \neq n$

$$A_{mn} = \sum_{i=1}^{4} (-1)^{i-1} Q_{ij} \left(\bar{g}_i'(\zeta_m | \eta_{n-1}; s) - \bar{g}_i'(\zeta_m | \eta_n; s) \right) -$$

$$- (\gamma A)^2 \Delta_n \sum_{i=1}^{4} Q_{ij} \left(\bar{S}_i(\zeta_m | \kappa_n) \bar{g}_i(\zeta_m | \kappa_n; s) \right)$$

b) $m = n$

$$A_{mn} = \sum_{i=1}^{4} (-1)^{i-1} Q_{ij} \left(\bar{g}_i'(\zeta_m | \eta_{m-1}; s) - \bar{g}_i'(\zeta_m | \eta_m; s) \right) -$$

$$- (\gamma A)^2 \Delta_m \sum_{i=2}^{4} Q_{ij} \left(\bar{S}_i(\zeta_m | \kappa_m) \bar{g}_i(\zeta_m | \kappa_m; s) \right) -$$

$$- (\gamma A)^2 Q_{ij}(I)$$

where $I = I_1 + I_2 + I_3 + I_4$ from (7.6.16)-(7.6.19)

and the integral evaluation points can be put at the arc length midpoint of the intervals.

To exactly calculate the η_n describing equal arc length partitions requires solving

$$u(\eta_n-\eta_{n-1}) = \int_{\eta_{n-1}}^{\eta_n} \left(A^2\sin^2\eta + B^2\cos^2\eta \right)^{\frac{1}{2}} d\eta = \Delta u \qquad (7.6.22)$$

numerically for each value of η_n, where Δu is the partition width (for constant arc length partitions.) This is quite difficult and time consuming. Instead, approximate the differential arc length as

$$\frac{du}{d\eta} = A\left(\sin^2\eta + \frac{B^2}{A^2}\cos^2\eta\right)^{\frac{1}{2}} \simeq \frac{\Delta u}{\Delta \eta} \qquad (7.6.23)$$

Then proper pulse widths, matching points, and integral evaluation points can be calculated by subdividing Δu into about ten portions and and incrementing numerically from η=0 to $\eta=\pi/2$. The last partition will end at $\eta>\pi/2$ due to the inaccuracy in approximating the arc length in this fashion. Thus, as a last step, it is necessary to correct all the points by multiplying by $\frac{\pi}{2}/\eta_N$.

To calculate the partition width, it is necessary to know the perimeter (actually, ¼ of the perimeter) of the ellipse quite accurately. This is done by calculating the complete elliptic integral

$$E(B^2/A^2) = \frac{\text{perimeter}}{4A} = \int_0^{\pi/2} \left(\sin^2\eta + \frac{B^2}{A^2}\cos^2\eta \right)^{\frac{1}{2}} d\eta \qquad (7.6.24)$$

Rather than calculate this numerically, it is possible to estimate the value of the perimeter via the following formula [71]

$$E(m) = 1 + \sum_{i=1}^{4} a_i m_1^i - \log(m_1) \sum_{i=1}^{4} b_i m_1^i + \varepsilon(m) \qquad (7.6.25)$$

where

$$m_1 = 1-m = \frac{B^2}{A^2} \qquad (7.6.26)$$

and

$$\begin{aligned} a_1 &= 0.44325141463 & b_1 &= 0.24998368310 \\ a_2 &= 0.06260601220 & b_2 &= 0.09200180037 \\ a_3 &= 0.04757383546 & b_3 &= 0.04069697526 \\ a_4 &= 0.01736506451 & b_4 &= 0.00526449639 \end{aligned} \qquad (7.6.27)$$

and

$$|\varepsilon(m)| < 2\times10^{-8} \qquad (7.6.28)$$

7.7 Numerical Results

The natural frequencies and modal current distributions of the thin wire elliptical loop scatterer are determined by solving equation (7.5.59). Little insight is gained, however, by haphazardly solving for roots to the determinantal equation. A much more informative and systematic approach can be conceived, as follows.

It was mentioned earlier that the special case of a circular loop (B/A = 1, or zero eccentricity) has been handled in great detail by Blackburn and Wilton [16]. By solving an equation similar to (7.3.16), they have been able to identify three general "types" of poles. There is one Type I pole for each value of the modal index n, and it is located in the complex plane near ω=n. There are n+1 Type II poles for each n, and they lie in layers to the left of the Type I layer. Lastly, there are an infinite number of Type III poles for each n, and they lie in a layer nearly parallel to the $s=j\omega$ axis. Since the Type I poles have the smallest damping coefficients, they provide the greatest contribution to the late-time portion of the scattered field waveform, and are thus of the greatest interest.

The values of the Type I natural frequencies of the circular thin wire loop can be calculated by solving equation (7.3.16). Those corresponding to n=1 through n=10 have been computed and are shown in Figure 7.7.1. The plotted values are normalized by c/b, where b is the loop radius and c is the speed of light, and they correspond to a wire radius given by a=0.01b. As predicted, they lie in a layer with ω=n c/b. Their numerical values are given in Table 7.7.1. As the circular loop is deformed into an ellipse, the Type I natural

Table 7.7.1 First ten Type I poles of a circular loop of radius b and wire radius a=0.01b.

n	$s_n/(c/b)$
1	-0.09617 + j1.046
2	-0.1425 + j2.062
3	-0.1794 + j3.074
4	-0.2115 + j4.084
5	-0.2406 + j5.092
6	-0.2677 + j6.099
7	-0.2933 + j7.106
8	-0.3177 + j8.112
9	-0.3412 + j9.118
10	-0.3639 + j10.12

Table 7.7.2 First five Type I poles of circular loop found by moment method solution to elliptical loop EFIE with B/A=1, a/A=0.01, using 15 partitions.

n	$s_n/(c/A)$
1	-0.09783 + j1.036
2	-0.1436 + j2.038
3	-0.1783 + j3.029
4	-0.2062 + j4.008
5	-0.2287 + j4.974

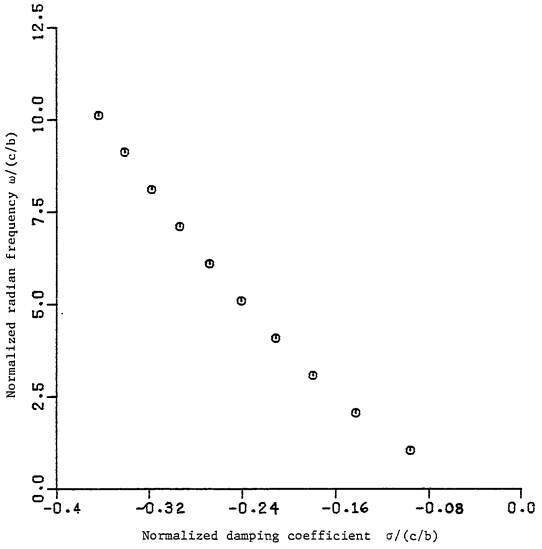

Figure 7.7.1. First ten Type I natural frequencies of a circular loop of radius b and wire radius a=0.01b.

frequencies should change smoothly into a special class of the natural frequencies of the elliptical loop scatterer. These will be examined extensively.

The natural frequencies of the elliptical loop are determined by solving the determinantal equation dictated by (7.5.59). These frequencies will be infinite in number and, like those of the circular loop, will probably fall into groups determined by their position in the frequency plane. Of greatest present interest are those frequencies with the smallest damping coefficients. It is hypothesized that since the Type I poles have the smallest damping coefficients for the circular loop, the frequencies derived from them as the eccentricity of the ellipse is perturbed from zero will have the smallest damping coefficients for the elliptical loop. The behavior of the Type I frequencies as the loop is deformed is investigated by solving (7.5.59) for the special case of B/A = 1, and then slowly decreasing B/A while using the previous solutions as initial guesses.

Equation (7.5.59) has been solved with B/A = 1, using 15 partitions. The results for the first five Type I poles are displayed in Table 7.7.2, and correspond to a wire radius of a=0.01A. It is seen that they do not exactly match the values determined via the Fourier series solution. This is not surprising, since the moment method approach introduces many additional approximations. The accuracy is worst for the higher order modes, where 15 partitions may not be enough to adequately represent the current distribution.

A scrutiny of the elliptical loop symmetry cases given in Figure 7.5.1 reveals that for the degenerate situation B/A = 1, circular

modes of odd order n correspond to both elliptical symmetry cases 1 and 2, while circular modes of even order n correspond to both symmetry cases 3 and 4. Since each symmetry case is expected to produce a separate mode when B/A < 1, each of the circular Type I poles should split into two distinct natural frequencies as the loop is deformed. This is verified by solving (7.5.59) for various values of B/A, beginning with B/A = 1. Using 15 partitions of equal arc length (the approach of section 7.6) and a/A = 0.01 gives the results shown in Figures 7.7.2 through 7.7.6. Here normalized values of natural frequency have been plotted for values of B/A ranging from 1 down to 0.1. As predicted, each of the Type I circular poles splits into two separate natural frequencies as B/A is decreased.

An especially interesting feature seen in the frequency plots is the trajectories of the case 2 and case 4 frequencies. With $B/A \to 0$, the elliptical loop approaches a transmission line with both ends shorted. The natural frequencies of such a transmission line are easily determined: they have zero real parts and have imaginary parts equal to $k \frac{\pi}{2} c/A$, k=1,2,... . The current distribution on the transmission line corresponds with case 2 and case 4 symmetry (current a maximum at each end.) It is thus encouraging to see in Figures 7.7.2 through 7.7.6 that the trajectories of the case 2 and case 4 frequencies approach the frequency values of the transmission line. This is shown with the dotted curves. Unfortunately, as $B/A \to 0$, a/B becomes larger and the thin wire approximation breaks down before the transmission line limit is reached. Indeed, the loop probably ceases to be an electrically thin wire before B/A = 0.2, as the figures seem to show.

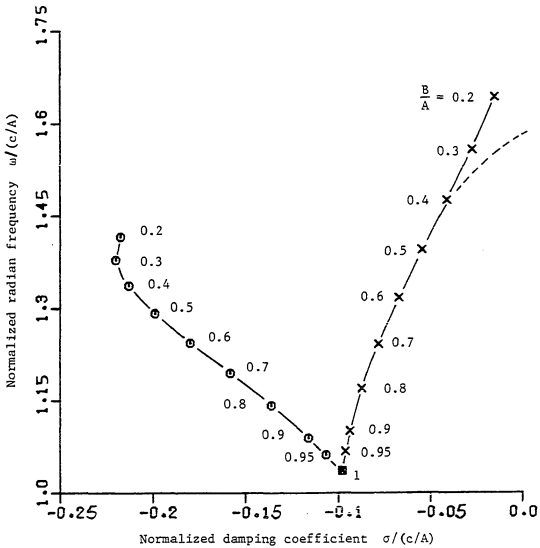

Figure 7.7.2. Case 1 (circles) and case 2 (crosses) natural frequencies of thin wire ellipse of wire radius a=0.01A arising from n=1 circular mode, for various values of B/A. Dotted line shows expected trajectory for transmission line limit.

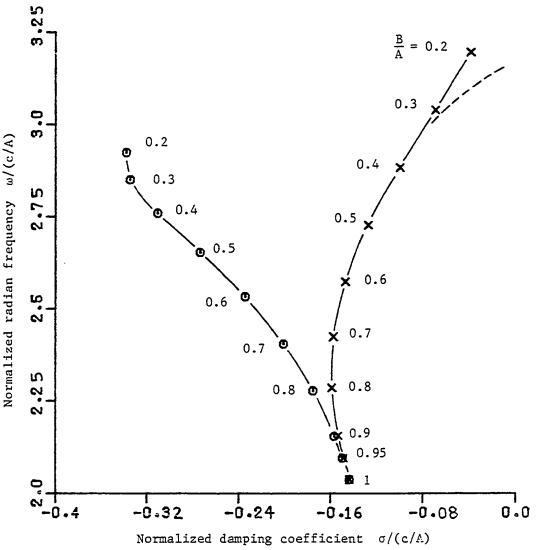

Figure 7.7.3. Case 3 (circles) and case 4 (crosses) natural frequencies of thin wire ellipse of wire radius a=0.01A arising from n=2 circular mode, for various values of B/A. Dotted line shows expected trajectory for transmission line limit.

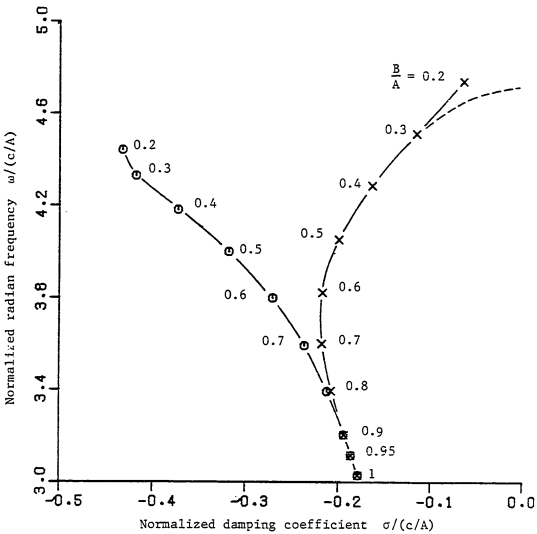

Figure 7.7.4. Case 1 (circles) and case 2 (crosses) natural frequencies of thin wire ellipse of wire radius a=0.01A arising from n=3 circular mode, for various values of B/A. Dotted line shows expected trajectory for transmission line limit.

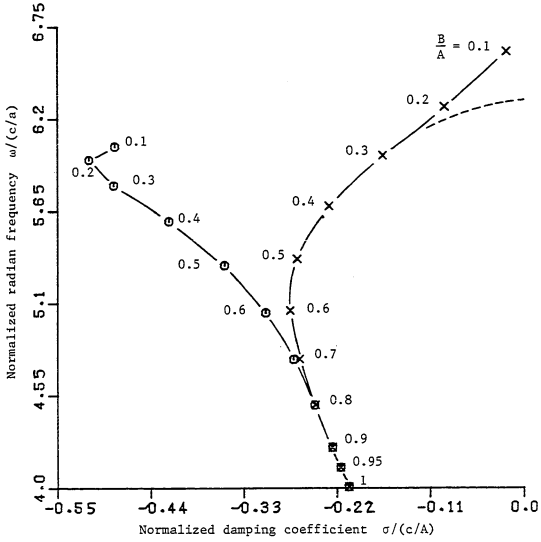

Figure 7.7.5. Case 3 (circles) and case 4 (crosses) natural frequencies of thin wire ellipse of wire radius a=0.01λ arising from n=4 circular mode, for various values of B/A. Dotted line shows expected trajectory for transmission line limit.

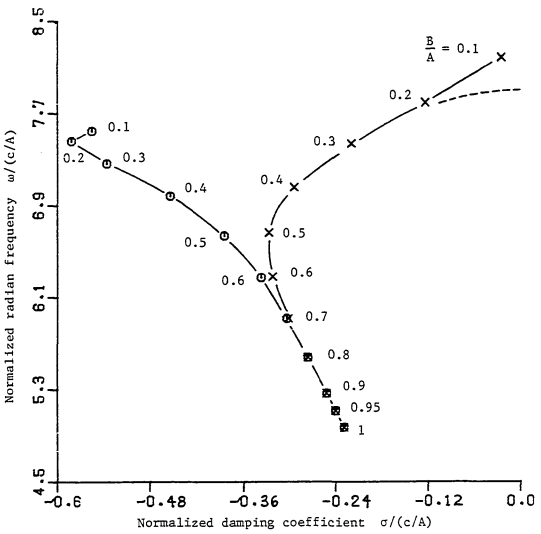

Figure 7.7.6. Case 1 (circles) and case 2 (crosses) natural frequencies of thin wire ellipse of wire radius a=0.01A arising from n=5 circular mode, for various values of B/A. Dotted line shows expected trajectory for transmission line limit.

However, the limit can be approached further by decreasing a/A. With a/A = 0.001, and using 60 partitions, the case 2 frequency which splits off from the the first Type I pole is found to converge to $s = -0.00017 + j1.565$ c/A by B/A = 0.025. This is very close to the limiting transmission line value of $s = 0 + j1.571$ c/A.

It is also possible to describe the limiting behavior of the natural frequencies corresponding to case 1 and case 3 symmetry. As $B/A \to 0$, the current associated with these symmetries approaches that on an open circuited transmission line. The natural frequencies of this structure have been investigated by Chuang [73] by analyzing parallel coupled thin wires. For a pair of wires each of length L and radius a=0.01L/2 at a separation of D=0.2L, he has obtained a value of $s = -0.21 + j1.40$ c/(L/2) for the first open circuit mode. Figure 7.7.2 shows that the first open circuit mode of the elliptical loop (case 1 symmetry) has a natural frequency of $s = -0.22 + j1.42$ c/A when B/A = 0.2. This is a very close match.

The current distributions corresponding to two sets of elliptical modes have also been plotted, for B/A = 0.4, and are shown in Figures 7.7.7 through 7.7.10. Figure 7.7.7 shows the real part of the currents which correspond to the two modes arising from the n=2 Type I circular mode, while Figure 7.7.8 shows the imaginary part. Similarly, Figure 7.7.9 displays the real part of the currents associated with the modes arising from the n=3 Type I circular mode, while Figure 7.7.10 shows the imaginary part. Each of these current distributions is plotted versus normalized arc length position (not angle.) The real parts are seen to be quite close to sinusoidal distributions, despite a

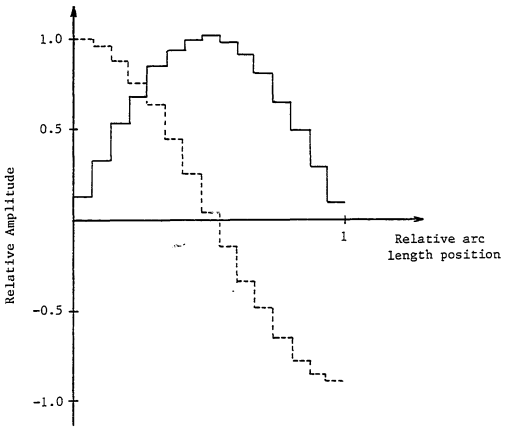

Figure 7.7.7. Real part of current distribution on ellipse with B/A=0.4, for case 3 (solid line) and case 4 (dotted line) symmetries arising from n=2 circular mode.

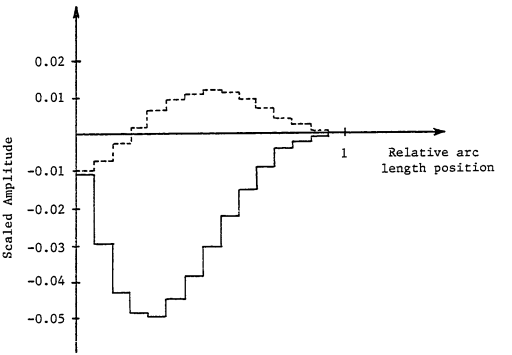

Figure 7.7.8. Imaginary part of current distribution on ellipse with B/A=0.4, for case 3 (solid line) and case 4 (dotted line) symmetries arising from n=2 circular mode. Amplitude is scaled relative to real part.

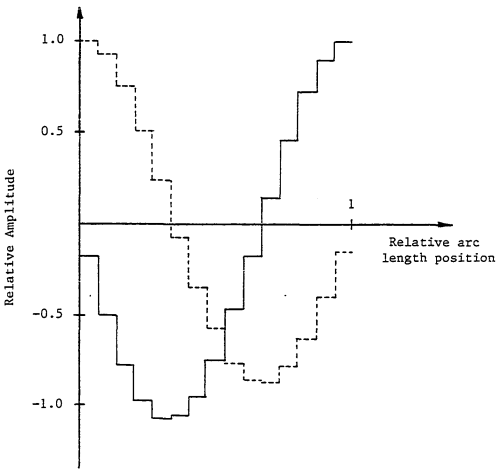

Figure 7.7.9. Real part of current distribution on ellipse with B/A=0.4, for case 1 (solid line) and case 2 (dotted line) symmetries arising from n=3 circular mode.

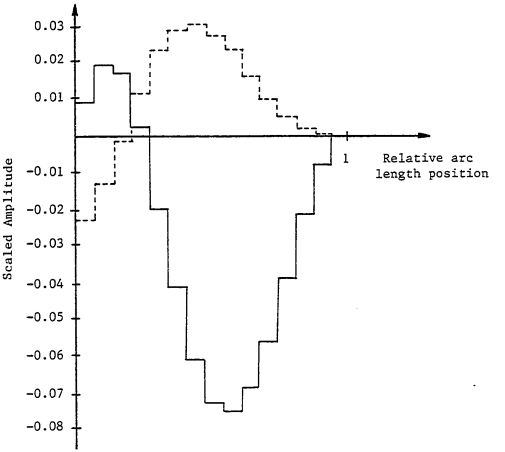

Figure 7.7.10. Imaginary part of current distribution on ellipse with B/A=0.4, for case 1 (solid line) and case 2 (dotted line) symmetries arising from n=3 circular mode. Amplitude is scaled relative to real part.

value of B/A directly intermediate between a circle (B/A = 1) and a transmission line (B/A = 0).

Figures 7.7.2 through 7.7.6 show that each Type I pole splits into frequencies which have very similar imaginary parts, but different real parts. Thus, it might seem at first that a measurement of the response of this target would provide a good means of checking the ability of natural frequency extraction schemes to separate nearly degenerate modes. However, the present experiment only allows transmission over a conducting ground screen. Because of the image effect, this allows current distributions obeying only symmetry cases 1 and 3 or only 2 and 4 to be present at one time (depending upon whether the long or short axis of the ellipse is perpendicular to the ground screen.)

It is now apparent that Type I circular modes split into elliptical modes which make important contributions to the late-time response. The question remains as to whether any Type II or Type III circular modes become important elliptical modes. That is, do any of the Type II or Type III poles split into natural frequencies which have trajectories carrying them near to the imaginary axis? It is also important to ask whether any elliptical frequencies exist which do not arise from circular poles. An extensive search of the complex frequency plane has not been performed, and thus the latter question cannot be answered. However, a preliminary investigation into the properties of the Type II poles has been undertaken.

The n=1 frequency of the first layer of Type II poles is found by solving equation (7.3.16) to be $s = -1.35 + j1.55\ c/A$. Figure

7.7.11 shows the trajectories of the two elliptical loop frequencies which split off from this pole. Each is seen to have damping coefficients which increase (negatively) as B/A is decreased. This means that this set of poles does not correspond to modes which make important contributions to the late-time response of the elliptical loop. Figures 7.7.12 and 7.7.13 show the real and imaginary parts of the current distributions associated with these natural frequencies, for a value of B/A = 0.4.

With the above information, it is not a bad assumption that only Type I circular poles give rise to elliptical modes which make important contributions to the late-time response of the elliptical loop scatterer. Thus, it is possible to construct E-pulses which should do a good job of extinguishing the late-time response of this target. Figure 7.7.14 shows a minimum duration natural E-pulse designed to eliminate the first five Type I modes of the circular loop (whose natural frequencies are shown in Figure 7.7.1.) The similarity between this E-pulse and the thin cylinder E-pulse of Figure 5.5.1.2 is most striking, but easily explained by the similarities in the distributions of the natural frequencies of the two objects. Figure 7.7.15 shows an E-pulse designed to eliminate the ten elliptical modes which arise from the first five Type I circular modes, for B/A = 0.4. This E-pulse waveform is quite different from that of the circular loop, but is still very well behaved. This suggests that natural E-pulses synthesized to eliminate nearly degenerate modes can be quite smooth, an important fact since most realistic targets will probably have such modes.

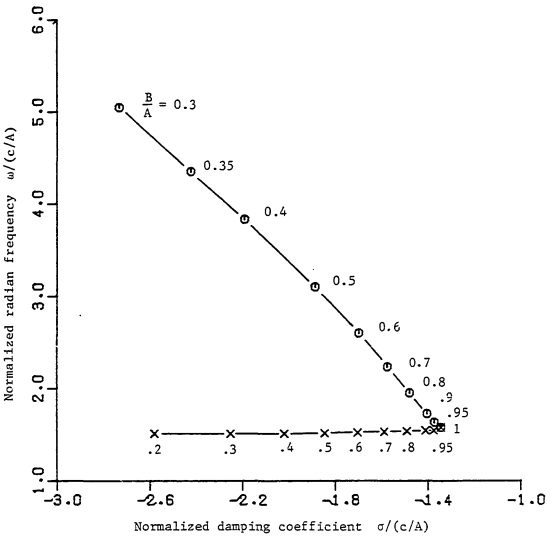

Figure 7.7.11. Case 1 (circles) and case 2 (crosses) natural frequencies of thin wire ellipse of wire radius a=0.01A arising from first layer Type II n=1 circular mode, for various values of B/A.

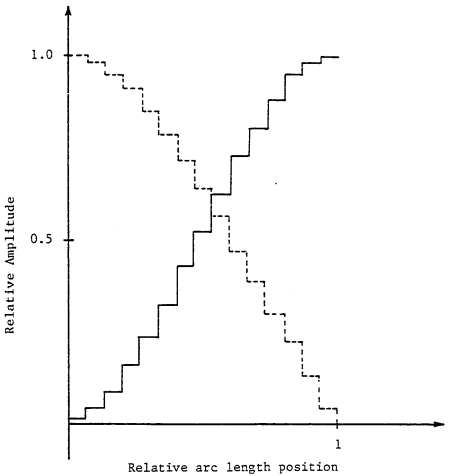

Figure 7.7.12. Real part of current distribution on ellipse with B/A=0.4, for case 1 (solid line) and case 2 (dotted line) symmetries arising from first layer Type II n=1 circular mode.

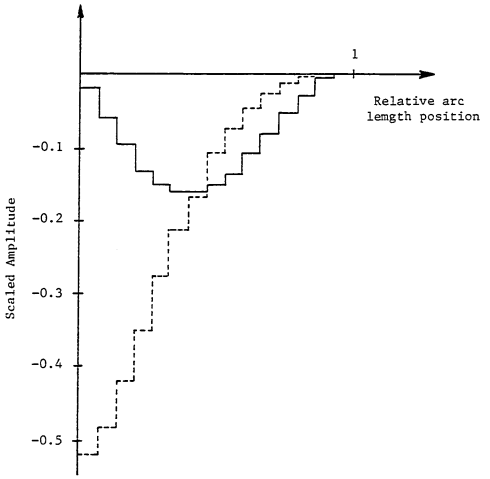

Figure 7.7.13. Imaginary part of current distribution on ellipse with B/A=0.4, for case 1 (solid line) and case 2 (dotted line) symmetries arising from first layer Type II n=1 circular mode. Amplitude is scaled relative to real part.

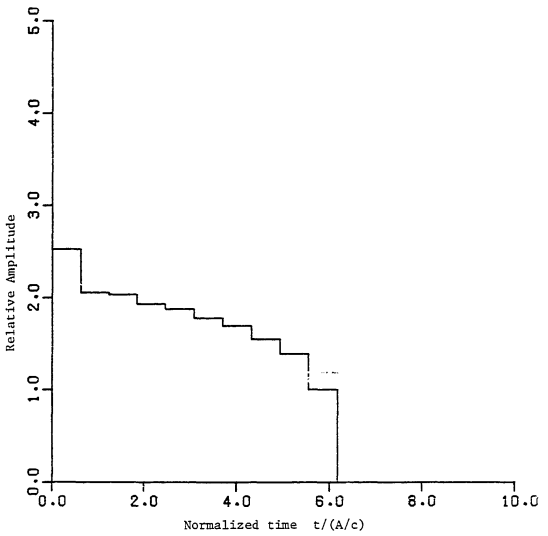

Figure 7.7.14. Natural E-pulse of minimum duration synthesized to eliminate the first five Type I modes of the circular loop scatterer.

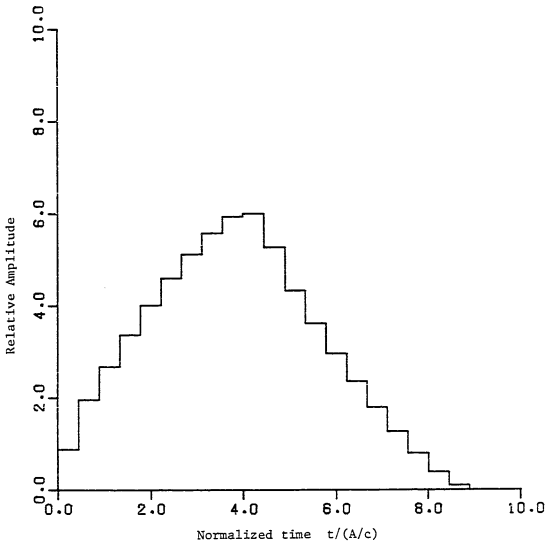

Figure 7.7.15. Natural E-pulse of minimum duration synthesized to eliminate the ten modes of the elliptical loop scatterer arising from the first five Type I circular modes, for B/A=0.4.

CHAPTER 8

EXPERIMENT

8.1 Introduction

Besides providing a basic description of the MSU scattering range and measurement facilities, this chapter has two main purposes. The first is to present experimental justification for using the SEM expansion of the late-time target scattered field waveform. This is accomplished by comparing the natural frequencies of a thin cylinder target obtained from a time domain measurement of scattered field or surface current with those predicted from SEM analysis. A verification of the aspect independence of target natural frequencies will also be given, via time domain surface current measurements taken at multiple aspects. Note that each of these tasks requires the utilization of a natural frequency extraction scheme, and thus also provides a practical test for the techniques of chapter 6.

Second, with the legitimacy of the SEM expansion strengthened by empirical observation, an experimental verification of the E-pulse concept can be sought. This is done using the scattered field measurements of two aircraft scale models -- those of a Boeing 707 and a McDonnel Douglas F-18.

8.2 Experimental Facility and Measurement System

A facility for the measurement of the time domain scattered field, surface current, and surface charge response of radar targets has been established at Michigan State University. A rough sketch of this transient scattering range is shown in Figure 8.2.1.

Target excitation is provided by an incident electromagnetic wave radiated by a monocone antenna suspended over a large conducting ground screen. The antenna has an axial height of 2.4 meters, a polar angle of 8°, and a characteristic impedance of 160Ω. It transmits a spherical TEM wave which approximates a plane wave polarized perpendicular to the ground screen at the position of the target. The ground screen consists of nine individual 4x8 ft aluminum sheathed modules, and has overall dimensions of 16x20 ft. This provides a "window" of approximately 14 nanoseconds in which to perform the measurements, before reflections from the edges of the ground screen and the top of the antenna return.

Figure 8.2.2 shows a schematic representation of the measurement system associated with the scattering range. Reception of the electromagnetic field scattered by a radar target is provided by the indicated (2 cm) monopole probe, which is located about 1.4 m from the transmitting antenna. Target surface charge or surface current can also be measured by placing a short monopole or a (5 mm diameter) shielded loop probe [75] directly on the surface of the target. The connections shown in Figure 8.2.2 remain unchanged.

The monocone antenna is driven by a Tektronix 109 pulser, which provides quasi-rectangular pulses (100 ps risetime) of approximately

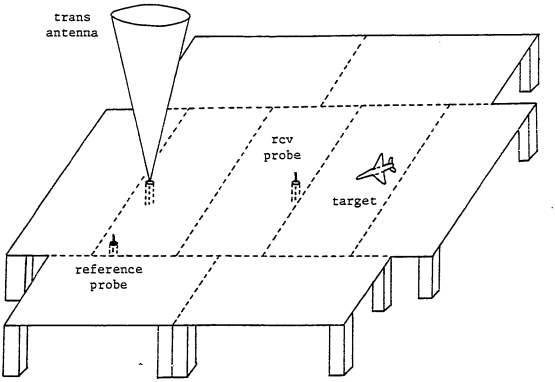

Figure 8.2.1. MSU transient scattering range.

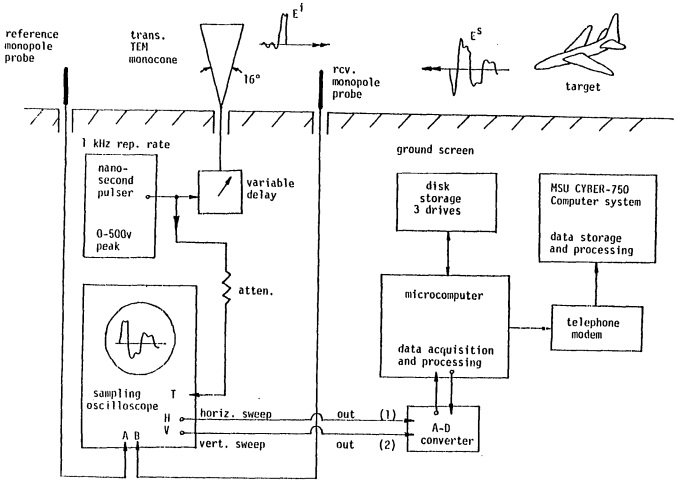

Figure 8.2.2. Transient scattering range measurement system.

nanosecond duration at a rate of 800 Hz. An external power supply allows pulse amplitudes of up to 500 volts. Since the antenna impedance is nearly constant over a large range of frequencies, the pulse is transmitted with little distortion. A variable delay is provided by adjusting the cable lengths in the system. This allows the movement of the target response relative to other events.

The output of the pulser is used to trigger a Tektronix ps-risetime sampling oscilloscope. Channel B of the scope is fed by the signal from the target response probe, while channel A of the scope is connected to a reference probe located at a position convenient for timing purposes. The reference probe is used to measure changes in timing and amplitude between runs. An analog-to-digital converter interfaces the sampling oscilloscope with a TRS-80 microcomputer, which acquires the measured data under software control. Each of the horizontal sweep voltage and the vertical voltages of channel A and channel B of the oscilloscope is accessed through a separate channel in the A/D converter.

Once measured data has been acquired and is in the micro-computer memory, it can be processed and placed on local disk memory or transmitted via telephone lines to the MSU Cyber-750 mainframe computer system.

8.3 Data Acquisition and Processing Procedure

As mentioned in the previous section, reception of target scattered field is provided by means of a short monopole probe. The reason for using such a low gain antenna is that its transfer function

is easily modeled as a pure differentiator. This allows the effects of the receiving antenna to be removed by applying simple integration to the measured data. The effects of a higher gain antenna, such as a horn, do not manifest themselves so simply, and require a deconvolution process for the separation of the target response from the measured data.

The low gain of the receiving probe results in a measured signal that is severely hampered by the presence of random noise. To combat this problem, the data acquisition process involves making repeated measurement runs and averaging the results. This has been found to increase the signal to noise ratio considerably. However, inconsistancies in the measurements between runs due to oscilloscope triggering jitter, inaccurate reproduction of sampling density, and drifting of the vertical amplifier characteristics and the external power supply voltage neccessitate the implementation of fairly sophisticated data acquisition and processing software.

Figure 8.3.1 shows what might be viewed as a typical trace on the sampling oscilloscope, displaying both the signal from the target probe and the signal from the reference probe. Because the A/D converter will only accept voltage values between zero and five volts, the DC offset on the vertical amplifiers of each channel of the scope must be adjusted so that any portion of the trace which is to be measured accurately falls inside this range. The first large positive going and negative going peaks on both the target response and reference probe traces represent the differentiated version of the incident pulse waveform. The amplifier gain on the scope is turned up

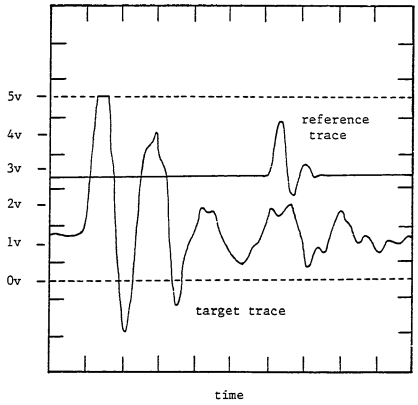

Figure 8.3.1. Typical target and reference traces on CRT of oscilloscope.

to near maximum on the channel which involves the target trace, to accentuate the late-time portion of the target response. However, this causes the initial two peaks to venture outside the five volt range allowed by the A/D converter. Fortunately, the positive going peak is limited at five volts by the scope itself, and so does no damage. The negative going peak falls below the zero volt level, and temporarily interrupts the acquisition of data. This is an important fact which must be emphasized: whenever the A/D converter is presented with a negative voltage, measurements of ALL signals are interfered with, and become inaccurate. Fortunately, the A/D converter recovers rapidly after the negative voltage is removed.

Scope gain and DC offset on the reference channel are adjusted so that the entire waveform, especially the first positive going peak, are well within the five volt range allowed by the A/D converter. The height and time position of the first peak are used as time and amplitude references for adjusting each data run before averaging. As such, it is important that the relative position of this peak is removed in time from the position of the first negative going peak of the target trace, for the reasons mentioned above. This is easily accomplished by choosing the correct cable lengths, or by adjusting the internal scope delay via the "B delay" knob.

Figure 8.3.2 shows a flowchart of the data acquisition and processing routines. The data acquisition phase consists of making several (typically ten) separate traces, first with the target present, and then with the target removed. The oscilloscope sampling density is adjusted such that each data run takes roughly five seconds to

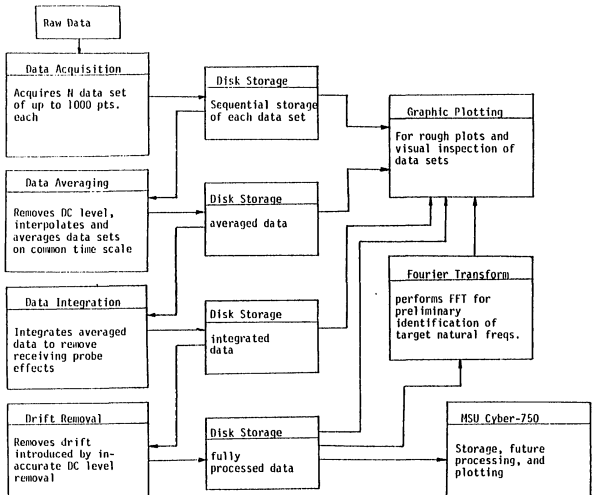

Figure 8.3.2. Flowchart for microcomputer controlled data acquisition and processing.

complete. It is important that the sampling density be high enough for the target response to be accurately reproduced. Data acquisition software (a FORTRAN program) allows the selection of A/D converter sampling rates varying from zero to 1000 samples per second. However, the amount of available microcomputer memory puts a limit on the number of points allowed in each data run: 400 when using program DATPROC for processing, and 1000 when using routine DATPROL. Thus, a sampling rate of 400 samples/5 seconds = 80 samples/sec is typical.

The data acquisition phase begins by running the FORTRAN program DATACQ. This program controls the A/D converter and interfaces with the experimenter via keyboard control. It begins by asking for the number, N, of target runs (target present) and clutter runs (target absent) the operator wishes to make, the A/D converter sampling rate desired, and the scope time per division used (typically one or two nanoseconds). It will then loop through the entire data acquisition process N times. At each step the operator indicates that he/she wants the acquisition of the current data set to begin. The program starts converting the horizontal voltage channel and waits for the voltage to exceed a preset level (around 50 mv). Thus, the system sits idle until the experimenter pushes the single sweep button on the scope. This initiates the trace and the computer begins to store data for the horizontal and the two vertical voltages in FORTRAN arrays.

It is important for the operator to adjust the timing so that the upward going edge of the first peak does not start until at least twenty samples into the trace. This first group of samples is used to determine the DC levels of the target and reference traces at the

beginning of the data run. It is also important that the A/D sampling rate be adjusted so that at least twenty samples are taken after the scope has performed its retrace. This group is used to calculate the DC levels at the end of the run. The DC levels are subtracted from the data during subsequent data processing.

After the data run has finished, the computer gives the operator the option of retaking the run (in case of problems incurred during the sweep), viewing the acquired data, resetting the sampling rate, or writing the data to floppy disk. Early versions of the data acquisition routine wrote each of the sampled horizontal and the two vertical voltages to disk. However, this is more information than needs to be saved. Program DATACQ still writes the target vertical voltage data series, but instead of writing the entire horizontal data set, it calculates and writes only the number of samples taken before the retrace. This determines the real time (scope) sampling density, which is assumed to remain constant during a trace. Next, rather than writing the entire reference vertical voltage data set to disk, the program calculates and writes the DC level at the beginning and the end of the reference trace (by averaging the samples), the sample time of the reference peak, and the vertical voltage values of the reference peak and its two nearest neighbors. It is important to keep the disk writing time to a minimum in order to make the entire data acquisition process as short as possible. This minimizes the amount of scope drifting between data runs.

After N runs are completed with the target present, an equal number of runs are taken with the target removed. If the target

surface current or surface charge is to be measured, then this step is eliminated. When the last data set has been written to disk, the data acquisition phase is complete.

Data processing begins by running either program DATPROC or DATPROL. Both programs are written in FORTRAN, and run automatically, without any user input. The reference data set for the first target run is read from disk into computer memory and the real time position (in nanoseconds) and the amplitude of the reference peak are calculated. The DC level of the reference signal is removed by performing linear interpolation between the beginning and ending DC levels, and subtracting. It is found that these two levels are rarely the same, due to drifting in the scope amplifiers during the data run. There is actually no reason to believe that this drift is linear, but such an approximation is all that is available. Also calculated from the first run is the scope sampling density. Each of these parameters is stored in memory and is used as a reference for comparison with later data runs.

The vertical target data set for the first target run is also read into memory. The beginning and ending DC levels are calculated by averaging the beginning and ending samples, and are subtracted off in the same linear fashion as above. This data set is then used as the basis with which to compare the remaining sets.

Following the analysis of the initial run, each additional data set is read into memory and processed. First the DC level of the reference signal is subtracted off, as before. Then the sampling density is read from disk, and the time scale is adjusted to match

that of the first data set. Next, the amplitude and time position of the reference peak are calculated. These are used to scale and shift the trace to match the reference signal of the first data set. The last step before averaging is to calculate the DC levels at the beginning and end of the target data set, subtract the DC level on a linear scale, and, finally, scale the target data set by the same amount as required to match the amplitudes of the reference peaks.

Now, since it is likely that neither the reference peak position nor sampling density will match that of the first run, it becomes necessary to employ an interpolation scheme in order to average subsequent data sets with the first. This is where routines DATPROC and DATPROL differ. Program DATPROC employs a cubic spline interpolation process [48], which requires a considerable amount of computer memory, and takes quite a bit of time to execute. However, it is very accurate. In contrast, program DATPROL performs a simple, less accurate linear interpolation between data points. The difference in execution time is quite substantial. For example, it takes about twenty minutes to process ten data and ten clutter runs on the TRS-80 using DATPROC, and only five minutes using DATPROL. Also, because it does not need splining arrays, DATPROL allows up to 1000 data points to be processed for each run, as opposed to the 400 points allowed by DATPROC. Most importantly, experience has shown that with the typically high experimental noise levels, using linear interpolation gives nearly identical results as using cubic splines. Thus, use of program DATPROL is suggested.

As a footnote, the FORTRAN routines ACQDAT and DATPRO1 are

slightly different versions of DATACQ and DATPROC, modified by Martin Perrine, which allow the measurement of target surface current and surface charge. These routines merely avoid the acquisition and processing of clutter waveforms.

Averaging of subsequent data sets is accomplished by using the first data set as a time basis. The data from the subsequent sets is interpolated to find the values at the times of the first set's points, and is added on to (for target runs) or subtracted off from (for clutter runs) the data in the first set. If everything has gone perfectly, when all the data sets have been processed, the net result is the clutter-free, differentiated response of the target. This response is finally written to floppy disk as the processed data.

The data processing as described above is fairly complex, and it is not wise to trust the software on measured data without first confirming its viability. To this end, program PROCTST has been developed which generates ten artificial target and clutter runs. Each run is given different sampling densities, starting and ending DC levels, reference waveform amplitudes, and reference waveform positions. The target response is constructed as a perfect sine wave, and the clutter + incident field waveform as a sinc function which is limited before reaching its peak (after the DC has been added). The reference waveform is also constructed from a sinc function, with a much smaller amplitude. The generated data is all written to disk using a format identical with program DATACQ. Thus, when DATPROC or DATPROL are employed, the result should be a perfect sine wave. This test has been performed, and has proven the validity of each routine.

A number of additional steps are available for further enhancement of the processed data. DATASUM is a FORTRAN program which integrates the processed data by using a simple running sum. This allows the differentiation introduced by the receiving probe to be removed. However, if the DC level of the measured response has not been handled adequately, there will be an unwanted ramp component added to the integrated data. Program DATADJ exists both as a BASIC and a FORTRAN program for the removal of this drift. The BASIC program is run first, allowing the user to choose the slope and intercept of a linear curve which is subtracted from the integrated data. The user can then have the result plotted on the CRT of the microcomputer, and view the response. If it is not to her/his liking, he/she can input new parameters. Once the slope and intercept of the best line have been determined, the FORTRAN version of DATADJ is run, writing the end result to floppy disk.

At any point in the data analysis, BASIC program DATPLOT allows the plotting of a disk file data set on the CRT screen, and also allows a hard copy to be printed. Also available is program FFTD, which is a BASIC program employing the fast Fourier transform algorithm [74] to obtain the Fourier spectrum of a disk file data set. This allows a preliminary identification of the imaginary parts of the target natural frequencies, which can then be used as initial guesses in the more sophisticated natural frequency extraction schemes of chapter 6.

One main goal of all the data processing routines discussed is to accomplish as much as possible in the laboratory using the TRS-80 microcomputer. At this time, everything but the natural frequency

extraction schemes can be completed quite rapidly in the lab. It is necessary as a last step to transmit the processed data over the telephone lines to the MSU Cyber-750 mainframe computer system to perform the frequency extraction.

An effort is currently under way to transfer all the data acquisition and processing responsibilities to an IBM PC computer. The additional memory and more rapid execution time of the IBM microcomputer should allow all the necessary steps of the E-pulse technique to be accomplished in the laboratory. This includes natural frequency extraction, E-pulse synthesis, convolution, and the processing of the convolved responses.

8.4 Experimental Investigation of SEM Validity

The E-pulse concept discussed in this thesis is based entirely upon the conjecture that the late-time scattered field response of a conducting target can be written as in equation (2.4.4) -- that is, it can be represented completely by a series of natural-resonance-based damped sinusoid functions. If this expansion is not correct, or if it is not complete, then the E-pulse concept will fail. It thus becomes extremely prudent to verify experimentally the natural resonance behavior of conducting targets.

Affirmation of the natural resonance description of the late-time response of a target can be accomplished by comparing the natural frequencies extracted from a measured target response with those obtained from a theoretical SEM analysis. To the extent that SEM involves implicitly the assumption of a pure natural resonance

description, close agreement between the two sets of frequencies would tend to substantiate the SEM expansion. This necessitates, however, the use of a target which has been analyzed theoretically. The target should also be a high Q structure, to make the frequency extraction easier. Two candidates obey these criteria -- the elliptical (or circular) loop of chapter 7, and the thin cylinder of chapter 5. Unfortunately, the response of the elliptical loop has not yet been measured. Thus, the comparison will be made for the thin cylinder.

A most visually striking confirmation of the natural resonance expansion is shown in Figure 8.4.1. This is the measured surface current response of a thin cylinder of length 15.87 cm and radius .317 cm placed perpendicular to the ground screen. (These and subsequent surface current measurements were performed by Martin Perrine.) Note the indicated late-time region, and the region where reflections from the edge of the ground screen begin to cause interfering clutter. It is obvious that this target response is dominated by a single natural mode -- the first mode of the thin cylinder. The spectral content of the incident pulse waveform does not have energy at the frequencies necessary to excite modes of higher order. Figure 8.4.2 shows a one mode best fit of the late-time clutter free region of the response, obtained using the continuation method from chapter 6. The analysis of chapter 5 indicates that the first natural frequency of this cylinder (including its image) should occur at $s=-0.246+j2.75 \times 10^9$ r/s. The one mode best fit from the continuation method ascribes a frequency of $s=-0.299+j2.79 \times 10^9$ r/s. The agreement is very good.

By lengthening the cylinder it is possible to lower the resonant

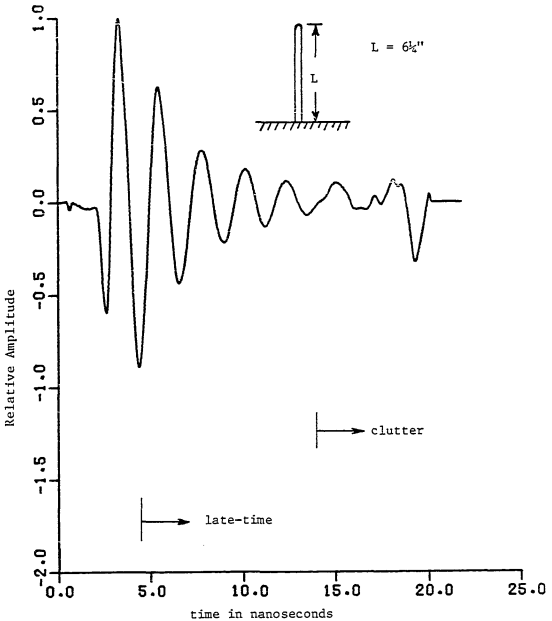

Figure 8.4.1. Measured surface current response of a thin cylinder of length 6.25 inches placed perpendicular to the ground screen.

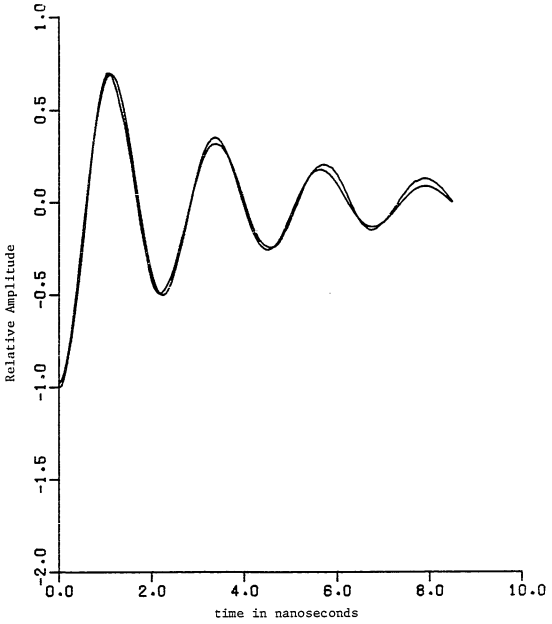

Figure 8.4.2. One mode best fit to late-time, clutter free portion of measured 6.25" thin cylinder surface current response.

frequencies and thus to excite higher order modes. Figure 8.4.3 shows the measured surface current response of a thin cylinder of length 46.36 cm placed perpendicular to the ground screen. This response is apparently not dominated by any single mode. The question then is: can the response be represented by a pure natural resonance series? Figure 8.4.4 shows evidence for answering yes. This figure displays the Fourier spectrum of the response obtained via the FFT. Three peaks very clearly dominate the spectrum, with evidence for a fourth, and they can be used to supply initial guesses for the continuation method. Due to the ground screen image effect, only the odd order modes of the thin cylinder will be excited, and the imaginary parts of the expected values correspond quite closely to the peaks in Figure 8.4.4. More conclusive evidence is provided by extracting the frequencies from the measured response. Figure 8.4.5 shows a two mode best fit to the late-time clutter free portion of the response, obtained using the continuation method. It is seen that the fit is quite good, implying that modes one and three are of greatest importance. An even better fit is shown in Figure 8.4.6, using four modes. The frequencies corresponding to these four modes, and the frequencies predicted from the SEM analysis are given as

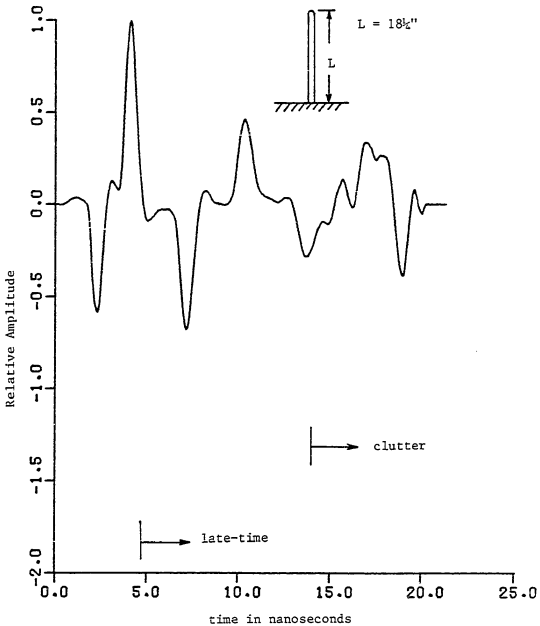

Figure 8.4.3. Measured surface current response of a thin cylinder of length 18.25 inches placed perpendicular to the ground screen.

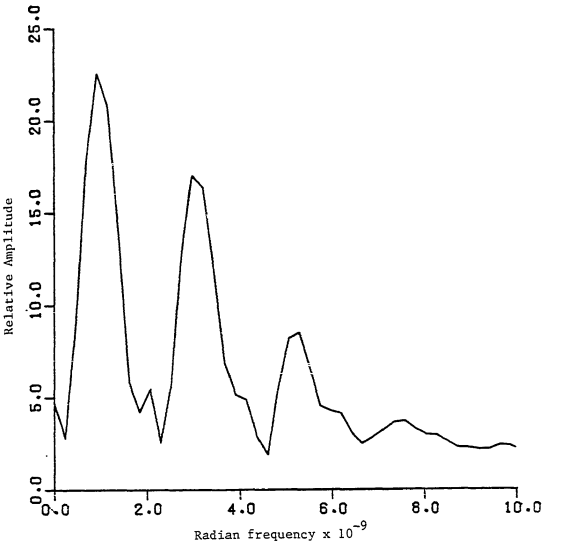

Figure 8.4.4. Fourier spectrum of 18¼" thin cylinder measured surface current response, obtained via FFT.

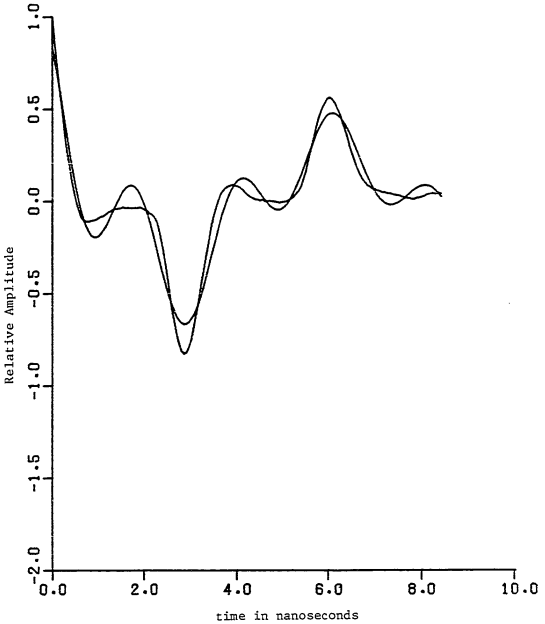

Figure 8.4.5. Two mode best fit to late-time, clutter free portion of measured 18¼" thin cylinder surface current response.

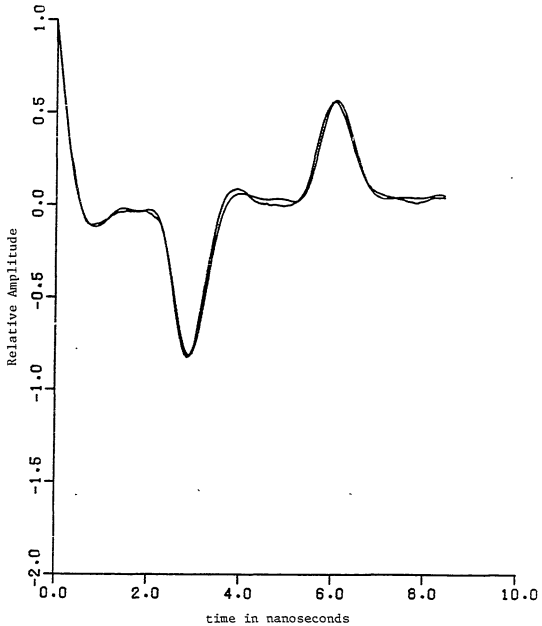

Figure 8.4.6. Four mode best fit to late-time, clutter free portion of measured 18½" thin cylinder surface current response.

mode	theoretical freq	extracted freq	extracted ampl
1	$-.0842 + j.940 \times 10^9$	$-.134 + j.945 \times 10^9$	0.613
3	$-.152 + j2.93 \times 10^9$	$-.142 + j2.97 \times 10^9$	0.439
5	$-.194 + j4.93 \times 10^9$	$-.137 + j4.99 \times 10^9$	0.171
7	$-.227 + j6.94 \times 10^9$	$-.211 + j6.97 \times 10^9$	0.0473

The imaginary parts of the natural frequencies compare extremely well. The damping coefficients are not quite as close, but experience has shown that it is always more difficult to extract the real parts of the natural frequencies.

Confirmation of the SEM expansion can also be provided through scattered field measurements. For example, Figure 8.4.7 shows the measured field scattered by a 15.87 cm wire placed perpendicular to the ground screen. It is obvious that the scattered field measurements are much noisier than the surface current measurements. In fact, there is a noticeable amount of noise on this waveform even though ten data runs were averaged together. This is also evident in Figure 8.4.8 which shows a two mode best fit to the late-time portion of the response. Because of the image effect, only the odd modes are again excited. It is more interesting to consider a thin cylinder target which is placed at an aspect that allows both even and odd modes to be excited.

Figure 8.4.9 shows the measured response of a 31.75 cm long thin cylinder raised 13.3 cm above the ground screen and inclined at an

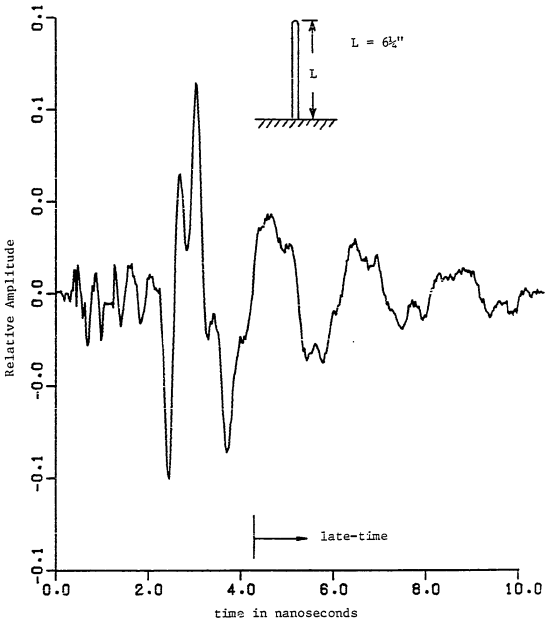

Figure 8.4.7. Measured scattered field response of a thin cylinder of length 6.25 inches placed perpendicular to the ground screen.

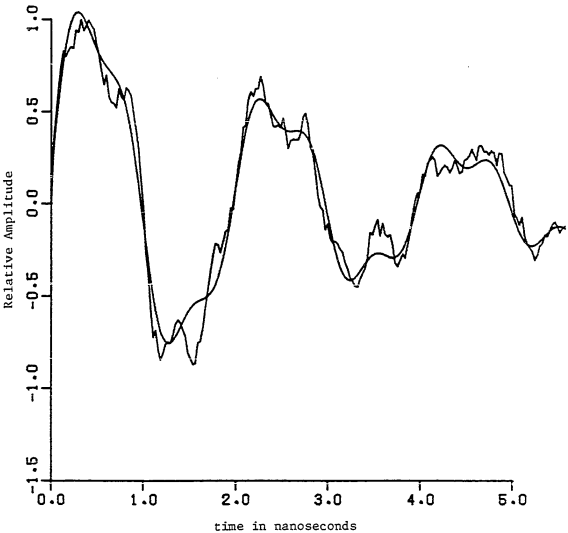

Figure 8.4.8. Two mode best fit to late-time portion of measured 6½" thin cylinder scattered field response.

angle of 45° directly toward the transmitting antenna. This arrangement actually represents a system of coupled wires, due to the image effect. This system has been analyzed [76] and the resulting natural frequencies are very close to those of the isolated wire. Figure 8.4.10 shows the Fourier spectrum of the response. It is obviously dominated by two modes which correspond in frequency quite closely to the first two modes of the isolated wire. There is also a possible third mode. Figure 8.4.11 displays a three mode best fit to the late-time portion of the response. The extracted natural frequencies and the frequencies of the first three modes of the coupled wire system are

mode	theoretical freq	extracted freq	extracted ampl
1	$-.215 + j2.71 \times 10^9$	$-.280 + j2.78 \times 10^9$	0.710
2	$-.287 + j5.70 \times 10^9$	$-.243 + j5.62 \times 10^9$	0.413
3	$-.465 + j8.57 \times 10^9$	$-.227 + j8.21 \times 10^9$	0.0496

The first two frequencies are quite close. The third is not as accurate, but this is expected, since the relative amplitude of this mode is fairly small.

Figure 8.4.12 shows the measured scattered field response of the coupled wire system after it has been rotated 45° about a line perpendicular to the ground screen, with the low end of the wire as a pivot point. This response is a very good demonstration of the sensitivity to aspect angle of the amplitudes and phases of the modes of a target.

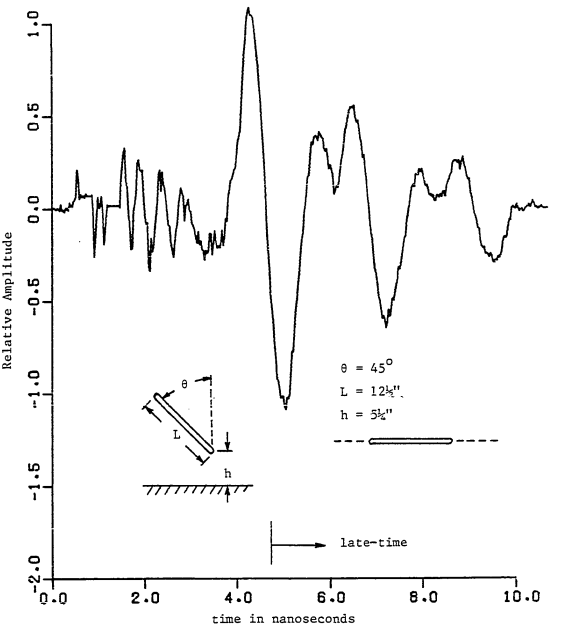

Figure 8.4.9. Measured scattered field response of a thin cylinder of length 12.5 inches raised 5.25 inches above the ground screen and inclined at 45° toward the transmitting antenna.

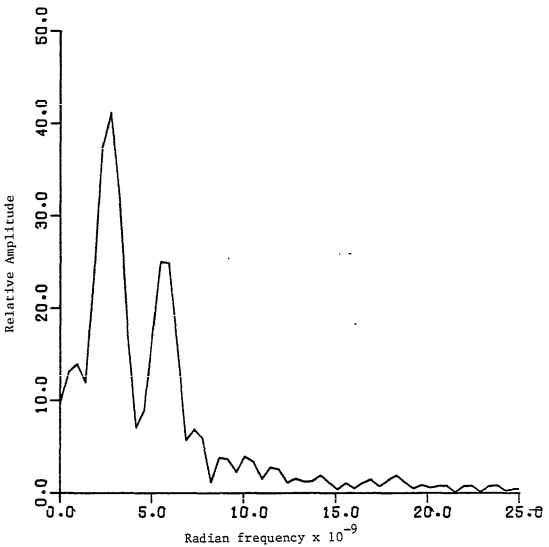

Figure 8.4.10. Fourier spectrum of measured 12½" inclined thin cylinder scattered field response, obtained via FFT.

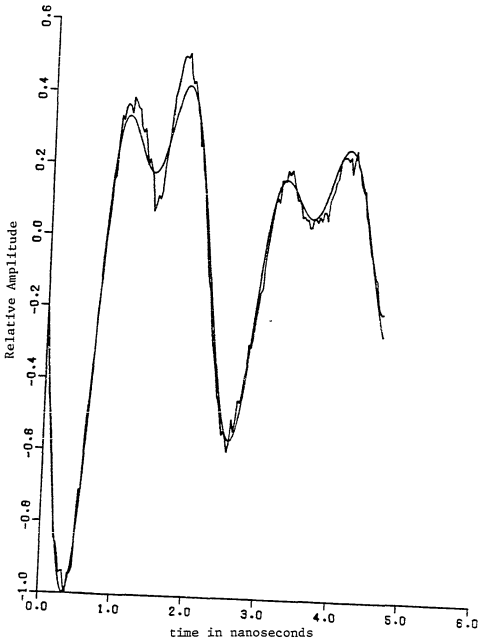

Figure 8.4.11. Three mode best fit to late-time portion of measured 12½" inclined thin cylinder scattered field response.

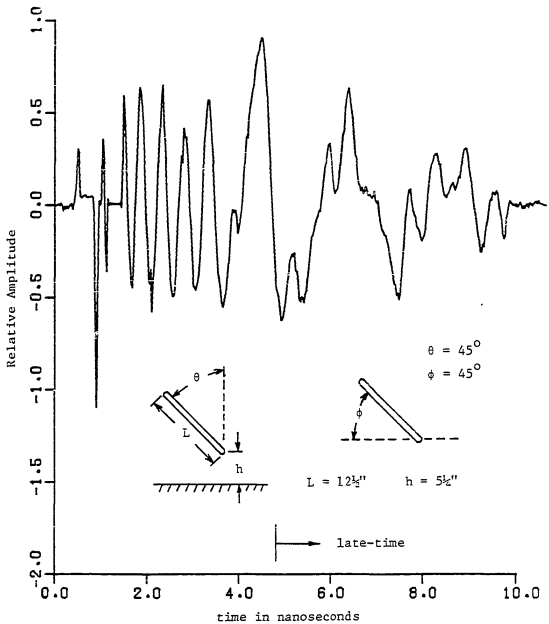

Figure 8.4.12. Measured scattered field response of a thin cylinder of length 12.5 inches raised 5.25 inches above the ground screen, inclined at 45° and rotated by 45°.

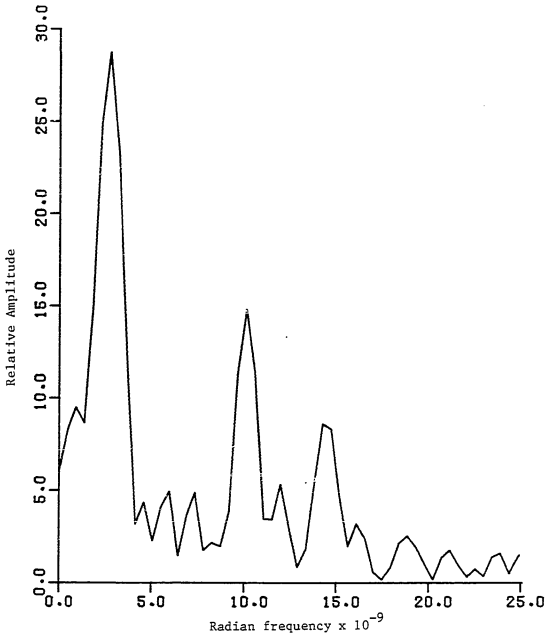

Figure 8.4.13. Fourier spectrum of measured 12½" inclined and rotated thin cylinder scattered field response, obtained via FFT.

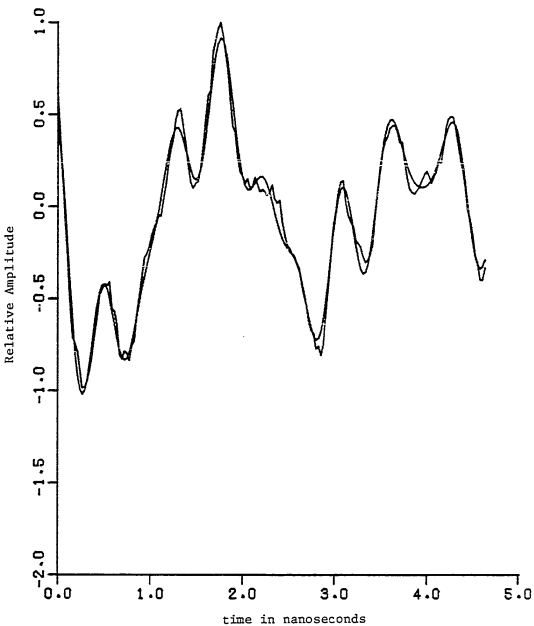

Figure 8.4.14. Five mode best fit to late-time portion of measured 12½" inclined and rotated thin cylinder scattered field response.

Figure 8.4.13 shows the Fourier spectrum of the response. Comparing this spectrum with Figure 8.4.10 reveals that at this aspect the second mode is not excited, while the third and fourth, which were not excited at the other aspect, are now present. In fact, a total of five modes can be detected to some extent, although the two not obvious in the spectrum have very small amplitudes. Figure 8.4.14 shows the five mode best fit to the late-time portion of the response provided by the continuation method.

These results for the thin cylinder provide a great amount of confidence in the natural resonance expansion of the late-time response of a conducting target. One last test can be conducted which provides the clinching evidence. If the expansion is indeed complete, then the natural frequencies extracted from the target response waveforms should be independent of target aspect. This has been shown to be true to some extent for the case of the coupled wire system above, but the independence should be investigated in more depth.

Figure 8.4.15 shows the late-time clutter free surface current response of a target composed of two 31.75 cm thin cylinders attached at a 45^{o} angle, as shown in the figure, and placed with one section perpendicular to the ground screen. By rotating this target and keeping the same section always perpendicular to the ground screen, the target aspect is easily changed. Figure 8.4.16 shows the Fourier spectrum of the response shown in Figure 8.4.15. There seem to be four dominant modes, but the peaks are not as distinct as with the simple straight wire. Since there is no theoretical analysis to compare with these measurements, it is difficult to tell whether some

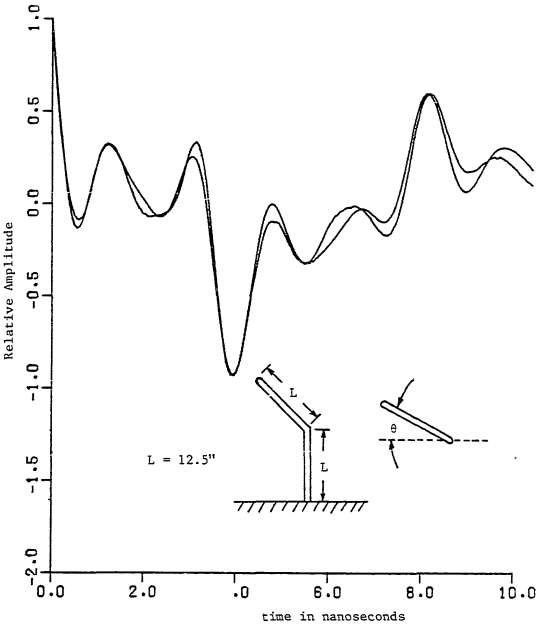

Figure 8.4.15. Late-time, clutter free portion of measured compund wire target surface current response for $\theta=0^{o}$, and four mode best fit.

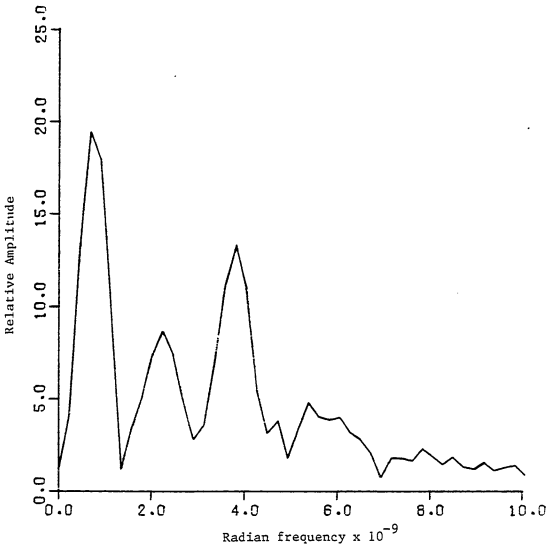

Figure 8.4.16. Fourier spectrum of measured compound wire target surface current response, obtained via FFT.

of these peaks might represent nearly degenerate modes. A four mode best fit given via the continuation method is also shown in Figure 8.4.15. Since the fit is very good, it can be assumed that these four modes comprise the majority of the excited portion of the target's natural mode spectrum.

A verification of the aspect independence of the first four natural frequencies of this compound structure can be obtained by making measurements at many aspects, and extracting the natural frequencies from each response. Table 8.4.1 shows the resulting natural frequencies, relative amplitudes, and relative phases for five different aspect angles. It can be seen that while the amplitudes and phases change dramatically, the natural frequencies remain remarkably constant.

This completes a very convincing validation of the natural mode series expansion.

8.5 Experimental Verification of the E-pulse Concept

With the natural resonance representation validated by the results of the previous section, the stage is set for an experimental verification of the E-pulse concept. An attempt will be made to discriminate between two aircraft scale models with similar dimensions by using the measured scattered field response of each target.

Figure 8.5.1 shows the measured scattered field response of a solid aluminum scale model of a Boeing 707 aircraft. The geometry of the model is shown in the same figure. Similarly, Figure 8.5.2 shows the measured scattered field response of a McDonnel Douglas F-18 scale

Table 8.4.1. Extracted natural frequencies, amplitudes, and phases for a compound wire target at various aspects.

Aspect Angle ϕ	Mode	Damping Coefficient $\times 10^{-9}$	Radian Frequency $\times 10^{-9}$	Relative Amplitude	Relative Phase
0°	1	-0.0252	0.716	1.0	0.0
	2	-0.115	2.23	0.814	0.392
	3	-0.133	3.72	1.22	1.18
	4	-0.155	5.21	0.432	1.59
45°	1	-0.0204	0.711	1.0	0.0
	2	-0.132	2.24	0.712	-0.122
	3	-0.130	3.72	0.709	0.743
	4	-0.190	5.21	0.335	0.610
90°	1	-0.0148	0.719	1.0	0.0
	2	-0.152	2.23	0.799	-0.968
	3	-0.101	3.71	0.363	1.63
	4	-0.201	5.11	0.244	-0.898
135°	1	-0.0477	0.742	1.0	0.0
	2	-0.135	2.22	0.912	1.39
	3	-0.135	3.75	0.918	-0.954
	4	-0.170	5.28	0.315	1.31
180°	1	-0.0121	0.754	1.0	0.0
	2	-0.162	2.24	1.07	1.36
	3	-0.124	3.75	0.987	-2.29
	4	-0.327	5.30	0.622	2.46

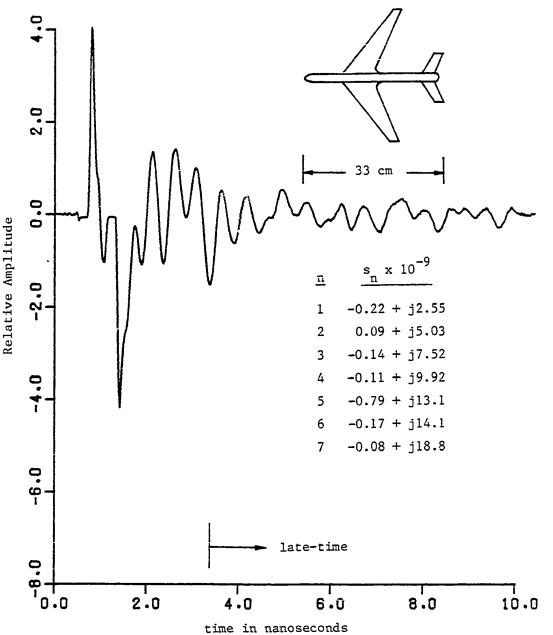

Figure 8.5.1. Measured scattered field response of a Boeing 707 aircraft scale model, and seven dominant natural frequencies.

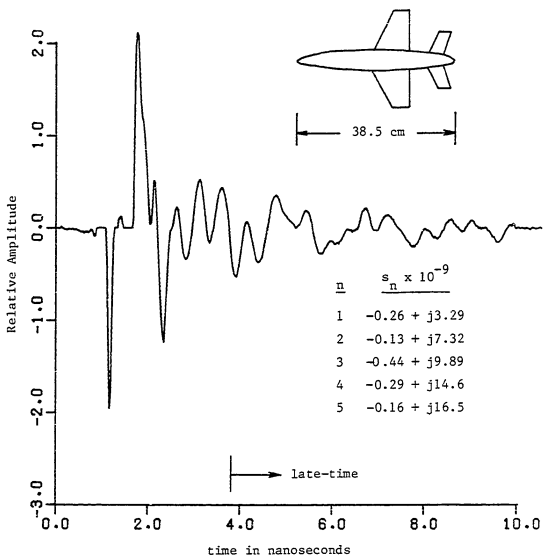

Figure 8.5.2. Measured scattered field response of a McDonnel Douglas F-18 aircraft scale model, and five dominant natural frequencies.

model. The Fourier spectrum of the late-time portion of the 707 response is shown in Figure 8.5.3. There are seven quite distinct modes evident in the spectrum of the 707, and similar analysis reveals a total of five dominant modes for the f-18. The natural frequencies corresponding to the modes of each target have been extracted using the continuation method, and are tabulated in Figures 8.5.1 and 8.5.2. The corresponding late-time best fits are shown in Figures 8.5.4 and 8.5.5.

The methods of chapter four have been used to construct rectangular pulse function based minimum duration natural E-pulses designed to eliminate the five tabulated modes of the F-18 and the seven modes of the 707. These waveforms are shown in Figures 8.5.6 and 8.5.7. Convolving the E-pulses with the target responses they are meant to extinguish results in the convolved responses displayed in Figures 8.5.8 and 8.5.9. While the late-time portions of these responses are not identically zero, they are quite small, and the E-pulses have done a very good job of eliminating the natural modes. In contrast, Figures 8.5.10 and 8.5.11 show the results of convolving the E-pulse waveforms with the responses of the opposite targets (i.e., not the targets for which they were designed). Now the late-time portions are seen to be quite large in magnitude. Discrimination between the two targets can thus be accomplished very convincingly by comparing the late-time portions of each of the convolved responses.

A corroboration of the discrimination decision based on the E-pulse convolutions can be provided by using single mode excitation signals. Rectangular pulse function based minimum duration natural

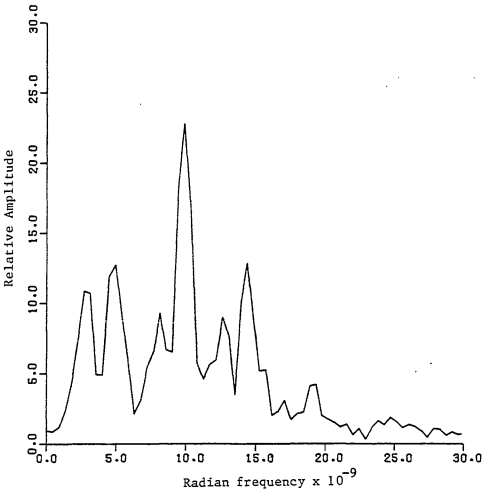

Figure 8.5.3. Fourier spectrum of measured 707 scattered field response, obtained via FFT.

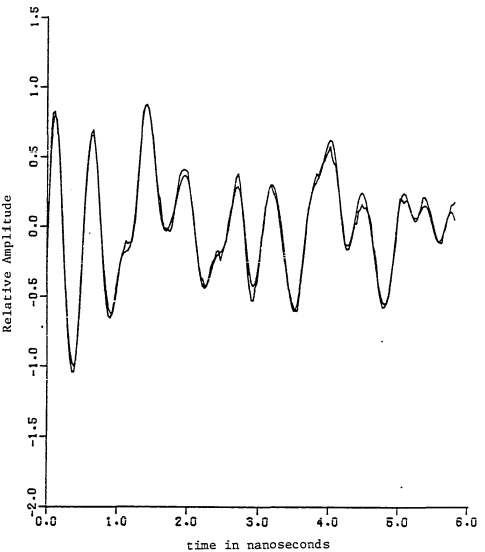

Figure 8.5.4. Seven mode best fit to late-time portion of measured 707 scattered field response.

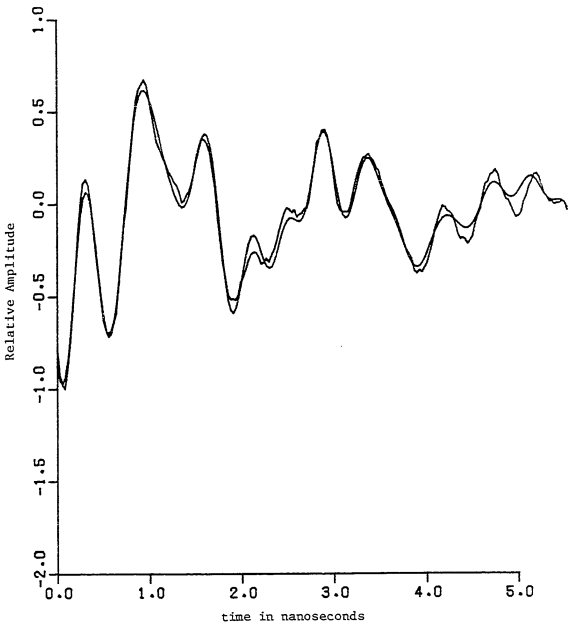

Figure 8.5.5. Five mode best fit to late-time portion of measured F-18 scattered field response.

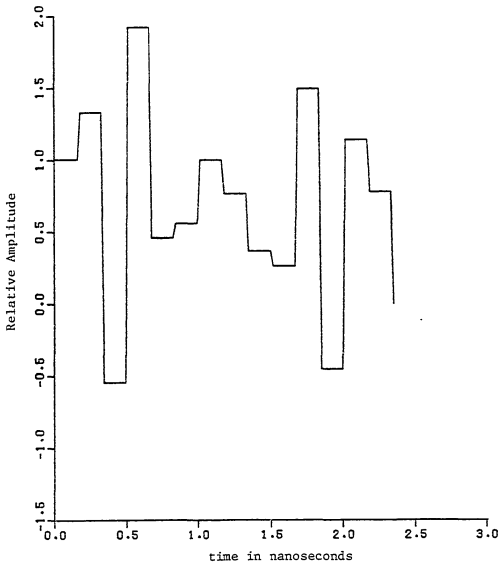

Figure 8.5.6. Natural E-pulse of minimum duration synthesized to eliminate the seven dominant modes of the measured 707 response.

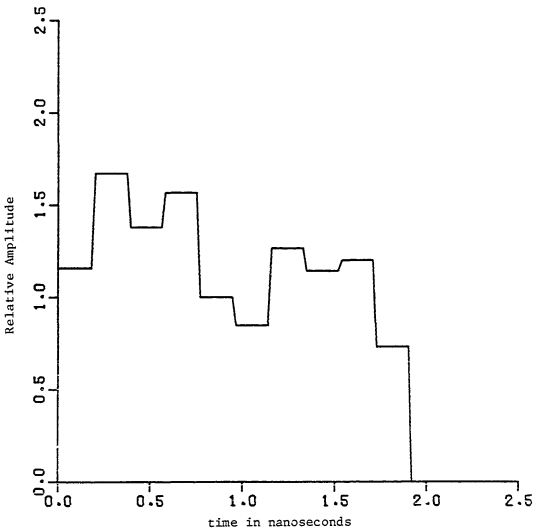

Figure 8.5.7. Natural E-pulse of minimum duration synthesized to eliminate the five dominant modes of the measured F-18 response.

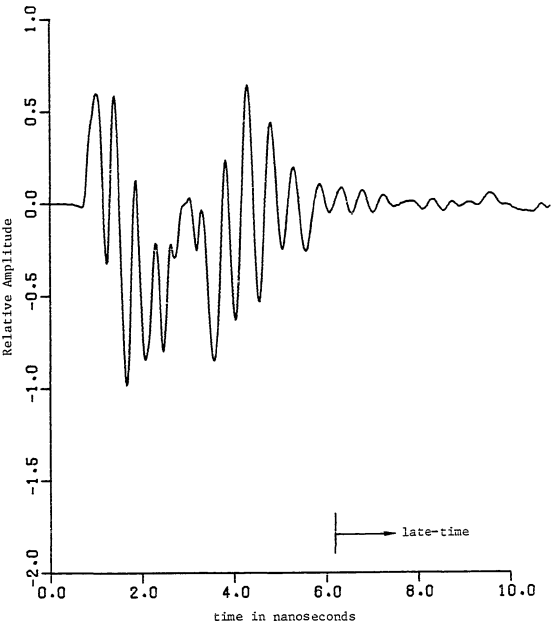

Figure 8.5.8. Convolution of 707 E-pulse with measured 707 response.

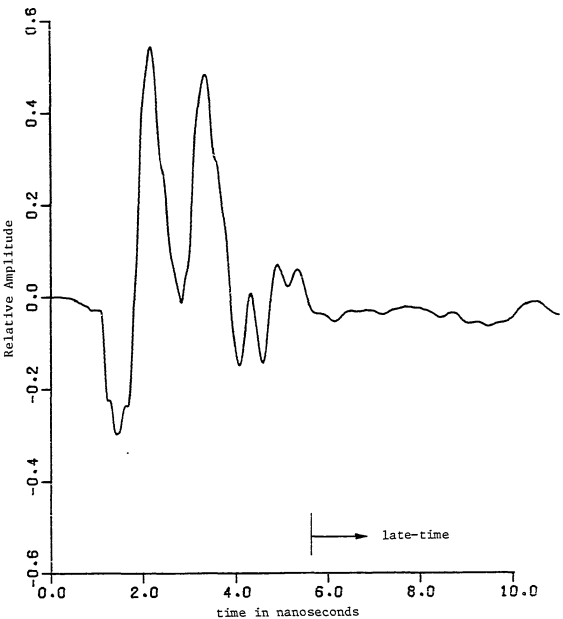

Figure 8.5.9. Convolution of F-18 E-pulse with measured F-18 response.

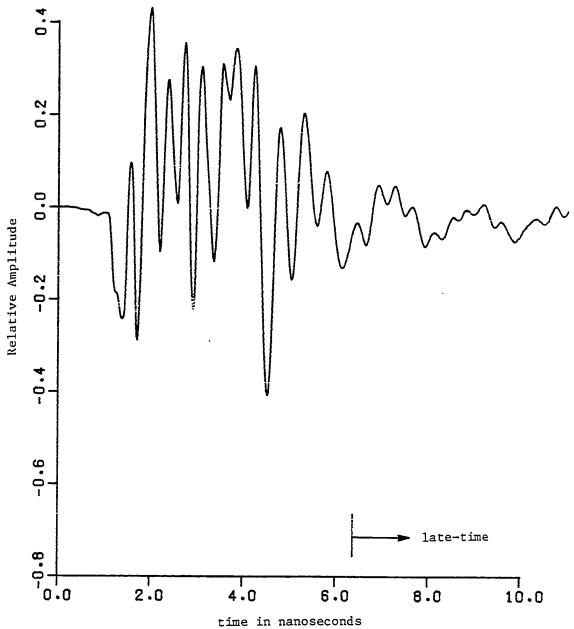

Figure 8.5.10. Convolution of 707 E-pulse with measured F-18 response.

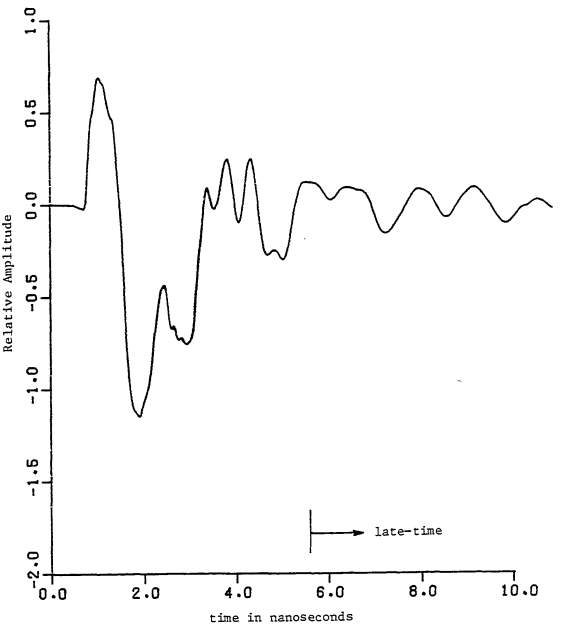

Figure 8.5.11. Convolution of F-18 E-pulse with measured 707 response.

sine and cosine single mode excitation signals have been synthesized to excite the first and the fourth modes of the 707 and to excite the first and third modes of the F-18. Each of these waveforms is then convolved with the measured responses of Figures 8.5.1 and 8.5.2. Although lack of space precludes showing each of the convolved responses, the response shown in Figure 8.5.12 is typical. This is the result of convolving the first mode cosine excitation signal for the F-18 with the F-18 measured response.

Figure 8.5.13 through 8.5.28 show the damping coefficient and radian frequency plots generated from each pair of convolved responses. The angular frequencies plots resulting from the convolution of the single mode signals with the responses for which they correspond (i.e. 707 with 707 and F-18 with F-18) are seen to lie parallel with the frequency lines of the expected modes in the late-time. While the damping coefficient plots are not as close, they do not deviate by a substantial amount. In contrast, the angular frequency plots generated from the convolution of the signals with the opposite responses (i.e. 707 with F-18 and vice versa) are seen to be far from parallel. In addition, the damping coefficient plots are all seen to be much less similar to the expected damping lines than were the convolutions of signals with the correct target responses.

The combination of the E-pulse convolutions and the single mode excitation signal convolutions allows the two targets to be discriminated with near certainty. Thus, for the case of these very realistic targets, the E-pulse technique has been verified experimentally.

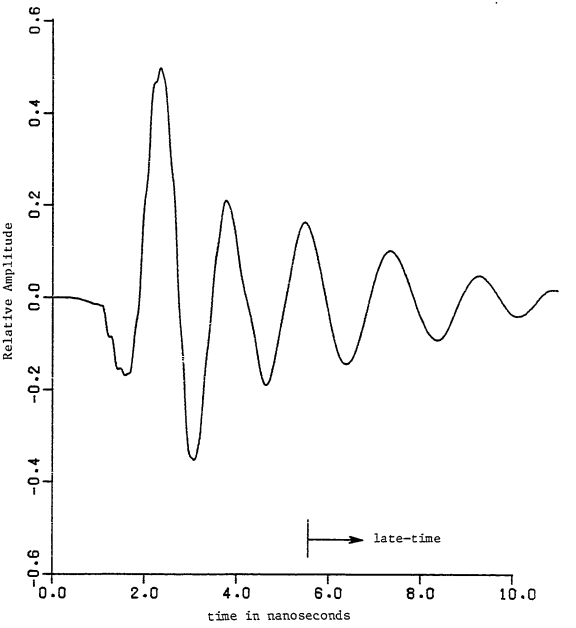

Figure 8.5.12. Convolution of F-18 cosine first mode excitation signal with measured F-18 response.

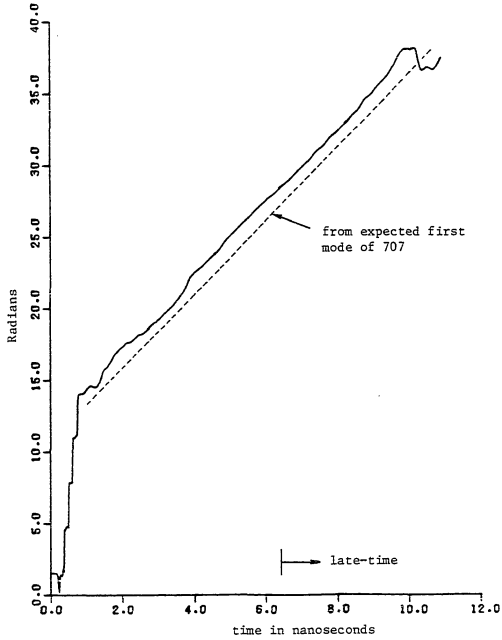

Figure 8.5.13. Radian frequency plot from convolution of first mode 707 excitation signals with measured 707 response.

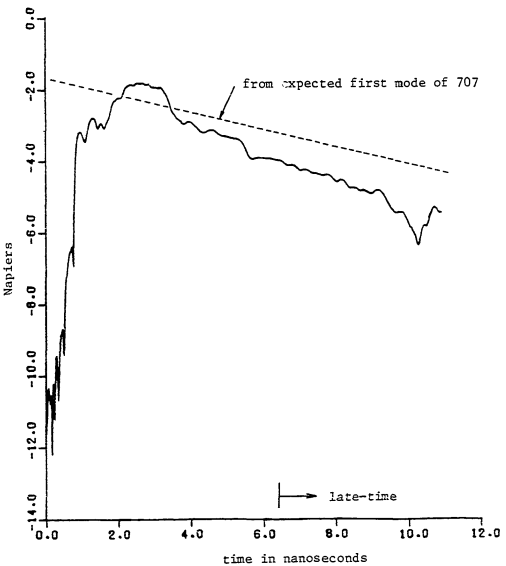

Figure 8.5.14. Damping coefficient plot from convolution of first mode 707 excitation signals with measured 707 response.

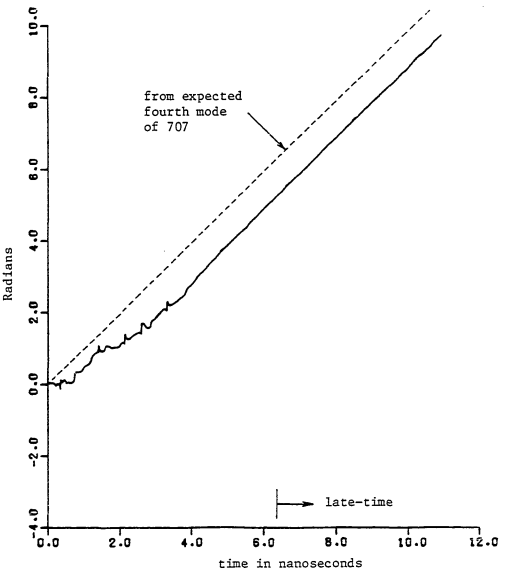

Figure 8.5.15. Radian frequency plot from convolution of fourth mode 707 excitation signals with measured 707 response.

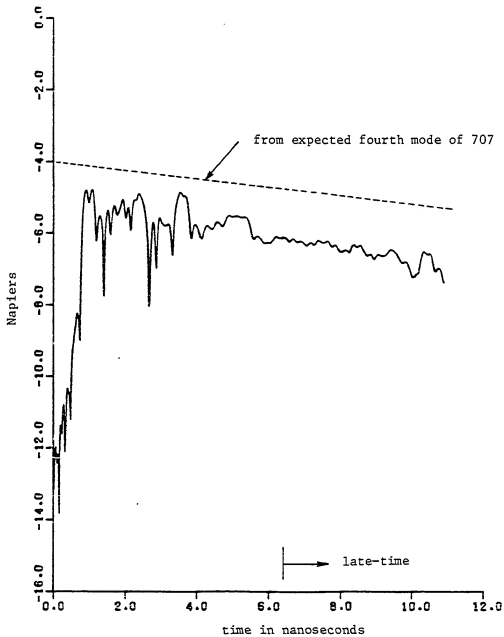

Figure 8.5.16. Damping coefficient plot from convolution of fourth mode 707 excitation signals with measured 707 response.

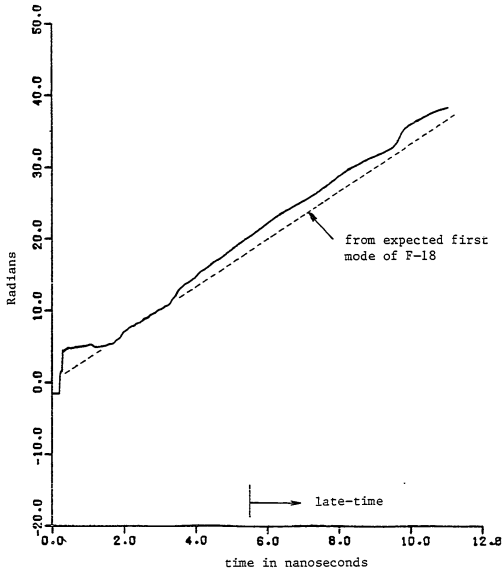

Figure 8.5.17. Radian frequency plot from convolution of first mode F-18 excitation signals with measured F-18 response.

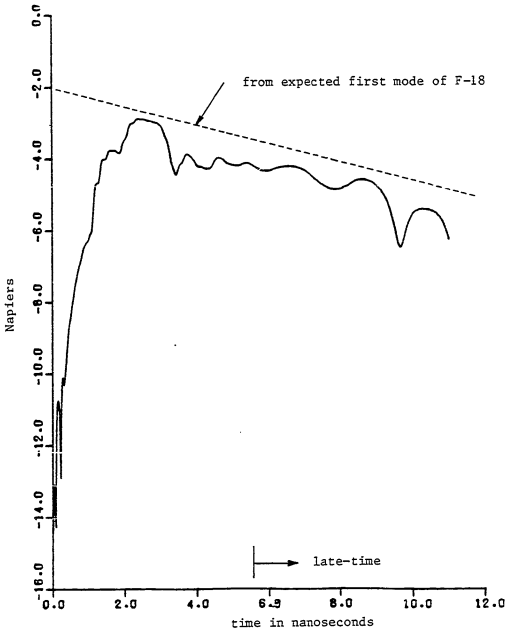

Figure 8.5.18. Damping coefficient plot from convolution of first mode F-18 excitation signals with measured F-18 response.

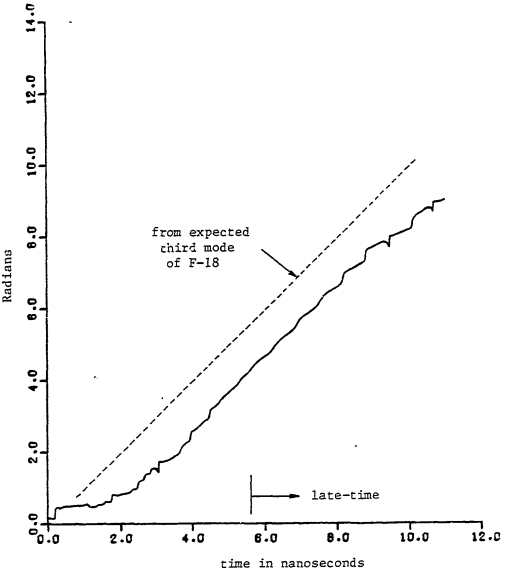

Figure 8.5.19. Radian frequency plot from convolution of third mode F-18 excitation signals with measured F-18 response.

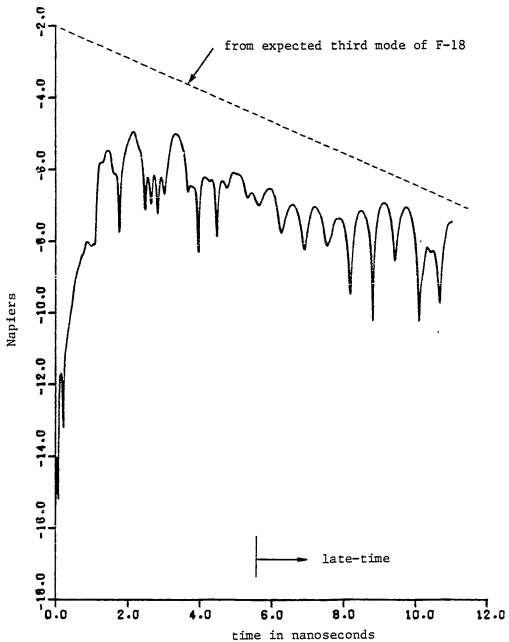

Figure 8.5.20. Damping coefficient plot from convolution of thind mode F-18 excitation signals with measured F-18 response.

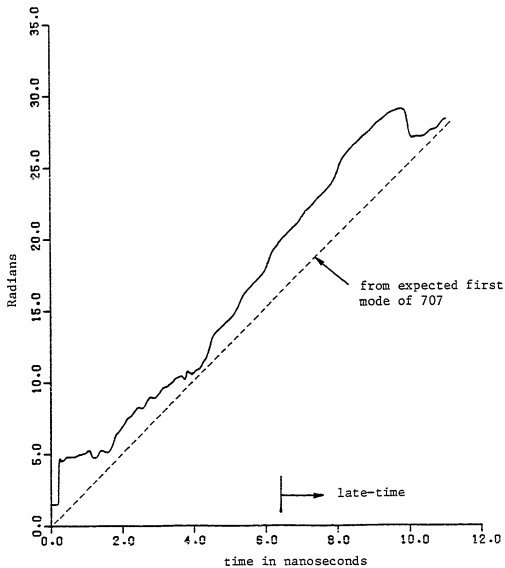

Figure 8.5.21. Radian frequency plot from convolution of first mode 707 excitation signals with measured F-18 response.

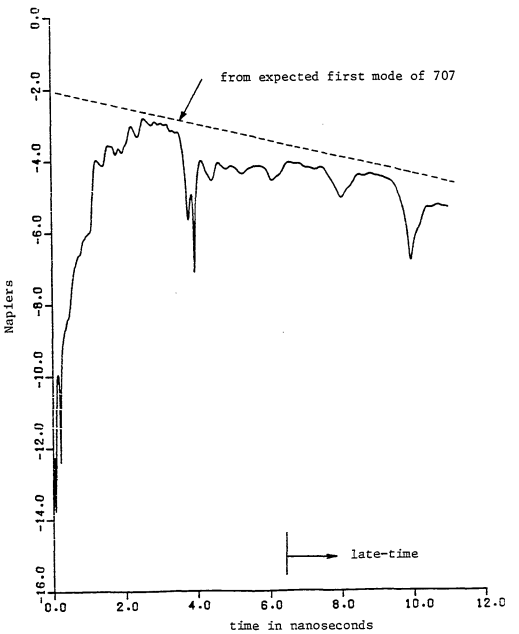

Figure 8.5.22. Damping coefficient plot from convolution of first mode 707 excitation signals with measured F-18 response.

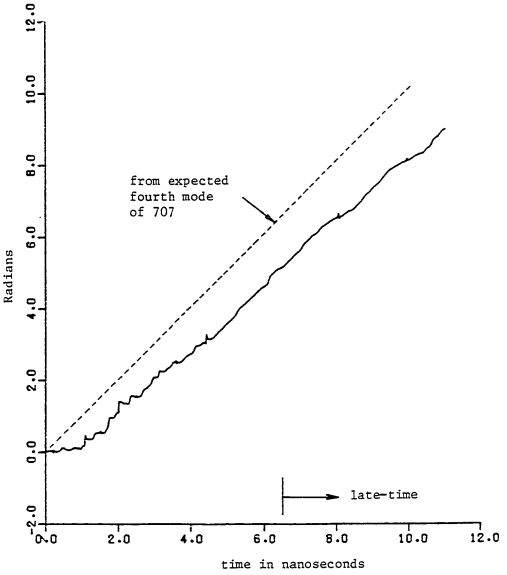

Figure 8.5.23. Radian frequency plot from convolution of fourth mode 707 excitation signals with measured F-18 response.

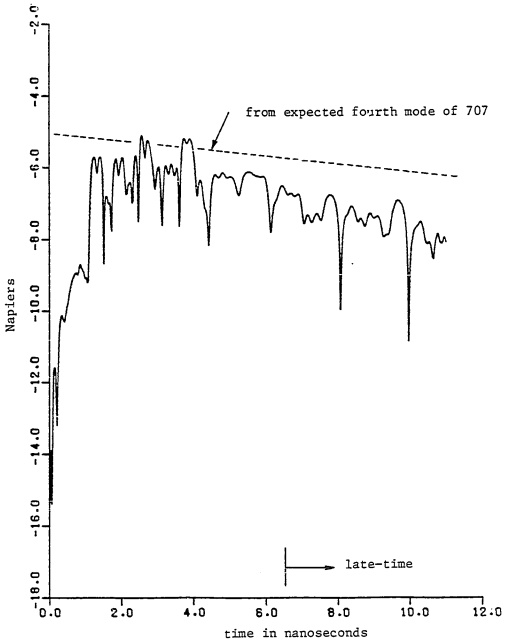

Figure 8.5.24. Damping coefficient plot from convolution of fourth mode 707 excitation signals with measured F-18 response.

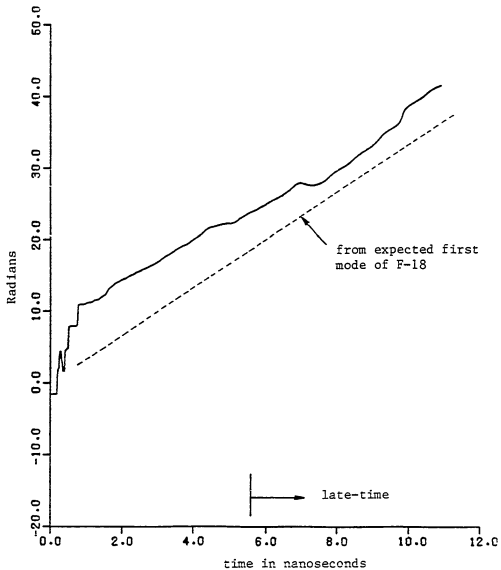

Figure 8.5.25. Radian frequency plot from convolution of first mode F-18 excitation signals with measured 707 response.

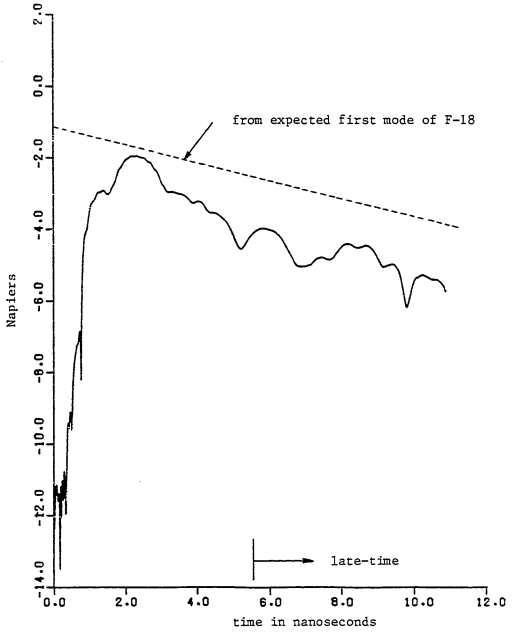

Figure 8.5.26. Damping coefficient plot from convolution of first mode F-18 excitation signals with measured 707 response.

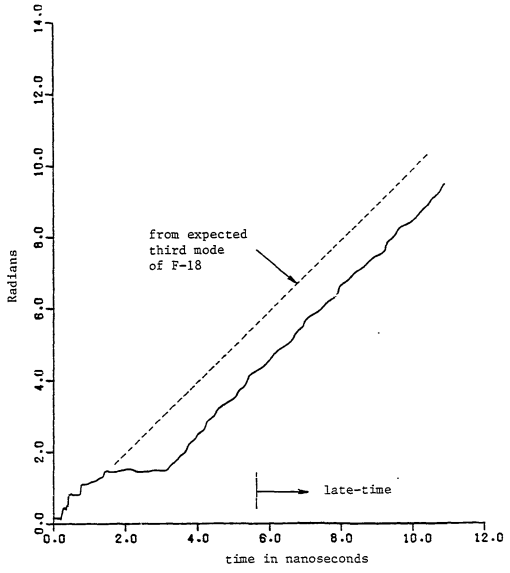

Figure 8.5.27. Radian frequency plot from convolution of third mode F-18 excitation signals with measured 707 response.

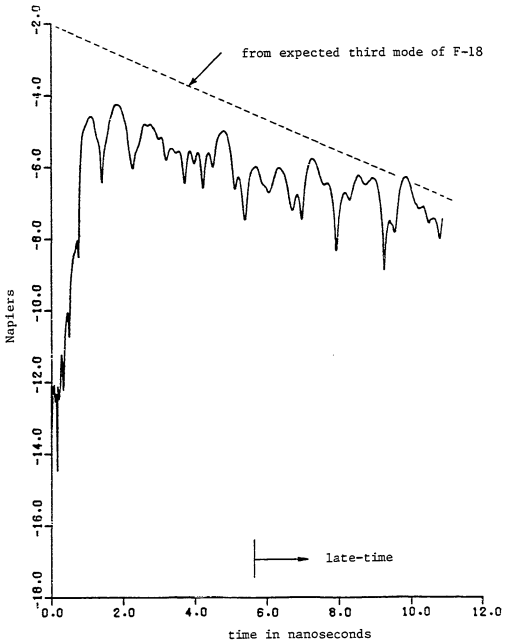

Figure 8.5.28. Damping coefficient plot from convolution of third mode F-18 excitation signals with measured 707 response.

CHAPTER 9

CONCLUSION

9.1 Summary

This thesis has introduced a scheme for radar target discrimination called the "E-pulse" technique. The E-pulse is a finite duration waveform which, upon interaction with a specific radar target, results in a scattered field which has only a pre-chosen component of the target's natural mode spectrum. An alternative approach has also been discussed, in which the E-pulse is not actually transmitted, but is merely convolved with the measured scattered field response of a target. The introduction of this technique has been shown to be warranted in the light of difficulties encountered using existing discrimination schemes.

Synthesis of E-pulse waveforms has been conducted in both the time and frequency domains by using an expansion in a set of properly chosen basis functions. The choice of basis functions has been shown to be important from the viewpoint of spectral content, noise averaging properties, and simplicity of calculations. A frequency domain interpretation of the E-pulse has been shown to be particularly insightful. Here the E-pulse is defined merely as a finite duration waveform whose Laplace spectrum has zero magnitude at the natural

frequencies of the target with which it corresponds.

Two fundamental types of E-pulses have been identified: forced and natural. The forced E-pulse waveform can have nearly any duration and consists of an arbitrary forcing component followed immediately by an extinction component, which is viewed as extinguishing the scattered field established by the forcing component. A less physical interpretation of the forced E-pulse is also allowed, by merely using one additional basis function in the E-pulse expansion. The natural E-pulse, on the other hand, has no forcing component, and is viewed as extinguishing its own resulting scattered field. This E-pulse waveform only exists for discrete values of duration.

Further types of E-pulses have been introduced, including DC and convolutional E-pulses. Distinction has also been made between E-pulses designed to eliminate the entire excited portion of the natural mode spectrum of a target, and those designed to eliminate all but a single mode. The latter are given the name "single mode excitation signals."

The pulse function basis set has been shown to be extremely useful in constructing E-pulse waveforms, due in greatest part to its simplicity. Indeed, explicit representations for the amplitudes of these pulses have been obtained, although they are not practical for performing the actual E-pulse calculation. However, a very efficient algorithm has been designed for the calculation of the pulse function amplitudes.

Comparison of natural E-pulses constructed from pulse and from Fourier cosine basis functions to eliminate the modes of a thin

cylinder target have been shown to be nearly identical. They also apparently converge to a unique waveform as the number of modes to be eliminated is increased. This suggests the possibility of E-pulse uniqueness. It has been shown that for an E-pulse to be unique, both the imaginary and real parts of the natural frequencies used in its construction must behave in a particular fashion. Of most importance are the imaginary parts, which determine the duration of the pulse function based E-pulses. This duration must converge to a specific value if the E-pulse waveform is to be unique.

Discrimination between differing thin cylinder targets has been demonstrated numerically, in the presence of random noise, with great confidence. From a frequency domain point of view, the natural DC E-pulse has been suggested as the "best" E-pulse for discriminating thin cylinders. Shaping of the E-pulse spectra has been undertaken as well, using the damped sinusoid basis set. This spectral manipulation has been shown to be potentially useful in the case of single mode excitation.

Discrimination has also been carried out using the measured scattered field response of aircraft model targets. The success of this practical demonstration has provided an empirical verification of the E-pulse concept. An experimental verification of the natural resonance expansion of target scattered field has also been accomplished.

Other topics pertinent to the E-pulse technique have been discussed as well. A group of methods for extracting the natural frequencies of targets from their measured scattered field responses

has been presented. These methods are needed to provide the basis for E-pulse construction for practical targets, where theoretical analysis is impossible. Five of the methods are completely new, and one utilizes the E-pulse concept itself. All the new methods have been shown to be successful in the presence of random noise, and with the number of modes present in the response underestimated. However, due to a lack of time, only the continuation method has been demonstrated on actual measured data.

The last topic introduced in this thesis is a theoretical analysis of a particular target -- a thin wire elliptical loop. An electric field integral equation has been derived for this structure, and it has been solved using the method of moments. The resulting natural frequencies have been shown to fall into four different categories, based upon the symmetry of the corresponding surface current distribution. The trajectories of these frequencies have been found to converge on the expected limiting cases of those of a shorted transmission line and those of two parallel wires.

9.2 Topics for Future Study

Many topics discussed in this thesis are either not fully complete, or have generated additional ideas which should prove interesting. This section shall consider several of them.

The shaping of the E-pulse spectrum considered in chapter 5 was obviously only of a preliminary nature. This topic should be pursued further by attempting discrimination in the presence of random noise. It is also possible to extend the analysis by using other basis sets,

or by actually specifying the magnitude of the spectrum at certain points. For example, the derivative of the spectrum magnitude could be forced to be zero at certain points, in an attempt to create maxima. Note that this also requires the introduction of additional basis functions.

Several of the natural frequency extraction schemes can be improved. It is possible to include variable step size in the continuation method, as well as corrections perpendicular to the path. In the schemes involving the construction of E-pulses, the inclusion of forced waveforms has been suggested. This would relieve the problem of the variation of the beginning to the late-time period. Each of the natural frequency extraction schemes should also be tested on measured data.

The theoretical analysis of the elliptical loop can also be improved, by using a Hallén type integral equation. In addition, it would be quite simple to calculate the coupling coefficients, and thus the scattered field response, from the surface current distributions. It would also be prudent to verify the analysis experimentally, by measuring the surface current response of the loop.

Lastly, the most interesting topic is also perhaps the most difficult. There remains the question as to whether the early-time portion of the scattered field response can be utilized for target identification purposes, despite its heavy dependence upon target aspect. To pursue this topic, it would be helpful to measure the early-time portion of the surface current or scattered field response of simple targets, for comparison with theory. However, this requires

the accurate removal of the system response from the measured data. Especially important is the exact removal of the receiving antenna response. To this end, an efficient and accurate deconvolution scheme must be established.

BIBLIOGRAPHY

BIBLIOGRAPHY

1. Baum, C.E., "On the Singularity Expansion Method for the Solution of Electromagnetic Interaction Problems," Interaction Note 88, December 1971.

2. Schmitt, H.J., et.al., "Calculated and Experimental Response of Thin Cylindrical Antennas to Pulse Excitation," IEEE Trans. Ant. Prop., vol. AP-14, pp. 120-127, March 1966.

3. Kennaugh, E.M., and D.L. Moffatt, "Transient and Impulse Response Approximations," Proc. IEEE, pp. 893-901, August 1965.

4. Bennett, C.L., et.al., "Transient Scattering from Conducting Cylinders," IEEE Trans. Ant. Prop., vol. AP-18, pp. 627-633, September 1970.

5. Marin, L., "Representation of Transient Scattered Fields in Terms of Free Oscillations of Bodies," Proc. IEEE, pp. 640-641, May 1972.

6. Marin, L., "Natural-mode Representation of Transient Scattered Fields," IEEE Trans. Ant. Prop., vol. AP-21, pp. 809-818, November 1973.

7. Marin, L., "Natural-mode Representation of Transient Scattering from Rotationally Symmetric Bodies," IEEE Trans. Ant. Prop., vol. AP-22, pp. 266-274, March 1974.

8. Baum, C.E., "The Singularity Expansion Method," Transient Electromagnetic Fields, L.B. Felsen Ed., Springer-Verlag, New York, 1975, pp. 130-176.

9. Baum, C.E., "Emerging Technology for Transient and Broad-band Analysis and Synthesis of Antennas and Scatterers," Proc. IEEE, vol. 64, pp. 1598-1616, November 1976.

10. Pearson, L.W., "A Note on the Representation of Scattered Fields as a Singularity Expansion," IEEE Trans. Ant. Prop., vol. AP-32, pp. 520-524, May 1984.

11. Felsen, L.B., "Comments on Early Time SEM," IEEE Trans. Ant. Prop., vol. AP-33, pp. 118-119, January 1985.

12. Dudley, D.G., "Comments on SEM and Parametric Inverse Problem," IEEE Trans. Ant. Prop., vol. AP-33, pp. 119-120, January 1985.

13. Morgan, M.A., "Response to Comments Regarding SEM Representations," IEEE Trans. Ant. Prop., vol. AP-33, p. 120, January 1985.

14. Tesche, F.M., "On the Analysis of Scattering and Antenna Problems Using the Singularity Expansion Technique," IEEE Trans. Ant. Prop., vol. AP-21, pp. 53-62, January 1973.

15. Chen, K.M., and D. Westmoreland, "Impulse Response of a Conducting Based on Singularity Expansion Method," Proc. IEEE, vol. 69, pp. 747-750, June 1981.

16. Blackburn, R.F., and D.R. Wilton, "Analysis and Synthesis of Impedance-loaded Loop Antenna Using the Singularity Expansion Method," IEEE Trans. Ant. Prop., vol. AP-26, pp. 136-140, January 1978.

17. Chen, K.M., et.al., "Radar Waveform Synthesis for Single-mode Scattering by a Thin Cylinder and Application for Target Discrimination," IEEE Trans. Ant. Prop., vol. AP-30, pp. 867-880, September 1982.

18. LePage, R., Complex Variables and the Laplace Transform for Engineers, Dover, New York, 1980.

19. Chen, K.M., "Radar Waveform Synthesis Method -- a New Radar Detection Scheme," IEEE Trans. Ant. Prop., vol. AP-29, pp. 553-566, July 1981.

20. Chen, K.M., and D. Westmoreland, "Radar Waveform Synthesis for Exciting Single-mode Backscatters from a Sphere and Application for Target Discrimination," Radio Science, vol. 17, pp. 574-588, June 1982.

21. Rothwell, E., et.al., "Radar Target Discrimination Using the E-pulse Technique," IEEE Trans. Ant. Prop., to appear 1985.

22. Webb, L., "Radar Target Discrimination Using K-pulses from a 'Fast' Prony's Method," Doctoral dissertation, Michigan State University, May 1984.

23. CRC Standard Mathematical Tables, W.H. Beyer Ed., CRC Press, Cleveland, Ohio, 1973.

24. Hanus, P.H., Theory of Determinants, Ginn and Co., Boston, 1886.

25. Muir, T., A Treatise on the Theory of Determinants, Dover, New York, 1960.

26. Gradshteyn, I.S., and I.M. Ryzhik, Table of Integrals, Series, and Products, Academic Press, New York, 1980.

27. Strang, G., Linear Algebra and Its Applications, Academic Press, New York, 1980.

28. Jordan, C., Calculus of Finite Differences, 1965.

29. Mese, E., et.al., "Target Identification by Means of Radar," Microwave Journal, pp. 85-102, December 1984.

30. Lin, H., and A. Ksienski, "Optimum Frequencies for Aircraft Classification," IEEE Transactions on Aerospace and Electronic Systems, vol. AES-17, pp. 656-665, September 1981.

31. Kennaugh, E., "Polarization Properties of Radar Reflections," Ohio State Univ., Project Rep. Contract No. RADC-AF28 (009)-90, Rep. 389-12 (AD2494), March 1952.

32. Copeland, J., "Radar Target Classification by Polarization Properties," Proc. IRE, pp. 1290-1296, July 1960.

33. Mieras, H., "Optimal Polarizations of Simple Compound Targets," IEEE Trans. Ant. Prop., vol. AP-31, pp. 996-999, November 1983.

34. Repjar, A., Ksienski, A., and L. White, "Object Identification from Multi-frequency Radar Returns," The Radio and Electronic Engineer, vol. 45, pp. 161-167, April 1975.

35. Ksienski, A., Lin, Y-T, and L. White, "Low-frequency Approach to Target Identification," Proc. IEEE, vol. 63, pp. 1651-1660, December 1975.

36. Young, J., "Radar Imaging from Ramp Response Signatures," IEEE Trans. Ant. Prop., vol. AP-24, pp. 276-282, May 1976.

37. Corrington, M., "Simplified Calculation of Transient Response," Proc. IEEE, vol. 53, pp. 287-292, March 1965.

38. Lin, Y., and J. Richmond, "EM Modeling of Aircraft at Low Frequencies," IEEE Trans. Ant. Prop., vol. AP-23, pp. 53-56, January 1975.

39. Chuang, C., and D. Moffatt, "Natural Resonances of Radar Targets via Prony's Method and Target Discrimination," IEEE Transactions on Aerospace and Electronic Systems, vol. AES-12, pp. 583-589, September 1976.

40. Berni, A., "Target Identification by Natural Resonance Estimation," IEEE Transactions on Aerospace and Electronic Systems, vol. AES-11, pp. 147-154, March 1975.

41. Van Blaricum, M., and R. Mittra, "A Technique for Extracting the Poles and Residues of a System Directly from its Transient Response," IEEE Trans. Ant. Prop., vol. AP-23, pp. 777-781, November 1975.

42. Miller, E., "A Study of Target Identification Using Electromagnetic Poles," Lawrence Livermore Laboratory, Livermore, California, Report UCRL-52685 (1979).

43. Auton, J., et.al., "On the Practicality of Resonance-based Identification of Scatterers," presented at the IEEE/AP-S Symposium and National Radioscience Meeting, Boston, Massachusetts, June 1984.

44. Morgan, M., "Time Domain Scattering Measurements," IEEE Antennas and Propagation Society Newsletter, vol. 26, pp. 5-9, August 1984.

45. Poggio, A., et.al., "Evaluation of a Processing Technique for Transient Data," IEEE Trans. Ant. Prop., vol. AP-26, pp. 165-173, January 1978.

46. Miller, E., "Prony's Method Revisited," Lawrence Livermore Laboratory, Livermore, California, Report UCRL-52590 (1978).

47. Kennaugh, E., "The K-pulse Concept," IEEE Trans. Ant. Prop., vol. AP-29, pp. 327-331, March 1981.

48. Gerald, C., Applied Numerical Analysis, Addison-Wesley, Reading, Massachusetts, 1978.

49. Prony, R., "Essai Experimental et Analytique sur les Lois de la Dilatabilite de Fluides Elastiques et sur Celles del la Force Expansive de la Vapeur de l'Alkool, a Differentes Temperatures," J. l'Ecole Polytech. (Paris), vol. 1, pp. 24-76, 1795.

50. Hildebrand, F.B., Introduction to Numerical Analysis, McGraw-Hill, New York, 1956.

51. Dennis, J.E., and R.B. Schnabel, Numerical Methods for Unconstrained Optimization and Nonlinear Equations, Prentice-Hall, Englewood Cliffs, New Jersey, 1983.

52. Stoer, J., and R. Bulirsch, Introduction to Numerical Analysis, Springer-Verlag, New York, 1980.

53. Golub, G.H., and V. Pereyra, "The Differentiation of Pseudo-inverse and Nonlinear Least Squares Problems Whose Variables Separate," SIAM J. Numer. Anal., vol. 10, pp. 413-432, 1973.

54. Kaufman, L.C., "A Variable Projection Method for Solving Separable Nonlinear Least Squares Problems," BIT, vol. 15, pp. 49-57, 1975.

55. Kaufman, L., and V. Pereyra, "A Method for Separable Nonlinear Least Squares Problems with Separable Nonlinear Equality Constraints," SIAM J. Numer. Anal., vol. 15, pp. 12-20, 1978.

56. Osborne, M.R., "Some Special Nonlinear Least Squares Problems," SIAM J. Numer. Anal., vol. 12, pp. 571-592, 1975.

57. Rice, Matrix Computations and Mathematical Software, McGraw-Hill, New York, 1981.

58. Phillips, "A Technique for the Numerical Solutions of Certain Integral Equations of the First Kind," ACM, vol. 8-9, pp. 84-89, 1961.

59. Tikhonov and Arsenin, Solutions of Ill-Posed Problems, Wiley, New York, 1977.

60. Dahlquist, D., and Å Björck, Numerical Methods, Prentice-Hall, Englewood Cliffs, New Jersey, 1974.

61. Drachman, B., and E. Rothwell, "A Continuation Method for Identification of the Natural Frequencies of an Object Using a Measured Response," IEEE Trans. Ant. Prop., vol. AP-33, pp. 445-450, April 1985.

62. Allgower and Georg, "Simplicial and Continuation Method for Approximating Fixed Points and Solutions to Systems of Equations," SIAM Rev., vol. 22, no. 1, January 1980.

63. IMSL User's Manual, Edition 9.2, International Mathematical and Statistical Libraries, Inc., Houston, Texas, 1984.

64. Keller, H.B., "Numerical Solutions of Bifurcation and Nonlinear Eigenvalue Problems," Applications of Bifurcation Theory, P. Rabinowitz, Ed., Academic Press, New York, 1977, pp. 359-384.

65. Linpack User's Guide, SIAM, Philadelphia, 1980.

66. Ortega, J.M., and W.C. Rheinboldt, Iterative Solutions of Nonlinear Equations in Several Variables, Academic Press, New York, 1970.

67. Harrington, R.F., Field Computations by Moment Methods, Macmillan, New York, 1968.

68. Wu, T.T., "Theory of the Thin Circular Antenna," J. Math. Phys., vol. 3, pp. 1301-1304, December 1962.

69. Storer, J.E., "Impedance of Thin-Wire Loop Antennas," Trans. AIEE, vol. 75, Part I, pp. 606-619, 1956.

70. Arfken, G., Mathematical Methods for Physicists, Academic Press, New York, 1970.

71. Abramowitz, M., and I.A. Stegun, Handbook of Mathematical Functions, Dover, New York, 1965.

72. Papoulis, A., Signal Analysis, McGraw-Hill, New York, 1977.

73. Chuang, C., "Transient Waveform Synthesis for Radar Target Discrimination," Doctoral dissertation, Michigan State University, 1983.

74. Otnes, R., and L. Enochson, Applied Time Series Analysis, John Wiley and Sons, New York, 1978.

75. Pearson, L., and Y. Lee, "SEM Parameter Extraction Through Transient Surface Current Measurement Using King-type Probes," IEEE Trans. Ant. Prop., vol. AP-30, pp. 260-266, March 1982.

76. Chuang, C., and D. Nyquist, "Perturbation Formulation for Nearly-degenerate SEM Modes of Loosely-coupled Bodies," presented at the National Radioscience Meeting, Boulder, Colorado, January 1984.